Modelling to guide the development of pharmaceutical interventions against malaria

Inauguraldissertation
zur
Erlangung der Würde eines Doktors der Philosophie

vorgelegt der
Philosophisch-Naturwissenschaftlichen Fakultät
der Universität Basel
von

Lydia Burgert

2022

Genehmigt von der Philisophisch-Naturwissenschaftlichen Fakultät

auf Antrag von

Prof. Dr. Melissa Penny, PD Dr. Jörg Möhrle und Dr. Lucy Okell

Basel, den 17.11.2020

Prof. Dr. Martin Spiess,
Dekan Philosophisch-Naturwissenschaftliche Fakultät

Contents

List of Figures

List of Tables

Abbreviations

A	Artemether.
ACPR	adequate clinical and parasitological response.
ACT	artemisinin combination therapy.
AIC	Akaike information criterion.
AQ	Amodiaquine.
AS	Artesunate.
AUC	area under the concentration time curve.
CHMI	controlled human malaria infection.
CI	confidence interval.
comp. erythr.	compensatory erythropoeisis.
const.	constant.
COVID-2019	Coronavirus disease 2019.
CQ	Chloroquine.
dd	density dependent.
DD	double dose.
DE	difference equation.

DHA	Dihydroartemisinin.
EIR	entomological inoculation rate.
EPI	Expanded Program on Immunization.
GP	Gaussian process.
h	hour.
i.v.	intravenous.
IPT-c	intermittent preventative treatment-children.
IPT-p	intermittent preventative treatment-pregnant women.
IRS	indoor residual spraying.
ITN	insecticide treated bed nets.
kg	kilogram.
LAI	long acting injectables.
LLOD	lower limit of detection.
LLOQ	lower limit of quantification.
LN	log-normal distribution.
LOD	limit of detection.
MalDA	Malaria Drug Accelerator.
M and S	modelling and simulation.
mAb	monoclonal antibody.
mg	milligram.
MIC	minimum inhibitory concentration.

mL milliliter.

MMV Medicines for Malaria Venture.

nM nanomolar.

NMRI Naval Medical Research Institute.

ODE ordinary differential equation.

OFV objective function value.

P. *Plasmodium*.

p.o. peroral, oral application.

PCE parasite clearance estimator.

PCR polymerase chain reaction.

PD pharmacodynamic.

PfATP4 plasma membrane P-type cation translocating ATP-ase.

PfDHODH *Plasmodium* dihydroorotate dehydrogenase.

PI4K phosphatidylinositol 4-kinase.

PK pharmacokinetic.

PKPD pharmacokinetic-pharmacodynamics relationship.

pmf parasite multiplication factor.

PPQ Piperaquine.

PRR parasite reduction ratio.

QD quadruple dose.

qPCR quantitative polymerase chain reaction.

RBC red blood cell, see also erythrocyte.

SCID severe combined immunodeficiency.

SD single dose.

SMC seasonal malaria chemoprevention.

SMC-SP+AQ seasonal malaria chemoprevention with Sulfadoxine-Pyrimethamine + Amodiaquine.

SP Sulfadoxine-Pyrimethamine.

SPAQ Sulfadoxine-Pyrimethamine + Amodiaquine.

TCP target candidate profile.

TD triple dose.

TPP target product profile.

VIS volunteer infection study.

WAIC Watanabe-Akaike information criterion.

WHO World Health Organization.

Acknowledgements

This thesis would not have been possible without the extensive and unconditional support that I have received over the last years.

My sincerest thanks to my supervisor Melissa Penny, whose guidance and eye for the bigger picture have always motivated and pushed me throughout the years. Thank you for making this thesis a truly outstanding experience and for providing me with so many opportunities. Additionally, I would like to thank my second-supervisor Jörg Möhrle, for his support. Your insights into the field and current ongoings of antimalarial drug development have been invaluable.

I would also like to acknowledge all my collaborators and colleagues at Swiss TPH including Monica Golumbeanu, Tamsin Lee, Tom Smith, Matthias Rottmann and Sergio Wittlin. Your feedback and discussions helped me to find my path through the jungle that is malaria research. It has been a pleasure to work with you. Thanks also to all the people, who dared to read the countless paper and thesis drafts for their tireless feedback.

My special thanks goes to Theresa Reiker and Fabienne Fischer who helped me in any and every way throughout the years and during the writing of this thesis. Without you, my plots would only be half as aesthetically pleasing and I don't even want to think about the state of my climbing and running abilities.

Finally, I would like to thank all the other crucial people in my life who have always been there for me with countless motivational speeches and distractions. My parents, Karin and Jürgen, who have always provided a safe haven to flee to over the years, full of open ears, too much to eat and endless support. Jonas, thank you for the ever ready coffee in the morning. Susi and Paul, who shooed me up almost every wall or a hill. And of course Dobby and Penny, for always being cute and not in the least impressed by all human-world problems.

Summary

The development of new antimalarial compounds and regimens is more urgent than ever as continued burden reduction and ultimately the elimination of malaria are threatened by emerging resistance against current treatments, and sub-optimal adherence to treatment schedules. Throughout this thesis, I have sought to develop a thorough understanding of parasite-host dynamics along the clinical development pathway of new antimalarials for clinical case management and to evaluate drug efficacy measures, their translation, and their limitations. I analysed parasite growth data from murine and human experiments in the absence of treatment and captured parasite growth in an ensemble of mechanistic mathematical models. Subsequently, I investigated the sensitivity of the experimental efficacy endpoint of parasite clearance after treatment to host-, parasite-, and drug-dynamics throughout the clinical development pathway. Our findings show that the experimental background and/or host dynamics strongly influence parasite clearance with differential impact between the experimental systems. The work culminates in a discussion of the multitude of different host-parasite dynamics in the development stages that compromise the translatability of drug efficacy estimates between the infection experiments.

I then shift the focus to the development of new anti-infective interventions in form of long acting injectables. These are envisioned to protect children living in highly seasonal transmission settings against malaria. I employ a simulation-based approach using an individual-based stochastic model of malaria that allows the efficient investigation of a large range of plausible product properties and deployment modalities and their potential to reach predefined health and impact targets. A non-inferiority analysis to currently implemented drug-based chemoprevention measures reveals the trade-offs between tool and coverage optimisation for the development of new tools. The results assist the specification of use cases and definition of efficacy targets in target product profiles to guide the future development of long-acting injectables.

Through the use of mechanistic parasite growth and individual-based models, the work reported here creates a sound foundation for a comprehensive assessment of experimental and clinical testing results through exploring, understanding and quantifying host-, parasite-, and experimental-factors that influence intervention efficacy and impact.

Chapter 1

Introduction

1.1 Malaria: disease, treatment and prevention

Malaria still takes around 405 000 lives each year, 67% of which are children under five years of age. It remains a wide-spread infectious disease with estimates of over 228 million cases in 2018 [WHO, 2019]. The majority of burden is caused by the *Plasmodium (P.) falciparum* parasite, transmitted to humans by the bite of an infected female *Anopheles* mosquito. Since the year 2000, burden reductions in malaria cases (-16%) and deaths (-48%) have been achieved following the large-scale introduction of interventions targeting mosquito abundance, preventing the transmission of malaria to humans and ensuring a timely treatment of malaria cases. The estimated total number of clinical cases averted lies at 663 (542–753 credible interval) million since 2000. Of these cases averted, 68% are estimated to be attributable to insecticide treated bed nets (ITNs), 10% to indoor residual spraying (IRS) and 22% to treatment with artemisinin combination therapy (ACT) [Bhatt et al., 2015]. In contrast to the preventive measures of IRS and ITN, the primary purpose of ACTs is the aversion of severe disease and death.

However, the efforts for continued burden reduction let alone elimination are compromised by numerous challenges: lack of funds for malaria control programs [Haakenstad et al., 2019], difficulties in reaching remote populations [WHO, 2015a], insecticide resistance [Ranson and Lissenden, 2016] and antimalarial drug resistance [Ménard et al., 2016]. The weakening of malaria control programmes or reintroduction of malaria transmission in previously malaria free areas could lead to a resurgence of malaria cases as has been observed multiple times over the last century [Cohen et al., 2012]. In 2014/2015, the Ebola outbreak in Liberia and Sierra Leone disrupted the distribution of ITNs, caused the closing of health care facilities and less testing for malaria by a reduction in resources allocated to malaria control programs [Edelstein et al., 2015]. Currently, the COVID-19 pandemic threatens to disrupt supply chains for malaria

diagnostics and treatment and the implementation of ITN distribution campaigns resulting in an increase in malaria case numbers and deaths and a potential increased spread of drug resistance [Rogerson et al., 2020].

As progress made in fighting malaria is challenged by these obstacles and stagnation in worldwide burden reduction was observed over the recent years [WHO, 2018; Whitty and Ansah, 2019], new innovative interventions for vector control, treatment and personal protection are needed to reach the goal of malaria control and elimination [Rabinovich et al., 2017; Hemingway et al., 2016].

1.1.1 The malaria parasite life cycle

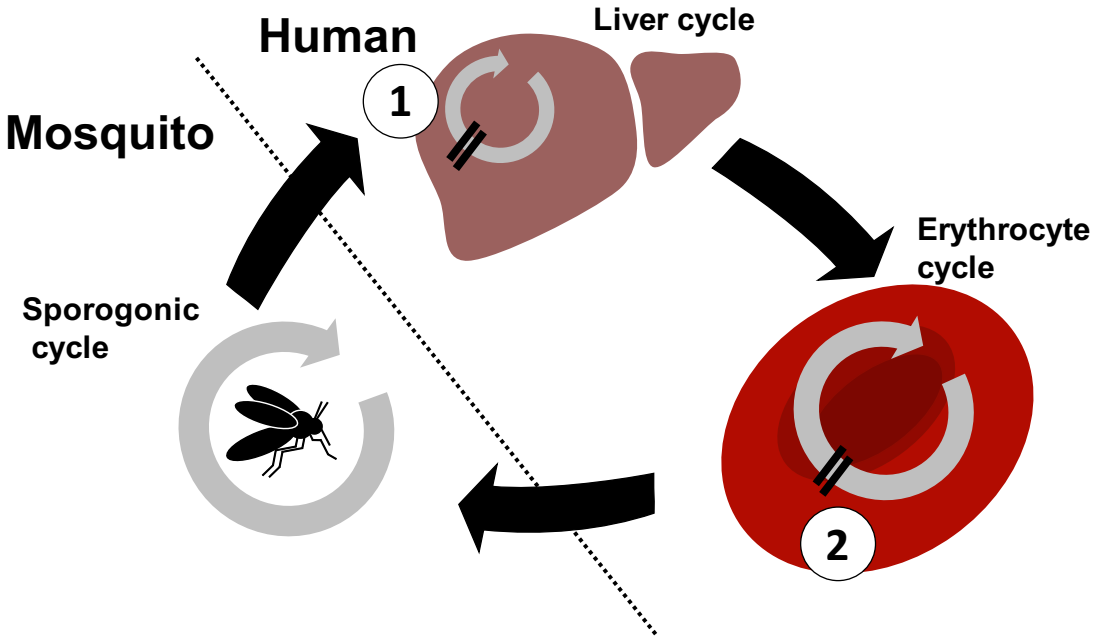

Figure 1.1: Overview of the malaria life cycle. The malaria life cycle consists of three stages; the sporogonic cycle in the mosquito and the liver and erythrocyte cycle in the human. The interruption of the malaria life cycle in humans is achieved through either targeting the liver cycle, therefore preventing blood stage infection (1), or treatment of blood-stage malaria (2).

The malaria parasite life cycle relies on two hosts: an insect (mosquito) and a vertebrate (human) host. It can be split into three stages; the sporogonic cycle in the mosquito and the exo-erythrocytic (liver) and erythrocytic (blood) cycle in the human (Fig. 1.1). Briefly, female *Anopheles* mosquitoes transmit the malaria parasite to humans through the inoculation with sporozoites during feeding. The sporozoites infect hepatocytes and subsequently mature into schizonts which rupture and release merozoites to infect new hepatocytes. After 6-7 days,

the merozoites are released into the blood stream, where they enter the erytrhocytic life cycle (asexual reproduction) consisting of the continued infection of erytrocytes (red blood cells, RBCs), maturation through the ring (trophozoite) and schizont stages, and subsequent release of new merozoites every 48 hours. After 3-10 days, a small proportion of parasites develop into the sexual gametocyte stage, which are ingested by mosquitoes during feeding. In the mosquito gut, the sporogonic cycle takes around 10-14 days and is completed with the production of new sporozoites, which migrate to the mosquitoes salivary gland for transmission to humans during the next blood meal [Cowman et al., 2016].

Clinical symptoms of malaria are caused by the periodic sequestration of infected RBCs to the blood vessels and release of new merozoites into the blood stream by lysis of infected RBCs. The aetiopathology is dependent on multiple factors such as the innate and acquired immunity of the host [O'Flaherty et al., 2017], the initial parasite burden before treatment [White et al., 2009] and the efficacy of treatment [WHO, 2009]. Severe malaria, which can cause multi-organ damage and coma (cerebral malaria), occurs in 1-2% of cases. Death occurs in 10-20 % percent of these severe cases, depending on aetiopathology and patient age [Wassmer et al., 2015].

The aim of all interventions against malaria is the effective interruption of the malaria life cycle leading to a reduction in malaria transmission and malaria burden (Fig. 1.1). Malaria transmission between mosquitoes and humans is targeted by decreasing the mosquito population through e.g. indoor residual spraying and larviciding, or hindering mosquitos from biting through e.g. insecticide treated nets [Pryce et al., 2018]. However, once a human has been bitten by an infectious mosquito, preventing progression to blood-stage infections or the prompt treatment after the onset of symptoms, is the only way to alleviate substantial burden from malarial disease.

1.1.2 Treatment of malaria

Historically, blood-stage malaria was treated with monotherapies consisting of e.g. Chloroquine (CQ), Sulfadoxine-pyrimethamine (SP), Amodiaquine (AQ) or Quinine. However, resistance against all of these compounds emerged within 5 to 20 years of their respective introduction and is now widespread [McClure and Day, 2014] (Table 1.1). The recommendation of artemisinin combination therapies (ACTs) as first-line treatment by the WHO in 2006 and the introduction of cheaper, fixed dose ACTs between 2009 and 2012 lead to higher treatment successes through simpler administration schedules [Bosman and Mendis, 2007; WWARN, 2015].

The spread of resistance is slowed by protecting the fast-acting artemisinin derivative with a longer-acting partner drug, which kills remaining parasites. However, treatment with ACTs requires a three day dose regimen [WHO, 2015b], making it prone to poor adherence and thus treatment failure [Challenger et al., 2017], thereby promoting the emergence and spread

Table 1.1: Overview of the compound class, (suspected) mode of action and time resistance development after introduction for a selection of old and new antimalarials. The information was extracted from [1] [Blasco et al., 2017], [2] [McClure and Day, 2014] [3] [Tse et al., 2019], [4][Boss et al., 2016]. ACT-artemisinin combination therapy

Class	(Suspected) mode of action	Drug	Introduction	Resistance reported	Ref.
4-aminoquinolines	Interference with haem detoxification in digestive vacuoles	Amodiaquine	1950	1971	1
		Chloroquine	1945	1957	2
		Piperaquine (PPQ)	1978	1989 (now as DHA+PPQ)	1
Artemisinin derivatives (endoperoxides)	Not well known, suspected parasite protein damage through generation of free radicals	Artemether (A) in ACT: A+ L	1992	-	2
		Artesunate (AS) in ACTs:			
		AS+SP	2003	2011	1
		AS+MQ	1994	2002	1
		AS+AQ	2007	-	1
		Dihydroartemisinin (DHA) in ACT: DHA+PPQ	1997	2010	1
Anti-folates	Dihydrofolate reductase (DHFR) inhibitor	Proguanil	1948	1949	2
Amino-alcohols	Unknown	Halofantrine	1960s	-	2
		Lumefantrine (L) in ACT: A+L	1992	-	2
		Mefloquine	1977	1986	2
		Quinine	1632	1910	2
Quinone	Blocking mitochondrial electron transport	Atovaquone	1996	1996	2
Sulfonamides with diaminopyrimidines	Folate biosynthesis pathway	Sulfadoxine- pyrimethamine	1967	1967	2
New antimalarial compounds					
Class	**(Suspected) mode of action**	**Drug**	**Discovery**	**Development stage**	**Ref.**
Triazolopyrimidines	PfDHODH inhibition	DSM265	2011	Phase II	3
Aminopyridine	PfP14K inhibition	MMV048	2012	Phase IIa	3
Endoperoxides	(Suspected) oxidative stress	OZ439 (Artefenomel)	2011	Phase II	3
		OZ277 (Arterolane)	2004	Licensed in India	3
Imidazolopiperazine	Unknown (potentially new)	KAF156	2012	Phase IIb	3
Spiroindolone	PfATP4 inhibition	KAE609/Cipargamin/NITD609	2010	Phase IIb	3
Phenylalanine	(Suspected) PfMDR1 inhibition	ACT-451840	2016	development halted	4

of resistance [White et al., 2009]. The emergence and spread of resistance against ACTs is assessed by monitoring the *P. falciparum* gene encoding the kelch (K13)–propeller domain and cure rates after treatment [Ariey et al., 2014]. Resistance to ACTs has already been detected in the Greater Mekong subregion, endangering yet another antimalarial treatment [Imwong et al., 2020]. For now, resistance to ACTs with a measurable impact on antimalarial treatment efficacy is mainly prominent in Southeast Asia and China [Ménard et al., 2016; Phyo et al., 2016b]. However, mutations potentially promoting the emergence of resistance against ACTs in Africa were discovered recently [Uwimana et al., 2020].

Therefore, the development of new drugs with different modes of action and easier administration plays a key role in successful case management through effective treatment [Burrows et al., 2017]. Table 1.1 lists examples of new antimalarial compounds and their (suspected) mode of action. The lack of commercial incentive for the development of new antimalarials initiated the foundation of the Medicines for Malaria Venture (MMV), a not-for-profit public-private partnership dedicated to the discovery, development, and delivery of new antimalarial drugs. Currently, there are around 33 molecules in different stages of research and discovery, translational and product development phases in the MMV development pipeline (https://www.mmv.org/research-development/mmv-supported-projects). However, late phase drug attrition is high because of uncertainties in dose selection, deficiencies in efficacy and safety concerns [Pellicciari, 2017]. Estimates show that, on average, 48 new candidate molecules are needed to launch one new treatment [Burrows et al., 2017]. This emphasises the need for the efficient and timely discovery and development of new anti-malarial treatments.

1.1.3 Prevention of malaria

The prevention of infection using ubiquitous personal protection through long-lasting preventative measures in the form of vaccines or chemoprevention has long been a goal in fighting malaria [Hoffman et al., 2015]. There have been numerous attempts at vaccine development including the most advanced candidate RTS,S/AS01 [RTS,S Clinical Trials Partnership, 2014]. It prevents blood-stage infection by targeting the sporozoite stage that occurs in the liver cycle of the *Plasmodium* life cycle (Fig. 1.1) [Cohen et al., 2010]. However, clinical field trials showed a protective efficacy of only 55% against all episodes in children and 33% in infants [RTS,S Clinical Trials Partnership, 2014]. Although a vaccine with high protective efficacy would be the ultimate goal in fighting malaria, the difficulties in developing such a vaccine are numerous including partial natural immunity even after multiple infections with malaria and active antigenic variation of the malaria parasite [Doolan et al., 2009].

Chemoprevention through intermittent preventative treatment (IPT) via the administration of a full antimalarial treatment course with SP during the malaria season was introduced to ease the malaria burden in vulnerable populations. At fixed time-points infants and pregnant

women receive IPT through the Expanded Program on Immunization (EPI) (IPT-i, [WHO, 2010]) and antenatel care programs (IPT-p, [WHO, 2016]). In 2012, the WHO released a guideline, recommending the use of Sulfadoxine-Pyrimethamine and Amodiaquine(SP-AQ) as seasonal malaria chemoprevention (SMC) in children between 3 and 59 months in areas of high malaria transmission [WHO, 2012]. Monthly administration throughout the transmission season aims at clearing existing infections and preventing new infections by targeting the liver cycle of malaria (Fig. 1.1). However, operational constraints, rising resistance and the restriction of implementation to regions with highly seasonal malaria transmission restrict the area of implementation for SMC [WHO, 2013].

Chemoprotection through a specifically designed, prophylactic regimen with long acting injectables (LAIs), in form of small molecule drugs or monoclonal antibodies, could provide an alternative prevention tool by simplifying the deployment and reducing the risk of resistance [Macintyre et al., 2018]. LAIs are molecules which provide protection for a longer period of protection than conventional drugs, thereby requiring less administration cycles over one season. The decrease in required doses (e.g. once per season) and a long protective efficacy potentially simplify the delivery and thereby increase the impact in vulnerable populations such as children and pregnant women. Towards reaching elimination, also the malaria transmission patterns and epidemiology change [Cotter et al., 2013]. With less exposure to malaria, people acquire less immunity, making them more susceptible to the occurrence of clinical malaria episodes and severe disease [Reyburn et al., 2005]. The implementation of an LAI promises the alleviation of a substantial amount of malaria burden. Protecting populations moving between high and low transmission areas (e.g. migrant workers) could also prevent the reintroduction of malaria to previously malaria free areas [Fowkes et al., 2016].

All in all, the need for the prompt development of new human-targeted pharmaceutical interventions, in form of personal protection and effective treatment of malaria cases, is evident to ensure a continued success in fighting malaria.

1.2 The development process of new antimalarials

The development process of human-targeted interventions is costly and time consuming as the finished products must meet multiple conditions spanning safety, efficacy, administration, and production requirements. From first hit in a compound screening to patients in the field, the development of a new antimalarial takes about 12-15 years [Burrows et al., 2017]. The need for combination therapy of minimum two compounds, to fight the rise of resistance, puts an additional constraint on the development of new treatment regimens. Finding effective combinations of antimalarial compounds is challenging as drug-drug-interactions, impacting the pharmacokinetic and pharmacodynamic profiles of the individual drugs, and the safety of the treatment

regimen and interactions with other medications have to be considered.

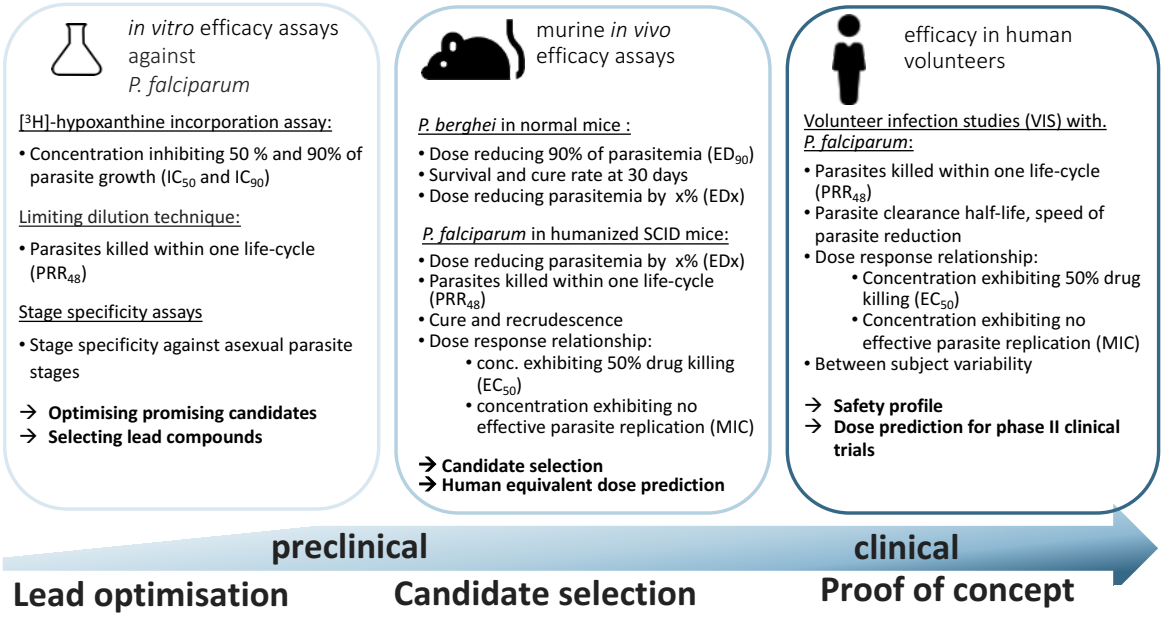

Figure 1.2: Summary of experiments and efficacy indices used to assess new antimalarial compounds during the translational phase of the development process.

To accelerate antimalarial discovery, drug discovery platforms such as the MalDA (MaLaria Drug Accelerator) consortium [Murithi et al., 2020] and initiatives to openly share promising candidate molecules and data for research [Duffy et al., 2017; Charman et al., 2020] were established. High throughput screening efforts of large compound libraries with phenotypic, whole-cell based assays identified over 25,000 active molecules in the recent years [Burrows et al., 2017]. This whole cell-based screening approach increases the chance to find first-in-class molecules with new modes of action or efficacy through multiple modes of action. Promising molecules are further analysed *in vitro* to determine general molecule properties including crude potency, toxicity, cost of synthesis and novelty. Furthermore, the investigation of structure activity relationships facilitates an increase in potency [Flannery et al., 2013]. Molecules selected for further development then enter the translational phase of antimalarial drug development which can be split into two phases; preclinical and clinical development. An overview over the different phases of the *in vitro* and *in vivo* efficacy experiments performed during the translational phase and the main decision criteria for efficacy at each stage can be found in Figure 1.2. The aim of the translational phase is to accompany antimalarial drug development from candidate selection to proof-of concept in patients.

In vitro efficacy assays against *P. falciparum*

The *in vitro* assays used to evaluate antimalarial candidates in pre-clinical development include various experiments to assess crude efficacy of the compound as well as stage-specificity and mode of action. The [^{3}H]-hypoxanthine incorporation assay estimates the ability of the compound to kill parasites *in vitro* by measuring remaining metabolic activity and therefore growth [Desjardins et al., 1979]. These experiments allow the quantification of crude efficacy indices such as the concentration where x% of parasite-growth is inhibited (IC_x). Using the limiting dilution technique [Rosario, 1981] that estimates the number of parasites viable at several time points after treatment, the *in vitro* parasite reduction ratio (PRR) can be estimated [Le Bihan et al., 2016]. The identification of stage-specificity and metabolic profiling to investigate the mode of action [Murithi et al., 2020] allow the evaluation of compound novelty and eligibility for their future use case.

Murine *in vivo* efficacy assays

Murine malaria models have a long history in compound selection in preclinical antimalarial development [Flannery et al., 2013]. They are used to investigate the drug-concentration profile over time (PK: pharmacokinetics), as well as drug efficacy (PD: pharmacodynamics). A commonly used experimental system to investigate crude efficacy is infection of NMRI (Naval Medical Research Institute) mice with *P. berghei*. With a life cycle length of 24 hours in the murine host, parasitemia (the percentage of infected RBCs) increases rapidly and infection is lethal within five to seven days. Nonetheless, parasite morphology and development exhibit overall similarity to human malaria infections [Flannery et al., 2013]. Multiple experiments were developed over time, with single- or multiple-dose treatment regimens commencing 4-48 hours after inoculation with infected RBCs and parasitemia being measured 4-5 days afterwards [Jiménez-Díaz et al., 2014a]. This experimental system is primarily used for compound selection through crude efficacy measurements and preliminary dose-response curves. However, enzymatic differences between the *P. berghei* and *P. falciparum* parasite have resulted in drugs showing parasiticidal activity in one experimental system and not the other [Phillips et al., 2016], therefore introducing a selection bias in preclinical candidate evaluation.

Since 2008, further investigation of drug efficacy towards human application is often undertaken in severe combined immunodeficiency NOD $^{\text{scidIL-2R'c-/-}}$ (SCID) mice to study *P. falciparum* blood-stage infection. These mice lack a fully functioning immune system, facilitating the engraftment with human RBCs to host the human malarial parasite *P. falciparum* [Angulo-Barturen et al., 2008; Jimenez-Diaz et al., 2009]. The mice are injected with human erythrocytes to reach a sufficient human to mouse erythrocyte ratio to carry infection with *P. falciparum*. Experiments can last for over 30 days and time-series data on parasite clearance after treatment and potential re-growth of parasites after non-curative treatment (recrudescence) can be collected. These data allow a first description of the dose-response relationship and are used to

inform human equivalent dosing. Both, *P.berghei*-NMRI and *P. falciparum*-SCID infection, have been widely used in drug development for compound selection [Charman et al., 2011; Paquet et al., 2017; Le Bihan et al., 2016]. Compared to *P.berghei*-NMRI experiments, SCID mouse infection studies are more costly and labor-intensive due to the continued human RBCs injections. However, they allow first insights into *in vivo* antimalarial activity against *P. falciparum*.

Efficacy against *P. falciparum* in human volunteer infection studies

During clinical development phases, controlled infection of volunteers with *P. falciparum* (volunteer infection studies, VIS) allows for the investigation of drug efficacy in malaria-naive humans [Engwerda et al., 2012; McCarthy et al., 2011]. Compounds showing blood-stage (e.g. OZ439 [McCarthy et al., 2016c]) as well as prophylactic liver-stage activity have been assessed using this approach (e.g. DSM265 [Sulyok et al., 2017]). Healthy volunteers are inoculated with infected erythrocytes or by bite of infectious mosquitoes. The assessment of blood-stage activity is conducted by treatment of volunteers 7-9 days after inoculation and the measurement of parasite clearance curves. The prophylactic potential of new compounds treatment is assessed by evaluating the ability to prevent blood-stage infection through treatment administration before parasite inoculation. In VIS, the extensive sampling of parasite- and drug-concentration over time allows the development and formalisation of concentration-effect relationships (PKPD-relationships). Coupled with information on inter-individual patient variability these experiments provide insights into the reachability of efficacy targets such as cure rates and speed of parasite clearance. Data from these experiments informs drug evaluation and dosing in phase II clinical trials [Stanisic et al., 2018].

Target product profiles to guide the development of new antimalarials

Along the translational pathway from compound selection to proof of concept (Fig. 1.2), target product profiles (TPPs) guide decisions on compound selection. They are strategic documents that capture the requirements for interventions spanning efficacy, safety and implementation specifications (Table 1.2). During the development of new antimalarials, they are used to benchmark new compounds against the desired product profiles, thereby providing means to evaluate and select promising compounds. The requirements listed in TPPs are informed by the future use case including health goals and impact targets, economic considerations, expert opinion and in comparison to existing tools. TPPs are continuously evaluated and updated to reflect changes in product requirements and incorporate new findings [Burrows et al., 2017]. Between 2013 and 2017, the refinement of efficacy measures such as the parasite reduction ratio for treating blood stage-malaria and additional specifications to treat and protect vulnerable populations was undertaken due to the progress made in the development of new drugs and reports of resistance against ACTs [Burrows et al., 2013; Burrows et al., 2017]. The efficacy requirements for blood stage targeting compounds include a fast reduction in parasite load and

a high cure rate. Additional specifications include desired dosing regimens and transmission blocking properties [Burrows et al., 2017]. To address the need for new tools for chemoprevention, a separate TPP for LAIs details the use cases and requirements for new protective tools [Macintyre et al., 2018].

The development of new antimalarials therefore requires the ability to systematically benchmark efficacy measured during the drug development process to these target product profiles to select promising candidates as early as possible.

Table 1.2: Overview of the efficacy and administration requirements as specified in the target product profile for malaria case management [Burrows et al., 2017] and protection from infection [Macintyre et al., 2018].

		Case management Treatment of acute uncomplicated malaria in children or adults		**Protection from infection**	
Target product profile (TPP)	Product	Combination therapy of at least 2 active molecules		Injectable prophylactic medicine: Combination of at least two molecules (depending on predicted resistance development)	
		minimum essential	**ideal**	**minimum essential**	**ideal**
	Antimalarial activity	• at least one component acts immediately • 24 h fever clearance • parasite-free (day 7)	• both components act immediately • 24 h fever clearance • parasite-free (day 7)	• blood schizonticides • at least one molecule has causal prophylactic activity (liver stage) • protection within 72 h	• both molecules have causal prophylactic, blood-stage and transmission blocking activities • immediate protection
	Clinical efficacy	• ACPR: >95% PCR-corrected on day 28 • non-inferior to standard of care	• ACPR >95% PCR-corrected on days 42–63; • non-inferior to standard of care	• ≥ 80% protective efficacy	• ≥ 95% reduction in incidence • of symptomatic malaria
	Treatment regimen	• oral • two or three doses	• oral • one dose	• monthly • intramuscular	• once per three months • intramuscular or sub-cutaneous
	Additional requirements	combination of two or more molecules with TCP-1 activity, plus reduction in transmission and relapse prevention		combination would ideally have causal prophylaxis (preventing blood-stage and liver stage activity)	
Target candidate profile (TCP)		**TCP-1 profile, molecules clearing asexual parasitaemia**		**TCP-4 profile, part of a prophylactic combination**	
		minimum essential	**ideal**	**minimum essential**	**ideal**
	Dosing regimen	•oral •single dose	•oral •single dose	•injectable: subcutaneous or intramuscular •once per month	•injectable: subcutaneous or intramuscular •once per three months
	Efficacy requirements	•rapid clearance of parasites at least as fast as MQ (≤72 h) •projected >10^6-fold reduction in parasites	•immediate and rapid clearance of parasites at least as fast as Artesunate •projected >10^{12}-fold reduction in parasites	•preclinical: liver schizont stage activity and 100% protective efficacy •clinical: predicted > 80% protective efficacy (VIS)	• preclinical: liver schizont stage activity and 100% protective efficacy • clinical: predicted 95% protective efficacy (VIS)

1.3 Supporting the development process of new antimalarial entities with modelling

1.3.1 Within-host modelling in antimalarial drug development

A comprehensive understanding of disease biology and drug efficacy throughout the development process is essential to ensure timely and cost-saving development of new tools. However, especially early in the translational pathway, detailed efficacy data on single compounds is sparse as many compounds are being tested in *in vitro* experiments. Later on data becomes more expensive to generate the further a compound is developed since *in vivo* experiments are more labour and resource intensive than *in vitro* experiments. Additionally, throughout the drug development process, many experimental systems with differing background in parasite and host set-up, and experimental designs are used (Fig. 1.2). Modeling and simulation studies facilitate the use of data from multiple sources in a common framework thereby connecting experiments and insights. They facilitate an effective and overarching use of data to assist the evaluation of new compounds.

Model-based approaches aimed to understand disease biology and drug efficacy throughout the development process include pharmacokinetic analyses describing drug-concentration over time as well as pharmacokinetic - pharmacodynamic (PKPD) analyses to describe the effect of treatment. Because of the complexity of the within-host malaria parasite life cycle, within-host parasite-growth models are increasingly used to explicitly capture the effect of drugs on parasite growth [Simpson et al., 2014].

In antimalarial drug development, parasite growth models assuming exponential growth have been widely used. In these models, parasite growth is described by an exponential function, defined by the initial parasite burden and growth rate, capturing parasite replication and death. Although they manage to capture the trends of parasite growth and treatment fairly well in the time-limited murine and human malaria infection experiments [McCarthy et al., 2016c; Krause et al., 2016; McCarthy et al., 2016a], they drastically simplify potential parasite-host dynamics which may be of great importance in patients. These aspects include host reactions to infection such as immune dynamics and parasite growth pattern adaptations with many possible consequences for translational efforts and future treatment of clinical cases.

Mechanistic models of within-host parasite growth and treatment formalise the underlying parasite growth patterns through equations explicitly following the life cycle of the parasite and parasiticidal effect of treatment. Parasite growth is commonly captured by tracking the development of the parasite throughout its life cycle in a system of ordinary differential equations (ODE), difference equations, delay differential equations, or partial differential equations. Their application is versatile as they allow the description of the parasite life cycle in varying levels of

detail and explore new hypothesis on parasite-, host-, and drug-dynamics. Through modelling, different scenarios and assumptions can be investigated in virtual experiments. This potentially saves cost and time by reducing experimental efforts through locating the dosing range of interest and designing experiments accordingly.

Early within-host parasite models were similar to those of viral infection and captured the dynamics of uninfected RBCs, their invasion by malaria parasites and subsequent release of new parasites into the blood-stream after the completion of the intra-erythrocytic life cycle [Anderson et al., 1989; Hetzel and Anderson, 1996; Austin et al., 1998]. Since then, within-host parasite growth models have developed in various directions according to their purpose, including investigations of mechanisms of the host (e.g. immunity), the parasite (e.g. maturation, life cycle length, sequestration), as well as the drug (e.g. stage specificity) [Khoury et al., 2018]. Most of these models were developed as a proof of concept to describe parasite dynamics via within-host models and to investigate parasite behaviour. However, the inclusion of drug efficacy in this models is mostly restricted to the exploration of treatment efficacy within one experimental system and for one antimalarial compound to develop dose adjustment strategies and investigate the impact of resistance [Simpson et al., 2014]. As of now, mechanistic modelling has not been used to systematically assess treatment efficacy across multiple compounds and *in vivo* infection experiments.

1.3.2 Individual-based models of malaria epidemiology, treatment, and prevention

Estimating the population impact of antimalarial interventions, requires the consideration of the whole malaria life cycle, including parasite replication in the mosquito and transmission dynamics between humans and mosquitoes (Fig. 1.1). Complex and setting dependent interactions between the force of transmission, seasonality in malaria transmission and the level of immunity influence disease prevalence, clinical incidence, severity [Wassmer et al., 2015] and even treatment success depending on the drug used [O'Flaherty et al., 2017].

The basis of modelling malaria transmission was laid by Ross in 1911 [Ross, 1911] and further refined by Macdonald [Macdonald, 1957] almost half a century later, to include additional epidemiological findings such as entomological theories, superinfection and reinfection [Smith et al., 2012]. Since then, several individual-based models, capturing the human host characteristics (e.g. immunity) as well as mosquito characteristics (e.g. species abundance, feeding behaviour) have been developed [Griffin et al., 2014; Eckhoff, 2011; Smith et al., 2006]. They were used to explore malaria epidemiology and investigate the impact of interventions such as the RTS,S/AS01 malaria vaccine on disease burden [Penny et al., 2016].

OpenMalaria is a stochastic individual-based simulator of malaria infection in human popula-

tions [Smith et al., 2006; Chitnis et al., 2008]. It captures mosquito abundance and transmission of malaria to humans as well as individual parasite densities in human individuals. Heterogeneity within a population is considered on multiple levels including host exposure, susceptibility, infectivity [Ross et al., 2006] and immune response [Maire et al., 2006], allowing the simulation of variability in human behaviour and response to treatment. Its wide range of application includes exploration of malaria epidemiology [Pemberton-Ross et al., 2015], informing policy on intervention packages to reach a certain health goal [Runge et al., 2020; Camponovo et al., 2019], investigating the cost-effectiveness of interventions [Penny et al., 2016] and guiding the specifications of new tools [Golumbeanu et al., 2022].

All in all, a wide spectrum of parasite, host and implementation dynamics influences the assessment of new pharmaceutical interventions against malaria, whether they are a new blood-stage drug or protective entity, as they move along the clinical development pathway from the first *in vitro* assays to application in humans and impact in populations after deployment. Accounting for parasite-host dynamics, by quantifying their influence on endpoints in antimalarial drug development, supports interpretation of antimalarial drug efficacy for translation. Similarly, drug efficacy in individuals can only be translated to population or public health impact by additionally accounting for malaria epidemiology. Conversely, understanding the public health impact of ranges of drug and tool efficacies allows one to understand criteria to select new tools for further development and ultimately implementation. Capturing these dynamics and quantifying their influence on endpoints to assess tools via mechanistic models of disease dynamics can facilitate a more comprehensive understanding of malaria disease and epidemiology and the potential impact of interventions.

1.4 Objectives and Outline

The aim of this thesis was the development and use of a series of models and data-model analysis tools to assess and thus gain a thorough and systematic understanding of efficacy and impact of pharmaceutical interventions against malaria along their development pathway. This thesis is based on the foundation of strong collaborations including academic and industry partners and inform our models by extensive preclinical and clinical data, and expert opinion. This work facilitates a comprehensive assessment of experimental and clinical testing results through exploring, understanding and quantifying factors that influence intervention efficacy and impact using mechanistic parasite growth and individual-based models of malaria disease. These insights support the acceleration of the development of human-based interventions for the treatment and prevention of malaria.

The aims will be achieved via several objectives:

- **Objective 1:** Understanding and assessing parasite-host dynamics in murine and human infection experiments for testing antimalarial efficacy during antimalarial drug development
- **Objective 2:** Comparison of experimental outcomes of murine and human malaria infection experiments to investigate the underlying dynamics influencing measured drug efficacy
- **Objective 3:** Assessment of experimental outcomes and their potential for translating drug efficacy between the clinical development stages to support the definition of inter-experimental efficacy indices
- **Objective 4:** Understanding determinants of protective efficacy for malaria chemoprevention with long acting injectables to guide the definition of TPPs

Chapter 2 investigates parasite host dynamics in the two murine *in vivo* infection experiments of *P. berghei*-NMRI and *P. falciparum*-SCID mouse infection. The mechanistic parasite-growth and treatment models developed and presented in this chapter are informed by experimental data from three laboratories and four antimalarial compounds. This chapter assesses the influence of interactions between host, parasite, drug, and experimental background in preclinical murine systems for evaluating existing and novel antimalarials. Additionally, the analysis of parasite recrudescence behaviour in the models compared to observed data raises awareness on the importance of investigating parasite-growth dynamics in unobservable parasite concentration ranges.

Chapter 3 builds on this foundation by developing and parameterising parasite-growth and treatment models for human volunteer infection studies and comparing them to the findings of Chapter 2 with regards to data structure and model structure. A subsequent simulation study demonstrates the varying influence of parasite-, host-, and treatment-dynamics on parasite clearance and therefore measured drug efficacy throughout the investigated *in vivo* antimalarial efficacy experiments. This chapter reveals the difficulties in an efficient translation of drug efficacy indices between the translational development stages.

Chapter 4 is a discussion piece that culminates the work of Chapter 2 and Chapter 3. It argues why thoughtful reconsideration and redefinition of commonly used drug efficacy indices during the antimalarial drug development process is needed. It highlights the shortcomings of currently used efficacy indices for benchmarking antimalarial candidates and proposes a new approach for translating drug efficacy between development stages that incorporates the mode of drug action.

Chapter 5 approaches the definition of target product profiles for new preventive anti-infective entities by using a simulation based approach that estimates tool impact throughout a large parameter space of protective efficacy decay. It quantifies the trade-offs between tool properties and deployment coverage, thereby providing arguments for future product or coverage optimisation depending on the use case and transmission setting.

The final chapter discusses the lessons learned throughout this thesis and gives recommendations on a path forward to incorporate mathematical modelling in decision making processes along the development pathway from pre-clinical experiments to later implementation. It addresses the challenges of an efficient translation of antimalarial efficacy indices along the development pathway and predicting population impact. Finally, it provides an outlook for future roles of modelling in the development of pharmaceutical interventions against malaria.

Chapter 2

Ensemble modelling highlights importance of understanding parasite-host behaviour in preclinical antimalarial drug development

Lydia Burgert[1,2], Matthias Rottmann[1,2], Sergio Wittlin[1,2], Nathalie Gobeau[3], Andreas Krause[4], Jasper Dingemanse[4], Jörg J. Möhrle[1,2,3], Melissa A. Penny[1,2]

[1]Swiss Tropical and Public Health Institute, Basel, Switzerland
[2]University of Basel, Basel, Switzerland
[3]Medicines for Malaria Venture, Geneva, Switzerland
[4]Idorsia Pharmaceuticals Ltd, Clinical Pharmacology, Allschwil, Switzerland

This manuscript has been published in Scientific Reports, March 2020 [Burgert et al., 2020] (https://doi.org/10.1038/s41598-020-61304-8).

The supplementary information can be found in Appendix A.

Abstract

Emerging drug resistance and high-attrition rates in early and late stage drug development necessitate accelerated development of antimalarial compounds. However, systematic and meaningful translation of drug efficacy and host-parasite dynamics between preclinical testing stages is missing. We developed an ensemble of mathematical within-host parasite growth and antimalarial action models, fitted to extensive data from four antimalarials with different modes of action, to assess host-parasite interactions in two preclinical drug testing systems of murine parasite *P. berghei* in mice, and human parasite *P. falciparum* in immune-deficient mice. We find properties of the host-parasite system, namely resource availability, parasite maturation and virulence, drive *P. berghei* dynamics and drug efficacy, whereas experimental constraints primarily influence *P. falciparum* infection and drug efficacy. Furthermore, uninvestigated parasite behaviour such as dormancy influences parasite recrudescence following non-curative treatment and requires further investigation. Taken together, host-parasite interactions should be considered for meaningful translation of pharmacodynamic properties between murine systems and for predicting human efficacious treatment.

2.1 Introduction

Scale-up of vector control and treatment strategies have led to large reductions in *Plasmodium falciparum* malaria prevalence and clinical cases over the last decade [WHO, 2018]. However, malaria remains a major cause of morbidity and mortality worldwide and recent successes are challenged by emerging resistance against several recommended first line treatments of artemisinin combination therapy [Tanner et al., 2015; WHO, 2017]. Although the current pipeline for new antimalarials is healthy; late stage drug attrition in antimalarial development and the need to develop combination therapies necessitates a continued search for new compounds [Wells et al., 2015]. Host-parasite dynamics and their influence on treatment results are important to consider throughout drug development to understand and interpret observed drug efficacy. Coupled with data, mechanistic modelling and simulation enables exploration of these host-parasite interactions along the preclinical development pathway. Such models facilitate translation from preclinical murine systems to clinical use, and thus potentially reduce time and costs to develop new antimalarial treatments.

In preclinical antimalarial development stages, murine systems of malaria infection are employed to evaluate drug pharmacokinetics (PK), drug effects (pharmacodynamics), efficacious exposure, and to inform human dose prediction. Pharmacodynamic (PD) measures of evaluation include parasite reduction compared to a control group, index numbers of drug efficacy such as concentrations inhibiting growth or resulting in a certain level of parasiticidal activity, and parasite recrudescence behaviour following non-curative treatment [Jiménez-Díaz et al., 2014a; Burrows et al., 2017; Flannery et al., 2013].

Two murine systems are commonly employed to investigate in vivo blood-stage efficacy of orally administered antimalarials; infection of normal mice with the *P. berghei ANKA* strain [Jiménez-Díaz et al., 2013] and infection of immunodeficient NOD$^{scidIL-2R'c-/-}$ (SCID) mice with *P. falciparum* [McCarthy et al., 2016a; Jiménez-Díaz et al., 2009; Angulo-Barturen et al., 2008]. The murine malaria parasite *P. berghei* causes severe, ultimately deadly malaria in mice while exhibiting similar parasite morphology and developmental characteristics observed in human malaria infection [Jiménez-Díaz et al., 2014a; Langhorne et al., 2011]. SCID mice engrafted with human erythrocytes (RBCs) are able to support infection with *P. falciparum*, providing the opportunity to investigate the efficacy of compounds against the human parasite in vivo [Angulo-Barturen et al., 2008; Jimenez-Diaz et al., 2009]. The main difference between the two parasite species is the length of the intra-erythrocytic life cycle being approximately 24h for *P. berghei* and approximately 48h for *P. falciparum* [Jiménez-Díaz et al., 2014a]. While the *P. berghei* murine system is used to test crude efficacy of blood-stage antimalarial drugs in shorter experiments, murine infection with *P. falciparum* is employed in longer experiments investigating the course of infection and parasite recrudescence behaviour. Recently the SCID mouse system has been utilised to facilitate translation of results between mice and humans

[McCarthy et al., 2016a], including testing of drug combinations, and to avoid issues where potentially active compounds against *P. falciparum* are not active against *P. berghei* due to enzymatic differences between the parasites [Phillips et al., 2015].

Mechanistic mathematical parasite growth models inform the drug development process by combining information on within-host behaviour of the parasite, the host itself, and the treatment [Simpson et al., 2014; Slater et al., 2017]. Several within-host models that include descriptions of the asexual blood-stage parasite life cycle and host properties have been developed for preclinical [Hetzel and Anderson, 1996; Patel et al., 2014; Patel et al., 2013; Austin et al., 1998] and clinical development stages [Hietala et al., 2010; Simpson et al., 2014; Svensson et al., 2002; Molineaux et al., 2001]. However, modelling is not used to systematically compare potential consequences of host-parasite interactions in different host-parasite systems and to investigate their impact on drug treatment outcomes and decisions during antimalarial development. Comparing performance of models capturing different aspects of biology can indicate importance of those aspects, or point to knowledge gaps.

We report an ensemble of mechanistic within-host parasite growth and antimalarial action models that are combined into a modelling workflow that handles data management, model development, parameterisation, and simulation for the analysis of antimalarial drugs in murine experimental systems. The models are based on previously described parasite characteristics such as erythropoiesis, parasite growth, erythrocyte and parasite clearance, and changes in parasite characteristics over the course of infection [Khoury et al., 2018]. Model selection is based on their potential relevance for assessing drug efficacy in preclinical antimalarial development. Our ensemble therefore highlights the diversity of potential parasite-host dynamics and the consequential influence on experimental insights and drug evaluation in the space of limited data resolution of the parasite life cycle. Parameterisation was conducted using multiple control and treatment experiments of four antimalarials with different modes of action. We evaluated the models based on their ability to describe laboratory data and to account for the biological and experimental background to understand parasite dynamics relevant for treatment effects. The workflow enables the analysis of *in vivo* drug efficacy against *P. berghei* and *P. falciparum* and thus facilitates comparison of results between laboratories. To the best of our knowledge, this is the first study to systematically investigate host-parasite interactions, antimalarial action, and drug effects across murine experimental systems, laboratories, and drugs from different drug classes. This analysis provides insights into antimalarial efficacy predictions, highlights processes of host-parasite interaction relevant to malaria in humans and informs on the advantages and disadvantages of each preclinical system.

2.2 Results

Data

The following drugs, for which data on both murine systems was available, were used for analysis: ACT-45184024 [Le Bihan et al., 2016], chloroquine (CQ) [Phillips et al., 2017], MMV39004827 [Paquet et al., 2017], and OZ439 (INN: artefenomel) [Dong et al., 2017; Charman et al., 2011] (Appendix A, Supplementary Table S2.1). Data from 43 experiments containing information about *P. berghei* in Naval Medical Research Institute (NMRI) mice and 32 experiments containing information about *P. falciparum* in SCID mice before and after treatment were analysed. Each experiment involved two to five control mice and two to ten mice per dose. An overview of the data used can be found in the Appendix A Supplementary Table S2.2. Parasite density data in the form of percentage of infected RBCs was used for model parameterisation. In SCID mice *models f* and *g*, hematocrit (percentage of human RBCs) was used as additional information.

Models of parasite growth

We developed five mathematical models of parasite growth for *P. berghei* (*models a* to *e*) and four models for *P. falciparum* in SCID mice (*models f* to *i*). Each model captures different levels of details and assumptions concerning RBC dynamics of the host (NMRI or SCID mice), the influence of the parasite on RBC dynamics, and parasite growth characteristics (Fig. 2.1).

A previous within-host model capturing RBC and parasite dynamics [Hetzel and Anderson, 1996] described by a set of ordinary differential equations (ODEs) was used as our base model (*model a*) for our *P. berghei* and *P. falciparum* growth models. This model captures parasite growth as well as RBC dynamics. It assumes constant production ν [cells/h] and decay μ [1/h] of healthy RBCs X [Hetzel and Anderson, 1996], that are infected by merozoites M dependent on the infectivity parameter β [cells/mL h]. Infected RBCs Y burst on average after one parasite life cycle $1/\ \alpha$ h later and subsequently release r new merozoites that die with rate δ [1/h]. In contrast to [Hetzel and Anderson, 1996], for all *models a* to *h*, the intra-erythrocytic parasite stage was split into n age compartments ($n = 12$, based on stability analysis of the base model structure (Appendix A, Supplementary Fig. S2.5)) with a transition rate of $\alpha_n = \alpha\ n$ [1/h] between compartments. Although *models b* to *h* can be considered as expansion of *model a (base)*, we deliberately illustrate them separately to compare model conclusions regarding influences of parasite-host dynamics on drug efficacy estimates. Therefore, we decided against nested model building.

In addition to our base model, we accounted for other parasite host interactions for *P. berghei*, whereby *model b (bystander)* included a bystander-death rate γ [1/h] of uninfected RBCs

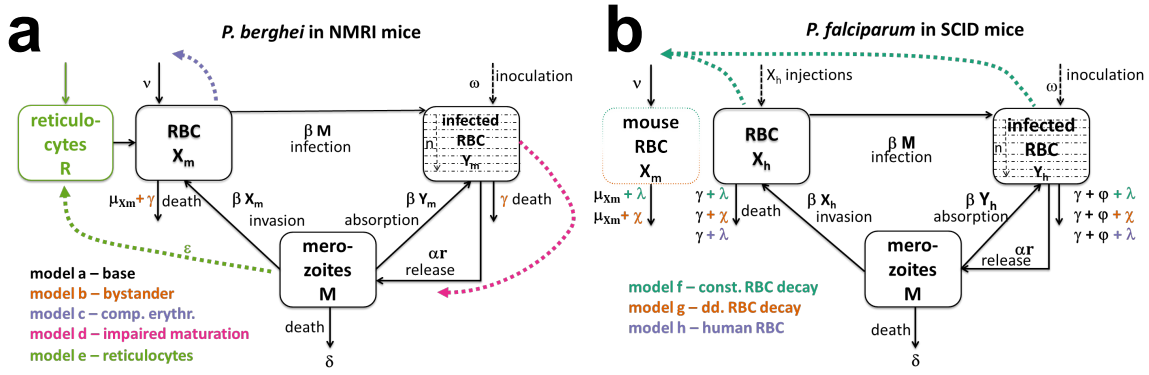

c

	P. berghei in NMRI mice					P. falciparum in SCID-mice			
	a base	b bystander	c comp. erythr.	d impaired maturation	e reticulo-cytes	f const. RBC decay	g dd. RBC decay	h human RBC	i expo-nential
Mouse RBC dynamics	✓	✓	✓	✓	✓	✓	✓		
Human RBC dynamics						✓	✓	✓	
Reticulocyte dynamics					✓				
Bystander death of RBCs		✓				✓	✓	✓	
Compensatory erythropoiesis			✓			✓			
Target cell dependent parasite growth	✓	✓	✓	✓	✓	✓	✓	✓	
Density dependent RBC decay								✓	
Maximal parasitemia P_{max} [%]	95	79	94	97	85	30	39	30	100
Time of P_{max} [h]	115	111	114	120	120	206	206	236	252
Anemia at P_{max} [%]	28	10	31	55	22	33	40	-	-

Figure 2.1: Schematic representations of the mechanistic within-host parasite growth models for *P. berghei* (a) and *P. falciparum* (b), with summary model details (c). The base model by [Hetzel and Anderson, 1996] is represented in black with model modifications added in color, for all models erythrocytic parasite stage was split into n age compartments ($n = 12$). **(a)** *Model a* to *e* for *P. berghei* mainly capture processes dictated by the host-parasite system such as reactions of the host to increasing infection in *model b (bystander)* and *model c (comp. erythr.)*, changes in parasite dynamics over the course of infection *model d (impaired maturation)*, and host cell preferences of the parasite *model e (reticulocyte)*. **(b)** In turn, *model f* to *h* for *P. falciparum* dynamics are primarily influenced by the experimental set-up of continued human RBC injections. Whereas *model f (const. RBC decay)* and *g (dd. RBC decay)* additionally explicitly model mouse RBCs, *model h (human RBC)* only captures human RBC populations. RBC or parasite transitions are represented with solid lines and influencing processes with colored dashed lines. **(c)** Selected index numbers characterising the growth of parasites in the respective mechanistic mouse models for the experiment shown in Fig. 2.3. Anemia is defined as the percentage of RBCs compared to values prior to infection.

caused by the reaction of the innate immune system to parasite growth [Cromer et al., 2006]. Compensatory erythropoiesis, caused by anemia through RBC destruction, was considered in *model c (comp. erythr.)* [Cromer et al., 2006; Lamikanra et al., 2007]. Potential changes to parasite properties was examined in *model d (impaired maturation)* assuming an increase in

parasite densities causes lengthening of the intra-erythrocytic parasite life cycle from 24 to 37h [Khoury et al., 2017b]. *Model e (reticulocytes)* allowed for an age preference of the parasite by including immature RBC (reticulocyte) dynamics [Cromer et al., 2006].

In order to adequately represent RBC and parasite dynamics as a consequence of the continued RBC injections, we extended and adapted *model a (base)* for *P. falciparum* growth in SCID mice by including human RBC dynamics in *models f* to *h*. To capture base decay rates of mouse and human RBCs, we assumed a constant decay rate λ [1/h] in *model f (const. RBC decay)* and *model h (human RBC)* as well as total RBC density-dependent (dd.) decay χ [1/h] in *model g (dd. RBC decay)* as a mouse reaction to continued RBC injections [Angulo-Barturen et al., 2008]. Additionally, we implemented parasite density-dependent clearance of RBCs by phagocytes γ [1/h] to account for infection-induced dynamics of RBC clearance and splenic/liver clearance φ [1/h] in all *models f* to *h*. While *model f* and *g* included human and mouse RBC dynamics, *model h (human RBC)* assumed mouse RBC dynamics to be negligible and only captured human RBC dynamics. Our last model, empirical *model i (exponential)*, assumed exponential parasite growth without explicit host-parasite dynamics and no resource depletion.

For all mechanistic *models a* to *h*, we assumed that parasite age was uniformly distributed at time of inoculation and asynchronous parasite growth based on previous descriptions of *P. berghei ANKA* infections desynchronizing after inoculation [Deharo et al., 1996]. Data resolution was too low to inform models of synchronous parasite growth in SCID mice. Since the *P. berghei ANKA* strain in NMRI mice is very aggressive (fatal within six days) and there is no fully functioning immune system in SCID mice, the dynamics of the adaptive immune system were not considered in either mice system.

The mechanistic *models a* to *h* used the time of parasite inoculation as a starting point for modeling whereas time of drug administration (72h post-infection) was chosen as the start of the exponential growth phase for *model i (exponential)* due to data availability. Data was pooled per experiment for all parameter estimations with an experiment defined as a group of mice having the same control group. No individual parameter estimation per mouse was conducted. An overview of our modeling workflow, model ODEs and specifications of parameters estimated or fixed to literature and experimental values are given in the Supplement (Appendix A).

Model fits to data

Models a to *h* were able to account for changes in experimental setting by using experimental information on parasite inoculation time and amount, and RBC injections, as input to the models. Additionally, for *model f* and *g*, the initial percentage of human RBCs H_0 was estimated per experiment, while constrained to value ranges extracted from laboratory protocols.

The differences in experiments are likely a consequence of variation in laboratory procedures, such as thawing of parasites, age and infection status of the donor mouse, altered parasite virulence due to serial passage of the parasite, or inoculum size. We therefore assessed the ability of either the infectivity parameter β (which effectively represents differences in parasite fitness and virulence) or the viability of the parasite inoculum ω (representing differences in thawing protocols) to capture differences between experiments.

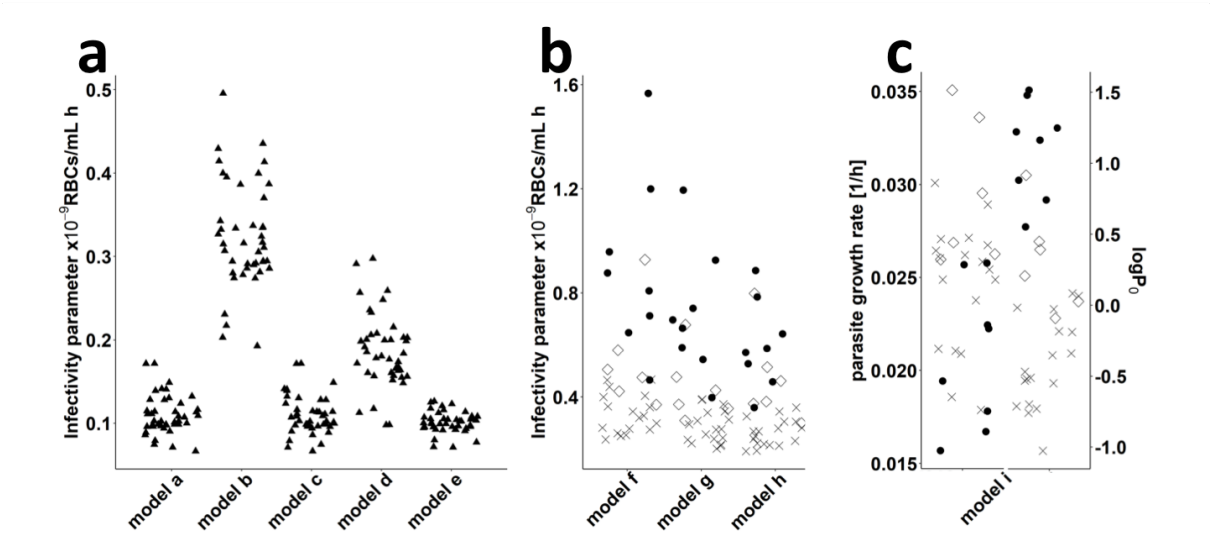

Figure 2.2: Estimated values of the infectivity parameter β by model for both murine experimental systems. Each symbol represents the value estimated for one experiment. **(a)** Values estimated for murine *P. berghei* infection. *Model a (base)*, *c (comp. erythr.)* and *e (reticulocyte)* show similar results whereas higher values were estimated for *model b (bystander)* and *d (impaired maturation)* **(b)** Estimated β-values for infection of humanized mice with *P. falciparum* using the mechanistic *models f (const. RBC decay)*, *g(dd. RBC decay)*, and *h (human RBC)*. **(c)** Parasite growth rate p_{gr} and parasitemia at start of the exponential growth phase P_0 (72h post-infection) estimated for *model i (exponential)*. The laboratories are denoted by different symbols (not identified here).

The infectivity parameter β was able to account for observed differences in force of parasite growth between experiments and laboratories. By comparing β values, we found consistent differences between each laboratory and model (Fig. 2.2). Our estimates of β for *P. berghei* and *P. falciparum* range from 6.7×10^{-11} to 5.0×10^{-10} and 1.2×10^{-10} to 1.6×10^{-9} cells/mL/h, respectively. For *model i (exponential)* an adjustment of base parasitemia P_0 at treatment start and parasite growth rate p_{gr} was necessary to capture inter-experimental differences. Estimates of parasite growth rates for *model i* range between 0.016 and 0.035 [1/h] (Fig. 2.2).

Even though the mechanistic parasite growth *models a* to *e* for *P. berghei* and *models*

f to *h* for *P. falciparum* showed similar parasite growth patterns in their respective murine hosts, several distinct characteristics affecting parasite growth and treatment patterns became apparent in our analysis.

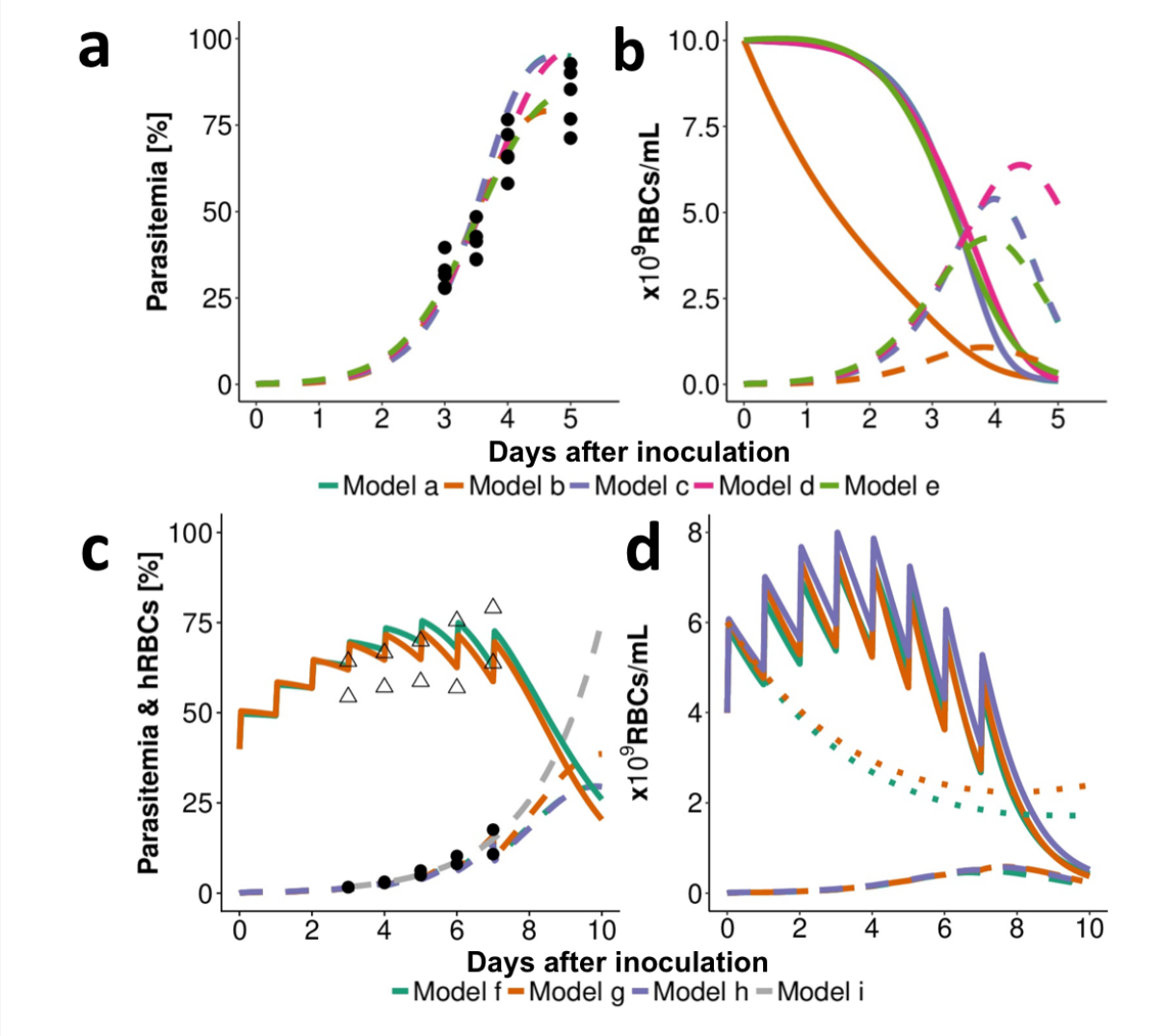

Figure 2.3: Representative fit of the within-host models to data. (a) Data (black points) and model predictions (dashed lines) of infection with *P. berghei* with an inoculum of 2×10^7 infected RBCs *(i.v.)* show a steep increase in parasitemia three days after inoculation. **(b)** Model output for unobserved total numbers of RBCs show an increase in infected RBCs (dashed line) with a simultaneous decrease in uninfected RBCs (solid line) resulting in anemia. However, the total number of human and murine RBC populations differs between model predictions (compare *model b (bystander)*), given that the estimated percentage of infected RBCs is compared to observed. Further differences in models become apparent comparing predicted time of, and total parasite numbers at, peak parasitemia P_{max} (see Fig. 2.1c). **(c)** Infection of SCID mice with *P. falciparum* through an inoculum of 3.5×10^7 infected RBCs (*i.v.*). Human RBCs (Δ) are injected daily until day seven post-infection, increasing total human RBC counts (solid line). **(d)** As uninfected RBCs (solid line) increase the predicted number of mouse RBCs (dotted line) decrease due to random clearance of excess RBCs. After RBC injections are ceased, the model predicts a steep decline in human RBCs. Data (points) and *models f* to *h* (dashed line) show lower values of predicted peak parasitemia compared to *model i*.

As expected, a steep decline of uninfected RBCs was predicted with increasing parasite load of *P. berghei* (Fig. 2.3). This resulted in anemia, defined as the percentage of RBCs compared to values prior to infection, of up to 10% (Fig. 2.1). Dependent on model choice, different time courses for total (un)infected parasite populations were observed (Fig. 2.1c and 2.3b) resulting in a range of maximal parasitemia values between 79% and 97%. Continued human RBC injections prevent the occurrence of anemia during *P. falciparum* infection. However, if human RBC injections cease *models f* to *h* predicted a steep decrease in human RBCs, also observed in laboratory experiments (Appendix A, Supplementary Fig. S2.4), emphasising the importance of capturing experimental RBC replenishment and clearance mechanisms. Compared with base clearance of mouse RBCs (0.001 [1/h], Appendix A, Supplementary Table S2.4) we estimated base clearance of human RBCs to be increased by a factor of 10 with *model f (const. RBC decay)* and *model h (human RBC)* estimating λ of 0.01 and 0.08 [1/h] and *model g (dd. RBC decay)* estimating a maximum base clearance χmax of 0.018 and $k_{\chi,50}$ of 1.05×10^{10} RBCs/mL (Appendix A, Supplementary Table S2.7). Total RBC counts tracked by *model f (const. RBC decay)* and *model g (dd. RBC decay)* reached a maximum value of 1.2×10^{10} RBCs/mL (*model h*; mouse RBCs not considered). The base death rate of RBCs λ was estimated to be smaller than the maximum parasite density-dependent death rate λmax for all models.

Drug action models and predicted translation between murine systems

Following our workflow detailed in Fig. S2.1, the parasite growth models were combined with compartmental PK models to investigate drug efficacy. The change in parasite death rate α was chosen as the pharmacological action for PD models (Appendix A, Supplementary Table S2.6). Parameters of parasite growth and PK models were fixed to previously estimated values (Appendix A, Supplementary Tables S2.7 and S2.8) for calibration of EC_{50}, E_{max} and additional parameters describing drug action models (Appendix A, Supplementary Table S2.6) against treatment data. We compared EC_{50}, E_{max}, and the structural PD models across murine systems and parasite growth models to assess influences of parasite-, host- and drug-interactions on drug efficacy analysis (Fig. 2.4, parameter values in Appendix A, Supplementary Table S2.9) and to investigate potential translation between murine systems.

A typical fit of parasite growth and drug action models to treatment data of SCID mice is shown in Fig. 2.5. As expected, all models predicted decreasing parasite counts following non-curative treatment until an inflection point after which parasite counts increased again. This inflection point is generally below the lower limit of quantification (LLOQ) (microscopic detection limit: 0.01% parasitemia) for effective treatment (Fig. 2.5). Structural drug action models were compared for each combination of parasite growth model, murine system and drug (lowest AIC, Appendix A, Supplementary Fig. S2.2). In *P. berghei* infection, at least three out of five and in *P. falciparum* infection at least three out of four parasite growth models match with respect to the chosen structural PD model (Fig. 2.4). All PD models either implement a

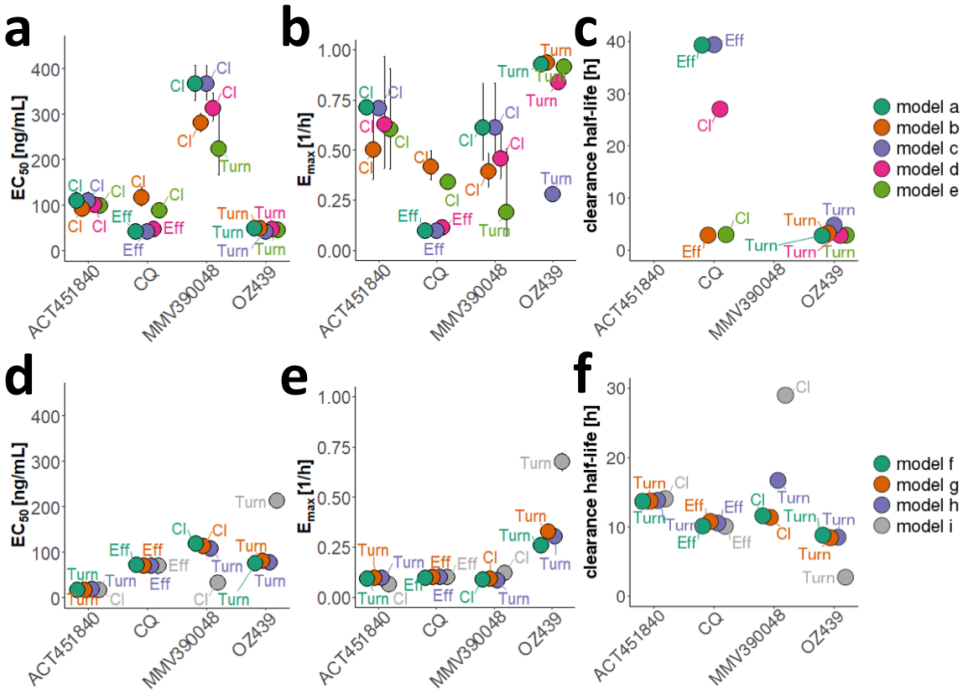

Figure 2.4: Comparison of drug efficacy estimates found for *P. berghei* in normal mice (a-c) and *P. falciparum* in SCID mice (d-f). EC_{50} [ng/mL], E_{max} [1/h] and the clearance half-life [h] are illustrated for each drug and parasite growth model. The drug action model showing the best fit to data was chosen based on ΔOFV (AIC), visual assessment of model fit and biological plausibility for each parasite growth model (with Turnover-model (Turn), drug action through an effect compartment (Eff) and delayed clearance of dead parasites (Cl)). See Appendix A, Supplementary Table S2.9 for parameter values.

delayed drug effect through an effect compartment or turnover model, or delayed clearance of dead parasites.

Although all drugs were active in both mouse systems, no apparent linear relationship was found when comparing estimated EC_{50}, E_{max}, and parasite clearance half-life values of the four drugs investigated between both murine experimental systems given chosen model of drug action and associated parameters (Appendix A, Supplementary Table S2.9). Parasite clearance half-life was generally lower for treatment of *P. berghei*.

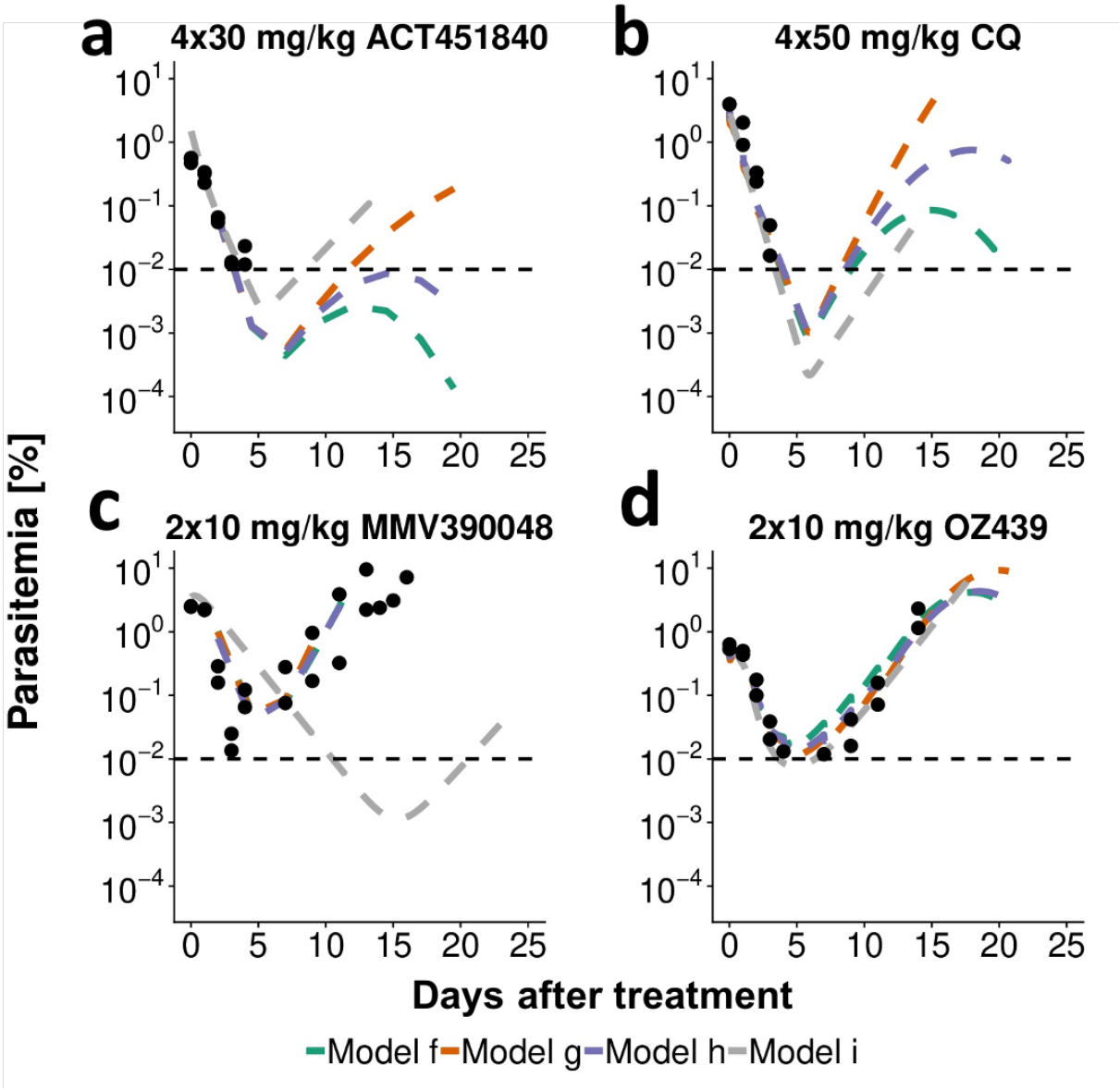

Figure 2.5: Representative fits of drug action models in SCID mice infected with *P. falciparum* at day 0 with an inoculum of 2×10^7 - 3.5×10^7 infected RBCs. The models were fitted to data of all administered doses with model predictions for the respective doses portrayed here. Treatment commenced three days after inoculation in dosing intervals of 24 hours. Mice were treated with 4×30 mg/kg ACT-451840, 4×50 mg/kg CQ, 2×10 mg/kg MMV390048 or 2×10 mg/kg OZ439. The cessation of human RBC injections in ACT-451840 and CQ experiments seven days after treatment leads to a decay of human RBCs and therefore also parasitemia 10-15 days after treatment (a,b). The horizontal dashed line represents the lower limit of quantification with 0.01% parasitemia. N = 2 mice for all doses shown.

Recrudescence

For the long-lasting recrudescence experiments conducted with MMV390048 and OZ439 in SCID mice, we were only able to capture recrudescence (occurring more than eight days after last measured parasitemia above the lower limit of detection) with the exponential growth *model i*. Although we capture recrudescence within eight days of last measurement, we were unable to describe recrudescence after this time, with the mechanistic parasite growth *models f* to h (Appendix A, Supplementary Fig. S2.3). Minimum parasite numbers predicted by the mechanistic growth models remain high, e.g., after dosing with 1 x 50 mg/kg OZ439, total parasite numbers of 3.3×10^6 parasites ($\approx 0.02\%$ parasitemia) are predicted by *model f (const. RBC decay)*. In contrast, *model i (exponential)* predicts a minimum parasitemia of 0.0003%. This indicates that additional parasite phenomena such as altered parasite maturation, dormancy, or stochastic extinction might be at play that have not been considered in the mechanistic models (Fig. 2.6: extension sources of variance and uncertainty of the parasite treatment curve described in [White, 2011] applicable to murine and human infections for antimalarial investigations). The inclusion of these additional parasite characteristics is also potentially influencing minimum inhibitory concentration (MIC) definition and estimates (Fig. 2.6a).

2.3 Discussion

By simultaneously capturing parasite growth and treatment, our mechanistic models provided insight into the influence of interactions between host, parasite, drug, and experimental background in preclinical murine systems for assessing existing and novel antimalarials. Mechanistic modeling and simulation enabled exploration of these host-parasite interactions along the preclinical development pathway to understand their potential effect on compound selection in preclinical models.

In general, we found that host-parasite dynamics and experimental set-up (e.g. in terms human RBC injections) had an influence on estimated parasite growth measured as parasite invasion rates, clearance and maturation rates, and the availability and replenishment of resources. Explicit inclusion of these mechanisms in our parasite growth models and subsequent analysis of translation of PD parameters and recrudescence identified the importance of considering dynamics of the murine system during analysis. The importance of host-parasite interactions for drug effect imply that careful consideration is needed to define and use appropriate mechanistic parasite growth models for translating, not only between murine systems, but also to humans and to predict human-equivalent dose.

We decided against nested parasite growth model building but rather we separately portrayed model predictions and fits and thus compared conclusions drawn in a non-weighted ensemble

approach, acknowledging the different assumptions in each model. Model averaging was forgone to illustrate uncertainty concerning underlying parasite-host interactions over time and their influence on drug efficacy estimates. This was also important in order to highlight if further mechanistic insights are needed due to limited data per mouse and experiment.

To parameterize our models to all the available experimental data we needed to consider inter-experimental differences in the infectivity parameter β. Our estimates of β for *P. berghei* and *P. falciparum* are similar to those described in literature [McCarthy et al., 2016a; Austin et al., 1998]. The variations in β, which effectively represent differences in parasite fitness and virulence, are likely a consequence of differences in laboratory procedures, such as thawing of parasites, age and infection status of the donor mouse, altered parasite virulence due to serial passage of the parasites and inoculum sizes.

We found properties of the host-parasite system to be the primary influence on undisturbed parasite growth of *P. berghei* in NMRI mice. Resource availability, in the form of RBCs, drives untreated parasite growth with mice exhibiting up to 90% peak parasitemia and 10% anemia five days post-infection. Similar anemia values ranging between 10% and 30% have been previously published [Cromer et al., 2006; Villeval et al., 1990]. As a consequence of RBC availability, *models a* to *e* predicted a decrease in total parasite densities after reaching peak parasite concentrations (Fig. 2.3b). Our analysis estimated that the preference of *P. berghei* for reticulocytes was less pronounced than found previously [Cromer et al., 2006]. This discrepancy could be due to the previous study using a mouse strain that tolerated longer lasting infections, during which activation of erythropoiesis led to increased reticulocyte numbers. This increase in infection length could facilitate age preference of parasites to be measurable. The influence of parasite-host interaction, in form of impaired parasite maturation, was found to be most prominent in advanced infections resulting in later and higher peak parasitemia. These time dependent parasite characteristics should therefore be considered in experimental design considerations.

In contrast, in the SCID mouse system, parasite growth is primarily influenced by the artificial replacement of erythropoiesis with injections of mature human RBCs containing negligible numbers of reticulocytes. Therefore, the analysis of erythropoietic processes and age preferences of the parasite are rendered irrelevant. The impairment of parasite maturation has previously been attributed to host immune mechanisms regulating parasite growth during early stages of infection [Khoury et al., 2017b]. For this reason, changes in parasite maturation were likely not observed in immunodeficient rag1$^{-/-}$-mice [Khoury et al., 2017b] and were therefore not considered in this analysis. To date the occurrence of this process in human and thus potential clinical implications remains unclear. To gain further insights into parasite-host dynamics influencing existing experiments, we suggest collecting additional data per experiment on total (un)infected RBC concentrations, and in SCID experiments on total mouse and human RBC concentrations. Resolution of present parasite age-stages could provide insights into parasite

maturation dynamics. Additional *in vitro* experiments investigating recrudescence patterns after treatment with different drugs could inform the analysis of potential parasite dynamics below the LLOQ [Nunes et al., 2009]. Influences of immunity on the efficacy of different drugs and recrudescence patterns could be assessed by utilizing chronic infection of mice [Nakazawa et al., 2002]. The differences elucidated between parasite growth patterns in the respective systems of murine malaria infection were also reflected in the analysis of antimalarial action. A comparison of drug efficacy parameters between host-parasite systems did not allow a direct translation between systems. The variability of the drug action parameters EC_{50} and E_{max} between murine systems could be caused by previously discussed differences in host-parasite interactions such as erythropoiesis, the ability to cause chronic infections, the development of anemia and differing parasite characteristics. Additionally, differences between parasites species on a molecular level are likely influencing anti-parasitic activities of compounds that are specific inhibitors of enzyme activity such as ACT-451840 and MMV390048 (Appendix A, Supplementary Table S2.1). We conclude that while the absence of erythropoiesis, anemia, and a functioning immune system described in SCID mice allows for an unperturbed investigation of the sole drug effect, direct translatability of drug action parameters to humans could be complicated should these processes be of importance in human infection.

However, in SCID mice underlying clearance of (un)infected RBCs could influence the analysis of drug efficacy data. Our mechanistic SCID models break down overall decrease in parasitemia into clearance mechanisms induced by experimental set-up, murine experimental system, and drug action. We estimated similar value ranges in terms of clearance attributable to host-reactions to infection γ_{max} (0.055-0.44) (Appendix A, Supplementary Table S2.7) and drug action E_{max} (0.065–0.33) (Appendix A, Supplementary Table S2.9) across all drugs and drug action models. Commonly used measures of drug efficacy such as parasite clearance half-life [Flegg et al., 2011], summarize all parasite clearance in a single index number [White, 1997; Marquart et al., 2015] when in fact parasite clearance is the net effect of multiple parasite clearance mechanisms [Khoury et al., 2018]. Therefore, the inclusion of delayed removal of parasites affected by the drug into mechanistic parasite growth models could prevent potential misinterpretation of parasite clearance half-life estimates. Analysis of more drugs and routine measurement of (stage-specific) parasite clearance rates would give valuable insight into clearance mechanisms and prevent misinterpretation of parasite clearance after treatment.

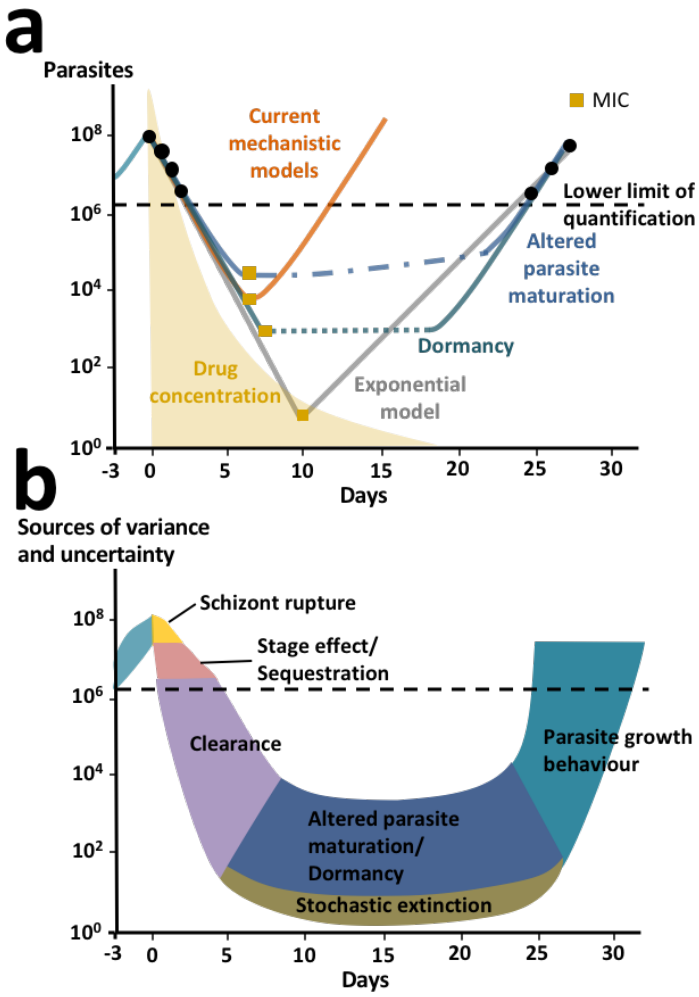

Figure 2.6: Schematics of *P. falciparum* parasite dynamics in SCID mice after treatment and potential factors explaining variance and uncertainty. (a) The mechanistic models (orange) presented in this paper assume parasite growth characteristics remain constant throughout treatment and are therefore not capturing late recrudescence. This is in contrast to the exponential model (grey) that compensates for late recrudescence by shifting the curve to low parasite and drug concentrations. Alternative to our mechanistic models, we propose some hypothetical parasite recrudescence curves (blue and green), that include additional phenomena such as altered parasite maturation and parasite dormancy offering possible explanations for late recrudescence. We cannot capture these mechanisms with models without additional data. MIC estimates important for experimental interpretation and translation to humans are shown by yellow square points and are likely to be very different given assumptions about parasite growth behaviour after treatment. **(b)** We hypothesise and extended the sources of variance and uncertainty of the parasite treatment curve described in [White, 2011] to schematically illustrate parasite phenomena during growth, treatment and recrudescence for antimalarial experiments (murine and possibly human). These extended phenomena include altered parasite maturation, dormancy, and stochastic extinction occurring below the lower limit of quantification hindering estimation.

We observed interactions between parasite and host system that resulted in parasite growth characteristics changing over time and with subsequent influence on observed drug efficacy. Thus, it is important to discuss the mechanisms of parasite recrudescence below the lower limit of quantification. Simple linear regression analysis showed a statistically significant prediction ($p = 0.0442$ after MMV390048 and $p = 6.8 \times 10^{-5}$ after OZ439 treatment) of recrudescence times using the slope of the parasite treatment curve, number of drug doses, and dose (Appendix A, Supplementary Tables S2.11 and S2.12). Our results indicate positive correlation between high drug exposure due to increasing doses and regimens and the time to recrudescence. The low proportion of explained variance (R^2) for MMV390048 may be caused by the data capturing both, alive and dead parasites due to the clearance model best describing drug action of MMV390048 in SCID mice (Appendix A, Supplementary Table S2.9). However, the mechanistic parasite growth models in SCID mice were not able to capture the range of incidence and times of recrudescence observed between and within experiments (Appendix A, Supplementary Table S2.10 and Fig. S2.3). Although parasite recrudescence generally occurred at later times with increasing doses in our models, time of recrudescence could not be mechanistically explained. Apart from variability in drug efficacy parameters such as EC_{50} and E_{max}, additional pharmacological or parasitic processes such as parasite dormancy [Hoshen et al., 2000; Thapar et al., 2005], impaired parasite maturation [Khoury et al., 2017a; Veiga et al., 2010], altered parasite clearance [Khoury et al., 2017a], and additional stochastic effects may be delaying recrudescence (Fig. 2.6). Previous studies indicated links between parasite virulence, parasite numbers at time of treatment, and treatment duration [Nakazawa et al., 2002; Schneider et al., 2012] as influencing frequency of recrudescence for different *Plasmodium* parasites. Overall, these findings suggest, that the current mechanistic models do not provide additional structural insight to late recrudescence (Fig. 2.6).

In comparison to mechanistic growth models, the exponential growth *model i* was not helpful in providing insights into mechanistic parasitic behaviour and drug action. Parasite growth parameter estimates for *model i (exponential)* are based on the exponential growth phase three days after inoculation (as no data is collected before), whereas the mechanistic models start at time of inoculation (using inoculum size) and therefore account for potential growth lag phases. Consequentially, the exponential model predicts a biologically implausible instant switch from drug suppressed growth to exponential growth after non-curative treatment. We found the direct influence of drug action on the estimated parasite growth parameter p_{gr}, which combines parasite growth and death, facilitates shifts of predicted recrudescence curves to fit recrudescence data (Fig. 2.6a). These lacks of mechanistic insights in the exponential model warrant caution in drawing conclusions from drug efficacy indices (e.g. MIC) derived directly from this model to translate to human clinical phases [McCarthy et al., 2016a]. In contrast, hypothetical growth curves including parasite dormancy and altered parasite maturation depicted in Fig. 2.6 allude to the fact that changes in growth behaviour are not captured in current models and that the MIC might not be a single concentration but rather a concentration range (dotted

lines). Investigations into clinical relevance of recrudescence mechanisms in humans might be worthwhile to forecast treatment efficacy in the field [Plucinski et al., 2015; Slater et al., 2005; White, 2002]. To date, neither mechanistic parasite growth models nor exponential growth models have been validated for human dose prediction. Further understanding of mechanistic background is necessary to understand their respective suitability and appropriate use cases for model simplification.

Despite our insights, our study comes with several limitations. Data availability and richness varied greatly between murine systems, experiments and antimalarials (Appendix A, Supplementary Table S2.2). Data per experiment was pooled as parasite density and drug concentration measurements and thus also parameter estimation could not be carried out per individual mouse due to constraints of the parasite-host system and experimental set-up (e.g. sampling frequency). Although we chose our model assumptions carefully based on current literature they are still simplifications of a complex system and do not fully capture the complexity of murine malaria infection, (e.g. synchronised growth of *P. falciparum* and antimalarial stage specificity).

To date, translation of drug efficacy parameters between experimental murine systems and humans is undertaken using PD parameters/indices such as parasite clearance estimator (PCE) or MIC. However, we demonstrated the influence of different mechanistic backgrounds of mouse systems and parasite clearance on drug efficacy estimates. Our analysis of parasite recrudescence behaviour in the models compared to observed data indicates additional unknown mechanisms influence parasite recrudescence timing and thus highlights potential pitfalls in using MIC for human-equivalent dose prediction. Further research on the importance of these mechanistic insights in humans and translation of PD indices between preclinical and clinical phases using historical preclinical and clinical data of existing antimalarials could accelerate the drug development process. Given the current standard of translation and dosing recommendation we conclude that, for now, further analysis of modelling results from both, preclinical experimental systems offers great potential to support optimal treatment of humans.

2.4 Material and Methods

Data

In vivo efficacy studies of *P. berghei ANKA*-infection were conducted at Swiss TPH as previously described [Le Bihan et al., 2016; Charman et al., 2011]. Briefly, NMRI mice were infected with 2×10^7 parasitized RBCs (*i.v.*), and treatment consisted of one to four doses (*p.o.*) commencing 4–72 h after infection. Parasitemia was measured 72 or 96 h after infection. Study outcomes are reduction in parasites compared to a control group, mouse survival, and mouse cure. In untreated mice, death usually occurs 6 days after infection.

In vivo efficacy experiments against *P. falciparum* Pf3D7$^{0087/N9}$ in NOD$^{scidIL-2R'c-/-}$ mice were conducted at GSK (GlaxoSmithKline), Swiss TPH and TAD (The Art of Discovery). Mice were engrafted with human RBCs by continued injections of human blood suspension, and infected with *P. falciparum* after a hematocrit of 40% - 75% was established. Treatment commenced 72 h post-infection. Original experimental outcomes were reduction in parasitemia compared to a control group, mouse cure, and parasite-recrudescence behaviour. Human blood injections were repeated every one to three days to maintain sufficient red blood cell levels and prevent occurrence of anemia throughout each SCID mouse experiment. For both murine systems, cure was defined as having no detectable parasites 30 days post-infection [Jimenez-Diaz et al., 2009; Angulo-Barturen et al., 2008]. The microscopic limit of detection is 0.01%, as a direct consequence of the total number of erythrocytes monitored for infection (10 000).

In *P. berghei* experiments, a wide range of doses were commonly tested with one measurement point per mouse (72 or 96 h after inoculation). In contrast, fewer doses were tested with fewer mice per dose in *P. falciparum* experiments. However, parasitemia and hematocrit were measured multiple times (at least once a day on day three up to day seven post-infection), with experiments lasting up to 32 days. All provided data was compiled into a database containing experimental data, along with information concerning experimental set-up and laboratory.

The animal experiments performed were approved by the Swiss Cantonal Authorities or by the Diseases of the Developing World Ethical Committee on Animal Research. The animal studies carried out at GSK were in accordance with European Directive 2010\63\EU and the GSK Policy on the Care, Welfare and Treatment of Animals and were accredited by the Association for Assessment and Accreditation of Animal Laboratory Care for the ones performed at Diseases of the Developing World Laboratory Animal Science facilities. The animal experiments carried out at the Swiss Tropical and Public Health Institute (Basel, Switzerland) are adhering to local and national regulations of laboratory animal welfare in Switzerland. Protocols are regularly reviewed and revised following approval by the local authority (Veterinäramt Basel-Stadt).

Modeling workflow

We developed a modelling workflow applicable for systematic analysis of antimalarial drugs which spans data handling, model development, parameterization, and simulation. The workflow is illustrated in Appendix A, Supplementary Fig. S2.1. In brief, we firstly developed multiple within-host parasite-growth models for both murine systems based on parasite characteristics described in the literature and via experimental background and settings (RBC clearance and replenishment in SCID mice). Models were described by ODEs (Appendix A, Supplementary Table S2.3) and were parameterised using available untreated parasite growth data with several parameters extracted from literature (Appendix A, Supplementary Table S2.4). Secondly, we tested, selected, and parameterized appropriate PK models to the concentration-time profile for

each drug given several tested doses. Thirdly, the undisturbed parasite growth model and the PK model were combined, and their parameters fixed, to estimate parameters of drug action using drug treatment data.

All parasite growth and PD modelling, data manipulation, and plotting was performed in R (Version 3.5) [*R Core Team. R: A Language and Environment for Statistical Computing.*] using the package IQRtools (Version 0.9.99) [Schmidt, 2017]. Parasite growth- and PD-parameters were estimated via a maximum likelihood approach on trust region optimisation. Multiple estimation starting points were utilised in order to guarantee identification of the global minimum.

Growth model evaluation was performed using visual comparison of data to model output, and assessment of biological plausibility of all parameters for all models. Several PD drug action models were fitted for each drug and murine experimental system to capture direct effect of drug concentration as well as delayed effects via effect compartment or indirect response models (Appendix A, Supplementary Table S2.2), and selected by ΔOVF (AIC) (Appendix A Supplementary Fig. S2.2). Hill coefficients were fixed to values between one and seven. The parasite clearance half-life was estimated from model simulations using the methodology described in [Flegg et al., 2011].

Several different PK models with varying number of compartments, absorption and clearance behaviour were tested to identify the PK model best describing each of the four drugs investigated (Appendix A, Supplementary Table S2.5). PK models were fitted to the concentration-time profiles simultaneously using nonlinear mixed-effects modelling in Monolix 2016R1 [Monolix version 2016R1, 2016]. The PK profile of each drug and murine system was chosen by comparing model AIC. Final PK models and parameter values can be found in the Appendix A Supplementary Table S2.8.

Data availability

The datasets analysed during the current study are available from the corresponding author on request and with permission of Medicines for Malaria Venture and Idorsia Pharmaceuticals Ltd.

Acknowledgements

We acknowledge our colleagues at the Swiss TPH Infectious Disease Modeling unit, our collaborators at MMV, Julie Simpson and Inigo Angulo Barturen for their valuable feedback and insights on this work. We further thank Henning Schmidt and Anne Kümmel at Intiquan GmbH for their technical support. The work was funded by the Swiss National Science Foundation through SNSF Professorship of M.A.P. (PP00P3_170702). Calculations were performed at sci-

CORE (http:\\scicore.unibas.ch\) scientific computing center at University of Basel.

Author contributions

L.B. conducted the analysis. M.A.P. conceived the study. S.W., M.R., N.G., A.K., J.D., J.J.M. provided data and input to the manuscript. L.B. and M.A.P. wrote the manuscript. All authors reviewed the manuscript. M.A.P. and J.J.M. supervised the project.

Chapter 3

Parasite-host dynamics throughout antimalarial drug development stages complicate the translation of parasite clearance

Lydia Burgert[1,2], Sophie Zaloumis[3], Saber Dini[3], Louise Marquart[4], Pengxing Cao[5], Mohammed Cherkaoui[6], Nathalie Gobeau[6],James McCarthy[4],Julie A. Simpson[3], Jörg J. Möhrle[1,2,6], Melissa A. Penny[1,2]

[1]Swiss Tropical and Public Health Institute, Basel, Switzerland
[2]University of Basel, Basel, Switzerland
[3]Centre for Epidemiology and Biostatistics, Melbourne School of Population and Global Health, University of Melbourne, Melbourne, Australia
[4]QIMR Berghofer Medical Research Institute, Brisbane, Australia
[5]School of Mathematics and Statistics, University of Melbourne, Melbourne, Australia
[6]Medicines for Malaria Venture, Geneva, Switzerland

This manuscript has been published in Antimicrobial Agents and Chemotherapy in March 2021 [Burgert et al., 2021] (https://doi.org/10.1128/AAC.01539-20).

The supplementary information and supplementary files can be found in Appendix B.

Abstract

Ensuring continued success against malaria depends on a pipeline of new antimalarials. Antimalarial drug development utilises pre-clinical murine and experimental human malaria infection studies to evaluate drug efficacy. A sequential approach is typically adapted, with results from each stage, informing the design of the next stage of development. The validity of this approach depends on confidence that results from murine malarial studies predict the outcome of clinical trials in humans. Parasite clearance rates (PRR) following treatment are key parameters of drug efficacy. To investigate the validity of forward predictions, we developed a suite of mathematical models to capture parasite growth and drug clearance along the drug development pathway and estimated PRR. When comparing the three infection experiments, we identified different relationships of PRR with dose, and different maximum PRR: in *P. berghei*-NMRI mouse infections we estimated a maximum PRR of 0.2 [1/h], in *P. falciparum*-SCID mouse infections 0.05 [1/h], while in human volunteer infection studies, we found a maximum PRR of 0.12 [1/h] and 0.18 [1/h] after treatment with OZ439 and MMV048, respectively. Sensitivity analysis revealed that host-parasite driven processes account for up to 25% of variance in parasite clearance for medium-high doses of antimalarials. Although there are limitations to translate parasite clearance rates across these experiments, they provide insight into characterising key parameters of drug action and dose response and assist in decision making regarding dose selection for further development.

3.1 Introduction and Background

Recent progress to reduce malaria burden is threatened by emerging resistance against current first-line treatments and sub-optimal adherence to existing treatment schedules. Thus, the development of new antimalarial treatments is more urgent than ever [WHO, 2019]. The requirements for new antimalarial treatment regimens are multi-facetted spanning safety, efficacy, and dose optimisation for all populations, including pregnant women, infants and children [Burrows et al., 2017].

Before testing compounds *in vivo*, promising compounds are identified *in vitro*, and their parasiticidal efficacy is assessed in whole cell or target-based assays [Flannery et al., 2013]. In pre-clinical stages, drug efficacy is often investigated using murine malarial infection. Historically, infection of normal mice with *P. berghei*, was shown to be a useful experiment to measure crude drug efficacy and select promising candidates [Jiménez-Díaz et al., 2013]. However, enzymatic differences between the human malaria parasite *P. falciparum* caused selection bias in candidate selection [Phillips et al., 2016]. More recently, the humanized mouse model of $\text{NOD}^{scidIL-2R'c-/-}$ (SCID) mice infected with *P. falciparum* has been shown to provide insights into efficacy against the human parasite *in vivo* [Angulo-Barturen et al., 2008; Jimenez-Diaz et al., 2009; McCarthy et al., 2016a] and further assists candidate selection. Early human efficacy studies via experimental infection of malaria-naïve individuals, termed volunteer infection studies (VIS) [McCarthy et al., 2011] or controlled human malaria infection (CHMI) studies, provide an opportunity to evaluate antimalarial activity in humans with low parasite burden in a controlled setting. These studies avoid the confounding factors of drug efficacy observed in clinical malaria cases such as acquired immunity, concomitant diseases and medication [Krause et al., 2016; McCarthy et al., 2016c; McCarthy et al., 2016b] .

Drug efficacy indices, used to summarise drug effect over time, represent key measures to inform the progression of drug candidates from the preclinical to clinical stages of the drug development pipeline. For malaria, pharmacodynamic/efficacy indices include: i) measurements of total or proportional parasite clearance such as the parasite clearance rate (PRR, or also referred to as the parasite reduction ratio when clearance is defined for specified time window) [McCarthy et al., 2016a] , ii) drug exposure typically reported by indicative drug concentrations such as the minimum inhibitory concentration (MIC), or iii) clinical endpoints such as adequate clinical and parasitological response (ACPR) [WHO, 2009]. The PRR is widely used in antimalarial drug development to guide compound selection [Burrows et al., 2017], and is also reported in clinical studies in endemic areas as a measure of drug efficacy [White, 2017].

In a previous paper, we developed a suite of mathematical models of parasite growth and drug-parasite dynamics to investigate murine malaria infection and malaria drug experimental tests. Via extensive simulation of these models and comparison to data for several drugs, we

found that the experimental systems and differences between the two murine malaria infections had appreciable effects on measured drug efficacy and treatment outcomes. More specifically, we found drug efficacy is influenced by host-parasite dynamics in *P. berghei*-NMRI mouse infection where resource limitation is caused by aggressive parasite growth, namely limitations of red blood cells (RBC) [Burgert et al., 2020]. In *P. falciparum*-SCID mouse infection, we found continued injections of human RBCs has a noticeable impact on subsequent clearance patterns of uninfected and infected RBCs. We additionally identified mechanisms of observed recrudescence patterns after non-curative treatment that are not discernible from the experimental data nor captured by current modelling approaches of antimalarial drugs. These unknown mechanisms may include altered parasite maturation or dormancy and affect experimental measures of cure, thus limiting interpretations of curative dose for a particular drug [Burgert et al., 2020].

In this study, we examined the ability of the PRR estimated from murine experiments to translate to estimates determined from human studies. This analysis used data from studies of two antimalarials MMV048 and OZ439 (artefenomel) in the *P. berghei*-NMRI mouse, *P. falciparum*-SCID mouse and *P. falciparum*-human infection experiments. Both compounds are part of the Medicines for Malaria Venture portfolio (https:\\www.mmv.org\research-development \mmv-supported-projects). OZ439 is a synthetic peroxide antimalarial candidate that is fast acting against all asexual erythrocytic parasite stages. It is currently being evaluated in combination with Ferroquine in phase II clinical studies [McCarthy et al., 2016c; Charman et al., 2011; Phyo et al., 2016a; Dong et al., 2010]. MMV048 is a Plasmodial phosphatidylinositol 4-kinase (PI4K) inhibitor efficacious against liver erythrocytic parasite-life cycle stages currently in phase IIa [Paquet et al., 2017; Sinxadi et al., 2020; McCarthy et al., 2020]. We modelled parasite growth and clearance following two new antimalarial treatments in murine and human malarial infections (Fig. 3.1a): model development and calibration). We included relevant and potentially important features of parasite growth, host, and drug dynamics in the models of all three testing systems following a comprehensive examination of their biological and experimental background. Via simulation and global sensitivity analysis of these models we explored and compared the estimates of PRR for a range of dosing regimens, and parasite and host assumptions in all three systems (Fig. 3.1b). Through this analysis, we demonstrated which of the factors; host, parasite, host-parasite and drug dynamics, primarily determine the relationship between PRR estimates across the antimalarial drug development pathway and assess implications for decision making in drug development.

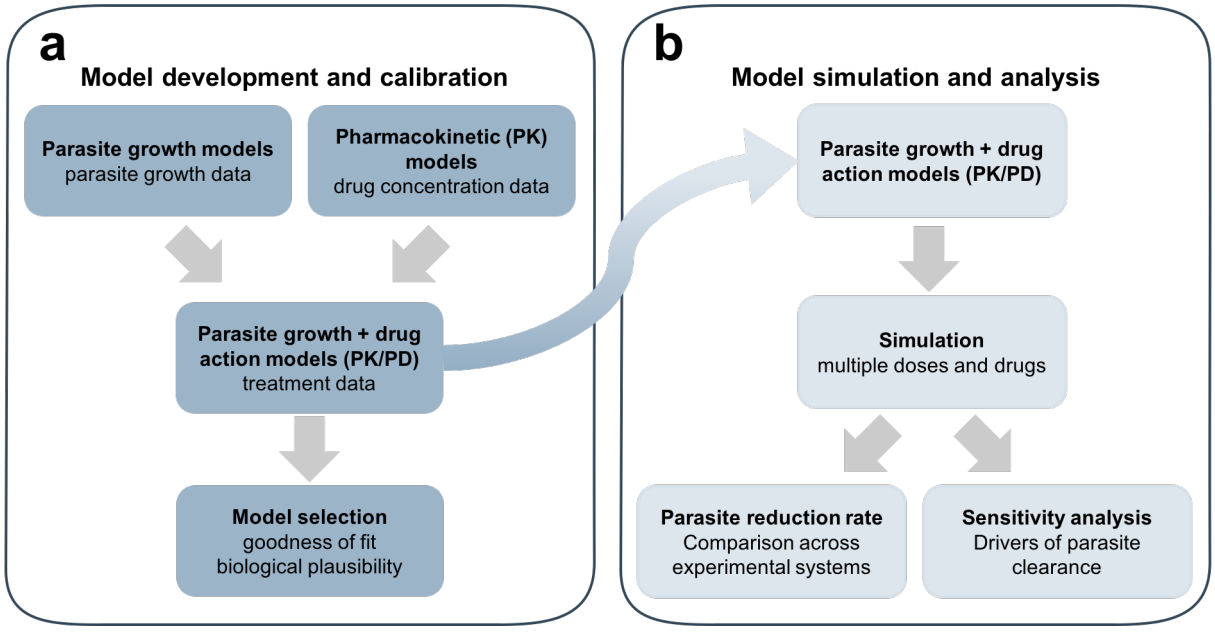

Figure 3.1: Standardised workflow for the systematic investigation of parasite-host-drug dynamics throughout the (pre)-clinical antimalarial development process. **(a)** Mechanistic models of parasite growth are calibrated to extensive undisturbed parasite growth (control) data in murine and human infection experiments on a population (mouse) or individual (human) level. Combined with models of drug-concentration (PK) over time, they are used to calibrate to treatment data over multiple doses and drugs. Models were selected for further analysis based on appropriate goodness of fit measures and assessment of biological plausibility. **(b)** Model simulation over multiple drugs and doses facilitates the comparison of the parasite reduction rate over all experimental systems. Subsequent sensitivity analysis allows the identification of parasite-, host-, or drug-dynamics as the drivers of experimental outcomes.

3.2 Results

The design of the studies/experiments used to evaluate the candidate antimalarials (MMV048 and OZ439) in normal mice, SCID mice and human volunteers are described in Table 3.1 and Fig. 3.2a (left side of panels a-c). Mice were infected with around 2×10^7 parasites or greater inocula resulting in progression to severe disease with high parasitemia of up to 60-80% (*P. berghei*, parasitised mouse RBCs) and 15-20% (*P. falciparum*, parasitised human RBCs) within a week of inoculation. By design, human volunteers do not progress to high parasitemia to avoid severe clinical illness [McCarthy et al., 2011]. Volunteers reach parasitemia of around 1×10^4 p/mL (corresponding to 0.0002% under the assumption of 6×10^9 RBCs/mL in male humans [Bates, 2017]) before treatment.

Parasite-host dynamics and experimental design influence treatment in murine malaria infection

In our previous work [Burgert et al., 2020], we developed several mathematical models of parasite and drug dynamics in both *P. berghei*-NMRI and *P. falciparum*–SCID mice (Fig. 3.1a). The experimental system and mathematical models are described in Fig. 3.2, panels a and b, respectively. Using the parameter estimates from the original paper (for both parasite growth and PKPD models), we simulated the models of murine infection to compare their results with our VIS simulations below (Fig. 3.1b). Here, we primarily compared PRR across the three testing systems (Fig. 3.1b: PRR comparison across experimental systems) as estimated from the models for a range of drug doses. We subsequently assessed influence of experimental design and parasite-host system on PRR throughout the antimalarial development pathway by sampling from the posterior distributions for VIS, and by sampling parameters from a log-normal distribution with 20% standard deviation for the murine models (Fig. 3.1b: sensitivity analysis).

In the two murine systems, several experimental and parasite-host traits were examined by including them in a suite of models (further details in Methods and Table S3.5) [Burgert et al., 2020]. From an experimental perspective, data availability and experimental design differ between the two murine infection systems. For example, in *P. berghei*-NMRI infection, the volume of blood sample needed for analysis and aggressive parasite growth limited the frequency of collection for measurements of parasitaemia. From the host perspective, we investigated and quantified adaptions of the host-system to increasing parasite burden. In *P. berghei*-NMRI infection, we included erythropoiesis [Cromer et al., 2006; Lamikanra et al., 2007] or clearance patterns, as well as parasite adaptions such as parasite maturation [Khoury et al., 2017b] and target-RBC preferences [Cromer et al., 2006] in our models to capture patterns of RBC availability and the occurrence of anemia (Fig. 3.2a). In *P. falciparum*–SCID infection experiments, continued injections of human erythrocytes hinder the occurrence of anemia and lead to an

increase in the proportion of available human host-cells throughout the experiment (Fig. 3.2b). The injected human RBC volume of 4.55×10^9 RBCs every two to three days (corresponds to 46% of total mouse RBCs) leads to a high clearance of excess erythrocytes throughout the experiments, thus likely affecting measures of drug efficacy [Angulo-Barturen et al., 2008]. Different hypotheses regarding the influences on RBC clearance mechanisms were formalised in our models of *P. falciparum*-SCID mouse infection (Fig. 3.2b).

Using a maximum likelihood approach, we estimated the parameters of our parasite growth models by fitting them to the pooled experimental control data of untreated parasite growth. The fitted models were then combined with the PD models to analyse the influence of the parasite-host dynamics and experimental design on the PRR.

We found a delayed parasite clearance, captured by clearance rate of dead parasites Cl_Y, after treatment with MMV048 in both murine hosts (Table S3.5 - clearance PD model selection: Cl_Y range of 0.036 to 0.041 (1/h) in *P. berghei*-NMRI and Cl_Y range of 0.068 to 0.071 (1/h) in *P. falciparum*-SCID infection over all mechanistic parasite growth models). In contrast, for OZ439, we observed a delayed drug effect through a turnover (Table S3.5 - turnover PD model selection: k_R range of 0.013-0.06 (1/h) in *P. berghei*-NMRI and k_R range of 0.013-0.016 (1/h) in *P. falciparum*-SCID infection over all mechanistic parasite growth models) [Burgert et al., 2020]. In both murine experimental systems, we found that assumptions on parasite-host dynamics result in differing estimates of parasite clearance times therefore influencing the evaluation of new compounds (Fig. 2.4 [Burgert et al., 2020]).

Table 3.1: Overview of the data and experimental outcomes in our analysis of murine and human malaria infection. Untreated parasite growth behaviour was informed by a separate control group in murine experiments, and by parasite growth data before treatment commences in human infection. Experimental outcomes evolve over the preclinical and clinical stages with increasing data richness per subject over time from crude efficacy measures such as activity and parasite reduction to more detailed concentration effect relationships. Measures of parasite reduction (e.g. parasite clearance rate or proportional antimalarial activity) are frequently used to evaluate compounds throughout the clinical development stages [Burrows et al., 2017]. SD: single dose, DD: double dose, TD: triple dose, QD: quadruple dose.

	***P. berghei ANKA* in NMRI mice**	***P. falciparum* in SCID mice**	***P. falciparum* in human**
no. subjects Control (Separate) MMV390048 OZ439	 215 (Y) 65 200	 132 (Y) 50 48	 177 (N) 20 24
no. subjects/dose	3-10	1-2	6-8
no. dose levels MMV390048 OZ439	 7 SD, 5 QD 14 SD, 3 TD	 2 DD, 6 QD 10 SD, 1 DD	 3 SD 3 SD
Min exp. length [d]	3-4 (up to 30)	8 (up to 31)	8 (up to 30)
Inoculum [iRBCs]	2×10^7	3.5×10^7	1800-2800 (viable parasites)
Total cure (no. mice) MMV048 OZ439	 4x3 mg/kg (3) 1x30 mg/kg (30)	 4x20 mg/kg (2) 1x100 mg/kg (2)	 1x80 mg (8) -
Outcomes	- Activity - Cure (Survival) (PRR)	- PKPD relationship - PRR - Cure	- PKPD relationship - PRR - Cure
Parasitemia output	Percentage of infected RBCs	Percentage of infected RBCs	Concentration of infected RBCs per mL

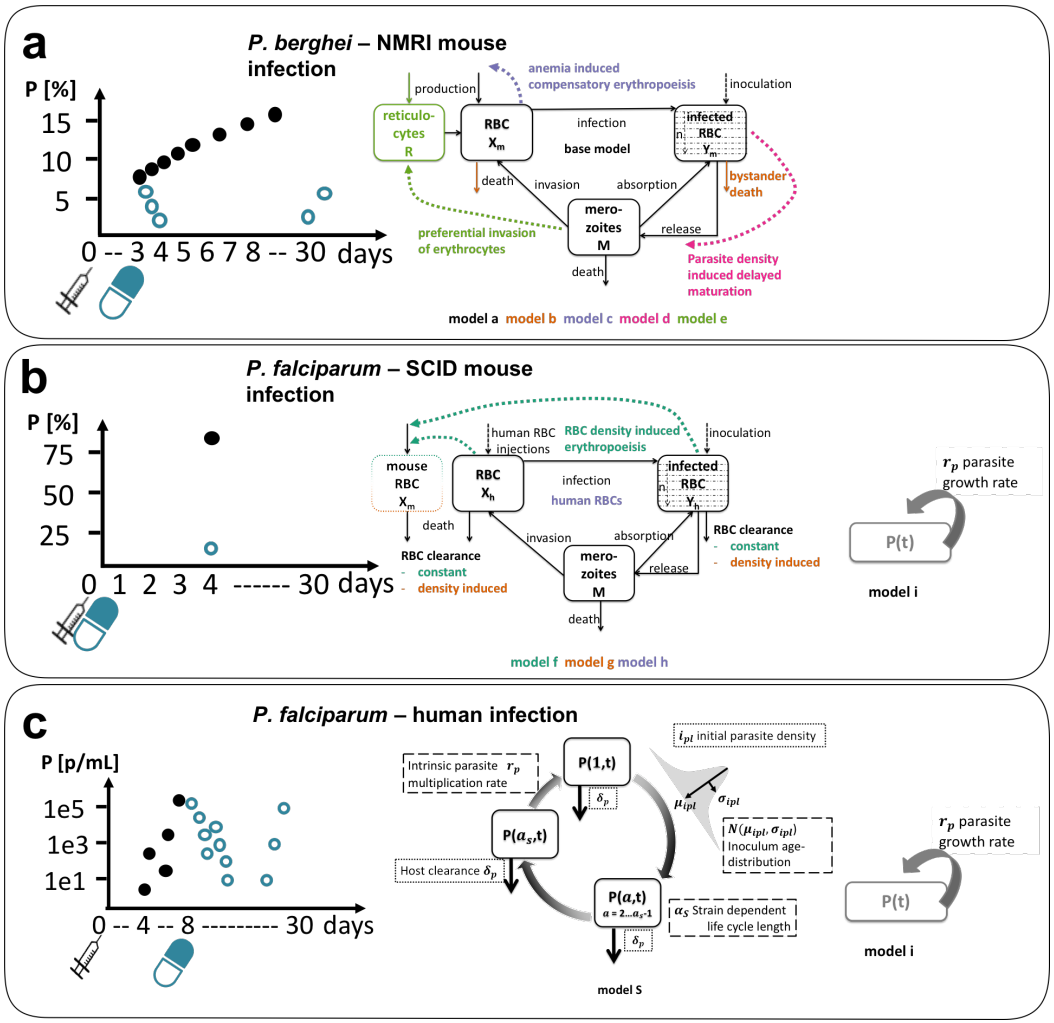

Figure 3.2: Experimental sampling design and investigated parasite-host dynamics in preclinical and clinical antimalarial drug development. Parasitemia of a typical subject in each experimental system is shown on the left side. Subjects are inoculated on day 0 (black syringe) and treatment (blue syringe, oral dose) commences on the same day or up to four days afterwards in murine malaria infection **(a, b)** and after seven to nine days in human infection **(c)**. Each dot represents one measurement, with black dots indicating untreated growth/growth before treatment and blue dots representing parasitemia after treatment. Separate control groups were measured in murine experiments. The murine infections are measured in percent of infected RBCs, and human infections are measured in infected RBCs per mL (Table 3.1). The schematics of mathematical models used to describe parasite growth in the respective system are shown on the right side. In murine malaria infection **(a, b)**, capturing uninfected (X) and infected (Y) RBCs dynamics is crucial to understand implications of resource limitation (*P. berghei*-NMRI infection) and resource replenishment (*P. falciparum*-SCID infection) [Burgert et al., 2020]. Details on murine model structure can be found in section 3.4 , Equations 3.1 to 3.6. In contrast, low total numbers of parasites P(t) in *P. falciparum*-human infection and increased number of measurements shift modelling focus on dynamics of intra-erythrocytic parasite-stages over time **(c)**. The exponential growth *model i* can only be used to capture parasite growth of *P. falciparum* in SCID mouse and human as data are not informative enough in *P. berghei*-NMRI infection.

Human volunteer infection studies exhibit large variation in observed parasite growth and clearance dynamics

We modelled parasite growth prior to treatment using data from 177 volunteers in 27 treatment cohorts in VIS conducted at Berghofer QIMR, Brisbane between 2012-2016 [Wockner et al., 2019]. These cohorts were part of 14 studies investigating new antimalarials in development and currently available antimalarials. Volunteers were infected with 1800-2800 infected RBCs and treated 7-9 days after inoculation [Wockner et al., 2019].

The frequent sampling of human volunteers over time was much greater compared to murine experiments, however, the number of measurements above the lower limit of quantification (LLOQ, 111 p/mL) varied between cohorts and volunteers with a median of five quantifiable measurements (ranging from one to eight). These detailed data allowed us to capture features of the parasite life cycle, such as the characteristic oscillation in parasite densities. This phenomena is caused by periodical sequestration of late stage asexual parasites stages to the deep microvasculature of the host organs [Khoury et al., 2018] and synchronicity in parasite growth determined by the distribution of parasite age in the inoculum [Zaloumis et al., 2012].

The models of asexual parasite growth in in human volunteers are described in Fig. 3.2c. We adapted a discrete time model [Saralamba et al., 2011] previously used to investigate antimalarial treatment [Zaloumis et al., 2012], resistance against artemisinin combination therapy [Zaloumis et al., 2018], and the impact of new antimalarial combinations [Dini et al., 2018]. A set of difference equations (*model S-parasite stages*, Equation 3.7) describes the parasite inoculation, capturing its size and age distribution, and the subsequent mechanism of intra-erythrocytic parasite development including ageing and parasite death. After 39 h [Wockner et al., 2019], the parasites replicate. For comparison, we tested a second model that assumes exponential parasite growth (*model i*, Equation 3.10), summarising parasite replication and death into one growth parameter. This model is the commonly used to capture parasite growth and treatment effects in antimalarial drug development [McCarthy et al., 2016a; McCarthy et al., 2016c].

We incorporated the models into a Bayesian hierarchical framework to estimate the posterior distributions of the model parameters from the VIS data. We investigated different levels of parameter variability, distinguishing between parasite and host dependent parameters by varying hierarchical parameter allocation in different parasite growth model specifications (Table S3.2, *models S1-S3*). *Model S3*, from here on referred to as *model S*, was selected based on the Watanabe-Akaike information criterion (WAIC) (Table S3.2). The parameters describing distribution of the initial parasite load (mean μ_{ipl} and standard deviation σ_{ipl}) and the intrinsic parasite multiplication factor, r_p, were found to vary on a cohort level whereas the initial parasite load i_{pl} and parasite death rate due to host clearance δ_p vary between individuals (Fig. S3.7). The population posterior predictions of the two parasite growth models (Fig. 3.3) begin on day four after inoculation, when quantifiable parasitemia measurements from the volunteers are first

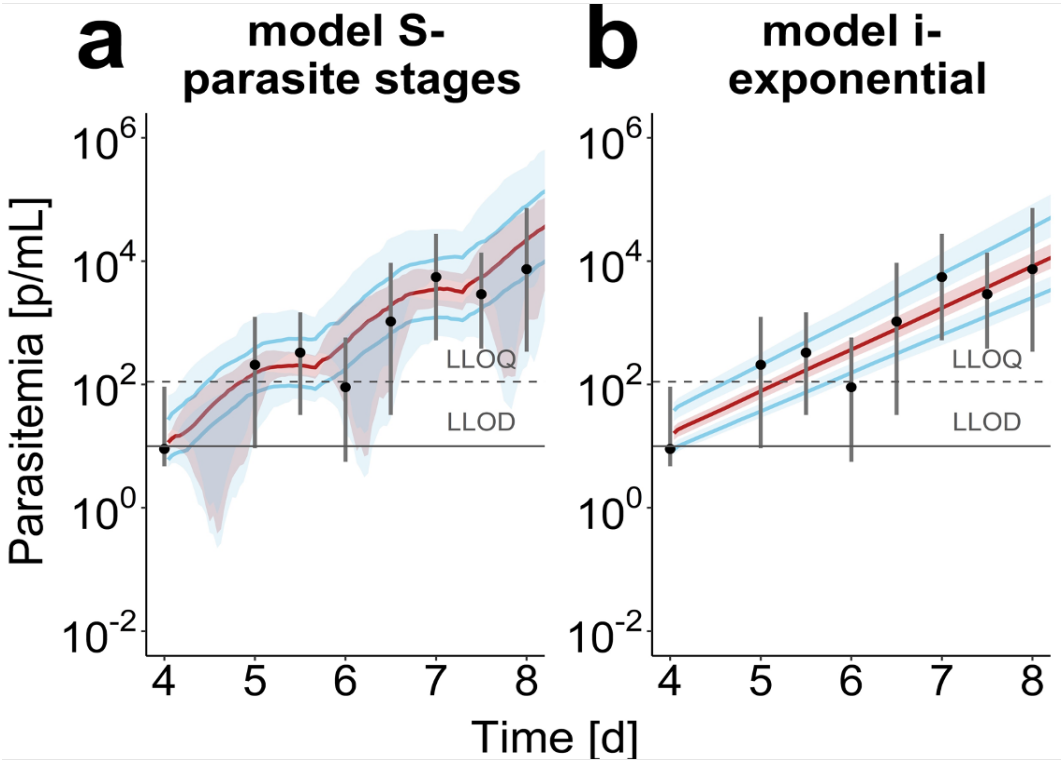

Figure 3.3: Population parasite growth prediction in VIS. Median parasite densities (black dots) with their 90-percentiles over the time starting four days after inoculation for the 177 subjects in VIS [Wockner et al., 2019]. Model predictions show the median (red) and 90th percentile (blue) with credible intervals over 100 trials with 20 subjects. **(a)** The mechanistic growth *model S* captures parasite growth trends well over time with discrepancies between data and prediction being centred around parasitemia under the lower limit of quantification (LLOQ) of 111 p/mL and lower limit of detection of 10 p/mL (LLOD). We found a population posterior median (credible interval) of the initial parasite load (four days after infection) of 2.59 (2.44-2.74) [log(p/mL)], a median parasite age μ_{ipl} of 14.0 h (12.1 – 15.6) with a standard deviation σ_{ipl} of 4.32 h (3.83-4.90). The intrinsic parasite multiplication rate r_p of 55.2 (46.3 – 68.5) and death rate δ_p of 0.0302 (0.0263-0-0353) [1/h] describe the intra-erythrocytic replication dynamics of the parasite. **(b)** The exponential parasite growth in *model i* leads to linear growth behaviour on the log-scale, so does not capture the oscillating parasite growth behaviour. We estimated a growth rate r_p of 0.0649 [1/h] (0.0620-0.0678). The posterior predictive checks are illustrated in Fig. S3.7 (*model S*) and Fig. S3.8 (*model i*).

available (Fig. 3.2). We estimated a parasite multiplication factor *pmf*, of 17.0 (15.3-20.0) over one life cycle of 39 h (Equation 3.7). Identifiability issues of growth rate r_p were detected by the partial congruency of the marginal prior and posterior distributions (Fig. S3.7). This means that data on parasite growth is not informative enough for estimating this parameter, similar to previous model analysis [Cao et al., 2019]. For exponential growth *model i*, we estimated a *pmf* of 12.61 (11.2 – 14.2) over one parasite life cycle. Differences in the parasite growth rate r_p between individuals within cohorts, could not be linked to cohort or subject specific parameters

for *model i* (Fig. S3.8).

Given our calibrated VIS parasite growth models, we incorporated PK models and modelled drug effects (pharmacodynamics) (Fig. 3.1a) to analyse single-dose treatment of 20 volunteers with MMV048 and 24 volunteers with OZ439 (Table S3.1). Drug concentrations after treatment were predicted using pharmacokinetic (PK) models (Equation S3.1 and S3.2) and individual PK parameters specified (Appendix B, Supplementary File 3.1). We simulated individual PK profiles to exclude large variation in drug-concentration as an influencing factor in the following analysis. Drug concentration over time was described by a two-compartment model with zero-order absorption for MMV048 and a 2-compartment model with linear absorption for OZ439. In the following section, we explain the results for OZ439. The analysis of MMV048 is detailed in the Supplement (Appendix B), and any deviations are highlighted and discussed here.

We incorporated a direct effect of drug concentration on parasite death (Equation 3.8) and additionally tested for drug concentration induced retarded parasite growth (Equation 3.9) due to the reduced parasite growth observed after non-curative dosing with OZ439 and the shift in oscillation patterns to a longer period. This phenomenon was also previously described for artemisinin derivatives [Teuscher et al., 2010]. A comparison of drug action model based on WAIC and additional observations is included in Table S3.3.

We detected drug-concentration dependent prolongation of parasite stages after treatment with MMV048 and OZ439, meaning that at sufficiently high drug concentrations each life cycle stage can be prolonged by 26 min or 65 min respectively (Equation 3.13). Through description of individual treatment effects via subject-specific parameters of drug efficacy (Fig. S3.9 to S3.12) we could capture individual parasite clearance and recrudescence curves after treatment with MMV048 (Fig. S3.3 and S3.4) and OZ439 (Fig. S3.5 and Fig. S3.6) for all subjects.

Although the posterior predictions of recrudescence (Fig. 3.4) fit the data well, we note that informed mechanistic models, and inclusion of experimental recrudescence outcomes and cure are hindered by limited data on cure probability since each cohort only consisted of eight subjects. Additionally, insights into minimum parasite concentrations for cure are missing.

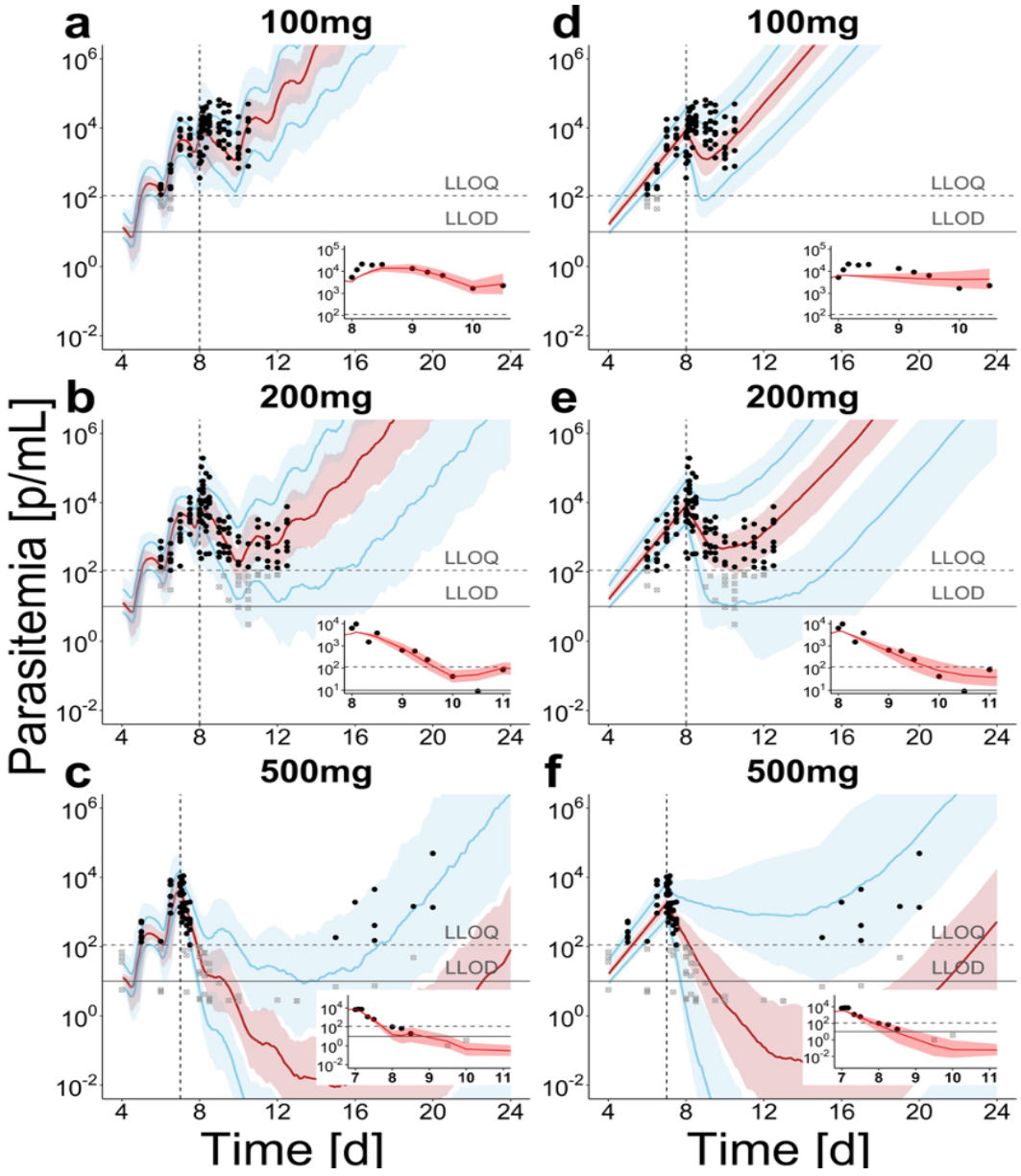

Figure 3.4: Population prediction after treatment with OZ439 in *P. falciparum*-human infection for mechanistic growth *model S* (a-c) and exponential *model i* (d-f). The simulated median (red) and 90th percentile (blue) with credible intervals over 100 trials with 20 subjects are compared to data of individual parasite densities (black dots) in the respective treatment group. For each treatment group, parasite clearance of a typical subject (Subject 1, 15 and 19) immediately after treatment is illustrated with individual predictions in the inset figures (for all subjects see Fig. S3.12 and Fig. S3.13). Immediately after treatment with 100 mg OZ439 **(a, d)** an increase in parasite densities, and transient decelerated parasite growth was observed which is captured by *model S* through the lengthening of the parasite life cycle. After treatment with higher doses **(b-c, e-f)**, this effect is less influential, with more prominent parasite killing by the drug. After treatment with 500 mg **(c, f)** only four out of eight volunteers exhibited parasite recrudescence (see individual data in Fig. S3.5 and Fig. S3.6 and posterior distributions in Fig. S3.11 and S3.12). Vertical line (—) indicates time of treatment and the horizontal lines the LLOQ of 111 p/mL and LLOD of 10 p/mL.

Parasite clearance rate (PRR) is unlikely comparable across the preclinical and clinical development pathway

The PRR was estimated from our model simulation for murine and human malaria infection (Fig. 3.1b) over a wide range of single doses of each drug. The range of doses and models facilitated comparison across preclinical and clinical stages. We chose seven doses per experimental system that capture realistic testing dose ranges. We simulated 1000 trials for each murine experiment with parameter estimates published in [Burgert et al., 2020] (see Table S3.5 for an overview) and variability added between trials and parameters fixed within one trial over all doses. In human-*P. falciparum* infections we simulated 100 trials with 20 subjects per dose and varied the parasite-dependent parameters between trials and the host-dependent parameters between subjects within a trial. The parameters of the PK models were fixed to population values for all model simulations to allow for adequate characterization of host-parasite dependent dynamics and variability. The simulation set-up is detailed in Table S3.4.

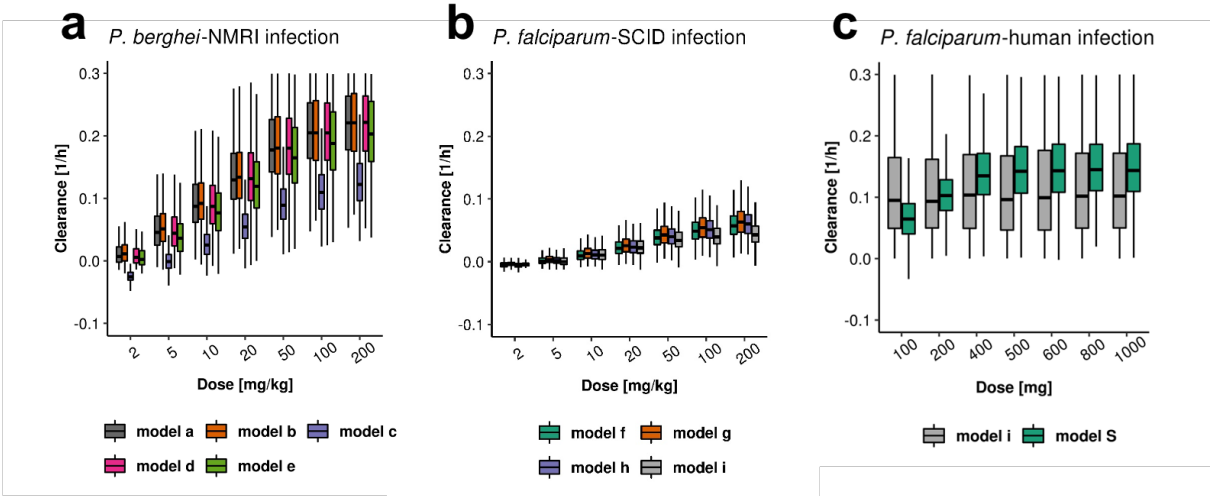

Figure 3.5: PRR across the murine and human experiments after single dose treatment with OZ439. Within one experimental system the predicted clearance rates are fairly consistent. **(a)** *Model c (comp. erythr.)* of *P. berghei*-NMRI infection estimated a lower maximum drug effect E_{max} resulting in lower clearance rates (Table S3.5). **(b)** Compared to panel a and c, *P. falciparum*-SCID infection shows less variability. **(c)** The wide clearance range observed in model predictions of the exponential growth *model i* for *P. falciparum*-human infection stems from the wide posterior distribution of the maximum drug effect E_{max}. Parasite clearance rates were calculated from simulation output using the methodology provided in [Flegg et al., 2011].

Fig. 3.5 compares PRR calculated from simulation output after single dose treatment of OZ439 over the two murine and experimental human infection experiments. We find different relationships of estimated PRR with doses across the experimental systems. Median estimates

of PRR plateau around 0.2 [1/h] in *P. berghei*-NMRI infection and 0.05 [1/h] for *P. falciparum*-SCID infection. Analysis for MMV048 shows similar maximum clearance rates in murine infection (Fig. S3.13) and different relationships with dose. In experimental *P. falciparum*-human infection the PRR for OZ439 plateaus with *model S* around 0.12 [1/h]. The ranges of the predicted clearance time of *P. falciparum*-human infection between *model i* and *model S* are also reflected in the wider posterior predictive intervals of the former after treatment with OZ439 (Fig. 3.4).

Parasite clearance is influenced by varying parasite-host dynamics throughout the analysed experiments of murine and human malaria infection. Despite the lack of comparability across experimental systems, the PRR predicted from mechanistic models within an experimental system are comparable, but with different levels of variation. Via a global sensitivity analysis, we thus identified which host-, parasite-, and drug-dynamics cause the highest variability in parasite clearance (PRR) after treatment with MMV048 and OZ439. We first partitioned variability by classifying parameters by their influence and dependency on parasite-, host- or drug-concentrations. For example, the parameters of infection induced RBC clearance γ in murine malaria models are classified as host-parasite parameters since they are induced by parasite concentration and influence overall RBC concentration (Table 3.2). We then undertook a global sensitivity analysis of the models on simulated PRR reducing computational time by using emulators and sobol-analysis, which calculates first order indices and total effect indices to evaluate individual and combined parameter contributions to the variance of PRR (see 3.4. Methods).

In general, we find in all experimental systems, that PRR is most sensitive to drug action parameters (Table 3.2). This is expected as we are measuring the effect of the drug in these systems. We also find that interactions of the drug action parameters (increased total effect over first-order effect) occur over all doses but decrease with increasing dose, evident in the convergence of first order and total effect values. However, in both the murine (Fig. 3.6 a and b) and human *P. falciparum* (Fig. 3.6c) infections, we find at lower doses an increasing influence of both the host or parasite, or host-parasite parameters. This indicates a greater influence of the experimental system on measured parasite clearance. Even in medium-high dose ranges, drug unrelated parameters and their interactions account for up 25% of variance in parasite clearance. This is mainly caused by sensitivity towards maximum infection induced RBC clearance γ_{max} and parameter φ, which capture splenic/liver clearance and maximum infection induced RBC clearance γ_{max}. The exponential growth *model i* shows diminishing dependence on parasite replication rate r_p with increasing doses in *P. falciparum*-SCID infection.

Estimated treatment effects of experimental *P. falciparum*-human infection are sensitive to the maximum drug action parameter E_{max}, resulting in a large range of PRR prediction throughout all doses. In the lower dose ranges of OZ439 treatment, the total effects of the age distribution parameters μ_{ipl} and σ_{ipl} of *model S* account for up to 50% of all variance (c). In

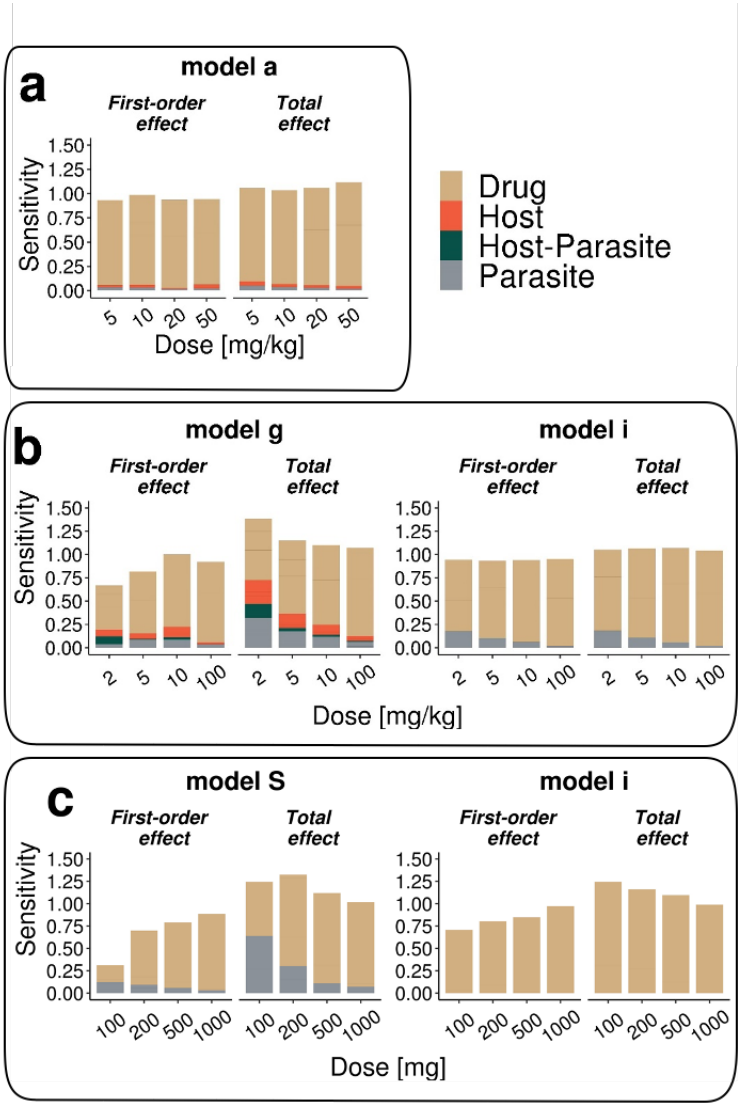

Figure 3.6: Exemplary results of the sensitivity analysis of parasite clearance after OZ439 treatment towards parameters of host, parasite, host-parasite, and drug dynamics for (a) *P. berghei*-NMRI, (b) *P. falciparum*-SCID, and (c) *P. falciparum*-human infection. Using sobol sensitivity analysis, first order effects measure individual parameter contributions and the total effect indices summarize individual and interactive parameter contributions to the outcome variance (see 3.4. Methods).

contrast, throughout all regimens, parasite parameters have negligible influence on clearance for MMV048 (Fig. S3.14). The full set of individual parameter contributions in all experimental systems can be found in Appendix B, Supplementary File 3.2. The complete set of results for both drugs are shown in Fig. S3.14 and Fig. S3.15.

Table 3.2: Classification of model parameters into host, parasite, host-parasite and drug parameters. Parameters were classified based on their dependency on host and parasite variables states and induction through those variables. Detailed description of parameters for murine models of *P. berghei*-NMRI and *P. falciparum*-SCID infection can be found in [Burgert et al., 2020]. Details on parameters of *P. falciparum*-human infection can be found in Fig. 3.2 and Table 3.3.

	***P. berghei* – NMRI**	***P. falciparum* – *SCID***	***P. falciparum* – human**
Host		• Initial percentage of human RBCs H_o • Base death rate of all RBCs λ • Parameters of RBC density dependent RBC clearance χ_{max} and $k\chi_{50}$	• Parasite death rate at each time stage δ_p
Parasite	• Infectivity parameter β • Number of merozoites per inf. RBC r • Attraction of parasite to reticulocyte ε • Parasite inoculum viability ω	• Infectivity parameter β • Number of merozoites per inf. RBC r • Parasite inoculum viability ω • Exp. parasite growth rate r_p • Initial parasitemia P_0	• Intrinsic parasite multiplication rate r_p • Distribution parameters of the initial parasite density μ_{ipl} and σ_{ipl}
Host- Parasite	• Parameters of infection induced RBC clearance γ_{max} and $k\gamma_{50}$ • Conc. of inf. Mouse RBCs achieving 0.5 growth retardation effect $k_{l,50}$	• Parameters of infection induced RBC clearance γ_{max} and $k\gamma_{50}$ • Base clearance of inf. RBCs φ	• Initial parasite density i_{pl}
Drug	• Parameters of concentration-effect relationship E_{max}, EC_{50} • Clearance rate for damaged parasites Cl_Y • First order rate constant for biological intermediate k_R	• Parameters of concentration-effect relationship E_{max}, EC_{50} • Clearance rate for damaged parasites Cl_Y • First order rate constant for biological intermediate k_R	• Parameters of concentration-effect relationship E_{max}, EC_{50} • Growth retardation parameter k_{ret}

3.3 Discussion

Our analysis of data from three unique experimental systems of drug action in *Plasmodium* infection: *P. berghei*-NMRI mouse infection, *P. falciparum*-SCID mouse infection and the human VIS, demonstrates a discrepancy in influencing parasite-, host- and drug-dynamics on parasite clearance between the pre-clinical and clinical antimalarial testing stages. This complicates the translation of results between these different experimental systems, aimed to collectively inform drug development. We initially intended to identify antimalarial drug efficacy indices that were reliable for translation. Although our analysis did not result in a unifying output, our insights into parasite-host dynamics across the preclinical murine and early clinical experimental infections in humans via the mathematical models provide a pathway to facilitate inference from the data. By describing the different experimental testing systems with data-calibrated mechanistic models, we used model predictions coupled with sensitivity analysis to identify factors significantly influencing experiments aimed to characterise drug efficacy. In addition to the drug and dose being tested, we identified differing magnitudes of host-parasite dynamics between the experimental systems as a driver of estimated parasite clearance rate.

By employing mechanistic models of parasite growth and drug effects in all three testing systems we found that several important dynamics affect translation of PRR and likely other parasitological outcome measures between preclinical and clinical systems.

Firstly, as expected, our sensitivity analysis of parasite clearance revealed a high sensitivity to parameters of drug action in higher dose ranges in all three experimental systems. In contrast, we found a variation in overall sensitivity of PRR to parasite-host dynamics in lower-medium dose ranges between the three experimental systems. In murine and human *P. falciparum* infection, parameters of parasite growth influenced PRR at lower doses. Additionally, the occurrence of clearance mechanisms of excess RBCs in *P. falciparum*-SCID infection, could place additional constraints on parasite growth. Overall, the increased susceptibility to the experimental set-up of the SCID system limits direct translation and comparison of results between laboratories and highlights the need for strict experimental protocols [Fidock et al., 2004; Burgert et al., 2020]. Thus, to predict human equivalent doses by exploiting the value of the *P. falciparum*-SCID mouse system, additional information is required concerning the interplay of disease dynamics and the experimental background which could be quantified with our modelling approach. For *P. berghei*-NMRI infection data, estimation of the PRR was less sensitive to parasite-host dynamics. However, the aggressive parasite growth in this experimental system might lead to host-cell limitations and therefore different growth dynamics compared to *P. falciparum* infection, challenging the translatability of drug efficacy measures. Although not investigated here, the uncertainties regarding clearance mechanisms may also hinder the investigation of drug-drug interactions. The testing of combination therapies relies on the ability to allocate contribution of individual drugs to parasite to estimate drug interactions. Hence testing combination therapies.

In vitro experiments could prove to be valuable alternatives in establishing formal descriptions of these interactions, which could thus be incorporated into mathematical models to predict the efficacy of combination [Dini et al., 2018].

Secondly, the sensitivity of PRR measured at lower drug doses due to factors other than the drug raises questions for current approaches to determine concentration-effect relationships (Equation 3.12) that rely on information gained in lower-medium dose ranges to define the concentration with half-maximum effect (EC_{50}). Additionally, other common drug efficacy indices such as the minimum inhibitory drug concentration (MIC) are influenced by EC_{50} measures (Equation 3.16). We therefore recommend that inferences based on data gathered at low-medium doses across the preclinical and clinical stages of drug development are assessed by considering factors connected to experimental and host-parasite pairing. For example, in *P. falciparum*-SCID and *P. falciparum*-human infection experiments, the sensitivity of the dose-response relationship of data obtained at lower dose ranges should be investigated for each drug candidate to avoid bias in decision making. In experiments with a new compound where drug efficacy analysis reveals a substantial influence of parasite-host dynamics in lower dose ranges, these data should not be used to characterise the MIC for decision making.

Thirdly, our earlier work indicated that recrudescence and thus estimates of MIC are potentially influenced by additional parasite mechanisms including retarded parasite growth in *P. falciparum*-SCID experiments [Burgert et al., 2020]. Experiments explicitly aimed at observing recrudescence are considered highly informative in understanding the dose-response relationships in these experimental systems. However, utilising these experiments for modelling proved that estimation or prediction of cure might be hindered by insufficient data on cure rates and curative doses in both murine and human malaria infection (Table 3.1). Thus, any analysis we could undertake on cure or recrudescence dynamics is driven by model assumptions, and therefore excluded from this analysis. We further excluded drug concentration dependent indices such as maximum concentration, time above a threshold concentration, and the area under the concentration time curve (AUC) because, especially in murine experiments, information on PK variability was missing.

How well the parasite clearance rate could be quantified varied in the murine and human volunteer experimental infection data. In the murine malaria experiments, there is limited repeated blood sampling of each mouse and evaluating progression of infection was limited to measuring percentage of infected RBCs (Fig. 3.2). Additionally, the evidence for delayed clearance of dead parasites after treatment with MMV048 for both murine models [Burgert et al., 2020] indicates that not only drug properties but also the host's ability to clear damaged/dead parasites are factors that are determining maximum clearance rate. In the VIS studies, drug treatment is typically administered at an earlier time-point at a lower parasitemia, when volunteers are typically asymptomatic. Thus, data from these studies are collected at parasitemia levels up to five logs below those studied in endemic settings, a factor that may confound analysis of maximal

parasite clearance.

We were able to compare drug efficacy as parasite clearance across the murine and human infection experiments measuring drug efficacy throughout antimalarial drug development because the models formally considered experimental background (parasite-host combination and experimental procedures) and parasite dynamics. Across the mathematical models of parasite growth and treatment, we found that different levels of detail between the preclinical and clinical infection experiments were required to capture parasite growth and thus drug effect. In the mechanistic models of murine malaria infection, high-parasitemia and RBC clearance mechanisms necessitate inclusion of host-cell dynamics in the models. Parasite-host dynamics were influenced by either rapidly increasing parasite load (in the case of *P. berghei*-NMRI infection) or the experimental set-up including the continued human erythrocyte injections (in the case of *P. falciparum*-SCID infection).

However, in VIS, explicit description of host-cell dynamics is not required due to lower parasite load and relatively short infection follow-up. This means, as patients are treated due to safety reasons when parasitaemia reaches a certain level, only few parasitaemia measurements during the initial growth phase are available and any effect of immune response on parasite dynamics is likely to be minimal, thus obviating the need to consider host responses in this model. Furthermore, due to the significant variability in parasite growth observed in the murine experiments, the parasite-growth models required calibrated parasite fitness parameters to capture differences between laboratories, as well as unmeasured differences in virulence of parasites transferred from donor mice in each experiment (ability of the parasite to infect new RBCS). Similarly, in VIS, parasite growth and synchronicity were dependent on the distribution of viable parasite life-cycle stages at inoculation, and models required estimates of these age distribution to recover observed oscillations.

For drug dynamics, we evaluated different pharmacodynamic models to capture the observed parasite clearance in murine and human infection. In murine experiments, delayed clearance of parasites damaged/killed by the drug and drug action through a turnover model were identified. Although *in vitro* experiments reported slight stage-specificity of OZ439 [Charman et al., 2011], with an increased action against trophozoites and schizonts, data was too sparse in the VIS study to inform a detailed analysis. We did not find evidence of delayed clearance of damaged or dead parasites [Khoury et al., 2018] for the two compounds analysed. However, this could change for other antimalarials depending on the mode of action, parasite load and data resolution.

Our estimated value of 17.0 (95% credible interval: 15.3 - 20.0) for the multiplication factor of the parasite every 39h life cycle in human is comparable to previous estimates of 16.4 (95% confidence interval: 15.1 - 17.8) [Wockner et al., 2019] and 21.8 (95% credible interval: 17.6 - 26.9, at a life cycle length of 42 h) [Cao et al., 2019] in VIS studies. The growth of parasitemia has been modelled using a variety of methods e.g. testing statistical models for quantification

[Wockner et al., 2019], assays for *in vivo* determination [Murray et al., 2017] and linking it to disease severity [Chotivanich et al., 2000]. However, we found a potential issue of statistical parameter identifiability for this rate where the intrinsic parasite multiplication rate exhibits weak identifiability and strong correlation with the parasite death rate. Nevertheless, we decided to maintain both dynamics, an intrinsic growth rate and parasite death rate in the model instead of a net growth rate to capture differences between cohorts and individuals, and to highlight gaps in knowledge. In theory, the synchronous parasite growth in VIS could inform these two parameters if information on parasite age-distributions throughout the parasite life cycle is collected [Greischar et al., 2019]. However, this information was not available in the cohorts analysed and in practice may be difficult to obtain. As parasite numbers after treatment are very low in VIS, the role of immunity for successful treatment is unknown from these studies. However, further analysis and modelling could combine information on parasite growth in clinical field trials in pre-exposed patients [Kingston et al., 2017; Douglas et al., 2011; O'Flaherty et al., 2019]. Thus potentially allowing the estimation of the effect of the immune system on parasite growth and clearance of new drugs to inform dosing recommendation.

The necessity for timely decisions regarding the progression of antimalarial compounds to the next experimental stages and design of future experiments might not allow for an extensive analysis of data through mechanistic models for each drug. However, the mechanistic models developed and validated in the context of this study could serve as a tool to assess potential influences stemming from parasite-host dynamics and help to improve the experimental design of future experiments providing more depth than the analysis of experimental data alone.

All three experimental systems are invaluable for compound selection; however we are currently not able to translate parasite clearance measures between the experimental systems. Our modelling shows that there are different underlying parasite-host dynamics in each system that influence experimental analysis and thus PRR results. A reliable strategy to translate efficacy measures and gain insights from drug-parasite-host dynamics between the development stages has not yet been identified.

As with all drug development, preclinical and early clinical testing of new antimalarial is expensive, especially when we consider the need to identify appropriate combination therapies in *P. falciparum*-SCID experiments [Rottmann et al., 2020] and *P. falciparum*-human infection in VIS [McCarthy et al., 2019]. We suggest that the value of *in vitro* data should be revisited in antimalarial development to support cost-efficient translation between experimental systems, candidate selection, and to inform early clinical dosing in real-life settings. By using mechanistic parasite growth models, we were able to understand these influencing mechanisms, and quantify them. This highlighted that we can compare antimalarial drugs within a system but to translate findings along the drug discovery experimental systems requires alternative strategies.

3.4 Materials and Methods

Data, parasite growth and PKPD models in murine experiments

Models of murine malaria infection (Fig. 3.2) were calibrated to extensive parasite growth data and subsequent treatment with multiple antimalarial drugs (Table 3.1). Here, we briefly present the base structure (*model a*) of the ordinary differential equations for the murine malaria infection model as specified in [Burgert et al., 2020]. Parasite growth within the host is described by ordinary differential equations capturing dynamics of uninfected murine host RBCs ($X_{m(murine)}$), infected RBCs (Y_{Xm}) and merozoites (M). RBC dynamics are incorporated with constant production ν [cells/h] and decay rate μ [1/h] and become infected through invasion with merozoites dependent on the infectivity parameter β [cells/mL h].

$$\frac{dX_m}{dt} = \nu - \mu_{X_m} X_m - \beta X_m M \tag{3.1}$$

Infected RBCs (Y) burst after $1\backslash\alpha$ hours to release r new Merozoites that die with rate δ [1/h]. The aging of the parasite throughout the parasite-life cycle is incorporated via n transit compartments.

$$\frac{dY_{Xm,i}}{dt} = \beta X_m M - \alpha Y_{Xm,i} \tag{3.2a}$$

$$\frac{dY_{Xm,i}}{dt} = \alpha Y_{Xm}, i-1 + \alpha Y_{Xm,i}, i = 2, ..., n \tag{3.2b}$$

$$\frac{dM}{dt} = -\beta(X_m + Y_{Xm})M + \alpha r Y_{Xm,n} - \delta M \tag{3.3}$$

The parasitemia, as percentage of infected RBCs, is calculated by summing over the parasite age-stages and dividing by the total number of RBCs:

$$Y_{Xm} = \sum_{i=1}^{n} Y_{Xm,i} \tag{3.4}$$

$$P = 100 \frac{Y_{Xm}}{X_m + Y_{Xm}} \tag{3.5}$$

The initial number of infected RBCs is informed by the inoculum size, its viability ω and the mouse blood volume V_n.

$$Y_{Xm,0,i} = \omega \frac{inoculum}{V_n} \tag{3.6}$$

For reference, population models for murine parasite growth and drug treatment were estimated via a maximum likelihood approach on trust region optimisation.

Data, parasite growth and PKPD models in human VIS experiments

Data in VIS

Parameters for the parasite growth models were estimated using previously published [Wockner et al., 2019] parasite growth data from 177 malaria-naïve healthy volunteers enrolled in 27 cohorts as part of 14 VIS studies. Briefly, volunteers were inoculated intravenously on Day 0 with human erythrocytes infected with *P. falciparum* (3D7 strain). Treatment commenced on day seven to nine after infection. Parasite growth was monitored using a quantitative PCR assay (*P. falciparum* 18S rRNA gene). Specifics of parasite growth monitoring and data processing can be found in [Wockner et al., 2019].

Parameters for drug efficacy were estimated from parasite clearance data (Table S3.1) collected from volunteers administered single doses of OZ439 (artefenomel) [McCarthy et al., 2016c] (Cohorts 4, 5, and 6) and MMV048 (Cohorts 15, 16, and 27) [Sinxadi et al., 2020]. In the MMV048 cohorts, gametocyte concentration data were also available, where parasite measurements were discarded if the gametocyte count exceeded 10% of the total parasite count. Further details of the data and clinical trial identifiers are given in Table S3.1. All data was previously published [McCarthy et al., 2016c; McCarthy et al., 2020]. As previously reported, all studies were approved by the QIMR-B Human Research Ethics Committee and all subjects provided informed consent [Wockner et al., 2019].

Pharmacokinetic models of OZ439 and MMV048 in VIS

Human Population pharmacokinetic (PK) modelling of the OZ439 and MMV048 concentration versus time profiles was performed using Monolix (Version Monolix 2018R1). A 2-compartment PK model with zero order absorption (Equation S3.1) best described MMV048 concentrations and a 2-compartment PK model with first order absorption described the OZ439 concentrations (Equation S3.2). Structural PK model specifications and individual parameter can be found in Appendix B, Supplementary File 3.1.

Mathematical models of within-host parasite growth and post-treatment parasite clearance in VIS

P. falciparum-human infection is described via difference equations able to capture the changing age-structure of the parasitemia over time. The difference equations for *model S* (Equations 3.7 to 3.9) and *model i* (Equations 3.10 and 3.11), with incorporated drug action as specified in the Results section are given below (Equations 3.7 to 3.11). We estimated parasite growth and treatment effects in a two-step sequential process. Firstly, parasite growth parameters were estimated from parasite growth data before treatment. Secondly, we fixed the individual

Table 3.3: Parameters of the parasite growth and treatment models. The bounds for parameter estimation were set to include all plausible values based on previously published models [Zaloumis et al., 2012; Zaloumis et al., 2018; Dini et al., 2018; Cao et al., 2019].

Parameter	Unit	Description	Bounds [lower, upper]
i_{pl}	[p/mL]	Parasite density four days after inoculation (log transformed)	[1, 15]
μ_{ipl}	[h]	Mean of the initial parasite age distribution	[5, 10]
σ_{ipl}	[h]	SD of the initial parasite age distribution	[2, 20]
δ_p	[1/h]	Drug independent parasite death rate	[0.001, 1]
r_p	[-]	Parasite replication rate	[40, 80]
α_l	[h]	Length of the parasite life cycle	fixed to 39 h
α_s	[h]	Sequestration age of asexual parasites	fixed to 25 h
pmf	[]	Parasite multiplication factor	-
EC_{50}	[mg/mL]	Drug concentration causing 50% of E_{max}	MMV048: [0.001, 0.8] OZ439: [1E-6, 0.1]
E_{max}	[1/h]	Maximum effect of the drug	[0.0001, 1]
γ	[]	Hill-coefficient, steepness of the C-E curve	-
k_{ret}	[1/h]	growth retardation due to drug treatment	-
$k_{ret,max}$	[1/h]	Maximum growth retardation	[0.0001, 1]

posterior median of parasite growth parameters and individual PK parameters to estimate parameters of drug efficacy (Fig. 3.1a). Treatment effect E incorporates parasite death through treatment as an increase in parasite death rate δ_p. The evaluated treatment models include a direct drug effect model and additional drug induced growth retardation causing a lengthening of the parasite life cycle length α_l. Model output of *model S* is the number of circulating parasites P_{circ} (Equation 3.14). The parasite multiplication factor *pmf* can be calculated for *model S* using the intrinsic parasite multiplication rate r_p and death rate δ_p. Details of the parameters are provided in Table 3.3.

Model S, mechanistic asexual parasite growth model incorporating parasite stages and drug effect:

Our mechanistic model of growth of parasite density P, over the life cycle of length $\alpha_l = 39$ hours, at age α and time t is given by:

$$P(\alpha, t) = \begin{cases} P(\alpha - 1, t - 1)e^{-\delta_p}, \alpha = 2, 3, ..., \alpha_l \\ r_p P(\alpha_l, t - 1)e^{-\delta_p}, \alpha = 1 \end{cases} \tag{3.7}$$

The direct drug effect on this model is incorporated via E (Equation 3.12) representing the

drug-concentration dependent increase of parasite death rate δ_p.

$$P(\alpha,t) = \begin{cases} P(\alpha-1,t-1)e^{-\delta_p-E}, \alpha = 2,3,...,\alpha_l \\ r_p P(\alpha_l,t-1)e^{-\delta_p-E}, \alpha = 1 \end{cases} \tag{3.8}$$

The direct drug effect model is extended to include drug concentration dependent growth retardation.

$$P(\alpha,t) = \begin{cases} P(\alpha,t-1)k_{ret}\frac{1-e^{-\delta_p-E-k_{ret}}}{\delta_p+E+k_{ret}} + P(\alpha-1,t-1)e^{-\delta_p-E-k_{ret}}, \alpha = 2,3,...,\alpha_l \\ P(\alpha,t-1)k_{ret}\frac{1-e^{-\delta_p-E-k_{ret}}}{\delta_p+E+k_{ret}} + r_p P(\alpha_l,t-1)e^{-\delta_p-E-k_{ret}}, \alpha = 1 \end{cases} \tag{3.9}$$

Model i, exponential parasite growth model incorporating drug effect:

Parasite growth for the exponential *model i* is modelled on the logarithmic scale with the initial parasite concentration P0 and parasite growth rate p_{gr}.

$$ln(P(t)) = P_0 + p_{gr}t \tag{3.10}$$

Treatment is included by decreasing parasite growth rate:

$$ln(P(t)) = P_0 + \int_0^t p_{gr} - E \tag{3.11}$$

Additional equations:

In both models, drug effect is given by E:

$$E = \frac{E_{max}C^\gamma}{EC_{50}^\gamma + C^\gamma} \tag{3.12}$$

and growth retardation in mechanistic *model S* by k_{ret}:

$$k_{ret} = \frac{k_{ret,max}C^\gamma}{EC_{50}^\gamma + C^\gamma} \tag{3.13}$$

The maximum possible parasite age stage prolongation is therefore given by $60\frac{1}{1-k_ret,max[h^-1]} - 1[h]$ where one hour is the original length of the age stage and 60 converts hours into minutes. In *model S*, the number of circulating parasites is given by summing parasite concentration up to the parasite-age stage α_s after which parasites sequester

$$P_{circ} = \sum_{\alpha=1}^{\alpha_s} P(\alpha,t) \tag{3.14}$$

The parasite multiplication factor over one parasite life cycle with length α_l for *model S* is given by

$$pmf = p_{gr} e^{-\delta_p \alpha_l}. \tag{3.15}$$

The parasite growth rate p_{gr} of exponential growth model i results in a parasite multiplication factor of:

$$pmf = e^{-p_{gr} \alpha_l}. \tag{3.16}$$

Under the assumption of exponential parasite growth (*model i*), the minimum inhibitory concentration, where parasite replication equals zero can be calculated with:

$$MIC = EC_{50} \left(\frac{p_g r}{E_{max} + p_{gr}} \right)^{\frac{1}{\gamma}}. \tag{3.17}$$

Parameter estimation

Parasite growth and pharmacodynamic parameters for humans were estimated in R (Version 3.6.0) with package RStan (Version 2.18.2 [Stan Development Team, 2020]) using a Bayesian hierarchical modeling approach. In brief, this means that subject and/or trial dependent parameters were defined as a second hierarchy level in addition to the population parameters. Parameters were estimated using a non-centred parameterisation approach [Papaspiliopoulos et al., 2007] and then transformed using inverse logit transformation within pre-specified lower and upper bounds [Stan Development Team, 2018] based on biological background information (Table 3.3). Prior distributions for the population mean parameters were given by standard normal distributions before the logit transformation. Priors for the inter-individual variability were defined by the Cholesky factors of the correlation matrices using a Cholesky LKJ correlation distribution with shape parameter of 2 for efficiency and computational stability [Stan Development Team, 2018]. We ran five chains with 4000 iterations each of which 2000 were used as a burn-in. The posterior samples were cumulated over all chains to illustrate the joint and marginal posterior distributions in Fig. S3.7 to S3.12. The 95% credible interval of each parameter is given by the 2.5% and 97.5% quantiles of the posterior distribution (Fig. S3.3 to S3.6). The M3-method was used for dealing with parasite measurements below the lower limit of quantification of 111 p/mL. Models were evaluated using the R-package bayesplot (Version 1.6.0) and loo (Version 2.1.0), and model selection was based on the Watanabe-Akaike information criterion (WAIC, [Watanabe, 2010]), and the effective sample size n_{eff}, an estimate of the number of independent draws from the posterior distribution. n_{eff} was required to be over 0.1 for all parameters. Additionally, divergences in any of the chains was evaluated visually and the convergence criteria $\hat{R}$ was calculated (potential scale reduction statistic should be less than 1.05). Posterior predictive checks were performed to visually assess how well the model fits the parasitological data.

Model simulation and analysis: PRR

We used the well calibrated models to estimate efficacy index PRR for a range of drug doses and regimes in both murine and human testing systems (Fig. 3.1b: PRR analysis). Simulation and subsequent analysis of murine *P. berghei*-NMRI and *P. falciparum*-SCID infection was executed in a pooled manner: one set of parameters was drawn and simulated over all doses for each experiment. Population parameter distributions are defined as a log-normal distribution LN(μ, 0.2μ) with the previously estimated mean μ (see Table S3.5 for a summary) [Burgert et al., 2020]. The experimental parameters infectivity parameter β and initial percentage of human RBCs H_0 were drawn from the pool of estimated parameter values. Simulations were performed using R-package IQRtools (Version 0.9.999). *P. falciparum*-human infection was simulated with parameter variability implemented on a trial and subject level. Within one trial subjects were allocated the subject-specific parameters i_{pl} and δ_p and shared the parasite related parameters μ_{ipl}, σ_{ipl} and r_p. Parameters were drawn from the estimated variance-covariance within the bounds specified for estimation (Table 3.3). Simulations were performed in R. Human PK parameters were fixed to population level parameters. Additional information on the simulations can be found in Table S3.4. Parameters not previously estimated were fixed to values previously reported [Burgert et al., 2020; Wockner et al., 2019]. Simulation results were processed to extract PRR as described in [Flegg et al., 2011]. Potential lag phases after treatment at the beginning of the clearance curve and tail phases at the end of the clearance curve are excluded from analysis as described in [Flegg et al., 2011]. The clearance rate is extracted from the clearance curve on the log scale using linear regression and corresponds to the slope of the parasite clearance curve.

Model simulation and analysis: sensitivity of PRR to host-parasite and drug dynamics

A global sensitivity analysis was performed to assess the sensitivity of PRR to the parameters describing drug action and parasite growth. We performed a global sensitivity analysis by decomposition of the variance of model output (in this case PRR) via sobol analysis [Sobol, 2001]. Calculation of the first order indices and total effect indices for all model parameters allows assessment of individual and combined parameter contributions to the variance of PRR across the whole parameter space [Zhang et al., 2015]. As sobol analysis is computationally intensive due to the required number of points across the input parameter space (n=200000) and bootstrap replicates (n=1000), we reduced computational time needed to simulate the parasite-PK-PD models by training emulators of the original models. We thus trained a Gaussian process model on simulation output for each of the parasite-growth models and doses analysed using R-packages hetGP (Version 1.1.2). We normalised input parameters and output to be between 0 and 1 due to the large differences in scales. The criterion for acceptance of our trained model

was out of sample prediction with a predictive accuracy of R^2 >0.97. The sensitivity analysis was performed using the function *soboljansen* in the R-packages *sensitivity* (Version 1.16.2) on the trained Gaussian-process model. Parameters contributing under 1% were excluded from further analysis. Remaining parameters were summarised into parameters of host, parasite, host-parasite, and drug dynamics for the visualisation of results according to Table 3.2.

Data availability

The datasets analysed during the current study are available from the corresponding author on request and with permission of Medicines for Malaria Venture.

Acknowledgments

We acknowledge and thank our colleagues in the Swiss TPH Disease Dynamics unit, and our collaborators at MMV, QIMR-Berghofer and University of Melbourne. The work was funded by the Swiss National Science Foundation through SNSF Professorship of MAP (PP00P3_170702). Calculations were performed at sciCORE (http:\\scicore.unibas.ch\) scientific computing center at University of Basel. JA Simpson is supported by an Australian National Health and Medical Research Council Senior Research Fellowship (1104975).

Chapter 4

Antimalarial drug development and the missing indices for cure

Lydia Burgert[1,2], Tamsin Lee[1,2], Theresa Reiker[1,2], Jörg J. Möhrle[1,2,3], Nathalie Gobeau[3], Melissa A. Penny[1,2]

[1]Swiss Tropical and Public Health Institute, Basel, Switzerland
[2]University of Basel, Basel, Switzerland
[3]Medicines for Malaria Venture, Geneva, Switzerland

Abstract

In the face of rising resistance against the current first-line treatment against malaria, the timely development of new compounds and regimens is more urgent than ever. Throughout the antimalarial development process, drug efficacy indices that quantify the parasiticidal effect are used to evaluate and select new drug candidates. In translational drug development stages, the drug efficacy indices are translated between experimental stages to ultimately predict curative doses in humans. Here, we provide an overview over the commonly used indices, their definition and measurement, and discuss their suitability to capture and translate drug efficacy. We argue that the different host-parasite pairings employed in *in vitro* and *in vivo* experiments and experimental singularities pose substantial challenges in the translation of drug efficacy indices from one stage to the next, thereby compromising the degree to which new promising antimalarial compounds can be evaluated and selected. We propose a new paradigm to capture drug efficacy in antimalarial drug development that builds on a thorough understanding of the mode of action of parasite killing. Through collaborations between multiple stakeholders, we envision a new, integrated approach to antimalarial testing that includes an experimental design tailored to subsequent analysis plans and that harnesses the advantages of modelling and simulation informed drug development from the earliest stages of drug development.

4.1 Introduction

Each year, *Plasmodium falciparum* malaria, transmitted by *Anopheles* mosquitoes, leads to around 228 million cases and takes the lives of 405 000 individuals, 67% of them in children under five years [WHO, 2019]. In addition to vector control, malaria burden is reduced by chemoprevention, and malaria mortality prevented through treatment of symptomatic individuals [Bhatt et al., 2015]. Treatment with antimalarial drugs prevents progression of clinical malaria to a severe presentation or death by a timely and enduring reduction in parasite load. The introduction of antimalarial artemisinin combination therapy (ACT) occurred in 2001, and since 2009, the WHO has recommended several highly effective, fixed dose ACTs as first line treatments against blood-stage malaria. ACTs consist of a three-day regimen of an artemisinin derivative paired with a partner drug covering two asexual life cycles of the *P. falciparum parasite* (ca. 96 h) [WHO, 2015b] (Fig. 4.1). However, the continued success in antimalarial treatment is threatened by incomplete adherence to multiple-day regimen and the emergence and spread of drug resistance [Ménard et al., 2016]. Therefore, effective case management of malaria requires continued development of new antimalarial treatment regimens with combinations of compounds which exhibit different modes of action, easier administration, and tailored to the most vulnerable populations.

The success of antimalarial drug development relies on accurately predicting the curative ability of new compounds in patients. Cure (under adequate clinical and parasitological response (ACPR) criteria), is defined as the absence of parasitemia on day 28 in patients who did not previously experience treatment failure, which results in the recrudescence of parasite after treatment [WHO, 2009]. In order to develop successful novel treatments against infectious diseases, product requirements are set to inform candidate molecule selection, and decisions for further development. These criteria are determined by experts and documented in living Target Product Profile (TPP), and Target Candidate Profile (TCP) documents [Burrows et al., 2017; *WHO Target Product Profiles*].

For the development of antimalarial treatments against asexual (blood-stage) *P. falciparum* parasites, these criteria include general guidance on efficacy, duration, and safety of treatment of clinical cases, and aim to enhance adherence and therefore ensure adequate curative ability (percentage of subjects cured after treatment) for resistance mitigation. The development of new treatments requires the screening of molecules and evaluation of potential new compounds in *in vitro* and *in vivo* efficacy experiments [Flannery et al., 2013]. To ensure an efficient development process, clinical requirements for products must be translated to screening and efficacy criteria. Meeting these criteria needs a systematic, target-oriented development process built on a thorough understanding of the dynamics of drug efficacy throughout the development process of new antimalarials. This ensures a streamlined development with efficient resource investment.

After whole-cell or target-based screening of compounds *in vitro* [Flannery et al., 2013], the main evidence for *in vivo malaria* drug efficacy against asexual parasites is provided by the following three experimental systems in a sequential approach, where results from each system contribute to compound and dose selection in the next system (Fig. 4.1):

- infection of mice with the highly virulent *P. berghei* parasite [Jiménez-Díaz et al., 2013];
- infection of immunocompromised, humanized NOD$^{scidIL-2R'c-/-}$ (SCID) mice with *P. falciparum* [Jimenez-Diaz et al., 2009]; and
- infection of malaria-naïve human volunteers with *P. falciparum* in volunteer infection studies (VIS) [McCarthy et al., 2011].

Translational approaches in malaria build on the confidence that the efficacy observed in one experimental system is transferable to the next testing stage. As testing occurs in four different host-parasite combinations (Fig. 4.1), including *in vitro* experiments, evaluating the treatment efficacy for a new drug requires an understanding of the drug action in different contexts. Thus, there is a clear need to quantify and evaluate the influence of host-parasite dynamics on observed drug efficacy in each system and to find meaningful ways to translate efficacy findings to the next development stage. Comparing drug efficacy within the different experimental stages in drug development is facilitated through drug efficacy indices, that summarise the efficacy of the drug (Fig. 4.1, Table 4.1).

For malaria, efficacy indices explored in development are constructed by relating drug doses or concentrations to measured parasite responses such as the speed and concentration-dependency of parasite killing (Fig. 4.1). However, to date, it has been difficult to demonstrate the data measured with the current experimental protocols and the quantitative approaches employed to assess or estimate efficacy indices, are sufficient to support translation [Burgert et al., 2021; Khoury et al., 2020].

In this review, we examine the common malaria efficacy indices in antimalarial development, how they are calculated and assessed with data from current and past experiments, and explore their explanatory power throughout the development process of new antimalarial compounds (Table 4.1). We discuss the implications for predicting drug efficacy in clinical studies and suggest, how the added value of modelling and simulation can be increased to support translation across pre-clinical and clinical development in the future.

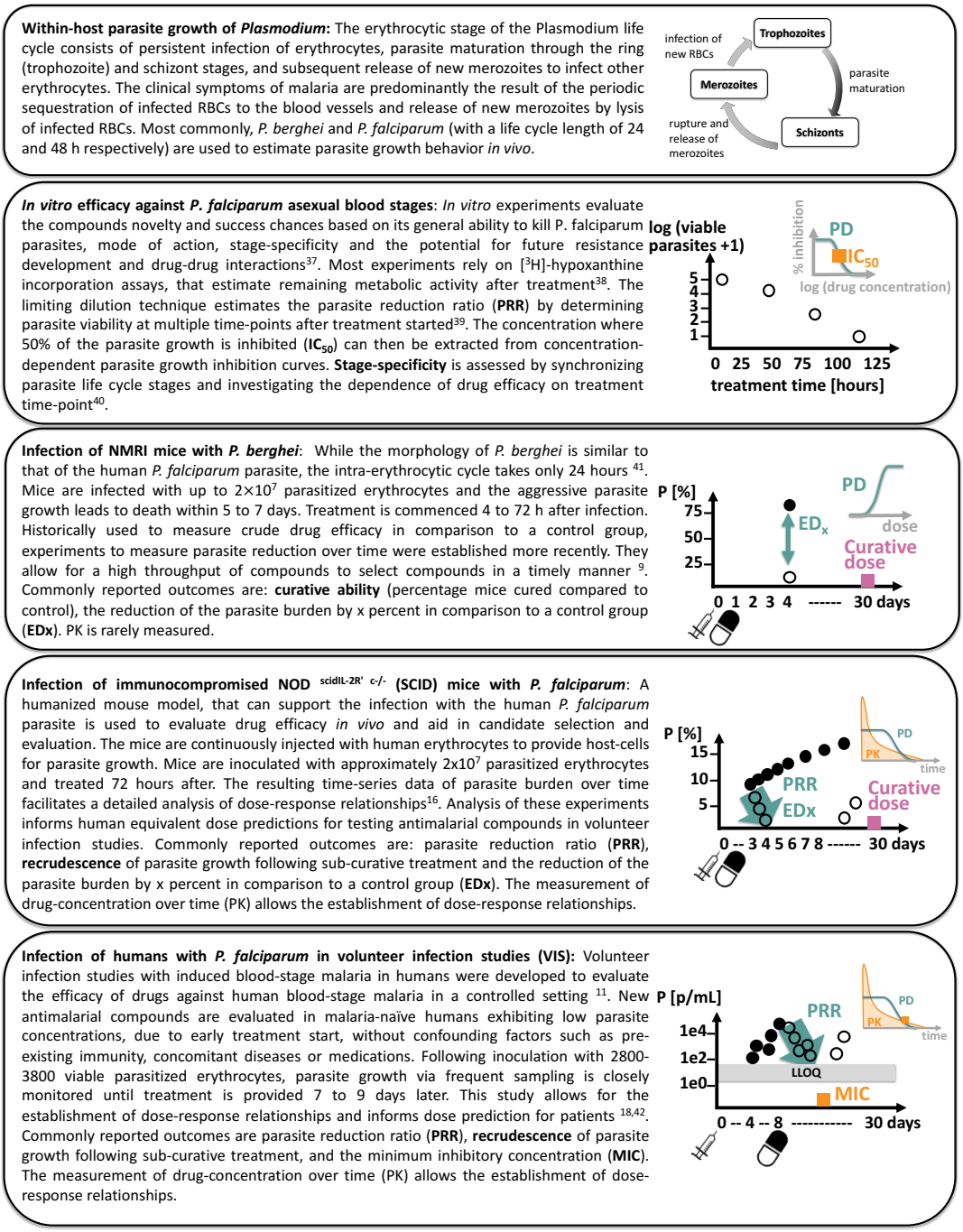

Figure 4.1: Parasite growth and drug efficacy indices used throughout the development process (four experimental stages) of new antimalarial drugs. [1][Murithi et al., 2020], [2][Desjardins et al., 1979], [3][Rosario, 1981], [4][Schleiferböck et al., 2013], [5][Langhorne et al., 2011], [6][Jiménez-Díaz et al., 2013], [7][McCarthy et al., 2016a], [8][McCarthy et al., 2011], [9][McCarthy et al., 2016c], [10][Gaur et al., 2020]. LLOQ-lower limit of quantification

4.2 Efficacy indices for new antimalarials: the barriers preventing translation

There are four groups of efficacy indices discussed in this review: curative behaviour, parasite clearance abilities, timing and period of parasiticidal effect, and pharmacokinetic parameters. Here we outline these, their measurement and complications in quantification and deduce their explanatory power in translating or estimating likely impact.

Curative ability and curative doses

Although estimates of **curative ability** (percentage of subjects cured after treatment) are a commonly used indicator for monitoring drug efficacy in phase 2 and 3 clinical trials and patient populations [Dahal et al., 2017], their ability to capture drug efficacy throughout and across the *in vivo* drug efficacy experiments is limited.

Firstly, the interpretation of curative ability and the ability to infer **curative doses** (lowest administered dose which results in 100% curative ability) are compromised by design of experiments and technical constraints in testing. Murine experiments usually report the dose with the highest curative ability (Table 4.1), which is the administered dose that achieved the highest percentage cure compare to controls in an experiment. However, the determination of curative ability between the two murine experiments is difficult due to the absence of a detailed dose-cure relationship and differences in tested dosing regimens. In contrast, human VIS are not designed to measure cure, as administration of curative doses provides no information on dose effects that can be gained from recrudescence curves after non-curative treatment. Rather, VIS experiments investigate the concentration-effect relationship of parasite clearance and the minimum inhibitory concentration for dose prediction in following clinical trials [Ashley and Phyo, 2018; McCarthy et al., 2016a]. Throughout all experiments, insufficient and inconsistent data on the dose-cure relationship hinder the prediction of curative doses.

Secondly, in both, murine and human experimental malaria infections, challenges exist to assess low parasite concentrations because of parasite quantification thresholds. Thus, there is considerable uncertainty in the limited data, as well as missing observations, that restricts direct analysis of cure and recrudescence dynamics. The lower limit of quantification (LLOQ) for parasites lies around 0.01% [Jiménez-Díaz et al., 2009] parasitised erythrocytes (flow cytometry) or 10-111 p/mL [McCarthy et al., 2016c; McCarthy et al., 2017] (qPCR). Therefore, parasite dynamics in a human under a total parasite load of around 550 000 parasites (qPCR, human total blood volume of 5 liters) or 1,500 000 parasites in a mouse (flow cytometry, murine total blood volume of 1.5 mL) cannot be quantified. Depending on the dose, parasite numbers disappear under the LLOQ 12 to 28 hours after treatment and recrudesce around 4 to 8 days (human)

[McCarthy et al., 2016c] or up to 26 days (mouse) [Burgert et al., 2020] later.

Thirdly, given that cure for all murine and human experiments occurs under the LLOQ, extrapolation by forward prediction of parasite clearance in dependence of drug-concentration is employed to infer curative abilities. Mathematical models of within-host parasite growth that incorporate treatment effects can be used to predict parasite numbers after treatment [Simpson et al., 2014], however there are limitations to their use given collected data. In the models, often a cure event is deemed to have occurred if the extrapolated minimum parasite concentration lies below a previously defined parasite concentration threshold. Generally, the thresholds for cure used to analyse human VIS [McCarthy et al., 2016c] or to predict the influence of imperfect drug adherence were arbitrarily defined [Challenger et al., 2017]. The definition of cure via a threshold concentration is highly unlikely to reflect the true dynamics of cure. Stochastic extinction events and additional influencing factors such as the ability of the individual host immune system to clear remaining parasites influence the probability of cure. To the best of our knowledge, generally, treating parasite clearance behaviour leading to cure as a stochastic process instead of deterministic has not been incorporated in analysis of experimental data.

Parasite clearance indicators

Measures of parasite clearance, summarising total or proportional parasite clearance, are continuously reported along the drug development pathway and are currently used to capture drug efficacy in all experimental stages (Fig. 4.1). They can be estimated directly from the parasite clearance data after treatment [Flegg et al., 2011] or through extrapolation of parasite clearance in modelling approaches [Burgert et al., 2020; Simpson et al., 2014; White, 2017]. However, the inconsistencies in reported parasite clearance indicators between the experimental systems hinder a direct comparison between experimental systems:

In murine efficacy experiments (especially *P. berghei* infection), the main clearance indicator is the **effective doses EDx** (reduction of the parasite burden by x percent in comparison to a control group). Although this can be estimated directly from experimental data, the differences in parasite growth behaviour [Burgert et al., 2020] and numbers of doses administered (Fig. 4.1) between experiments of one development stage hinder comparability across experiments of one development stage. Further, as parasite inocula and parasite growth behaviour differ between *P.berghei*-NMRI infection and *P. falciparum*-SCID infection [Burgert et al., 2020], the comparability of effective doses between development stages is missing. *In vitro* and *in vivo P. falciparum* infection experiments generally report the **parasite reduction ratio** (PRR_{48}, if specified over a parasite life cycle of 48 h) as a primary clearance indicator (Table 4.1). Given data availability, the PRR can be estimated directly from data [Flegg et al., 2011].

Table 4.1: Overview over antimalarials currently under development and the publicly available efficacy indices published throughout their development process. [1][Phillips et al., 2015], [2][McCarthy et al., 2017], [3][Llanos-Cuentas et al., 2018], [4][Phillips et al., 2015], [5][Novartis, 2016], [6][Hien et al., 2017], [7][Nagle et al., 2012], [8][Kuhen et al., 2014], [9][White et al., 2016], [10][Paquet et al., 2017], [11][McCarthy et al., 2020], [12][Charman et al., 2011], [13][Tse et al., 2019], [14][McCarthy et al., 2016c], [15][Ashley and Phyo, 2018], [16][Jiménez-Díaz et al., 2014b], [17][Gaur et al., 2020], [18][Le Bihan et al., 2016], [19][Thaithong et al., 1983]. SD-single dose, QD-quadruple dose.

		DMS265	KAE609	KAF156	MMV048	OZ439	SJ733	CQ
Drug properties	**Mode of action**	PfDHODH inhibitor[1]	PfATP4 inhibition [4]	Not established	PfP14K inhibition	(suspected) oxidative stress	PfATP4 inhibition	Blocking haem detoxification
	Drug class	Triazolo-pyrimidine[1]	Spiroindolone [4]	Imidazolo.-piperazine	Amino-pyridine	Endoperoxide	Quinolone	4-aminoquinolone
***In vitro P. falciparum* assays**	**IC_{50} (strain)**	1.8 ng/mL (3D7) [1]	0.5 nM (NF54) [4]	10 nM (NF54) [7]	28 nM (NF54) [10]	1.9 ng/mL (NF54) [12]	36 nM (3D7) [13]	11 nM (NF54) [18]
	Log10 PRR (strain)	3.1(3D7) [1]	-	-	2.7 (NF54) [10]	-	-	4.5 (3D7) [18]
***P.berghei* in NMRI mice**	**Curative dose** [a]	Not active	100 mg/kg (SD) [4]	100 mg/kg (QD) [8]	30 mg/kg (SD) [10]	20 mg/kg (SD) [12]	-	100 mg/kg (QD) [12]
	ED99[mg/kg]		5.3 (SD) [4]	1.4 (SD) [8]	-	-	-	8.4 (SD) [4]
	ED90 [mg/kg]		2.7 (SD) [4]	0.9 (SD) [8]	1.1 (QD) [10]	2 (SD) [13]	40 (QD) [16]	4.2 (SD) [4]
	ED50[mg/kg]		1.2 (SD) [4]	0.6 (SD) [8]	0.57 (QD) [10]	-	-	1.9 (SD) [4]
***P. falciparum* in SCID mice**	**$Log10\ PRR_{48}$**	-			2.2-2.7 [10]			-
	ED90	3 (QD) [1]			0.57 (QD) [10]		1.9 (QD) [16]	4.3 (QD) [1]
	MIC [ng/mL]	-			71 [10]		-	-
VIS with *P. falciparum*	**$Log10\ PRR_{48}$**	1·55 [2]	1.3-5.84 [5c]		2.6 [11]	4 [14]	4.1 [17]	-
	Parasite clearance half-life	9·4 h [2]	2.5-11.4 h [5c]		5.5 h [11]	3.6h [14]	3.56 h [17]	-
	MIC [ng/mL]	1040 [2]	-		83 [11]	4.1 [14]	122 [17]	-
	Curative ability [b], **(dose)**	0/7, (150 mg) [2]	-		3/8, (80 mg) [11]	4/8, (500 mg) [14]	0/8, (600 mg) [17]	-
Adult patients with *P.falc.*	**$Log10\ PRR_{48}$**	2.9 [3]	3.7 [6]	3.17 [9]		1.8 - 3.7 [15]		-
	Parasite clearance half-life	5.2 h [3]	1.5 h [6]	3.4 h [9]		4.1-5.6h [15]		-
	MIC [ng/mL]	520-1510 [3d]	0.126 [6]	-		-		300 [19]
	Curative ability [b], **(dose)**	11/13, 400mg [3]	3/6, 30 mg [6]	14/21, 800 mg [9]		-		-

[a] curative dose describes the lowest administered dose which results in 100% curative ability, [b] curative ability describes the dose-dependent percentage of subjects cured after treatment ,[c] study was terminated due to severe adverse events ,[d] could not be quantified with certainty due to lower limit of quantification.

However, there is a fundamental problem with quantifying and evaluating parasite clearance from observed data since the measurement of parasite numbers by microscopy or PCR, does not distinguish between dead and alive parasites. Therefore, the observed parasite clearance curves are generated by two overlapping processes: parasite killing and parasite clearance dynamics [Khoury et al., 2020]. Although modelling approaches can support the assessment of parasite clearance through models of within-host parasite growth that close data gaps and allow the calculation of PRR in sparse data experiments [Burgert et al., 2021], to date, models have generally struggled to differentiate between dead and alive parasites due to insufficient data. Both, data analysis techniques and modelling approaches struggle to disentangle these without more detailed information on all factors governing both processes.

Parasite killing is governed by drug action dynamics including the parasite stages present at time of treatment [Flannery et al., 2013; Khoury et al., 2016], the mode of action [Sanz et al., 2012], and potential cumulative drug effects [Cao et al., 2017]. Stage-specificity and the rate of onset of drug action have been linked to the occurrence of lag-times at the beginning of the parasite clearance curve directly after treatment [Sanz et al., 2012]. Furthermore, the mode of action [Sanz et al., 2012] and cumulative drug effects [Cao et al., 2017] influence the steepness of the parasite clearance curve and duration of drug effects.

The clearance patterns observed after treatment is affected by the ability of the host to clear damaged or dead parasites [Khoury et al., 2020]. Parasite clearance is induced by changes in parasite morphology or viability after treatment [Jiménez-Díaz et al., 2014b]. However, its magnitude also depends on the underlying parasite host dynamics and therefore varies between experimental systems [Burgert et al., 2021]. Different scales of infection between murine and human experiments complicate comparison of clearance estimates (Fig. 4.1). Infected mice carry a high parasite burden due to the inoculum size and cycle length (*P. berghei*). In contrast, the timing of treatment in VIS hinders the occurrence of high parasitemia [McCarthy et al., 2011]. Combined with the highest applied dose not chosen to be curative in VIS, the estimation of maximum parasite clearance rate might be compromised.

As parasite killing and parasite clearance dynamics interact, it is challenging to disentangle their individual influence on the estimated parasite clearance curve to extract only the killing effect of the drug.

In summary, the explanatory power of parasite clearance indicators as drug efficacy indicators is controversial as the common assumption of parasite clearance as a single constant rate neglects these time and experiment dependent host, parasite and drug dynamics and wrongly assumes independent processes of drug, host and parasite induced clearance mechanisms [Khoury et al., 2020; White et al., 2017].

Minimum inhibitory concentration

The uncertainties around quantification of parasite clearance below the LLOQ also affect the quantification of the **minimum inhibitory concentration (MIC)**. The MIC defines the drug concentration where parasite replication is equal to one. Hence, during the time where drug-concentration is above the MIC, parasite growth is inhibited by the drug and parasite clearance prevails. When evaluating drugs, the quantification of the MIC is theoretically advantageous as it allows one to infer the cumulative time of parasite killing if the time-concentration profile is known [Ambrose et al., 2007]. Its quantification has long been a goal in drug development efforts [Watson et al., 2018; Hien et al., 2017]. However, a reliable definition and quantification of the MIC is challenging:

Firstly, the MIC lies at the turning point of the parasite clearance curve to the recrudescence curve, which requires both detailed insights into parasite clearance and growth behaviour for quantification. Depending on the experimental set-up (especially in early preclinical development), this data might not be available.

Secondly, MIC evaluation is highly dependent on the lower limit of quantification (LLOQ). At lower dosages, the transition from inhibited parasite growth to recrudescence can lie above the LLOQ, making the MIC directly quantifiable. In contrast, if this turning point lies below the LLOQ, the MIC is deduced through backward projection of parasite numbers starting at the time-point of recrudescence. With more prominence in higher doses, parasite killing through cumulative exposure could shift the estimated MIC to values lower than the actual MIC. Extrapolation under the assumption of exponential parasite growth neglects lags in recrudescence after treatment due to the presence of dormant parasite stages or alterations in parasite growth through sub-MIC drug concentrations [White, 2017]. To date, these potential parasite behaviours are not quantified. As modelling approaches to estimate the MIC need to predict parasite behaviour under the LLOQ, they are not reliably informed.

Thirdly, at low parasitemia levels after effective treatment, the immune system's ability to clear the last remaining parasites could decide between the occurrence of cure or recrudescence. However, quantifying the contribution of the immune system is difficult for the different *in vivo* experiments: whereas the mice infected with the highly virulent *P. berghei* parasite have a functioning immune system, the *P. falciparum* infected SCID mice are immunocompromised. In human VIS, different abilities between individuals to clear remaining parasites [Burgert et al., 2021] could contribute to the observed recrudescence behaviour. Without further knowledge on the dynamics of recrudescence, quantification of the MIC heavily relies on assumptions about parasite growth behaviour and immune system response (or lack thereof) after non-curative treatment.

In summary, evidence on the ability of the MIC to predict curative behaviour is sparsely

reported (Table 4.1) and potential and strength of growth dynamics to influence the estimates are unknown.

Secondary pharmacokinetic parameters

Secondary pharmacokinetic drug efficacy indices such as the **time of maximum drug concentration** and the **area under the concentration-time curve (AUC)** can be linked to antimicrobial effect, such as survival after treatment or curative ability [Drusano, 2004] to evaluate drug efficacy. They were predominantly used in antibacterial drug development to distinguish between time of exposure or maximum-concentration driven compounds and to adjust dosing regimens accordingly [Craig, 1998].

The adaptation of this principle to antimalarial drug development faces several challenges: In murine experiments, the analysis of drug concentration over time is complicated by practical limits to number of measurements allowed over time due to required blood volume and missing information on variability between mice and experiments. In experimental human VIS, the between-subject variability in drug-concentration in time hinders the establishment of statistically significant relationships. However, filling these data gaps through richer sampling schemes and a higher sample size is costly. Additionally, split dose experiments would be required to distinguish between exposure and maximum concentration driven experimental outcomes. In these experiments, either the exposure or maximum concentration is kept constant over multiple doses to identify the driver of compound efficacy. Through optimisation of the pharmacokinetic profile (formulation, dosing regimen), the impact of the compound can then be improved.

4.3 Where can we go from here?

The main purpose of the drug efficacy indices discussed above is to enable the comparison of new candidate molecules and select them for the next experimental stage. They offer the opportunity to quantify, compare and evaluate antimalarial killing effects between compounds from the same drug class within one *in vivo* experimental system (e.g. during the development of new ozonides) [Charman et al., 2011].

However, only the first wave of parasite-growth after non-curative treatment is generally monitored in detail in the *in vivo* drug efficacy experiments (Fig. 4.1). This means that long term disease dynamics of natural infection that are influenced by interactions between parasite growth dynamics and immune reactions are not accounted for in any of the current experimental systems. *P. berghei* growth is highly virulent and deadly within six days, SCID mice are immunocompromised, and lastly human volunteers must be treated before onset of normal disease

symptoms that accompany natural malaria infection. Thus, the experimental malaria infection systems do not fully capture potentially clinically relevant parasite or host behaviour in natural infections.

Furthermore, the drug efficacy indices discussed in this review are difficult to compare across molecules of different compound classes and translation of efficacy or insights from one experimental system to the next is challenging. This is due to factors related to each experimental set-up and lack of general knowledge about parasite-, host-, and drug-dynamics in each of the experimental systems. These include the specific characteristics of each parasite-host combination, including parasite clearance patterns, host-responses to infection and potential parasite-life cycle adjustments. Additionally, to date, the technical constraints in quantifying indices measuring parasite growth dynamics around recrudescence or cure events in each system limit their explanatory power to translate to the subsequent testing system.

The unrealised potential of modelling and simulation

Historically, *in vivo* drug efficacy experiments were designed to directly observe drug efficacy indices (with the implicit assumption that they will be the same across animal species and parasite strains). However, as translation from data alone is limited, more recently modelling and simulation (M&S) approaches have been employed as an additional layer to attempt a translation of drug efficacy in the different experimental systems to treatment success in humans (assuming that the relationship between drug effect and unbound drug-concentration remains the same) [McCarthy et al., 2016a].

Despite its potential to collate and integrate different data into one analysis stream, M&S is often introduced late in the decision-making process, and is also constrained by the historical setup of the experiments. For instance, in translational drug development stages M&S analyses are often expected to facilitate the prediction of drug efficacy in the next experimental stages after the experiments have already been conducted. However, these experiments are designed to inform candidate selection and not to power models to analyse treatment dynamics and enable prediction of drug efficacy in the following development stage. The data is proving to be mostly insufficient, and the added value of M&S analysis has not yet reached its full potential.

Without appropriate data, translation of drug efficacy becomes challenging as too many assumptions are required to adequately inform decision making. For instance, pharmacokinetic data is often not recorded in *P. berghei*-NMRI infection, hindering the combined analysis of drug-concentration and parasite load. Additionally, it is not possible to reliably quantify drug efficacy indices such as the MIC given sparse data, and missing insights into the impact of parasite-host dynamics and the influence of cumulative drug exposure linked to the mode of drug-action. To date, the mechanism of drug-action and parasite-host dynamics are not routinely incorporated

into the analysis of drug efficacy, as insufficient data or knowledge is gathered to allow this. This leads to confounded drug efficacy estimates that are not translatable between experimental stages [Burgert et al., 2021].

A new paradigm for the translation of *in vivo* drug efficacy

Altogether, there is a need for systematic incorporation of further data and M&S into antimalarial drug development in an effort to support translation. This leads to a proposal of a modified approach for drug efficacy analyses during antimalarial drug development, that builds on a mechanistic understanding of drug action and constructs experiments noting the supportive role M&S will have for candidate selection and translation (Fig. 4.2):

Firstly, the *in vitro* concentration-effect relationship should be established by inclusion of the mechanism of drug-action and the dependence of parasite killing on the unbound drug-concentration (Fig. 4.2a). Knowledge on mode of action-based parasite killing allows to mechanistically capture parasite killing and establish a profile of drug-effect over time that includes lag-times, parasite stage-specificity, and cumulative drug effects. Additionally, it facilitates the classification of dead and alive parasites in parasite clearance curves. These modes of action include mechanisms such as the interruption of a metabolic pathway leading to starvation or the accumulation of toxic products.

Next, experiment specific within-host parasite growth dynamics are captured in mechanistic models of parasite growth. To do this well, strong and well-validated models of parasite growth in each experimental testing system in the absence of drugs need to be established. For testing of drugs, the concentration-time relationship in the respective host is subsequently quantified (Fig. 4.2b). The prediction of *in vivo* drug efficacy is facilitated through a combination of mechanistic descriptions of parasite-growth and drug-concentration in the respective experimental system with mechanism of action-based parasite killing models (Fig. 4.2c). Whereas traditional dose-response relationships previously used in antimalarial drug development [Simpson et al., 2014] are data-driven and lack biological explanations of parasite death, this new approach is based on a mechanistic understanding and description of parasite-growth as well as drug action. Beyond the quantification and prediction of drug efficacy, the incorporation of the detailed mechanism of action allows the effective combination of compounds for antimalarial combination therapy by pairing drugs with complementary modes of action and assessing the threat of resistance development. Within this framework, the experiments that support the prediction of drug efficacy throughout drug development are tailored to inform later analyses. We thereby move away from the status quo, where experimental design and procedure are often disconnected from the later analysis.

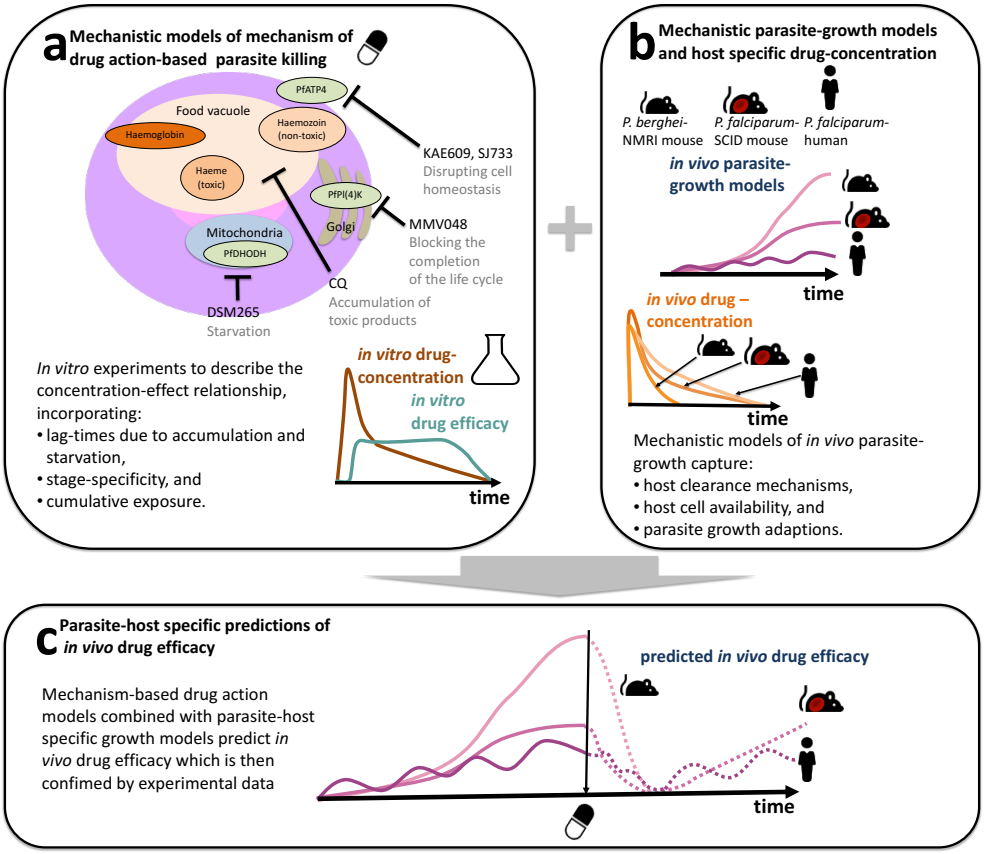

Figure 4.2: Schematic of the strategy to incorporate mechanism of action-based parasite killing into the analysis of in vivo drug efficacy experiments. (a) The mechanism of action-based parasite killing is investigated through *in vitro* experiments. Shown here are four exemplary mechanisms of drug-action of new or historical antimalarials (see also Table 4.1): DSM265 blocks the pyrimidine biosynthesis through inhibition of PfDHODH [Phillips et al., 2015]. Chloroquine (CQ) blocks the degradation of toxic haeme (intermediate product during the haemoglobin metabolisation) [Wunderlich et al., 2012]. MMV048 blocks the completion of the parasite life cycle through inhibiting *P. falciparum* phosphatidylinositol-kinase (PfPI(4)K), needed during ingression [McNamara et al., 2013]. KAE609 and SJ733 inhibit *P. falciparum* p-type ATP-ase 4 (PfATP4) needed for Na+ homeostasis during nutrient intake [Jiménez-Díaz et al., 2014b; Huskey et al., 2016]. **(b)** The drug-specific mode of action for each drug can be accounted for in mechanistic models of parasite killing. Thus, the concentration-dependent description of their parasite killing abilities incorporates, where appropriate, lag-times after dosing due to the accumulation of toxic products or starvation mechanisms, stage specificity, and/or the effect of cumulative drug exposure over time. **(c)** These models can then be coupled with host-parasite combination specific descriptions of *in vivo* parasite-growth and drug-concentration to inform parasite-host specific predictions of *in vivo* drug efficacy. The advantage over commonly used approaches to analyse drug efficacy is the use of mechanistic drug-action models. In contrast to data-driven empirical approaches to describe drug action, this approach is able to distinguish the sole effect of drug action on the parasite (mechanistic model of drug-action) from the parasite-host dynamics (mechanistic model of parasite-growth). If the mechanism of action cannot be determined *in vitro*, the different drug action and parasite growth models with could be used to explore possible explanations via model selection and sensitivity analysis, provided extensive data is available. The illustration of drug action (left upper panel a) is adapted from [Phillips et al., 2017].

However, this new approach to analyse drug efficacy during drug-development can only be realised through the design of experiment protocols that target both the need to screen and select promising candidates, but that also maximise chances of obtaining the information needed for translation through recognising the added value of M&S. This aim can only be achieved through strong collaborations between multiple stakeholders including infection biologists, drug developers, translational scientists, clinicians, and modellers. A careful assessment of current screening and efficacy protocols alongside what additional information could be realised with M&S, will enable a stronger approach to translational antimalarial drug development by supporting the optimisation of experiments for screening, candidate selection criteria and ultimately human dose prediction. The systematic engagement of M&S early in development promises to maximise the exploitation of information from each experiment and optimise the time needed for translational analysis and decision making along the development pathway. Any new or additional experiments would then be prioritised in the most promising candidates. This may result in a tiered approach of experiments with large scale initial screening of many compounds, and then more extensive data collection for potential candidates. A process will also need to be added for candidates where the mode of action is unknown so far, eg. KAF156 [Kuhen et al., 2014].

Conclusion

We have highlighted and discussed the strengths and drawbacks of different *in vivo* experimental systems and the drug efficacy indices used to evaluate compounds within these systems. These experimental systems have had far reaching success in selecting many promising new antimalarial treatments, however translation between these systems has been challenging and attrition of compounds high. To further support antimalarial development and translation between experiments and enable the prediction of human curative dosing, future efforts should focus on harnessing the added potential of M&S approaches from the earliest stages of development. Now is the time to invest in establishing a stronger experimental and modelling framework that builds on a mechanism-based descriptions of parasite death, and collection of data most informative to the processes currently restricting translation of efficacy indices. Overall, along with the important experimental systems, modelling can improve predictions of drug efficacy, and if used in a holistic approach with all stakeholders, has the potential to accelerate malaria drug development.

Chapter 5

Model informed target product profiles of long acting injectables for use as seasonal malaria prevention

Lydia Burgert[1,2], Theresa Reiker[1,2], Monica Golumbeanu[1,2], Jörg J. Möhrle[1,2,3], Melissa A. Penny[1,2]

[1]Swiss Tropical and Public Health Institute, Basel, Switzerland
[2]University of Basel, Basel, Switzerland
[3]Medicines for Malaria Venture, Geneva, Switzerland

This manuscript has been published in PLOS Global Public Health in March 2022 [Burgert et al., 2022] (https://doi.org/10.1371/journal.pgph.0000211).

The supplementary information can be found in Appendix C.

Abstract

Seasonal malaria chemoprevention (SMC) has proven highly efficacious in reducing malaria incidence. However, the continued success of SMC is threatened by the spread of resistance against one of its main preventive ingredients, Sulfadoxine-Pyrimethamine (SP), operational challenges in delivery, and incomplete adherence to the regimens. Via a simulation study with an individual-based model of malaria dynamics, we provide quantitative evidence to assess long-acting injectables (LAIs) as potential alternatives to SMC. We explored the predicted impact of a range of novel preventive LAIs as a seasonal prevention tool in children aged three months to five years old during late-stage clinical trials and at implementation. LAIs were co-administered with a blood-stage clearing drug once at the beginning of the transmission season. We found the establishment of non-inferiority of LAIs to standard 3 or 4 rounds of SMC with SP-amodiaquine was challenging in clinical trial stages due to high intervention deployment coverage. However, our analysis of implementation settings where the achievable SMC coverage was much lower, show LAIs with fewer visits per season are potential suitable replacements to SMC. Suitability as a replacement with higher impact is possible if the duration of protection of LAIs covered the duration of the transmission season. Furthermore, optimising LAIs coverage and protective efficacy half-life via simulation analysis in settings with an SMC coverage of 60% revealed important trade-offs between protective efficacy decay and deployment coverage. Our analysis additionally highlights that for seasonal deployment for LAIs, it will be necessary to investigate the protective efficacy decay as early as possible during clinical development to ensure a well-informed candidate selection process.

5.1 Introduction

Children carry the majority of the global malaria burden, with an estimated 67% of all malaria related deaths (272 000 in 2019) occurring in those under 5 years of age [WHO, 2019]. In addition to effective and timely treatment, prevention through vector control or drug-based prophylaxis has proven to be an effective approach, reducing incidence and mortality [Bhatt et al., 2015]. Especially in seasonal malaria transmission settings, where malaria transmission is linked to the rainy months, well-timed preventive malaria interventions that protect from infection during the transmission months can ease a substantial amount of malaria burden [WHO, 2019]. The WHO has recommended seasonal malaria chemoprevention (SMC) with monthly Sulfadoxine-Pyrimethamine+Amodiaquine (referred to as SMC SP+AQ) for children aged between 3 months and 5 years during the malaria transmission season since 2012 [WHO, 2012]. SP+AQ provides a two-stage effect: while AQ clears existing blood-stage infections, the long clearance half-life of SP prevents new infections. The impact of SMC in seasonal settings has been widely demonstrated [Baba et al., 2020], achieving a protective efficacy of roughly 80% against clinical episodes in a trial in Burkina Faso [Zongo et al., 2015], a reduction in incidence by 60% in routine implementation in Senegal (80% deployment coverage of all eligible children) [Cisse et al., 2016], and a reduction in the proportion of positive tests by 44% in routine implementation in Mali [Druetz, 2018].

Despite its potential, poor adherence limits the effectiveness of SMC and the spread of drug resistance has potential to limit the effectiveness of SMC. Additionally, the monthly delivery of SMC-SP+AQ (one day of SP and three days of AQ) throughout the transmission season is relatively expensive, due to human resources and especially due to operational constraints during the rainy season [Coldiron et al., 2017]. Consequently, in 2019, only 62% of children living in SMC-eligible areas in the Sahel subregion received SMC [WHO, 2019]. Throughout the transmission season, coverage subsequently decreased by 6% in Guinea [Loua and Milligan, 2019] and 20% in Mali [Diawara et al., 2017]. Investigation of the adherence to the three-pill AQ regimen within one treatment course in a clinical trial in Niger showed that only 20% of children received the full regimen [Ding et al., 2019]. A recent clinical trial reported 93–100% coverage of SMC in Burkina Faso and Mali, which could be considered as part of non-inferiority evaluation for LAIs [Chandramohan et al., 2021]. Additionally, the spread of resistance markers against SP was reported with increasing SMC deployment [Somé et al., 2014; Dieng et al., 2019], impacting the eligibility of regions for SMC [van Lenthe et al., 2019] as well as the protective efficacy after implementation [WHO, 2013].

The need for alternative prevention tools that simplify deployment and possess a reduced risk of resistance is pressing. In the absence of an effective vaccine being deployed, long-acting injectables (LAIs) with an anti-infective effect could provide potential alternative seasonal prevention tools by simplifying the deployment and reducing the risk of resistance through decreased

selection pressure for SP resistance [Macintyre et al., 2018]. LAIs are still in development and thus far from being used and deployed in malarious areas. Current candidate LAIs include small molecule drugs [Bakshi et al., 2018; Yuthavong et al., 2012] or monoclonal antibodies (mAbs) [Kisalu et al., 2018; Tan et al., 2018] that target the sporozoite stage or liver stage of the malaria parasite, thereby serving as anti-infectives. The successful development of a LAI entails the definition of appropriate product profiles and use cases which are specified in Target Product Profiles (TPPs). Precisely, these specifications include LAI efficacy and safety prerequisites as well as delivery modalities [Macintyre et al., 2018]. TPPs are living documents and therefore continuously updated as new evidence for product requirements becomes available.

To justify the implementation of LAIs under the use case of seasonal malaria prevention, non-inferiority to the existing intervention of SMC-SP+AQ must be met [Zongo et al., 2015]. For new tools with new modes of action and/or deployment modalities, proving non-inferiority to the standard of care is a crucial step and is usually established in non-inferiority clinical trials conducted at late stages of tool development. Currently, it is not yet known what clinical studies will be required for LAIs. In absence of efficacy data on LAIs, it is at the current stage impossible to obtain insights about the circumstances in which LAIs have the potential to be non-inferior. *In silico* modelling and simulation approaches of malaria transmission and control, allow the quantification of the impact of varying tool specifications in relation to varying operational and setting constraints which would not be feasible in real life clinical trials. They thus allow for the exploration of the potential to meet non-inferiority criteria. In the absence of non-inferiority evidence at the early stages of development, modelling and simulation approaches therefore provide a quantitative basis to further inform decision making. They guide tool development from the early stages by predicting potential public health impact (Fig. 5.1a) [Golumbeanu et al., 2022] and understanding non-inferiority criteria prior to clinical trial planning. Here, we investigate the potential public-health impact for various use cases of LAIs by conducting an *in silico* simulation analysis examining product properties and operational modalities supporting LAI implementation as a seasonal malaria prevention tool. Accordingly, in the simulated scenarios, LAIs were delivered to children under five once at the beginning of the transmission season with an antimalarial in settings currently approved for SMC deployment.

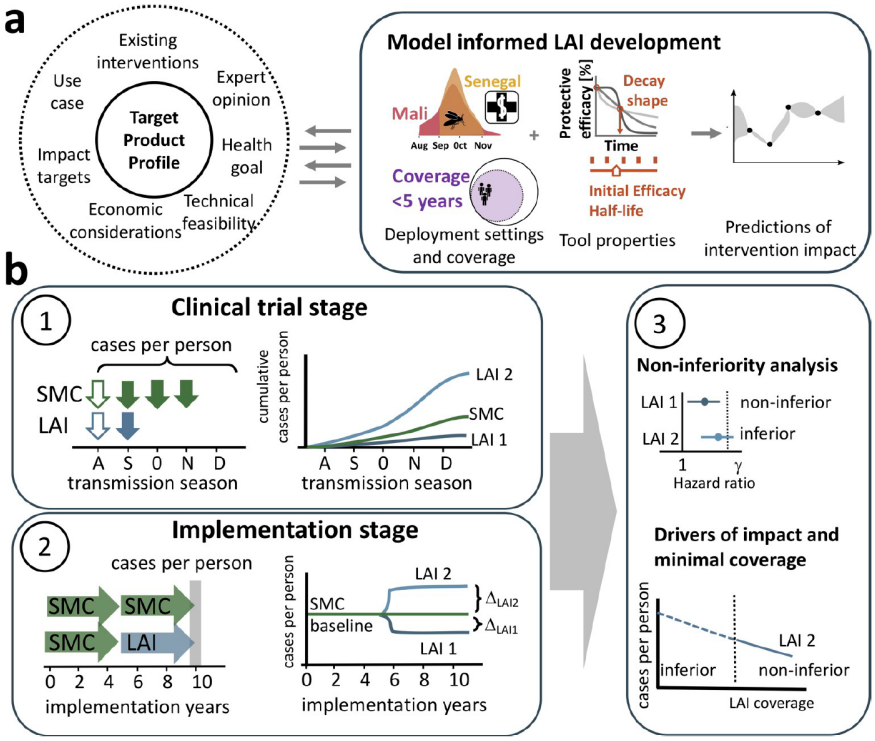

Figure 5.1: Workflow to assess the target product profile of LAIs. (a) In an iterative exchange between various stakeholders, definition of TPPs is informed by results from modelling approaches. Simulation of predefined scenarios with *OpenMalaria*, an individual-based model of malaria dynamics, allows to predict the likely intervention impact (incidence reduction, indicated by the model symbol) of LAIs in the context of deployment setting details (access to healthcare, indicated by the hospital symbol) and seasonality (indicated by the mosquito icon), deployment coverage of the target population and the tool properties (initial protective efficacy against infection, protective efficacy half-life and decay of protective efficacy). The resulting evaluation of LAI impact is communicated and discussed with stakeholders to refine the analysis as LAIs are developed. **(b)** The analysis in the clinical trial and implementation stage are illustrated on the example of two hypothetical LAIs with different efficacy profiles (denoted LAI 1 and 2). (1) In clinical trial stages, the minimum essential properties to reach a certain health goal are evaluated in a two-arm clinical trial. SMC with SP+AQ is administered (green arrows) three time during the months of September (S), October (O), and November (N) (as in Senegal, filled green arrows) or four times as well as in August (A) (as in Mali, filled and unfilled green arrows) times over the transmission season. LAIs are administered once at the beginning of the transmission season (blue filled arrow for Senegal or blue empty arrow for Mali). The cumulative cases per person over the trial period are tracked. (2) In implementation stages, SMC-SP+AQ is replaced with LAIs after five years of implementation. Impact is assessed in the last implementation year (grey bar) and compared to the baseline of SMC-SP+AQ implementation. Coverages of SMC-SP+AQ and LAIs are independent from each other. (3) Upper panel: The tool properties influencing the establishment of non-inferiority of LAIs to SMC are investigated in the clinical trial stage. Lower panel: At a fixed SMC deployment coverage, the minimum coverage of LAI deployment required to establish non-inferiority is identified.

Their protective effect was then compared with SMC-SP+AQ administered three or four times per season in monthly intervals. By combining disease modelling and simulation experiments with machine learning approaches, we efficiently explored the large space of possible parameter values describing intervention and transmission setting characteristics and analyzed tradeoffs between tool characteristics and operational constraints in a variety of transmission settings [Golumbeanu et al., 2022]. We conducted our malaria transmission simulations using *OpenMalaria*, an established individual-based stochastic simulation platform of malaria transmission and control [Maire et al., 2006; Penny et al., 2016]. Based on this approach, we defined a quantitative framework to assess the influence of tool properties and operational constraints on the impact of SMC and LAIs. Using this framework, we investigated two malaria transmission settings based on the malaria transmission profile in Senegal and Mali and assessed public health impact for a plethora of different tool properties, deployment coverages and over multiple transmission intensities. Our analysis was carried out along the clinical development pathway from late clinical trials through to implementation of future LAIs as an SMC replacement. By understanding the main drivers of impact to reach a pre-defined health goal in implementation stages and under operational constraints, we provide an assessment of endpoints in clinical trials of newly developed LAIs and identify efficacy requirements for further development.

5.2 Materials and Methods

The impact of novel anti-infective LAIs depends on the tool properties defining their efficacy profile, as well as on the operational constraints and the respective underlying malaria epidemiology, that influence tool suitability for implementation in a given setting (Fig. 5.1 a). We investigated the influence of tool properties over a large range of specified protective efficacies, as well as operational considerations (coverage of children) in several implementation settings varying in seasonality and access to healthcare. The drivers of predicted impact for preventive LAIs were analysed along their clinical development from clinical trials to implementation (Fig. 5.1 b) and compared with current standard of care (SMC-SP+AQ). Accordingly, we defined two analysis stages: in the *clinical trial stage*, we investigated the maximum incidence reduction and the ability to establish non-inferiority to SMC-SP+AQ over one malaria season (Fig. 5.1 b panel 1). In the *implementation stage*, we replaced SMC-SP+AQ with LAIs after five years of implementation at varying coverages, and we inferred the minimal LAI coverage at which LAIs are equivalent (non-inferiority) in public-health impact (incidence reduction) to a continued implementation of SMC-SP+AQ (Fig. 5.1 b panel 2). We adapted a previously developed framework to inform TPPs of new interventions against infectious diseases [Golumbeanu et al., 2022]. First, a set of simulated scenarios was defined. These were characterized by the delivery modality, tool specifications, and settings in which a concrete health target was analysed (in our case, incidence reduction). Second, a set of disease scenarios were simulated randomly over the entire parameter space to evaluate the health outcomes. The resulting database of simulations

was used to train a Gaussian process (GP) emulator, which predicts the health outcome given a set of input parameters. Third, the emulator was employed to perform sensitivity analysis and optimisation of tool properties with respect to health outcomes. We employed the use of emulators as it would be computational infeasible to simulate over the entire parameter-space, as well as to perform global-sensitivity analysis and utilize iterative optimization algorithms [Reiker et al., 2021]. This analysis allowed us to define the optimal product characteristics of a LAI that maximises the chance of achieving a desired health goal.

Malaria disease transmission model

We explored the dynamics of a preventive LAI against malaria using *OpenMalaria*, a stochastic, individual-based simulator of malaria infection in humans linked to a deterministic model of the mosquito feeding cycle [Chitnis et al., 2012; Chitnis et al., 2008]. *OpenMalaria* accounts for heterogeneity within a human population on multiple levels including host exposure, susceptibility and immune response [Maire et al., 2006; Smith et al., 2006; Ross et al., 2006]. The model allows the investigation of interventions against malaria at multiple points in the malaria life cycle (e.g., vaccination [Penny et al., 2016], insecticide treated bed-nets [Briët and Penny, 2013], and reactive case detection [Reiker et al., 2019]) while monitoring a variety of health outcomes (e.g., prevalence, incidence, and mortality) [Cameron et al., 2015].

Simulated disease scenarios

Using *OpenMalaria*, we simulated a range of transmission settings (Fig. A in Appendix C) and assumptions for the implementation of SMC and LAIs as a seasonal infection prevention intervention replacing existing prevention with SMC-SP+AQ. These assumptions are with regards to the properties of the setting (seasonality and intensity of transmission), health system (access to care and treatment of clinical cases with a first-line ACT), new and replacement intervention (Table 5.1). The intervention age-group consisted of children between 3 months and 5 years of age (accounting for ca. 16% of the total population).

The intervention age-group was chosen according to WHO recommendations [WHO, 2012], although some countries have implemented SMC for children up to 10-years-old [Baba et al., 2020]. We assumed a total population of 10,000 individuals to capture transmission settings within health facility catchment areas with an age-structure that represents a realistic age-distribution for African malaria-endemic settings [Ekström et al., 2016]. Access to treatment, defined as the percentage of the whole population who seek care for a symptomatic malaria episode, was chosen to represent settings with low or high health systems strength. The probability of symptomatic cases (mild or severe) to receive effective treatment within two weeks from the onset of symptoms (E_{14}) was set to 10% in low access to healthcare settings and 50% in high access to healthcare settings [Tediosi et al., 2006]. The malaria seasonality profile, mosquito

Table 5.1: Summary of simulation set-up used for the implementation experiments. The simulated transmission settings were defined using a factorial design covering all possible combinations of discrete health system and vector specifications. The parameters defining the efficacy and delivery profiles of LAIs (highlighted in bold in the third column) were sampled within the defined parameter space using Latin Hypercube Sampling and simulated for each combination of settings. The effective coverage E_{14} describes the probability that effective malaria treatment will occur within a 14-day period since symptoms onset. Additional information on simulated transmission intensity can be found in the Supplement (Appendix C, Fig. S5.1 and Table S5.1). [1] [Penny et al., 2015] [2] [Diouf et al., 2015] [3] [Traore et al., 2020].

	Parameter	Setting	Value					
Health system	Access to treatment (effective treatment coverage[1] E_{14})	High access	0.5					
		Low access	0.1					
	Diagnostics	-	Rapid diagnostic test					
	Malaria treatment	-	First line: ACT Treatment failure/Severe malaria: Quinine					
Malaria transmission	EIR [infectious bites per person per year] and yearly clinical incidence [$cpppy_{0.25\text{-}5y}$]	High access	EIR	5	9	20	47	150
		Long season	$cpppy_{0.25\text{-}5y}$	0.42	1	1.6	2.2	2.9
		Short season	$cpppy_{0.25\text{-}5y}$	0.49	0.95	1.52	2.04	2.83
		Low access	EIR	3	4	8	28	150
		Long season	$cpppy_{0.25\text{-}5y}$	0.41	0.71	1.4	2.4	3.3
		Short season	$cpppy_{0.25\text{-}5y}$	0.45	0.72	1.3	2.3	3.2
	Mosquito species Biting behavior	-	*An. gambiae* 60% indoor biting, 40% outdoor biting					
	Seasonality in malaria transmission [% yearly EIR]			Jul	Aug	Sep	Oct	Nov	Dec
		Senegal-like short season[2]		0	20	60	20	0	0
		Mali-like long season[3]		8	18	50	23	2	0
Interventions	Timing of interventions	Senegal-short season Mali-long season	3x SMC: Sep, Oct, and Nov 4x SMC: Aug, Sep, Oct, and Nov					
	Intervention cohort		3months to 5 years					
	Population treated		**Coverage: [40 - 100] %**					
	Protective efficacy LAI		**Initial efficacy: [70 - 100] %** **Half-life: [30-150] days**					
		exponential LAIs bi-phasic LAIs sigmoidal LAIs	Decay shape: Exponential decay, k=1 (Eq. 5.1) Bi-phasic decay, k=0.69 (Eq. 5.1) Sigmoidal decay, k= 8 (Eq. 5.2)					
	Protective efficacy SMC-SP+AQ		Initial efficacy: 100 % Half-life: 32 days Decay shape: Weibull, k= 5.4 (Eq. 5.1) Adherence declining by 10% over the season					

species and timing of interventions were parameterised to reflect those of Mali or Senegal, two countries in the Sahel region where SMC is implemented and clinical trials for malaria interventions are conducted frequently. In Mali, the malaria season is longer, starting in August and lasting until November (*long season*), and SMC is generally four monthly doses. In contrast, the malaria season in Senegal is only three months long, with a sharper profile (*short season*) and SMC is three doses one month apart (Fig. 5.1, Table 5.1, and Fig. B in Appendix C). Malaria prevalence in Senegal is generally low, with the highest *P. falciparum* prevalence in 2–10 years old ($PfPR_{2\text{-}10y}$) in the southern regions being around 8%. However, the $PfPR_{2\text{-}10y}$ in Mali is around 80% in the south of Mali but very low in the North [WHO, 2020].

To develop a broader understanding of the influence of transmission intensity on LAI impact, we simulated a range of initial incidence settings capturing the transmission heterogeneity of these two malaria-endemic countries (Fig. A and Table A in Appendix C). The simulated transmission intensity of each setting was defined by the entomological inoculation rate (EIR) modelled as the average annual number of infectious bites received by an individual, and the corresponding simulated $PfPR_{2\text{-}10y}$ (Table A and Fig. A in Appendix C). The protective efficacy of SMC-SP+AQ was implemented as being fully effective (no prevalent resistance against SP) or reduced duration of protection (prevalent resistance against SP).

Over all simulation experiments, the input parameter space for the protective efficacy and its decay, and the intervention coverage are as defined in Table 5.1. Parameters were randomly sampled using Latin hypercube sampling [Stein, 1987] by drawing 1500 parameter sets for each setting (capturing combinations of seasonality, health system access, EIR, and SP resistance), with 5 stochastic realizations (simulation replicates) for each point. All simulations were performed using *OpenMalaria* version 38. The source code and comprehensive documentation for *OpenMalaria*, including a detailed model of demography, transmission dynamics and interventions is available online [*OpenMalaria Github*] or in a recent publication [Reiker et al., 2021].

Delivery: Clinical trial and implementation assumptions

In our study, LAIs were implemented as anti-infective entities in the form of mAbs or small molecule drugs that prevent the development of blood-stage malaria through action on malaria parasites in sporozoite or liver stages. We assumed administration once at the beginning of the transmission season in combination with an artemisinin-based combination therapy (ACT) that cures prevalent blood-stage malaria infections with a 100% cure rate noting this was an optimistic assumption for ACTs. The same initial blood-stage clearance was applied for SMC-SP+AQ to focus on the investigation of protective efficacy. SMC-SP+AQ was administered monthly, administered for three months per season in Senegal-like settings (*short season*) and for four months per season in Mali-like settings (*long season*) with four seasonal cycles per year for each setting as recommended by the WHO [WHO, 2012] (Fig. B in Appendix C). We assume a decrease in SMC coverage by 3–4% between treatments (7% over the three and 10% over the

four month season for the treatment regimen), therefore lying between the two extremes of observed coverage decrease [Loua and Milligan, 2019; Diawara et al., 2017].

The *clinical trial stage* (Fig. 5.1 b panel 1) was simulated in the high case management setting to account for awareness of malaria symptoms. Initial deployment coverage levels for both, SMC and LAI, were set to 100%. Follow up visits, in the form of active case detection carried out by health workers at the community and household level for groups considered to be at high risk, were implemented two weeks after every administration round of SMC-SP+AQ in both trial arm. In addition to fully effective SMC-SP+AQ, we investigated a reduced length of protection by prevalent resistance against SP in the *clinical trial stage*.

In the *implementation stages* (Fig. 5.1 b panel 2), we analysed the impact of switching seasonal malaria prevention strategies from SMC-SP+AQ after five years of implementation to LAIs. After five years of LAI implementation, the cumulative clinical case incidence was compared with a control setting (no switching). LAIs and SMC-SP+AQ were implemented with varying coverages between 40–100%. Intervention cohorts, defined by the coverage in the intervention age group, were specified at the beginning of a transmission season for the whole season. An exemplary illustration of LAI and SMC-SP+AQ implementation is provided in Fig. D in Appendix C.

Intervention characteristics: SMC and LAI properties

As the decay of efficacy of LAIs is not yet known, we explored a range of possible scenarios. In both the clinical and implementation analysis, the prevention of infection by LAI was modelled as pre-erythrocytic protection from infection *E(t)* over time defined by the initial protective efficacy *E0* [%], protective efficacy half-life of decay L and shape parameter k (Fig. C in Appendix C). The decay shapes of protective efficacy were chosen such that they represent multiple development possibilities: exponential-like decay (referred to as *exponential LAIs*), malaria vaccine-like decay, namely biphasic-like decay [White et al., 2014a; Penny et al., 2015] (referred to as *biphasic LAIs*) and sigmoidal- like decay (referred to as *sigmoidal LAIs*). The protective efficacy decay over time *E(t)* for exponential and biphasic LAIs was modelled as either Weibull-like decay:

$$E(t) = E_0 e^{(-\frac{t}{L})^k log(2)}, \tag{5.1}$$

where $k = 1$ yields *exponential LAIs* and $k = 0.69$ yields *biphasic LAIs*. *Sigmoidal LAIs* were defined by the following Hill equation with $k = 8$.

$$E(t) = E_0 \frac{1}{1 + (\frac{t}{L})^k}. \tag{5.2}$$

The individual protection profile over time after one administration of SMC-SP+AQ, was parameterized using published clinical trial results [Zongo et al., 2015]. The protection profile

in preventing infections is not well understood [Griffin et al., 2010], and usually the protective efficacy of SMC-SP+AQ was assessed in clinical studies in terms of population survival estimates, risk reductions or a reduction in incidence [Diawara et al., 2017; Aponte et al., 2009]. To compare the impact of novel LAIs with SMC-SP+AQ, we parameterized the protective efficacy of SMC–SP+AQ to data from a clinical non-inferiority trial conducted in Burkina Faso [Zongo et al., 2015]. Our parameterization approach employs a Gaussian process regression model [Rasmussen, 2004] to determine the model parameters that reproduce the clinical trial data via minimization of the residual sum of squares between the observed and simulated SMC-SP+AQ protective efficacy. A detailed description of the parameterization process is given in Appendix C. Scenarios assuming SP resistance, the effect of resistance against the SMC component SP was implemented by decreasing the SMC half-life of protection from 32 to 20 days. The lower protection half-life due to resistance can be modeled as an increase in the drug concentration inhibiting the parasite growth by 50% (IC_{50}). Because SP has a long clearance half-life [Kock et al., 2018], we assume no impact of resistance on the initial efficacy.

The health targets analysed in this study were based on incidence reduction by LAIs, clinical cases averted by LAIs compared with SMC, and non-inferiority with regard to clinical burden in the modelled clinical trials. Clinical cases per person (cpp) in the intervention age group ($cpppy_{0.25\text{-}5y,\ int}$) over the clinical trial length (Fig. 5.1 A) ($cpp_{0.25\text{-}5y,\ int}$) or in the last implementation year only as cases per person per year (cpppy) ($cpppy_{0.25\text{-}5y,\ int}$) (Fig. 5.1 B) were calculated over the entire population at risk in the intervention age group ($N_{0.25\text{-}5y,\ int}$).

$$cpp_{0.25-5y,int} = \frac{totalcases}{N_{0.25-5y,int}} \tag{5.3}$$

The incidence reduction percentage inc_{red} was calculated via the cumulative incidence in the year before trial implementation cpp_{cont} and the cumulative incidence during the clinical trial cpp_{int}

$$inc_{red} = 100\frac{cpp_{0.25-5y,cont} - cpp_{0.25-5y,int}}{cpp_{0.25-5y,cont}} \tag{5.4}$$

Survival analysis on the number of clinical cases per person cpp_{int} was performed to analyse the establishment of non-inferiority of LAIs to SMC-SP+AQ as described in [Dahal et al., 2017]. The impact of a LAI is assumed to be non-inferior to SMC-SP+AQ if the upper bound of the 95% confidence interval of the hazard ratio between SMC-SP+AQ and LAI is less than the upper bound for non-inferiority. This upper bound is informed by the survival estimate of SMC-SP+AQ and the desired margin for non-inferiority. We assumed a 5% margin for non-inferiority. More information about the non-inferiority analysis is provided in Appendix C. Additionally, the intervention impact defined as clinical incidence difference between SMC-SP+AQ clinical cases per person per year $cpp_{0.25\text{-}5y}$, SMC and LAIs $cpp_{0.25\text{-}5y}$, LAI was compared using the

relative difference $diff_{cpp}$ as an indicator for the malaria burden.

$$diff_{cpp} = 100\frac{cpppy_{0.25-5y,SMC} - cpppy_{0.25-5y,LAI}}{cpppy_{0.25-5y,SMC}} \tag{5.5}$$

Gaussian process emulator approach to predict intervention impact

To perform a fast and efficient search of the parameter space of LAI properties, we used a database of *OpenMalaria* simulations to train heteroskedastic GPs for each LAI efficacy decay type in each seasonal and transmission intensity setting (R-package *hetGP*, function *mleHetGP*, Version 1.1.2.) [Binois and Gramacy, 2017]. The input parameters of the GPs in the *clinical trial stage* consisted of the tool properties including initial protective efficacy and protective efficacy half-life. In the *implementation stage*, the input parameters additionally included the respective SMC-SP+AQ and LAI deployment coverage. To define the covariance structure of the Gaussian process models, we used a Matérn kernel with smoothness parameter 5/2 accounting for the high variability in the parameter space [Binois and Gramacy, 2017]. The trained GPs were then used to predict the number of cases per person per year and the metrics related to the non-inferiority analysis (Table B in Appendix C) for any point in the parameter space. Emulator performance was ascertained by testing on a 20% holdout set after training on 80% of the data [Golumbeanu et al., 2022] (Table B in Appendix C).

Sensitivity analysis

We identified the main drivers of intervention impact via a global sensitivity analysis, performed using decomposition of variance via Sobol analysis on the emulator output predictions. We conducted an EIR-stratified sensitivity analysis to assess the potential change in drivers of impact over the whole transmission range. Within the pre-defined parameter space, the total effect indices quantify the interactions between individual parameter contributions to the emulator output variance [Sobol, 2001]. The total effect indices were normalized to obtain the relative importance of each parameter through division by their sum. The total effect indices were estimated with a Monte Carlo sampling approach using the function *soboljansen* in the R-package *sensitivity* (version 1.16.2) with 500000 sampled points and 1000 bootstrap replicates.

Intervention properties and coverage optimisation

In the *clinical trial stage*, we discretized the space of the initial protective efficacy and protective efficacy half-life of LAIs within the range of plausible values (Table 5.1), yielding a two-dimensional grid of parameter value combinations. At each grid point, we used the GP emulators to estimate the upper limit of the confidence interval of the hazard ratio between the survival estimates in the SMC and LAI arm and the non-inferiority margin and check if non-inferiority could be established for the given combination of parameter values (cf. Non-

inferiority Analysis in Appendix C). The contours of the resulting non-inferiority surface yielded the thresholds of the minimal initial protective efficacy and protective efficacy half-life needed to establish non-inferiority across different transmission settings (Fig. 5.2).

In the *implementation stage*, we additionally determined the minimum required LAI coverage and half-life at which non-inferiority to SMC-SP+AQ could be established. At each grid point, we conducted a constrained optimisation, translating the non-inferiority condition into an inequality constraint by requiring the difference between the upper limit of the confidence interval and the non-inferiority margin to be positive. The optimisation was conducted using an augmented Lagrange method (*gosolnp*, R-package *Rsolnp*, Version 1.16) with a minimum of 3 starting values and 200 simulations. To determine the benefits of reallocation of resources from reduced visits within a season towards increasing deployment coverage, we compared the number of cases per person per year in a simulation with SMC implemented at a given coverage to the number of cases per person per year with LAI at a coverage that was 20% higher than the optimal coverage.

5.3 Results

Decay shape and duration of protective efficacy influence LAI impact

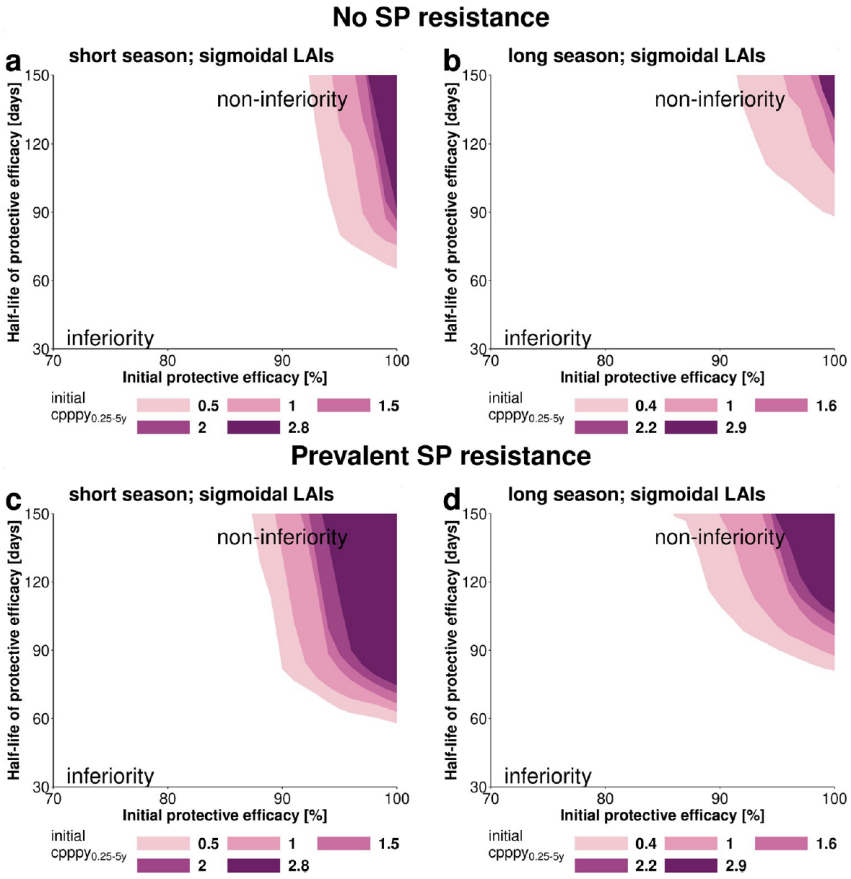

Figure 5.2: Parameter space under which *sigmoidal LAIs* achieve non-inferiority compared to SMC-SP+AQ in the *clinical trial stage*. We investigated the ability of sigmoidal LAIs to establish non-inferiority in clinical trials with an optimal deployment coverage (100%) in settings with a short **(a, c)** and long **(b, d)** malaria season and over varying initial malaria incidence (initial cases per person per year$_{0.25\text{-}5y}$). The minimum required LAI characteristics are defined as those parameter combinations that achieve non-inferior for different baseline incidence settings. **(a, b)** SMC–SP+AQ has an initial protective efficacy of 100% and a half-life of 32 days parameterised from previous clinical trial data [Zongo et al., 2015]. The influence of prevalent SP-resistance **(c, d)** was analysed by decreasing the protective efficacy half-life of SP from 32 days to 20 days (see Appendix C). The coloured area defines the limits of the parameter space where non-inferiority could be established through comparison of the difference hazard ratio δ between Kaplan-Meier survival estimates (see Appendix C). The white area describes the parameter space where LAIs are inferior. *Sigmoidal LAIs* can achieve noninferiority compared with SMC for lower durations of protection in a shorter malaria transmission season. *Exponential LAIs* and *biphasic LAIs* could not establish non-inferiority to SMC–SP+AQ.

We assessed the obtained malaria incidence reduction in the simulated scenarios of the *clinical trial stage* at high deployment coverage (100%) and found that the decay shape of LAI protective efficacy and protection half-life play an important role in achieving a targeted incidence reduction (Fig. 5.3) for each simulated clinical trial scenario. Additionally, we identified the parameter space in which a certain incidence reduction cannot be achieved following LAI deployment under different setting assumptions (below each curve in Fig. 5.3).

In settings with a more extended transmission season (Fig. 5.3 b, d, and f), a longer LAI half-life is required to reach the same predicted impact compared with the shorter season settings (Fig. 5.3 b, c, and e). A steeper initial decrease of initial protective efficacy (Fig. 5.1 a and Fig. C in Appendix C) led to lower estimated incidence reduction, with *biphasic* LAIs exhibiting the lowest predicted impact (Fig. 5.3 c and d), followed by *exponential* LAIs (Fig. 5.3 a and b). The predicted impact of *sigmoidal LAIs* was largely determined by their half-life compared with initial protective efficacy: an initial decrease in protective efficacy would require only a marginal increase of the half-life needed to reach the desired incidence reduction for half-lives greater than 90 days (Fig. 5.3 e and f). In contrast to *exponential* (Fig. 5.3 a and b) and *biphasic LAIs* (Fig. 5.3 c and d), where the force of infection increased the required minimum half-life of protective efficacy, the required minimum half-life for *sigmoidal LAIs* was not markedly increased by the force of transmission compared with the exponential and biphasic decays (Fig. 5.3 e and f). A longer malaria transmission season (Fig. 5.3 b, d and f) was predicted to increase the half-life requirements to reach a desired incidence reduction for all LAIs. In these longer transmission season settings, a predicted incidence reduction of over 80% was not possible for *exponential* and *biphasic LAIs*.

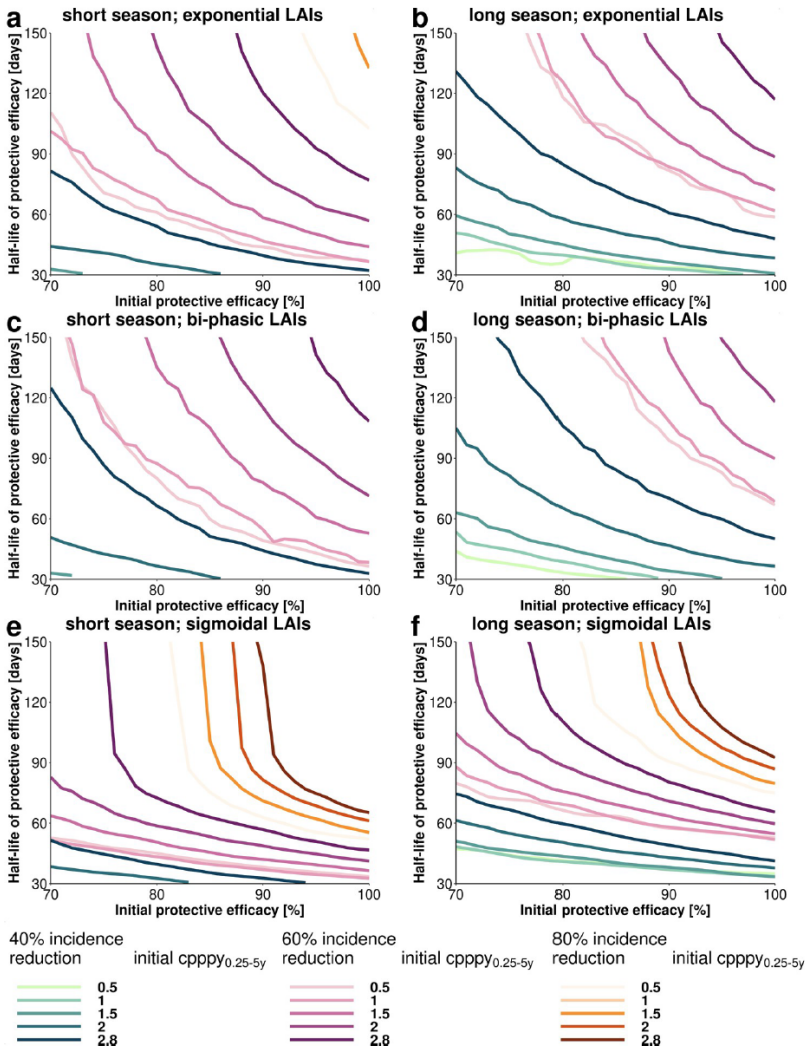

Figure 5.3: Achieving targeted malaria incidence reduction depends on the decay shape of the LAIs protective efficacy. Estimated relationships between initial protective efficacy and efficacy half-life for different incidence reduction criteria (40%, 60% and 80%, line style and color) and clinical incidence settings (increasing color intensity indicates an initial clinical incidence measured in cases per person per year in the target age group of 0.5, 1, 1.5, 2, and 2.8). Each line shows the minimum required LAI characteristics to reach the desired health goal at a 100% LAI deployment coverage at *clinical trial stage*, with all parameter combinations below a line failing to meet those requirements. The panels show the parameter space of attainable incidence reductions within the specified constrained ranges of initial protective efficacy and half-life for *exponential LAIs* **(a, b)**, *biphasic LAIs* **(c, d)** and *sigmoidal LAIs* **(e, f)** in settings with a short (Senegal-like **a, c, e**) or long (Mali-like **b, d, f**) malaria season. The incidence reduction was calculated by comparing the incidence over one transmission season after application of the LAI compared with the previous transmission season. The incidence reductions were obtained by predicting the cases per person per $\text{year}_{0.25\text{-}5\text{y}}$ via our emulator approach (see Appendix C) in a fine grid defined over the parameter space (increments of 0.1 h for half-life and 0.01% for initial protective efficacy) and calculating the incidence reduction by comparison to the initial clinical incidence measured in cases per person per $\text{year}_{0.25\text{-}5\text{y}}$ in the respective transmission intensity setting.

Fig. 5.3 shows the exemplary extraction of minimum essential efficacy properties for a LAI with a given half-life. For example, if the half-life of protective efficacy of a LAI was assumed to be 150 days, we predicted that an initial protective efficacy of 88%, 96%, and 76% was required for *exponential*, *biphasic* and *sigmoidal LAIs*, respectively (Fig. 5.3 a, c and e) to reach a clinical incidence reduction of 60% (short malaria transmission season, initial cases per person per $\text{year}_{0.25\text{-}5\text{y}}$ of 2.8).

Establishing non-inferiority of LAIs to SMC-SP+AQ in clinical trials is difficult

In the SMC-SP+AQ arm of the simulated *clinical trial stages*, we found a predicted mean achievable incidence reduction of 71% to 90% in Mali and Senegal-like seasonal settings (Table C in Appendix C). Our non-inferiority analysis (Fig. 5.1 B panel 3) demonstrated that the predicted establishment of non-inferiority of *sigmoidal LAIs* to SMC-SP+AQ under the assumption of 100% initial deployment coverage could only be met with LAI efficacy over 90% in both seasonal settings and half-life over 62 days in Senegal-like (short season) and 88 days in Mali-like (long season) seasonal transmission patterns (Fig. 5.2). In agreement with the analysis of attainable incidence reduction (Fig. 5.3), the predicted establishment of non-inferiority was more feasible in settings with a shorter transmission season and lower initial malaria incidence (Fig. 5.2 a). For settings with a lower initial incidence (between 0.5 and 1 initial cases per person per $\text{year}_{0.25\text{-}5\text{y}}$), the parameter space where non-inferiority could be established varied more than in higher initial incidence settings. If resistance against SP was prevalent, which we modelled as a shorter duration of protection through a decrease in protective efficacy half-life to 20 days (from 32 days), *sigmoidal LAIs* were predicted to be non-inferior in a wider range of tool property combinations (Fig. 5.2 c and d). Nevertheless, non-inferiority could not be established in any setting for any parameterization of *exponential* and *biphasic LAIs* under clinical trial coverage assumptions. We conclude that the efficacy decay profiles of LAIs play an important role for reaching the defined incidence reduction goals and establishing non-inferiority to SMC-SP+AQ.

The influence of protective efficacy half-life changes over the parameter space

Moving from clinical field trials towards *implementation stages*, where LAIs are administered as a replacement for SMC-SP+AQ (Fig. 5.1 b panel 2), we analyzed the influence of underlying LAI efficacy properties and deployment coverage on resulting intervention impact and non-inferiority to SMC-SP+AQ.

Our sensitivity analysis via decomposition of variance (Fig. 5.4) indicates that the influence of half-life of protective efficacy depends on the length of the transmission season in *implementation stages*. An increase in initial efficacy (Fig. 5.4 d) and deployment coverage (Fig. 5.4 e) resulted in a linear increase in predicted impact. In contrast, the influence of the protective efficacy half-life changed over the parameter space (Fig. 5.4 a-c), with a much steeper influence for changes

in lower half-life ranges.

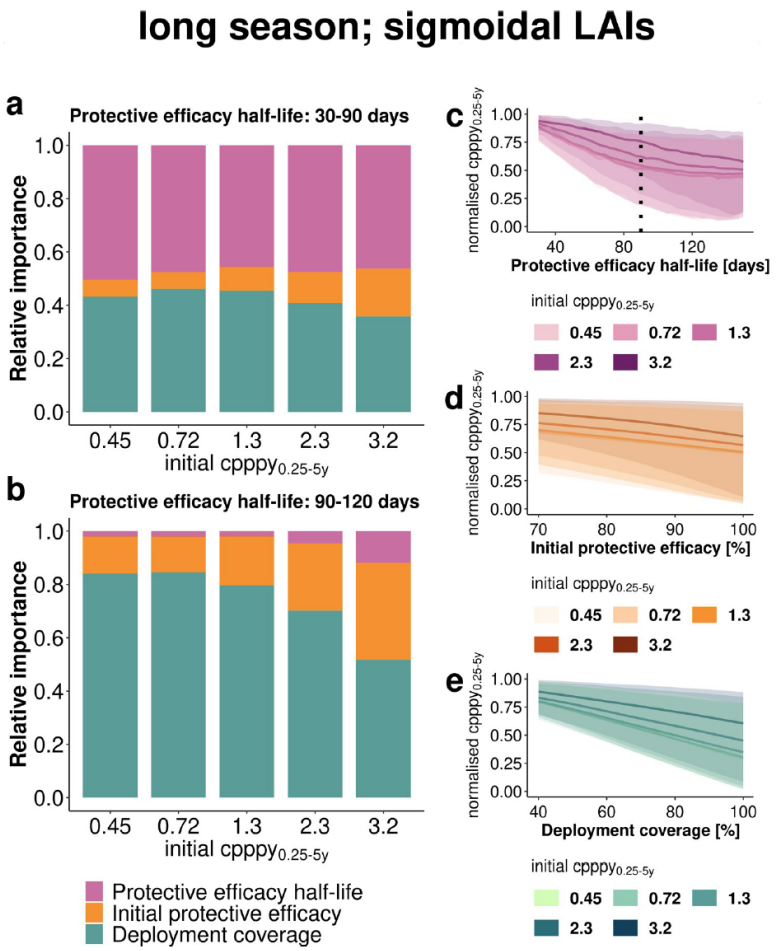

Figure 5.4: Estimated importance of LAI properties and operational factors on the level of clinical incidence reduction. Results are shown for the implementation stage for *sigmoidal LAIs* in a setting with low access to care and long malaria transmission season. **(a, b)** Sobol sensitivity analysis estimates the relative importance of LAI coverage, initial protective efficacy and half-life of protective efficacy to the variance of the emulator through decomposition of variance over the entire evaluated parameter space (coverage 40–100%, initial protective efficacy 70–100% and half-life **(a)** 30–90 days and **(b)** 90–150 days). Changes in clinical incidence measured as cases per person per year$_{0.25\text{-}5y}$ with increasing tool properties or deployment coverage across the parameter space are shown for **(c)** half-life (30–150 days), **(d)** initial protective efficacy (70–100%) and **(e)** coverage (40–100%). The lines represent the mean and the 95% confidence interval (shaded area) capture the distribution of incidence reduction across all sampled values. The dotted line in panel c indicates the split of half-life range for sensitivity analysis in panels a and b. Increasing color intensity represents increasing initial cases per person per year$_{0.25\text{-}5y}$. Further results for different decay shapes and length of transmission season are shown in the Fig. D and E in Appendix C.

We found a change in the main source of variance of the impact of *sigmoidal LAIs* with increasing protective efficacy half-life (shown in Fig. 5.4 a and d for a half-life threshold of 90 days). For instance, if the LAI half-life was less than 90 days (Fig. 5.4 a), the protective efficacy half-life and deployment coverage shared almost equal proportions of attributable variance, accounting for 38% to 52% of variance while the initial protective efficacy contributed between 7% and 19%, depending on transmission intensity. However, for half-lives greater than 90 days (Fig. 5.4 b) the importance of deployment coverage increased from 54% to 85% and importance of the initial protective efficacy from 14% to 38% (in these results we assumed LAIs of less than 70% initial protective efficacy are unlikely to be developed). In contrast, the relative importance of the protective efficacy half-life decreased to around 2% to 12%. In settings with a longer malaria transmission season (Fig. F panels a, d, and g in Appendix C), a sharper initial decrease in clinical incidence was predicted for a larger range of protective efficacy half-life than for shorter transmission seasons (Fig. E panels a, d, and g in Appendix C). Overall, this demonstrates the potential to explore how the impact determinants and their importance change based on efficacy duration cutoffs compared with the length of transmission season or alternative deployment.

Trade-offs between enhancing duration of protection and implementation coverage

These results illustrate the importance of setting-specific trade-offs between enhancing tool properties and improving implementation coverage (Table 5.2). For example, increasing the half-life of a *sigmoidal LAI* with an initial efficacy of 90% from 49 to 63 days reduced the predicted required LAI coverage to establish non-inferiority to SMC-SP+AQ in implementation (60% coverage) by 20% (from 100 to 80%) in a setting with an initial clinical incidence of 1.4 cases per person per $\text{year}_{0.25\text{-}5\text{y}}$. Furthermore, in settings with relatively high levels of initial clinical malaria incidence and corresponding high transmission intensity, namely cases per person per $\text{year}_{0.25\text{-}5\text{y}}$ >2.4 and EIR >150, a change in dynamics to establish non-inferiority was observed. In these settings, we predicted LAIs will likely fail to sufficiently protect the targeted population from clinical malaria even at very high deployment coverage (Fig. D in Appendix C). Therefore, we were unable to assess the required half-life of protective efficacy of LAI for high transmission settings.

For SMC-SP+AQ, we estimated that an additional 13% to 29% in incidence reduction could be achieved by increasing the coverage from 62% to 100%, dependent on initial clinical incidence before implementation (Fig. G in Appendix C). However, achieving high levels of SMC coverage at implementation is challenging [Cisse et al., 2016; Druetz, 2018], and increasing levels of coverage are associated with increasing costs.

As information on costs of LAI (costs of goods and supply chain) are not available as of now, we were unable to include detailed economic analysis in the assessment of LAIs in *implementation stages*. The main cost drivers of SMC-SP+AQ are deployment costs (remuneration of healthcare

Table 5.2: Illustration of the trade-offs between LAI protective efficacy half-life, initial protective efficacy and coverage in *implementation stages*. The table displays the estimated minimum half-life of LAI protective efficacy (measured in days, estimated values specified in the colored cells, increasing colour intensity illustrates increasing requirements) required to reach non-inferiority in implementation stages of various LAI profiles compared with SMC-SP+AQ deployed at 60% coverage for each of 3 or 4 rounds in a setting with low access to healthcare ($E_{14} = 0.1$). SMC-SP-AQ protective efficacy specifications are summarized in Table 5.1. Results are shown for different levels of LAI coverage, decay shapes (*exponential* or *sigmoidal*), initial protective efficacy and malaria incidence prior to deployment (initial cases per person per year$_{0.25\text{-}5y}$).

		Exponential LAIs Coverage [%]				***Sigmoidal LAIs*** Coverage [%]			
Efficacy [%]	**initial cpppy$_{0.25\text{-}5y}$**	**40%**	**60%**	**80%**	**100%**	**40%**	**60%**	**80%**	**100%**
70%	0.41	-	-	113	62	-	-	85	59
	0.71	-	-		70	-	-	87	63
	1.4	-	-	-	89	-	-	103	63
	2.4	-	-	-	93	-	-	105	79
	3.3	-	-	-	-	-	-	-	-
80%	0.41	-	-	109	54	-	-	71	52
	0.71	-	-	112	62	-	148	74	55
	1.4	-	-	132	64	-	-	77	57
	2.4	-	-	119	75	-	-	84	62
	3.3	-	-	-	-	-	-	-	-
90%	0.41	-	-	81	48	-	102	61	50
	0.71	-	-	79	52	-	86	64	52
	1.4	-	-	90	56	-	103	63	49
	2.4	-	-	92	62	-	97	72	56
	3.3	-	-	-	-	-	-	-	-
100%	0.41	-	112	62	46	-	78	58	47
	0.71	-	115	69	48	-	78	58	49
	1.4	-	131	71	49	-	78	58	47
	2.4	-	119	72	52	-	80	61	47
	3.3	-	-	-	-	-	-	-	-

workers) and cost of goods [Pitt et al., 2017; Gilmartin and Collins, 2016], with deployment costs increasing non-linearly with higher coverage. Therefore, we determined the minimal LAI coverage at which non-inferiority to SMC-SP+AQ (assuming initial SMC deployment coverage of 60%) was established, stratified by initial clinical incidence before implementation (Fig. 5.5 and Fig. H and I in Appendix C). We found that the parameter space where non-inferiority could be established shrank with increasing baseline malaria incidence (Fig. H and I in Appendix C). With regard to seasonality, LAIs were more likely to be non-inferior in shorter malaria transmission settings in the *implementation stage* (Fig. G and H in Appendix C). In settings with a high initial clinical incidence (EIR = 150, Table A in Appendix C), LAI coverage could not be optimised to be non-inferior to SMC-SP+AQ at 60% coverage because LAIs were unable to prevent malaria cases even at very high coverage levels (Fig. D panel D in Appendix C). We did not explore less seasonal profiles or transmission profiles with reasonable ongoing transmission in the dry season. However, longer duration LAIs might potentially be needed to reach non-inferiority for periods of evaluation extending into the dry season. Overall, the optimisation of LAI coverage in settings with a limited SMC-SP+AQ coverage illustrates the potential of LAI implementation in non-optimal coverage settings.

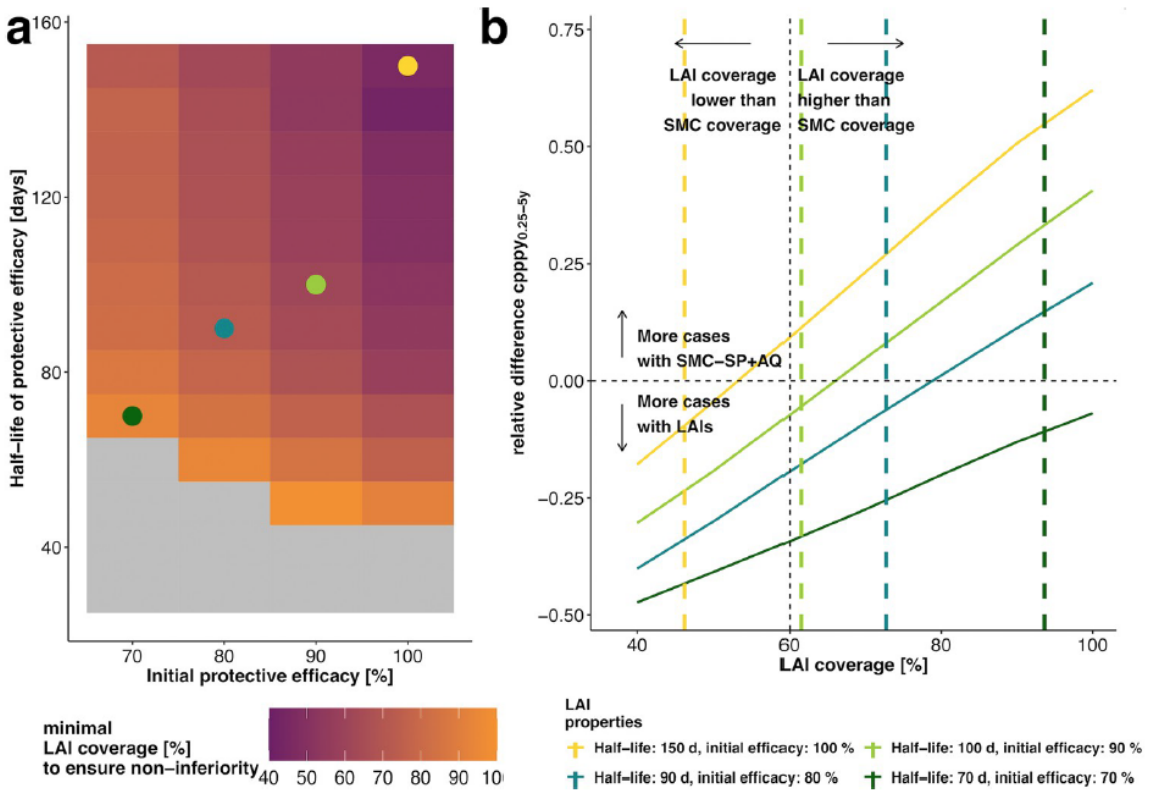

Figure 5.5: Estimated minimal LAI coverage required during implementation stages to achieve non-inferiority in a given setting and predicted gains in cases averted of subsequent *sigmoidal LAI* coverage increments. **(a)** Heatmap of the estimated minimal coverage (colour) of *sigmoidal LAIs* at which non-inferiority to SMC-SP+AQ (assuming a fixed SMC coverage of 60%) is achieved for different combinations of *sigmoidal LAI* efficacy and half-life. The results are displayed for intervention scenarios with an underlying disease burden of 1.4 cases per person per year$_{0.25\text{-}5y}$, long malaria transmission season and low access to treatment (E_{14} = 0.1). In the grey area, non-inferiority of LAIs could not be established for any coverage. The light blue frames capture the tool characteristics where non-inferiority could be reached with a LAI coverage under the reference SMC-SP+AQ coverage of 60%. Further results for additional settings and decay shapes are provided in the Appendix C (Fig. H and I in Appendix C). The coloured dots represent four illustrative LAI profiles for which the corresponding predicted relative differences in cases per person per year$_{0.25\text{-}5y}$ (Eq 5) are calculated in **(b-e)** five years after LAI introduction over all LAI coverages as compared with SMC-SP+AQ at 60% coverage (vertical dotted line). The predicted positive increase in relative difference in yearly clinical cases (above the dotted horizontal line) means more clinical cases are averted with LAIs than with SMC-SP+AQ. It thus illustrates the benefit of increasing *sigmoidal LAI*-coverage above the minimal required coverage to achieve non-inferiority (shown by the grey coloured area). Due to the chosen margin of non-inferiority (here 5%, see Material and Methods), LAIs are non-inferior for a slight negative relative difference in cases per person per year$_{0.25\text{-}5y}$. In the light-blue area in **(b)**, a LAI coverage lower than the SMC-SP+AQ coverage is sufficient to establish non-inferiority. The corresponding analysis for *exponential LAIs* can be found in Fig. J in Appendix C.

While non-inferiority could only be established in a small part of the parameter space of *sigmoidal LAIs* in long seasonal transmission settings (Fig. 5.2 b), it is possible to increase the potential area of applicability of *sigmoidal LAIs* by optimising their deployment coverage (Fig. 5.5 a, initial cases per person per year0.25-5y = 1.4). Deploying a *sigmoidal LAI* at 46% coverage with a half-life of 150 days and initial efficacy of 100% is sufficient to establish non-inferiority over SMC-SP+AQ at 60% coverage (Fig. 5.5 b). In contrast, sigmoidal LAIs with a half-life of 70 days and initial efficacy of 70% require a deployment coverage of 95% in order to be non-inferior (Fig. 5.5 e). For *sigmoidal LAIs* we found that increasing the deployment coverage over the estimated minimum required coverage to establish non-inferiority results in potential gains in terms of clinical incidence reduction compared with SMC-SP+AQ (Fig. 5.5 b-e).

Additionally, we found that even though non-inferiority of *exponential LAIs* to SMC-SP+AQ could not be established in *clinical trial stages*, coverage optimisation in *implementation stages* reveals their applicability. Deploying an *exponential LAI* at 52% coverage with a half-life of 150 days and initial efficacy of 100% was sufficient to establish non-inferiority over SMC-SP +AQ at 60% coverage (Fig. J panel b in Appendix C) and a half-life of 100 days and initial protective efficacy of 90% requires a deployment of 78% to establish non-inferiority (Fig. J panel c in Appendix C). *Exponential LAIs* with a half-life of 70 days and initial efficacy of 70% were always inferior to SMC-SP+AQ at a coverage of 60% (Fig. J panel e in Appendix C).

5.4 Discussion

The effective prevention of clinical malaria in children is crucial to prevent malaria mortality and reduce the overall global malaria burden [WHO, 2019]. Through modelling and simulation, we explored a broad range of LAI characteristics in multiple settings for clinical testing and deployment. This allowed us to understand the likely influence of LAI efficacy properties and operational factors on clinical incidence reduction in children under five years of age when LAI is deployed as a seasonal malaria prevention tool. We found that if the protective efficacy of a new LAI decays immediately after injection, for example an exponential or biphasic-like decay, then the LAI is unlikely to achieve non-inferiority over SMC-SP-AQ in current SMC settings in a clinical trial. This exploration assumed non-inferiority criterion is required for testing, and we only explored LAI half-life of protection in the range of 30 to 150 days. In contrast, when the protective efficacy of LAIs is long-lasting and decays only after some time (i.e. a sigmoidal decay), there is a stronger chance of achieving non-inferiority when the duration of protection is close to the transmission length. Beyond clinical stages, by assessing implementation factors versus LAI properties, we conclude that focusing on enhancing the duration of protective efficacy (half-life) is more likely to result in successful LAIs in a larger range of incidence and transmission settings. If the half-life of protective efficacy of a LAI approaches the length of

transmission season, and initial efficacy is sufficiently high (depending on the transmission intensity (Fig. 5.3)), then the development of new LAI should prioritize optimising operational delivery factors to ensure reasonable coverage to be as good as or better in averting clinical cases than current SMC-SP+AQ implementation.

The estimated impact of tool properties

In general, the duration of the half-life and its shape of decay are the most relevant tool properties for incidence reduction. This means that the development of new LAIs should focus on understanding the likely decay and half-life of protection (this is not the pharmacokinetic properties of a small molecule or the antibody longevity of a mAb). Over the analyzed transmission settings and parameter space, the estimated minimum essential (80%) and ideal (95%) incidence reduction targets for LAIs as defined by Macintyre et al. (2018) [Macintyre et al., 2018] are hard to achieve in clinical testing. A desired incidence reduction of <80% in clinical testing could only be achieved for LAIs with a sigmoidal decay shape and half-life over 60 days (Senegal, short season) and 80 days (Mali, long season). Our findings indicate that key to identifying and refining candidates for development of new LAIs is investigating the decay shape of efficacy as early as possible and providing a sufficiently long protection half-life. Before conducting large scale clinical trials, it will therefore be important to ensure the adequate means to establish the decay and duration of protection and the ability to extrapolate to paediatric indications.

We investigated three very different decay profiles of potential LAI protection because this information is currently unknown. While the pharmacokinetic profile of potential LAIs can be evaluated in pharmacokinetic studies, their protective efficacy profile and decay shape are harder to derive. Currently, murine [Flannery et al., 2013] or human challenge [NCT03707041, 2019; Sulyok et al., 2017] studies are being used to investigate these parameters. In these studies, subjects receive treatment before inoculation with sporozoites through the bites of infectious mosquitoes or direct venous injection [NCT03707041, 2019; Sulyok et al., 2017]. However, parasite growth in the liver, and therefore protective efficacy, cannot be directly quantified. Instead, the time and number of parasites entering the blood stream is used as a crude proxy for protective efficacy. We note, however, that sporozoite or mosquito human challenge studies with pharmacokinetic modelling will provide valuable information to refine the profiles of protection against infection investigated in our study. These data and PKPD models refining protective efficacy decay curves and incorporating them into the population modelling approach with *OpenMalaria* can provide more informed first insights into the potential public health impact of new LAIs.

In summary, our findings suggest that when defining key efficacy characteristics for TPPs for LAIs, there are two important processes that should be carried out: (1) evaluate the feasibility of existing or newly specified efficacy and duration requirements for LAIs [Macintyre et al., 2018] by estimating their public health impact using for example, modeling and simulation approaches,

and (2) translate the population-level protective efficacy of LAIs on the incidence of clinical cases into individual-level protection efficacy, and vice versa, using reasonable measures of protective efficacy from summations of animal or human studies.

Clinical non-inferiority trials

Our non-inferiority analysis (Fig. 5.2) highlights that the establishment of non-inferiority in *clinical trial stages* is challenging due to not only the high protective ability of SMC-SP+AQ but also clinical trial designs. This motivates an important discussion on the clinical development of LAIs under the use-case of SMC replacement: the necessity and extent of clinical trial testing or non-inferiority criteria should be assessed. We estimated SMC-SP+AQ in a clinical study results in incidence reductions of 71% to 90% in children under five, aligning to an efficacy of 86% (95% CI: 78–91%) in a clinical trial in Senegal [Cissé et al., 2006]. Monthly SMC-SP+AQ administration together with the estimated protective efficacy half-life of 32 days offers a high degree of protection and the blood-stage clearing effect of AQ eliminates remnant malaria infections, making optimally employed SMC a very powerful tool to prevent clinical malaria. This means it is difficult for most LAIs to achieve non-inferiority in a clinical trial with limited SP resistance when the LAI is only deployed once per season in combination with a blood stage clearing drug. Thus, at first glance, our non-inferiority results may offer a distorted picture of the ability of LAIs to compete with current SMC, as clinical non-inferiority trials do not reflect the reality of SMC implementation. Operational constraints result in reduced coverage over the number of rounds [Cisse et al., 2016; Druetz, 2018] and adherence [Ding et al., 2019], thus hindering SMC-SP+AQ from reaching its full potential. As SMC-SP+AQ effectiveness reduces with operational challenges, this presents a niche for LAIs. In 2018, among children under 5 years of age living in SMC-eligible areas in the 12 countries in the Sahel subregion that scaled-up SMC, only 62% (19 of 31 million) were administered SMC-SP+AQ [WHO, 2019], meaning that additional incidence reduction could be achieved by increasing coverage at each round.

Tool and coverage optimisation in implementation stages

Replacing SMC-SP+AQ with LAIs will likely prove beneficial in reducing deployment costs due to fewer deployment rounds. In the absence of information on costs of LAIs (costs of goods and supply chain), we are unable to adequately assess economic considerations and thus our results assume that coverage is the main driver of implementation cost. If LAIs are assumed to have a longer clearance half-life and therefore higher protective efficacy for longer than SP+AQ, resources are freed up through decreased deployment rounds within a season. These resources could be reallocated to increase the overall coverage in a single round of LAI in the target population, including populations in remote places. Additionally, the overall adherence to the blood-stage clearing co-administration of antimalarials could be increased, thereby reducing the probability of emergence of resistance. However, if transmission intensity is very high, we

found that the optimisation of protective efficacy half-life and deployment coverage is insufficient to adequately protect the targeted population. Instead, it might be necessary to expand the deployment of LAIs to multiple administration rounds within a transmission season.

The optimisation of deployment coverage of LAIs to reach non-inferiority to SMC-SP+AQ where optimal coverage cannot be met exposes an additional use case for LAIs. If external circumstances, such as the current COVID-19 pandemic, prevent the regular implementation of SMC and bed-nets campaigns, millions of children will experience an increased risk of malaria [Rogerson et al., 2020], LAIs may alleviate this burden. Our analysis can aid the identification of minimal LAI coverages necessary to achieve given population impacts and prevent a resurgence in malaria cases.

Framework and areas of application

Our modelling and simulation analysis provides important insights into the likely impact of new malaria tools that are currently under clinical development. Our modelling framework divides the unknown parameter space of realistic properties of new tools into setting-specific attainable incidence reduction by translating the decay of individual protection against infection of a new tool into estimates of population impact on clinical incidence. While in clinical trials often only one (high) deployment coverage and a limited number of trial-arms can be investigated, a simulation-based approach can explore the trade-off between operational constraints and tool properties to narrow down beneficial implementation settings and use cases without the need for expensive field studies. Not only does this approach offer the opportunity to assess the potential population impact of new tools currently under development, but it also provides a methodology to assess the potential clinical trial outcomes. It assists the evaluation of clinical trial scenarios that might be considered over several different malaria transmission and health-system settings to supporting thinking on appropriate population impact endpoints that are suitable to inform decision making. This is particularly true for existing interventions with high efficacy for which the establishment of non-inferiority in clinical non -inferiority trials is problematic, due to the required large sample sizes [Borrmann et al., 2008]. Here, our approach offers first insights into the outcomes of such trials and the additional possibility to develop clinical trial analysis tools.

Furthermore, beyond the current scope of our study, as more information on likely costs of LAIs become available and further certainty in implementation and cold-chain needed, this work can serve as a basis for cost-effectiveness or economic analysis.

As with all modelling studies there are limitations to our analysis. In this study, despite exploring a large range of characteristics on tool properties, deployment, and transmission settings, our results are constrained by the investigated parameter-space. First, we only investigated the impact of one administration round of LAIs with an antimalarial treatment and assumed that the time-point of administration would coincide with the first SMC application round. How-

ever, depending on the LAI profile, the time of deployment may need to be optimised. Second, the implementation of protective efficacy of LAIs is solely assumption-driven, as clinical data is not yet available. With additional information on likely achievable protective efficacy half-life, initial protective efficacy, and efficacy decay shapes, the preliminary LAI profiles can be further defined and re-evaluated as LAIs are developed. The re-definition of plausible parameter ranges will also impact the results of the sensitivity analysis and trade-offs, and potentially shift the recommended focus of development efforts. Additionally, target mediated drug disposition might change the pharmacokinetic profile of mAbs dependent on the transmission intensity and parasite growth within the human host and therefore also its efficacy profile [Kamath, 2016]. Third, the focus of this analysis was the investigation of the effect of the anti-infective LAIs. Our results are subject to change if LAIs are co-administered with different bloodstage clearing drugs (different efficacies and/or potential properties e.g. transmission blocking) or are deployed with other interventions such as insecticide-treated bed-nets. And lastly, we explored SMC or LAI replacement in only children under 5 years of age and in settings similar to where SMC is currently deployed such as Mali and Senegal. Further analysis could be undertaken to assess LAI as seasonal prevention in children under 10 years of age, however we expect conclusions to be similar in regards tool properties and coverage requirements. Our results also only hold for assessing LAI as replacing SMC; we did not explore use cases of deploying LAI in perennial or other settings in which SMC is not yet deployed. Alternative clinical metrics would need to be explored as LAI in these use-cases are not a replacement tools, rather new tools and non-inferiority trials are not relevant. Although this study focuses on the use of LAIs in seasonal malaria transmission settings, our findings regarding the importance of protective efficacy half-life do provide first insights for potential use of a LAIs in perennial malaria transmission settings. The protective efficacy half-life of a LAI will most likely dictate the number of applications to children during the yearly seasonal transmission to ensure effective clinical case reduction.

Current stage of development of mABs and duration of protection

Potential candidate LAIs include mABs and small-molecule drugs, and to date most known mAbs for use in malaria (largely by-products from research into whole sporozoite vaccines [Julien and Wardemann, 2019]) have been shown to prevent blood-stage infection in *in vitro* and/or *in vivo* murine malaria infection experiments [Kisalu et al., 2018; Tan et al., 2018]. As the natural clearance half-life of antibodies ranges between 2 and 21 days [Kontermann, 2009], strategies to increase the half-life of mAbs have been introduced via modifications to the tail (Fc) region of antibodies that interacts with the receptors on the surface of cells. Fc-modified mAbs have exhibited extended half-lives ranging from, 100 days [Robbie et al., 2013] and 80 to 112 days [Yu et al., 2017] in healthy human adults. Our results suggest that these extended half-lives, if functional malaria protection is maintained, are crucial to establish non-inferiority to standard SMC. A second stream of LAI development is focused around small-molecule drugs such as atovaquone [Bakshi et al., 2018] and P218 [Yuthavong et al., 2012]. Although these compounds

show promising liver-stage activity, the estimated clearance half-life of enhanced formulation atovaquone of 32 days in humans [Bakshi et al., 2018] and 8.9–19.6 hours of P218 in first-in-human trials [Chughlay et al., 2020] are again likely insufficient in the use cases explored in our study and emphasize the need for longer-lasting formulations to be useful as SMC replacements when deployed only once per season. Further use may be possible for multiple applications within a season.

5.5 Conclusion

Here, we provided the first quantitative evaluation of the TPPs of future LAIs for malaria as a seasonal prevention tool in children. Simulation analysis of LAIs in real-life implementation settings revealed that the ability of LAIs to prevent clinical cases in children is strongly dependent on the length of the malaria transmission season and transmission intensity. We also found it is important to focus on improving the protective efficacy duration (half-life) of LAIs in development, as the speed of protective efficacy decay is a key driver of overall impact (a crucial consideration for TPP development) or the chance to meet non-inferiority criteria compared with SMC-SP+AQ. However, if a reasonable duration is possible (longer half-life and sigmoidal decay that supports protection close to the length of transmission season) then development should focus on increasing deployment coverage to optimise the LAIs chance of higher impact. This provides evidence for the potential trade-offs between tool properties and operational constraints as LAIs are developed and deployed. In general, our findings support the need for a thorough and combined investigation of tool properties and use cases in the future development of LAIs. This combined effort includes earlier modelling alongside clinical studies to provide evidence of translation of impact at population levels before late stage clinical studies and optimise the success of new malaria tools. Our research here provides an initial foundation to support dialogue between stakeholders, scientists, and clinicians at each clinical development stage of novel anti-infective LAI's to reduce clinical malaria incidence. LAIs have the potential to be a game changer in protecting vulnerable populations from malaria. Our analysis serves as a stepping stone for the refinement of TPPs for LAIs, thereby assisting the target-oriented use-case of development and implementation of new LAIs.

Supporting information

Appendix C. Fig. A: Prevalence—incidence relationship in the simulated Open Malaria settings. Fig. B: Modelled malaria transmission pattern and simulated prevalence defining seasonality settings. Fig. C: Simulated protective efficacy decay shapes of long acting injectables (LAI) and seasonal malaria chemoprevention (SMC) over one transmission season. Fig. D: Exemplary illustration of incidence and survival estimates of sigmoidal LAIs and SMC-SP+AQ in implementation stages over one implementation year. Fig. E: Estimated impact of LAI properties

and operational factors on the level of clinical incidence reduction. Fig. F: Estimated impact of LAI properties and operational factors on the level of clinical incidence reduction. Fig. G: Incidence reduction achieved through implementation of SMC-SP+AQ over varying deployment coverage. Fig. H: Estimated minimal LAI coverage required during implementation stages to achieve non-inferiority in a given setting. Fig. I: Estimated minimal LAI coverage required during implementation stages to achieve non-inferiority in a given setting. Fig. J: Estimated minimal LAI coverage required during implementation stages to achieve non-inferiority in a given setting and predicted gains in cases averted of subsequent exponential LAI coverage increments. Fig. K: True over predicted RSS of the GP. Fig. L: Decay of protective efficacy of SMC-SP+AQ over time. Fig. M: Cumulative hazard of malaria in children who received SMC with SP-AQ (blue) compared to controls (black). Fig. N: Prevalence of malaria in children who received SMC with SP-AQ (blue) compared to controls (black) over the trial. Table A: Simulated prevalence–incidence settings. Table B: Emulator performance for the investigated outcomes. Table C: Incidence reduction achieved through implementation of SMC-SP+AQ in a clinical trial setting. Table D: Inputs into OpenMalaria (OM) to check adequate parameterization of SMC-SP-AQ. Table E: Results of the GP optimization. Table F: Comparison of trial results of Zongo et al., 2015 and model outputs using the model specification in Table D with the best parameter set.

Acknowledgments

We acknowledge and thank our colleagues in the Swiss TPH Infectious Disease Modeling unit for their valuable insights and feedback. Calculations were performed at sciCORE (scicore.unibas.ch) scientific computing center at University of Basel.

Author Contributions

Conceptualization: Lydia Burgert, Melissa A. Penny., Formal analysis: Lydia Burgert, Melissa A. Penny., Funding acquisition: Melissa A. Penny., Investigation: Lydia Burgert, Theresa Reiker, Monica Golumbeanu, Jörg J. Möhrle, Melissa A., Penny., Methodology: Lydia Burgert, Monica Golumbeanu, Melissa A. Penny., Project administration: Melissa A. Penny., Supervision: Melissa A. Penny., Visualization: Lydia Burgert., Writing - original draft: Lydia Burgert., Writing – review and editing: Lydia Burgert, Theresa Reiker, Monica Golumbeanu, Jörg J. Möhrle, Melissa A. Penny.

Chapter 6

Discussion

> Such calculations are useful because they help to define and classify our ideas; but no one imagines that the same dose will always have the same effect.
>
> Colonel Sir Ronald Ross, on calculating curative regimens of quinine (1921)

The overall aim of this thesis was the development and use of a series of models and data analysis tools to guide decision making along the development pathway of new pharmaceutical interventions against malaria. I was able to develop and further refine new models and approaches to capture the impact of blood-stage treatment and liver-stage prevention and to develop new methodologies to evaluate experimental data and modelling results. This work was facilitated by strong collaborations with academic and industry partners, that include the exchange of data, but also modelling expertise and valuable insights into experimental dynamics.

As a result, this thesis presents different approaches to capture and analyse the efficacy of pharmaceutical interventions against malaria, to enhance the understanding of the determinants of intervention success and to explore implications for their pharmaceutical development. It provides new insights into intervention properties and operational and setting characteristics, be it in experimental malaria infection studies or in the field, that drive, but also limit intervention impact. The systematic modelling methodologies to analyse the impact of pharmaceutical interventions against malaria presented in this thesis, advance the definition of efficacy indices and attainable impact targets in product profiles.

I developed a comprehensive modelling and analysis workflow to investigate the influence of underlying parasite-, host-, and drug-dynamics in antimalarial drug development (Chapters 2 and 3). By collating data and insights from many different sources, we showed that incorporating mechanistic parasite-growth models into the analysis of drug efficacy can extract the

different sources of variability in parasite-clearance between the murine and human infection experiments. Further, this methodological approach assists the evaluation of commonly used drug efficacy indices and future definition of new indices which are meaningful throughout the drug development process (Chapter 4). It therefore enables the prediction of drug efficacy between development stages. This workflow has the potential to function as a decision support tool throughout the drug development process by assisting drug efficacy analysis, but more importantly by guiding thinking on how to approach and what to consider in experimental analysis.

By analysing minimal tool profiles for new long acting injectables (LAIs) (Chapter 5), we further developed a workflow that supports the definition of use cases and efficacy targets for target product profiles. This workflow efficiently identifies the parameter space in which impact targets for desired health goals are reachable and non-inferiority to existing interventions can be established. Hence, it allows the quantification of the potential population impact of new preventative interventions currently under development, providing a basis for tool refinement and selection.

The findings of this work are multi-facetted, including new methodologies to analyse experimental data and intervention efficacy resulting in a quantitative and qualitative assessment of intervention impact and evaluation. The following discussion contains the overall conclusions and recommendations of this thesis and provides an outlook for future prospects of modelling in the development of pharmaceutical interventions against malaria. The following points will be elaborated in the remaining of the discussion:

- The importance of a holistic experimental analysis approach: Parasite growth and treatment have to be analysed in the context of the underlying parasite-host pairing as well as the experimental context.
- The missing pieces of antimalarial dose-response relationships: The incorporation of treatment effect into parasite growth models needs to be based on a mechanistic understanding of the mode of drug action.
- The need for systematic model validation: A comprehensive and systematic validation of the different modelling approaches and assumptions is required.
- The critical examination of experimental outcomes: Varying parasite-host dynamics influence the efficacy indices used to evaluate and prioritise new compounds in antimalarial drug development.
- The right tool for the right place: Modelling and simulation reveals the trade-offs between tool properties and future deployment modalities during the development of new tools.

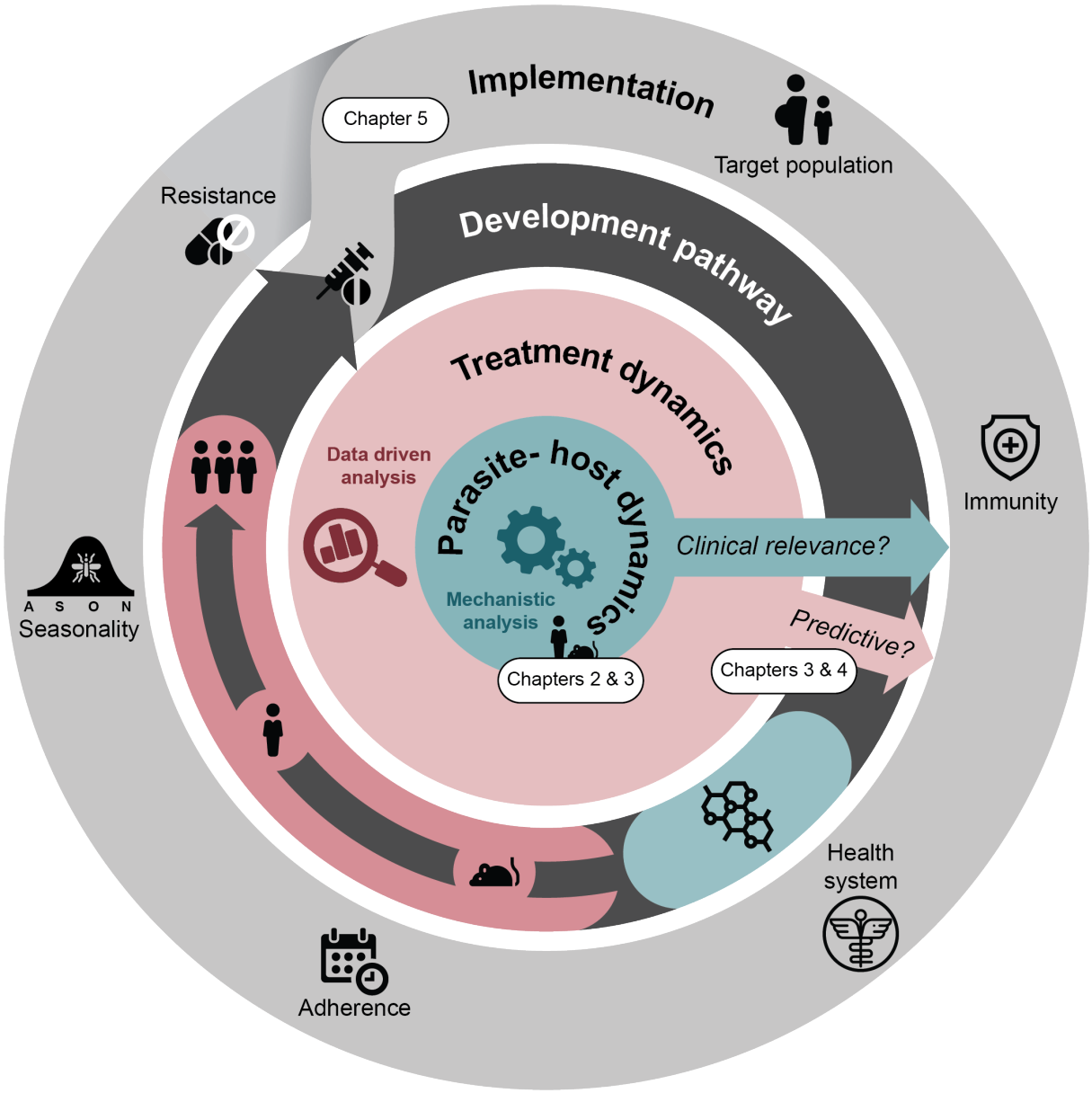

Figure 6.1: Future perspectives to guide decision making during the development and implementation of new human-targeted pharmaceutical interventions. The above figure contextualises the individual chapters of my thesis. In Chapters 2 and 3, I quantified the influence of parasite-host dynamics on the measurement of *in vivo* drug efficacy during the development of new antimalarials. These dynamics potentially influence the decision making process in evaluating and selecting promising antimalarial candidates. Therefore, I recommend a careful examination of parasite-host dynamics and their clinical relevance in implementation settings. In Chapters 3 and 4, I discussed the suitability of drug efficacy indices to predict treatment dynamics between the development and implementation stages. Here, I propose the employment of mechanistic models of drug action instead of empirical approaches, to aid the translation and prediction of drug efficacy between development and into implementation stages. In Chapter 5, I quantified and discussed the influence of future use case and implementation setting on tool requirements in TPPs.

6.1 The importance of a holistic experimental analysis approach

The successful development of new pharmaceutical antimalarial interventions requires a comprehensive understanding of the underlying dose-response relationship. An important aspect in the assessment and evaluation of this relationship is the disentanglement of factors confounding efficacy measurements. Traditional population analyses in clinical drug development mostly consider patient characteristics as covariates to explain the observed variability in responses. We found that this approach is insufficient to assess the dose-response relationships of new antimalarial interventions. The research presented in Chapters 2 and 3 shows that parasite dynamics within the host are additional confounders of intervention efficacy. Their evaluation is therefore crucial to guarantee an efficient development of much needed antimalarial interventions.

We developed and analysed an ensemble of within-host models of parasite growth and treatment of murine and human malaria infection on the foundation of data from various sources (Chapters 2 and 3). These include observational data from different experiments and laboratories, but also previous descriptions and observations of parasite growth and treatment efficacy.

We found that differences in experimental set-up (e.g. parasite inocula and treatment times) as well as varying parasite and host dynamics between the murine and human experimental infection systems result in different parasite growth patterns. These differences in parasite-host pairing and experimental set-up result in varying sources of the observed variability between the experimental systems and should dictate data collation and analysis. For example, experimental design efforts should optimise sampling measures, times, and repetitions under the premise of experimental constraints to ensure an efficient allocation of experimental resources and optimal exploitation of data [Kreutz and Timmer, 2009]. The incorporation of new data into the developed workflow is then simplified by the ability to account for the identified sources of experimental variability.

Further, the influence of underlying parasite and host dynamics on observed parasite clearance after treatment can be quantified by using a holistic experimental analysis approach based on mechanistic models of parasite growth. It thereby assists the evaluation of new antimalarial compounds (Chapter 3, Fig. 3.2): In the *P. berghei*-NMRI infection experiments, the large inoculum size coupled with a highly virulent parasite strain, leads to resource limited parasite growth. This non-linearity in parasite-growth likely compromises the explanatory power of efficacy measures that compare parasite abundance in a control and treatment group (Chapter 4). In contrast, the continued human RBC injections in *P. falciparum*-SCID infection experiments hinder the occurrence of resource limitation but induce an increased clearance of (un-)infected RBCs. The different underlying clearance patterns complicate the distinction between host and drug induced parasite clearance. The observed variability between murine experiments was captured by adjusting the virulence of parasite growth (as the ability of the parasite to infect

new RBCs) (Fig. 2.2).[1] Therefore, parasite growth and treatment data could be pooled at an experimental level for the subsequent analysis of drug efficacy (Chapter 2).

In experimental human volunteer *P. falciparum* infection studies (VIS), testing is only conducted at low parasite burden. Coupled with the restricted length of experiments, a reliable analysis of detailed parasite-host dynamics is infeasible. Instead, identifying the sources of inter-individual and inter-cohort variability in parasite growth is crucial. In VIS, the (human) host as well as the parasite contribute to the observed variability between individuals and cohorts (Fig. 3.3).[2] Parameters of parasite clearance were identified as host-dependent, whereas the parameters of the initial age distribution and parasite replication were identified as parasite-dependent (Fig. S3.7, Appendix B). This implies, that in the analysis of VIS, individual host as well as cohort characteristics must be considered.

Therefore, the focus of parasite growth models and modelling methodology needs to be adjusted between the experimental systems. Consequently, I recommend a broad and systematic validation of sources of variability in experiments throughout the drug development to avoid the introduction of screening bias due to underlying parasite host-dynamics.

In summary, our analysis of parasite-host dynamics provides an important foundation in i) identifying the potential underlying parasite-host dynamics influencing parasite-growth in the experimental systems and ii) assigning the observed variability in parasite growth behaviour to parasite-, host-, or experimental-sources.

6.2 The missing pieces of antimalarial dose-response relationships

In recent years, large screening efforts for new blood-stage antimalarials have brought forward many new molecules exhibiting new modes of action [Burrows et al., 2017]. Several new compound classes now populate the antimalarial drug development pipeline (e.g. spiroindolone [Rottmann et al., 2010] and ozonides [Charman et al., 2011]) and have progressed as far as phase II clinical trials [White et al., 2014b], where they are now being tested in new combination therapies [Macintyre et al., 2017]. In addition to the continued search for a malaria vaccine, new interventions based on small molecules or monoclonal antibodies or the repurposing of existing drugs, offer exciting opportunities for universal personal protection [Macintyre

[1] Differences in experimental protocols including thawing of parasite inocula, inocula sizes, and infection status of the donor mouse cause a variation in parasite virulence between experiments. This analysis was informed by undisturbed parasite growth data in 215 *P. berghei* infected NMRI mice over 43 experiments and 132 *P. falciparum* infected NOD$^{scidIL-2R'c-/-}$ (SCID) mice over 32 experiments [Burgert et al., 2020].

[2] This analysis is based on extensive data of parasite-growth before treatment in 177 individuals within 27 different cohorts.

et al., 2018]. Several new drug or monoclonal antibody based entities showing preventative potential in murine experiments by targeting the *P. falciparum* liver stage are currently under development [Chughlay et al., 2020; Kisalu et al., 2018].

The pharmacokinetic profiles of these pharmaceutical interventions describe their concentration over time. They can be quantified for different populations, such as children, adults, and hospitalised patients, with reasonable efforts in population PK studies [Guidi et al., 2019; Ding et al., 2019]. In contrast, their pharmacodynamic profiles are harder to quantify because of technical constraints in measuring low parasite concentrations and additional influences of host clearance mechanisms on the clearance profile of parasites (Chapters 2 and 3). While in VIS parasite-growth data before treatment is available, in clinical field trials, only data after treatment can be collected. Therefore, information on inter-individual differences in parasite-growth are missing which complicates the establishment of dose-response relationships in different patient populations.

Throughout Chapters 2 and 3, we captured drug efficacy by combining mechanistic parasite growth models with different descriptions of dose-response relationships. In Chapter 2 (Table S2.7), we tested several pharmacodynamic models to capture the observed parasite killing and clearance after treatment in murine malaria infection including:

- a direct effect model, assuming direct dependence of parasite killing on drug-concentration and an immediate clearance of dead parasites;
- a turnover model, assuming an indirect response of the parasite killing to drug-concentration;
- an effect compartment model, assuming a direct drug effect with additional effect compartment incorporating a time-delay in drug action, and;
- a delayed clearance model, accounting for potential delays in clearance of damaged or dead parasites by including an extra compartment for dead parasites.

In Chapter 3, we included

- a delayed parasite growth model, incorporating drug-concentration dependent parasite growth retardation that causes a temporary lengthening of the parasite life cycle

to describe parasite killing after treatment in human VIS (Equation 3.9).

However, in contrast to the mechanistic parasite-growth models, the dose-response relationships presented here are primarily data-driven drug effect models that derive their structure and parameters from empirical observation. Therefore, they often lack direct physiological explanation. For example, despite the ability of the presented drug action models to capture a lag-time

in drug effect after dose administration[3] or the delayed clearance of dead parasites through additional parasite compartments[4], the underlying details of biological mechanism responsible for the observed lag times are rarely known. For now, a possible explanation includes the different developmental stages of the parasite present in the host at the time of treatment coupled with stage-specificity of the compound [Khoury et al., 2016] and cumulative drug effects [Cao et al., 2017]. Without further knowledge of the underlying dynamics, the quantification of drug efficacy and correct mapping of pharmacodynamic functions is highly dependent on data quality and quantity. Hence, the ability of these data-driven models to accurately capture cumulative drug-effects and additional parasite reactions to drug exposure is lacking.

The same considerations apply to new entities preventing blood-stage infection by either attacking the liver-stage or early blood-stage of the malaria life cycle (Fig. 1.1). Detailed data on parasite numbers and drug effects in the liver are missing, since they have to be estimated by backwards prediction of the number of parasites released into the blood after the liver cycle has been concluded. The effect of preventive interventions was therefore modelled by defining their ability to prevent blood-stage infection over time. Here, insights into inter-individual variability in protective efficacy and detailed mode of action could assist in further specifying the efficacy decay shape and therefore intervention impact. Our work could help in establishing dose-response relationships for preventative pharmaceutical interventions from two angles: by estimating efficacy decay curves from clinical trials (see Appendix C) and by providing a foundation for the development of mechanistic drug action models.

In summary, while the concentration-time profiles of pharmaceutical interventions are frequently established, the dose-response relationships often lack biological insights. They therefore compromise the predictive ability of these models which is needed for out-of-sample predictions, the prediction of drug efficacy in the next development stage or the estimation of the population impact. These findings call for further research to establish the mechanism of action driven dose-response relationship (see 6.6.) and highlight the need for rigorous model validation exercises (see 6.4).

6.3 Critical examination of experimental outcomes

Currently, efforts to quantify drug efficacy indices throughout the development process build on the confidence, that the results from one development stage are able to predict drug efficacy in subsequent developmental stages. A unifying approach to translate and predict drug efficacy between and within the experimental development stages could guide drug development efforts

[3] CQ and OZ439 in *P. berghei*-NMRi infection and ACT-451840, CQ, and OZ439 in *P. falciparum*-SCID infection (Fig. S2.10, Appendix A)

[4] ACT-451840 in *P. berghei*-NMRi infection and MMV390048 in *P. falciparum*-SCID infection (Fig. S2.10, Appendix A)

by providing compound selection criteria and assisting in dose prediction. However, our analysis and evaluation of efficacy indices as predictors for cure revealed, that, as of now, neither the data, nor the mechanistic drug efficacy insights for such an analysis are available. I found that i) different efficacy indices are employed to measure e.g. parasite clearance at the different experimental stages (Chapter 4), ii) these indices are potentially influenced by different underlying parasite-host dynamics (exemplary analysis of PPR in Chapter 3) and iii) some indices cannot be reliably examined with the available data and methodological approaches (e.g. the MIC) (Chapters 2, 3, and 4).

A (non-systematic) review of reported experimental outcomes for antimalarials currently in various development stages of the MMV development pipeline revealed a plethora of different measures for parasite clearance throughout the analysed *in vivo* drug efficacy experiments (Table 4.1). For example, in murine infection experiments, commonly reported parasite clearance indices include the effective dose EDx reducing the parasite abundance by x% after treatment in comparison to untreated control mice. In VIS, it is more common to report the parasite reduction ratio (PRR), that summarizes the magnitude of parasite clearance compared to parasite concentration before treatment (Table 4.1). Here, modelling approaches allowed the quantification and comparison of parasite clearance rates, that could not be calculated from raw data (Fig. 3.5) and the subsequent investigation of the underlying mechanisms that influence observed parasite clearance.

An extension to the work in Chapter 3 would be the systematic analysis of further drug efficacy indices such as the minimum inhibitory concentration (MIC). However, in the absence of further data and insights, we must conclude that although this analysis could be conducted for the previously described drug efficacy indices through extrapolation from parasite-growth behaviour, the scientific foundation for confident quantification and prediction of these drug efficacy indices is missing. The general lack of recrudescence data in *P. berghei*-NMRI mouse infection experiments, and the missing information on the causes of delayed recrudescence in *P. falciparum*-SCID mouse infection experiments, coupled with the general lack of insights into parasite growth behaviour under the LLOQ, constitute an insurmountable obstacle. Common approaches to estimate the MIC employ extrapolation of exponential growth model [McCarthy et al., 2016a; Hien et al., 2017]. However, the development of mechanistic parasite-growth models for parasite behaviour below the LLOQ requires additional (extensive) assumptions. These assumptions on (for now) unobservable parasite growth behaviour increase the uncertainty around model predictions, therefore, potentially lead to squandering of experimental resources if estimated MICs are used in experimental design efforts (e.g. dose prediction). Further analysis of drivers of cure such as maximum concentration or drug exposure metrics (e.g. area under the concentration-time curve) was hindered by insufficient drug-concentration data in mice and the inter-individual variability in drug-concentration profiles in humans.

Overall, several limitations, including conceptual, technical and analytical aspects, to cur-

rently employed drug efficacy indices were found. While the comparison of candidates within one experimental system is feasible with current methods, I illustrated the challenges in translating efficacy indices between experimental systems. Identification of efficacy indices that capture efficacy in a meaningful way throughout the development and implementation of interventions would assist in the construction of a platform to comparing and selecting promising compounds. These platforms could serve as a place to collect and collate data from different experiments and analysis streams. The effort to identify (non-)promising candidates as early as possible would accelerate drug development efforts and decrease late phase drug attrition due to lacking efficacy. Systematic model validation exercises that investigate the plausibility and applicability of currently used parasite-growth and treatment models in antimalarial drug development could then identify the most promising analysis tools for an efficient translation of drug efficacy indices.

6.4 The need for systematic model validation

The development strategies of new pharmaceutical antimalarial interventions are built on a sequential design, where insights into drug efficacy gained in one development stage are used to inform predictions of drug efficacy in the next development stage - from mice to experimental human infection and further on to patients [McCarthy et al., 2016a; Langhorne et al., 2011]. To guarantee reliable predictions between development stages, the predictive tools (in this case mathematical models of parasite growth and treatment) have to be assessed under three aspects:

- their biological plausibility, to allow for out-of-sample prediction;
- their ability to capture the observed parasite growth and treatment patterns; and
- the clinical relevance of incorporated parasite-host dynamics.

In Chapters 2 and 3, we illustrated that several models incorporating many different assumptions are able to capture the same parasite growth patterns based on the data available (Fig. 2.3 and Fig. 3.3). While models could be selected based on goodness of fit measures (e.g. AIC, BIC, WAIC), these commonly used selection criteria fail to incorporate approaches that consider biological plausibility. For example, of the within-host parasite-growth models analysed and developed as part of this thesis (Chapters 2 and 3), the simplest parasite growth model, namely exponential parasite growth in the absence of treatment[5], also incorporates the strongest assumption. This assumption can only hold true for the first wave of infection as any underlying

[5] *model i* in Chapters 2 and 3

parasite-host dynamics and secondary symptoms of long-term malaria infection are neglected[6]. By incorporating drug-action as a direct counteraction of parasite growth (Equation 3.11), the exponential growth model could not capture delayed parasite clearance behaviour and shifts in parasite growth after non-curative treatment in VIS (Fig. 3.4) or resource limitation in murine infection (Fig. 2.3). In contrast, using more complex, mechanistic, models of parasite growth, we were able to capture some of the observed dynamics such as RBC limitation in murine infection and the oscillation in parasite-growth in human infection (Fig. 3.3 and Fig. 3.4), but not others such as the late recrudescence observed in murine infection (Fig. 2.6 and Fig. S2.3, Appendix A).

To portray these different model assumptions and their influence on evaluating drug efficacy, I decided to illustrate and compare all growth models with the aim of initiating a dialogue between infection biologists, physicians and data analysts on the assumptions experimental analyses are based on. The insights and observations of product developers into compound properties and experimental sequence and singularities could support model building exercises and result in the identification and quantification of underlying confounders of experimental outcomes. In turn, the model analyses presented in Chapters 2 and 3 can assist in experimental design, but also provide additional guidance throughout the development process by illustrating the influence of different assumptions on host-parasite dynamics and assisting the definition of robust drug efficacy indices.

As different assumptions on parasite-growth and drug effect potentially result in different evaluations of drug efficacy and therefore potentially bias drug evaluation (Fig. 2.4), I propose the development and implementation of rigorous model validation exercises within these iterative exchanges. These validation steps should include the discussion of model assumptions and their influence on model predictions, and, if possible, calibration to data. The work in this thesis serves as a starting point for the development of systematic model validation tools (see 6.4 and 6.6).

6.5 The right tool for the right place

New preventive tools against malaria are urgently needed to protect vulnerable populations from clinical malaria in the face of rising drug resistance and operational difficulties to reach high coverages of existing preventive interventions such as seasonal malaria chemoprevention (SMC) with SP+AQ [WHO, 2019; Macintyre et al., 2018]. Anti-infective long acting injectables (LAIs) protecting from blood-stage infection, have the potential to provide universal personal

[6]These include host adaptions such as changes in erythropoeisis due to the occurrence of anemia [Lamikanra et al., 2007] and immune system responses to increasing parasite numbers [Cowman et al., 2016], as well as parasite adaptations such as changes in parasite growth rate and antigenic parasite variation [Kyes et al., 2007].

protection from infection in the absence of an effective malaria vaccine. As first *in vivo* data on their potential duration of protection and efficacy estimates are becoming available [Bakshi et al., 2018; Yuthavong et al., 2012; Kisalu et al., 2018; Tan et al., 2018], the timing is right to evaluate their prospective impact and shape their future product profiles. I employed model-based analysis of LAI properties to estimate LAI impact under the use case of protection against seasonal malaria and implementation as SMC-SP+AQ replacement in clinical trial and implementation stages. Our analysis revealed the potential trade-offs between LAI properties and implementation modalities, guiding future directions of LAI development and optimisation.

As such, the work presented in Chapter 5 provides the first quantitative analysis of LAI requirements to achieve significant public health impact and constitutes a starting point of an iterative and interactive process of exchange with all stakeholders. These include relevant development partners such as academic partners including biologists and immunologists, industry partners such as pharmaceutical companies, but also other stakeholders such as representatives of national malaria control programs, who are able to provide insights into the operational and logistic requirements and constraints. The aim of this process is to define and refine efficacy requirements, but also to determine favourable use cases and implementation settings in the Target Product Profile (TPP) of LAIs. It entails quantitative specification of LAI product properties as well as evaluation of resulting impact at the population level. Our analysis thus addresses this need by defining efficacy criteria and developing methodologies for the evaluation of LAIs on two intertwined levels: i) the duration of protection of individuals and ii) the cumulative population impact.

The embedment of modelling and simulation approaches throughout the development of new tools, facilitates a direct translation of experimental data, insights and future implementation requirements at every development stage into the TPP (Fig. 6.2). Overarching efficacy indices, impact targets and analysis methodologies are needed to assess the possibilities of new LAIs to meet the desired health goals.

The Target Candidate Profile (TCP) for molecules employed as part of a prophylactic intervention in form of a LAI states minimum essential and ideal protective efficacies of >80% and >95% respectively in human challenge studies [Macintyre et al., 2018]. The LAI product profile envisions a combination of at least two molecules. In the population implementation of LAIs in endemic settings, efficacy evaluated in human challenge studies should translate into an incidence reduction of >80% and >95% (minimum essential and ideal requirements) [Macintyre et al., 2018]. The conversion of these clinical endpoints of human challenge experiments into measures that reflect LAI population impact in implementation settings and over time is challenging:

In human challenge experiments, the time until the asexual parasite concentration in the blood exceeds a certain threshold serves as an endpoint, since liver stage activity can not be

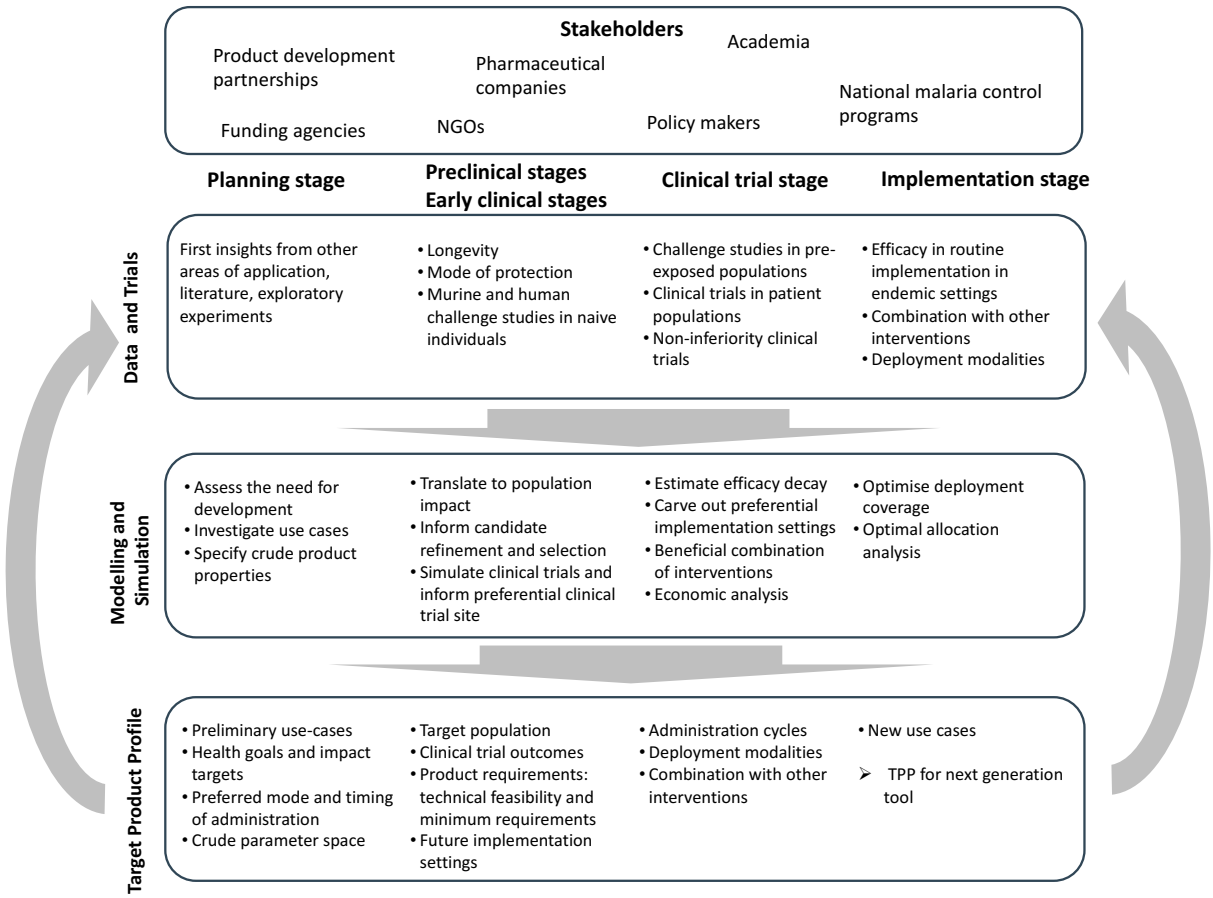

Figure 6.2: Guiding the definition of TPPs for new preventive interventions throughout their development. There is a huge potential for modelling and simulation approaches to accompany the development of new interventions from planning up to implementation stages, by serving as a platform to exchange new data and insights and subsequently update the product requirements in the TPP.

directly measured [Stanisic et al., 2018; Sulyok et al., 2017; NCT03707041, 2019]. To predict the potential population impact from these clinical trials, the experimental endpoints have to be translated into the duration and decay of individual protection. In Chapter 5, the decay of individual protection was defined by the initial protective efficacy, efficacy decay shape and the protective efficacy half-life (Equations 5.1 and 5.2). To reconcile these two approaches of defining LAI efficacy, endpoints to translate experimental data to protective efficacy parameters at population level implementation are needed. The future development of LAIs thus relies on the identification and validation of appropriate screening criteria to be used for benchmarking during candidate molecule selection processes.

Transmission intensity and length of the malaria transmission season play an important

role in the estimated population impact of LAIs and their ability to establish non-inferiority to existing preventive interventions. Our analysis revealed the limitations of LAIs in terms of product profile and use case. Under the investigated use case of SMC replacement, we found that with increasing length of the transmission season and increasing transmission intensity, the requirements for protective efficacy half-life and coverage of LAIs increase. In very high transmission settings (EIR of 150 and yearly clinical incidence over 3.3 cases per person in the target age group), LAIs need a substantially longer protective efficacy half-life or multiple applications per season, to be considered as a non-inferior SMC-SP+AQ replacement (Fig. D, Appendix C). Additionally, a thorough economic analysis is needed to investigate the value and potential advantages of LAIs in highly seasonal transmission settings, where SMC with SP+AQ is already implemented, to determine if upscaling and optimising the SMC coverage is equally or more beneficial.

Other potential use cases to be investigated with the methodology presented in Chapter 5 (Fig. 5.1) include the protection of vulnerable populations in settings with prevalent SP resistance (mostly in Eastern Africa [Okell et al., 2017]) or perennial transmission settings with multiple LAI applications over the year.

In summary, guidelines for LAI development should not only cover the inherent tool properties but couple them to the desired implementation setting and the prevalent epidemiological background. This poses new challenges in intervention allocation, as transmission settings, even within one country, are diverse and can span wide prevalence and incidence ranges [Weiss et al., 2019].

6.6 Perspectives: Harmonising the instruments of analysis

Throughout the conducted analyses, one missing piece towards refining intervention efficacy is the lack of incorporation of the mode action, meaning the way an antimalarial damages or kills parasites, into impact estimations. In recent years, progress has been made to identify the mechanism of action for many new (and old) blood-stage antimalarials [Chaparro et al., 2018]. Our approach to include mechanism of drug-action-based parasite killing into modelling and simulation analysis was introduced in Chapter 4 (Fig. 4.2). Here, we further illustrate its benefits for the development of curative blood-stage as well as preventive liver-stage antimalarials and provide a more detailed proposal for implementation. The approach comprises the following steps:

1. **Model of mode of drug action-based parasite killing**: Although the determination of mode of action is difficult, it becomes increasingly important to understand preclinical and clinical measures of drug efficacy. *In vitro* data on drug-concentration and drug-

exposure dependent parasite death through e.g. the accumulation of toxic substances or the disruption of important metabolic pathways could be used to inform the development of mechanism-based models of parasite death. For instance, these models could describe the detailed metabolic pathways that are interrupted and lead to death of the parasite.

2. **Combined mechanistic model of parasite growth and drug action**: The mechanism-based drug-action models are combined with mechanistic models of parasite-growth. The parasite-growth model of any experimental system is implemented by following these steps:

   (a) Parasite growth in the respective experimental systems (e.g. mouse or human) is captured through mechanistic models of parasite growth (Chapters 2 and 3).

   (b) Descriptions of drug-concentration over time in the respective experimental system are established (PK models).

   (c) Host-parasite pairing dependent values for the clearance of dead parasites are adjusted through estimating parasite clearance rates from parasite clearance curves after treatment.

3. *(if required)* **Model simplification**: The resulting models can be highly complex and computationally demanding, thus requiring a model simplification step before further use.

   (a) **Model reduction**: Models themselves are simplified through model reduction techniques that decrease the complexity of the models by identifying variables with limited impact on the dose-response relationship [Knöchel et al., 2018].

   (b) **Emulation**: Gaussian process emulators of highly complex models save computational time in further model analysis e.g. sensitivity analysis [Golumbeanu et al., 2022].

The resulting models can capture both the host-parasite characteristics of interest including information on underlying variability between experimental systems, and the mechanism of drug action dependent parasite killing, constant throughout all host-parasite combinations. The application of these models is diverse: The mechanistic models of drug action on the parasite could be used in modelling and simulation exercises to identify the drivers of parasiticidal efficacy for a specific compound. In a next step, the prediction of drug efficacy throughout the development process and into the implementation stages of new interventions could improve experimental design efforts through an optimisation of dosage regimens and sampling times. Furthermore, the incorporation of (simplified) drug-action models into individual-based malaria simulators offers the possibility to estimate the population impact in different settings, including varying underlying malaria transmission dynamics and case management, before clinical trials are implemented (see Chapter 5). Additionally, these complex, mechanism-based models could serve as the gold standard to validate simpler models of parasite growth and treatment through

definition of a parameter space, where approximation with simpler models accurately predicts treatment efficacy[7].

6.7 As far as the data goes - the boundaries of modelling and simulation

Models of malaria biology and epidemiology represent the knowledge, but also knowledge gaps, that define our understanding of underlying epidemiological and disease dynamics. As such, they will likely never manage to reproduce all real life dynamics and dependencies.

The analysis of drug efficacy in antimalarial drug development in Chapters 2 and 3, relies on data of four antimalarials in preclinical antimalarial development and two of those four in human volunteer infection experiments. While the combined data used to calibrate the parasite-growth and treatment models is extensive, it is intrinsically biased. The investigated compounds all showed promising antimalarial efficacy and progressed into (at least) human volunteer infection studies. However, the success rates for compounds in preclinical development and the following clinical phase 1 and phase 2a development stages are 50%, 70%, and 75% respectively [Burrows et al., 2017]. Therefore, the analysed experiments provide a one sided view on antimalarial efficacy, as the data only contains information on the dose-response relationship of efficacious antimalarials. Data on missing or insufficient antimalarial efficacy that lead to the attrition of potential compounds is absent from our analysis. A complete picture on indicators for successful antimalarials can only be developed from the combined analysis of these failed antimalarials in comparison with successful ones. This analysis could be crucial to support the definition of criteria for decision making in candidate selection.

In this thesis modelling and simulation techniques were used to understand the determinants of antimalarial efficacy during the development of pharmaceutical antimalarial interventions. Although, the evidence provided in Chapter 5 can be used to inform the development process of new interventions by supporting the decision making process, evidence in form of data is needed to validate our results. This includes the identified sources of experimental variability in Chapters 2 and 3 as well as the LAI properties identified in Chapter 5. The long-term integration of model-informed drug discovery and development (also known as MID3) into research and development approaches requires an integrated and consistent modelling approach, that is accepted by decision makers along the clinical development process as well as regulatory authorities [Marshall et al., 2016]. The foundation for these approaches has been laid. Now, data to validate these new insights is needed to further the routine implementation of model informed drug development. In the absence of further data, a careful dissemination and communication of the

[7] such as exponential growth models or models concentration on specific parasite-stages to analyse stage-specificity

assumptions the models and analysis are based on is crucial to build confidence of collaborators and potential stakeholders in our analysis results.

6.8 Conclusion - Modelling to guide development of pharmaceutical interventions against malaria

This thesis demonstrates how modelling can assist and guide the development of pharmaceutical interventions against malaria from candidate selection to product implementation.

The work in this thesis evaluates the underlying dynamics influencing the assessment of drug efficacy. It thereby paves the way for improvement of experimental design and definition of efficacy indices and targets, leading to a more informed evaluation of drug candidates. Additionally, this work highlights the importance and use of modelling and simulation approaches in facilitating a combined analysis of intervention characteristics and the future experimental and implementation settings. Through the estimation of potential public health impact of new interventions, this work helps to refine TPPs and steer compound development and selection from a population perspective.

During the extensive development process of new antimalarial interventions, the combined amount of data generated is extensive. Yet, the efficient combination and exploitation of this information are challenging and the full potential of these insights to inform decision making is often lost. Furthermore, the siloed analysis between experiments and compounds complicates the efficient translation of information between development stages. In general, the process of model building promotes the collation and synthesis of knowledge from various sources, fostering the dialogue between stakeholders and researchers from different disciplines. I would thus like to emphasise the urgent need for a model-informed development approach for pharmaceutical interventions against malaria, spanning the definition of product requirements, experimental analysis and implementation settings and involving all stakeholders.

This thesis showed that modelling and careful reflection on its limits and potentials exhibits great prospects as a tool for decision-making. Specifically, I hope that the undertaking of this thesis has advanced the sharing of data and crucial insights into malaria biology, epidemiology and the effect of antimalarial interventions.

Bibliography

Ambrose, P. G. et al. (2007). "Pharmacokinetics-Pharmacodynamics of Antimicrobial Therapy: It's Not Just for Mice Anymore". In: *Clinical Infectious Diseases* 44.1, pp. 79–86.

Anderson, R. M. et al. (1989). "Non-Linear Phenomena in Host-Parasite Interactions". In: *Parasitology* 99 Suppl, S59–79.

Angulo-Barturen, I. et al. (2008). "A Murine Model of Falciparum-Malaria by in Vivo Selection of Competent Strains in Non-Myelodepleted Mice Engrafted with Human Erythrocytes". In: *PLOS ONE* 3.5, e2252.

Aponte, J. J. et al. (2009). "Efficacy and Safety of Intermittent Preventive Treatment with Sulfadoxine-Pyrimethamine for Malaria in African Infants: A Pooled Analysis of Six Randomised, Placebo-Controlled Trials". In: *The Lancet* 374.9700, pp. 1533–1542.

Ariey, F. et al. (2014). "A Molecular Marker of Artemisinin-Resistant Plasmodium Falciparum Malaria". In: *Nature* 505.7481 (7481), pp. 50–55.

Ashley, E. A. and A. P. Phyo (2018). "Drugs in Development for Malaria". In: *Drugs* 78.9, pp. 861–879.

Austin, D. J. et al. (1998). "The Dynamics of Drug Action on the Within-Host Population Growth of Infectious Agents: Melding Pharmacokinetics with Pathogen Population Dynamics". In: *Journal of Theoretical Biology* 194.3, pp. 313–39.

Baba, E. et al. (2020). "Effectiveness of Seasonal Malaria Chemoprevention at Scale in West and Central Africa: An Observational Study". In: *The Lancet* 396.10265, pp. 1829–1840.

Bakshi, R. P. et al. (2018). "Long-Acting Injectable Atovaquone Nanomedicines for Malaria Prophylaxis". In: *Nature Communications* 9.1, p. 315.

Bates, I. (2017). "2 - Reference Ranges and Normal Values". In: *Dacie and Lewis Practical Haematology (Twelfth Edition)*. Ed. by B. J. Bain et al. Elsevier, pp. 8–17.

Bhatt, S. et al. (2015). "The Effect of Malaria Control on Plasmodium Falciparum in Africa between 2000 and 2015." In: *Nature* 526.7572, pp. 207–211.

Binois, M. and R. B. Gramacy (2017). *hetGP: Heteroskedastic Gaussian Process Modeling and Design under Replication.* Version Version 1.1.2.

Blasco, B. et al. (2017). "Antimalarial Drug Resistance: Linking Plasmodium Falciparum Parasite Biology to the Clinic". In: *Nature Medicine* 23.8 (8), pp. 917–928.

Borrmann, S. et al. (2008). "Revisiting the Design of Phase III Clinical Trials of Antimalarial Drugs for Uncomplicated Plasmodium Falciparum Malaria". In: *PLOS Medicine* 5.11, e227.

Bosman, A. and K. N. Mendis (2007). "A Major Transition in Malaria Treatment: The Adoption and Deployment of Artemisinin-Based Combination Therapies". In: *The American Journal of Tropical Medicine and Hygiene* 77 (6 Suppl), pp. 193–197.

Boss, C. et al. (2016). "Discovery and Characterization of ACT-451840: An Antimalarial Drug with a Novel Mechanism of Action". In: *ChemMedChem* 11.18, pp. 1995–2014.

Briët, O. J. and M. A. Penny (2013). "Repeated Mass Distributions and Continuous Distribution of Long-Lasting Insecticidal Nets: Modelling Sustainability of Health Benefits from Mosquito Nets, Depending on Case Management". In: *Malaria Journal* 12.1, p. 401.

Burgert, L. et al. (2020). "Ensemble Modeling Highlights Importance of Understanding Parasite-Host Behavior in Preclinical Antimalarial Drug Development". In: *Scientific Reports* 10.1, p. 4410.

Burgert, L. et al. (2021). "Parasite-Host Dynamics throughout Antimalarial Drug Development Stages Complicate the Translation of Parasite Clearance". In: *Antimicrobial Agents and Chemotherapy* 65.4, e01539–20.

Burgert, L. et al. (2022). "Model-Informed Target Product Profiles of Long-Acting-Injectables for Use as Seasonal Malaria Prevention". In: *PLOS Global Public Health* 2.3, e0000211.

Burrows, J. N. et al. (2013). "Designing the next Generation of Medicines for Malaria Control and Eradication". In: *Malaria Journal* 12.

Burrows, J. N. et al. (2017). "New Developments in Anti-Malarial Target Candidate and Product Profiles". In: *Malaria Journal* 16.1, p. 26.

Cameron, E. et al. (2015). "Defining the Relationship between Infection Prevalence and Clinical Incidence of Plasmodium Falciparum Malaria". In: *Nature Communications* 6.1 (1), p. 8170.

Camponovo, F. et al. (2019). "Mass Campaigns Combining Antimalarial Drugs and Anti-Infective Vaccines as Seasonal Interventions for Malaria Control, Elimination and Prevention of Resurgence: A Modelling Study". In: *BMC infectious diseases* 19.1, p. 920.

Cao, P. et al. (2017). "A Dynamic Stress Model Explains the Delayed Drug Effect in Artemisinin Treatment of Plasmodium Falciparum". In: *Antimicrobial Agents and Chemotherapy* 61.12.

Cao, P. et al. (2019). "Modeling the Dynamics of Plasmodium Falciparum Gametocytes in Humans during Malaria Infection". In: *eLife* 8, e49058.

Challenger, J. D. et al. (2017). "Assessing the Impact of Imperfect Adherence to Artemether-Lumefantrine on Malaria Treatment Outcomes Using within-Host Modelling". In: *Nature Communications* 8.1 (1), p. 1373.

Chandramohan, D. et al. (2021). "Seasonal Malaria Vaccination with or without Seasonal Malaria Chemoprevention". In: *New England Journal of Medicine* 385.11, pp. 1005–1017.

Chaparro, M. J. et al. (2018). "Efforts Aimed To Reduce Attrition in Antimalarial Drug Discovery: A Systematic Evaluation of the Current Antimalarial Targets Portfolio". In: *ACS Infectious Diseases* 4.4, pp. 568–576.

Charman, S. A. et al. (2011). "Synthetic Ozonide Drug Candidate OZ439 Offers New Hope for a Single-Dose Cure of Uncomplicated Malaria". In: *Proc Natl Acad Sci U S A* 108.11, pp. 4400–5.

Charman, S. A. et al. (2020). "An in Vitro Toolbox to Accelerate Anti-Malarial Drug Discovery and Development". In: *Malaria Journal* 19.1, p. 1.

Chitnis, N. et al. (2012). "A Periodically-Forced Mathematical Model for the Seasonal Dynamics of Malaria in Mosquitoes". In: *Bulletin of Mathematical Biology* 74.5, pp. 1098–1124.

Chitnis, N. et al. (2008). "A Mathematical Model for the Dynamics of Malaria in Mosquitoes Feeding on a Heterogeneous Host Population." In: *Journal of biological dynamics* 2.3, pp. 259–285.

Chotivanich, K. et al. (2000). "Parasite Multiplication Potential and the Severity of Falciparum Malaria". In: *The Journal of Infectious Diseases* 181.3, pp. 1206–1209.

Chughlay, M. F. et al. (2020). "First-in-Human Clinical Trial to Assess the Safety, Tolerability and Pharmacokinetics of P218, a Novel Candidate for Malaria Chemoprotection". In: *British Journal of Clinical Pharmacology* 86.6, pp. 1113–1124.

Cisse, B. et al. (2016). "Effectiveness of Seasonal Malaria Chemoprevention in Children under Ten Years of Age in Senegal: A Stepped-Wedge Cluster-Randomised Trial". In: *PLOS Medicine* 13.11, e1002175.

Cissé, B. et al. (2006). "Seasonal Intermittent Preventive Treatment with Artesunate and Sulfadoxine-Pyrimethamine for Prevention of Malaria in Senegalese Children: A Randomised, Placebo-Controlled, Double-Blind Trial". In: *Lancet* 367.9511, pp. 659–667.

Cohen, J. et al. (2010). "From the Circumsporozoite Protein to the RTS,S/AS Candidate Vaccine". In: *Human Vaccines* 6.1, pp. 90–96.

Cohen, J. M. et al. (2012). "Malaria Resurgence: A Systematic Review and Assessment of Its Causes". In: *Malaria Journal* 11.1, p. 122.

Coldiron, M. E. et al. (2017). "Seasonal Malaria Chemoprevention: Successes and Missed Opportunities". In: *Malaria Journal* 16.1, p. 481.

Cotter, C. et al. (2013). "The Changing Epidemiology of Malaria Elimination: New Strategies for New Challenges". In: *The Lancet* 382.9895, pp. 900–911.

Cowman, A. F. et al. (2016). "Malaria: Biology and Disease". In: *Cell* 167.3, pp. 610–624.

Craig, W. A. (1998). "Pharmacokinetic/Pharmacodynamic Parameters: Rationale for Antibacterial Dosing of Mice and Men". In: *Clinical Infectious Diseases: An Official Publication of the Infectious Diseases Society of America* 26.1, 1–10; quiz 11–12.

Cromer, D. et al. (2006). "Preferential Invasion of Reticulocytes during Late-Stage Plasmodium Berghei Infection Accounts for Reduced Circulating Reticulocyte Levels". In: *International Journal for Parasitology* 36.13, pp. 1389–1397.

Dahal, P. et al. (2017). "Statistical Methods to Derive Efficacy Estimates of Anti-Malarials for Uncomplicated Plasmodium Falciparum Malaria: Pitfalls and Challenges". In: *Malaria Journal* 16.1, pp. 430–430.

Deharo, E. et al. (1996). "The Erythrocytic Schizogony of Two Synchronized Strains of Plasmodium Berghei, NK65 and ANKA, in Normocytes and Reticulocytes". In: *Parasitology Research* 82.2, pp. 178–182.

Desjardins, R. E. et al. (1979). "Quantitative Assessment of Antimalarial Activity in Vitro by a Semiautomated Microdilution Technique." In: *Antimicrobial Agents and Chemotherapy* 16.6, pp. 710–718.

Diawara, F. et al. (2017). "Measuring the Impact of Seasonal Malaria Chemoprevention as Part of Routine Malaria Control in Kita, Mali". In: *Malaria Journal* 16.1, p. 325.

Dieng et al. (2019). "Contrasting Asymptomatic and Drug Resistance Gene Prevalence of Plasmodium Falciparum in Ghana: Implications on Seasonal Malaria Chemoprevention". In: *Genes* 10.7, p. 538.

Ding, J. et al. (2019). "Adherence and Population Pharmacokinetic Properties of Amodiaquine When Used for Seasonal Malaria Chemoprevention in African Children". In: *Clin Pharmacol Ther.*

Dini, S. et al. (2018). "Investigating the Efficacy of Triple Artemisinin-Based Combination Therapies for Treating Plasmodium Falciparum Malaria Patients Using Mathematical Modeling". In: *Antimicrobial Agents and Chemotherapy* 62.11.

Diouf, I et al. (2015). "Détermination Des Paramètres Du Paludisme Au Sénégal à Partir de Données Météorlogiques de Stations et de Réanalyses". In: *XXVIIIe Colloque de l'Association Internationale de Climatologie, Liège 2015.*

Dong, Y. et al. (2017). "Structure-Activity Relationship of the Antimalarial Ozonide Artefenomel (OZ439)". In: *Journal of Medicinal Chemistry* 60.7, pp. 2654–2668.

Dong, Y. et al. (2010). "The Structure-Activity Relationship of the Antimalarial Ozonide Arterolane (OZ277)". In: *Journal of Medicinal Chemistry* 53.1, pp. 481–491.

Doolan, D. L. et al. (2009). "Acquired Immunity to Malaria". In: *Clinical Microbiology Reviews* 22.1, pp. 13–36.

Douglas, A. D. et al. (2011). "Substantially Reduced Pre-Patent Parasite Multiplication Rates Are Associated with Naturally Acquired Immunity to Plasmodium Falciparum". In: *Journal of Infectious Diseases* 203.9, pp. 1337–40.

Druetz, T. (2018). "Evaluation of Direct and Indirect Effects of Seasonal Malaria Chemoprevention in Mali". In: *Scientific Reports* 8.1, p. 8104.

Drusano, G. L. (2004). "Antimicrobial Pharmacodynamics: Critical Interactions of 'Bug and Drug'". In: *Nature Reviews Microbiology* 2.4 (4), pp. 289–300.

Duffy, S. et al. (2017). "Screening the Medicines for Malaria Venture Pathogen Box across Multiple Pathogens Reclassifies Starting Points for Open-Source Drug Discovery". In: *Antimicrobial Agents and Chemotherapy* 61.9.

Eckhoff, P. A. (2011). "A Malaria Transmission-Directed Model of Mosquito Life Cycle and Ecology". In: *Malaria Journal* 10.1, p. 303.

Edelstein, M. et al. (2015). "Ebola: The Challenging Road to Recovery". In: *The Lancet* 385.9984, pp. 2234–2235.

Ekström, A. M. et al. (2016). "INDEPTH Network: Contributing to the Data Revolution". In: *The Lancet Diabetes & Endocrinology* 4.2, p. 97.

Engwerda, C. R. et al. (2012). "Experimentally Induced Blood Stage Malaria Infection as a Tool for Clinical Research". In: *Trends in Parasitology* 28.11, pp. 515–521.

Fidock, D. A. et al. (2004). "Antimalarial Drug Discovery: Efficacy Models for Compound Screening". In: *Nature Reviews. Drug Discovery* 3.6, pp. 509–20.

Flannery, E. L. et al. (2013). "Antimalarial Drug Discovery - Approaches and Progress towards New Medicines". In: *Nature Reviews Microbiology* 11.12, pp. 849–62.

Flegg, J. A. et al. (2011). "Standardizing the Measurement of Parasite Clearance in Falciparum Malaria: The Parasite Clearance Estimator". In: *Malaria Journal* 10.

Fowkes, F. J. I. et al. (2016). "Immunity to Malaria in an Era of Declining Malaria Transmission". In: *Parasitology* 143.2, pp. 139–153.

Gaur, A. H. et al. (2020). "Safety, Tolerability, Pharmacokinetics, and Antimalarial Efficacy of a Novel Plasmodium Falciparum ATP4 Inhibitor SJ733: A First-in-Human and Induced Blood-Stage Malaria Phase 1a/b Trial". In: *The Lancet Infectious Diseases*.

Gilmartin, C and D Collins (2016). *The Costs of Seasonal Malaria Chemoprevention (SMC) in the Sahel Sub-Region of Africa: A Multi-Country Cost Analysis of the ACCESS-SMC Project*.

Golumbeanu, M. et al. (2022). "Leveraging Mathematical Models of Disease Dynamics and Machine Learning to Improve Development of Novel Malaria Interventions". In: *Infectious Diseases of Poverty* 11.1, p. 61.

Greischar, M. A. et al. (2019). "The Challenge of Quantifying Synchrony in Malaria Parasites". In: *Trends in Parasitology* 35.5, pp. 341–355.

Griffin, J. T. et al. (2014). "Estimates of the Changing Age-Burden of Plasmodium Falciparum Malaria Disease in Sub-Saharan Africa". In: *Nature Communications* 5.1 (1), p. 3136.

Griffin, J. T. et al. (2010). "Protective Efficacy of Intermittent Preventive Treatment of Malaria in Infants (IPTi) Using Sulfadoxine-Pyrimethamine and Parasite Resistance". In: *PLOS ONE* 5.9, e12618.

Guidi, M. et al. (2019). "Population Pharmacokinetics and Pharmacodynamics of the Artesunate-Mefloquine Fixed Dose Combination for the Treatment of Uncomplicated Falciparum Malaria in African Children". In: *Malaria Journal* 18.1, p. 139.

Haakenstad, A. et al. (2019). "Tracking Spending on Malaria by Source in 106 Countries, 2000–16: An Economic Modelling Study". In: *The Lancet Infectious Diseases* 19.7, pp. 703–716.

Hemingway, J. et al. (2016). "Tools and Strategies for Malaria Control and Elimination: What Do We Need to Achieve a Grand Convergence in Malaria?" In: *PLOS Biology* 14.3, e1002380.

Hetzel, C. and R. M. Anderson (1996). "The Within-Host Cellular Dynamics of Bloodstage Malaria: Theoretical and Experimental Studies". In: *Parasitology* 113, pp. 25–38.

Hien, T. T. et al. (2017). "Estimation of the in Vivo MIC of Cipargamin in Uncomplicated Plasmodium Falciparum Malaria". In: *Antimicrobial Agents and Chemotherapy* 61.

Hietala, S. F. et al. (2010). "Population Pharmacokinetics and Pharmacodynamics of Artemether and Lumefantrine during Combination Treatment in Children with Uncomplicated Falciparum Malaria in Tanzania". In: *Antimicrobial Agents and Chemotherapy* 54.11, pp. 4780–4788.

Hoffman, S. L. et al. (2015). "The March toward Malaria Vaccines". In: *Vaccine*. Advancing Vaccines and Immunization 33, pp. D13–D23.

Hoshen, M. B. et al. (2000). "Mathematical Modelling of the Within-Host Dynamics of Plasmodium Falciparum". In: *Parasitology* 121 (Pt 3), pp. 227–35.

Huskey, S.-E. W. et al. (2016). "KAE609 (Cipargamin), a New Spiroindolone Agent for the Treatment of Malaria: Evaluation of the Absorption, Distribution, Metabolism, and Excretion of a Single Oral 300-Mg Dose of [14C]KAE609 in Healthy Male Subjects". In: *Drug Metabolism and Disposition: The Biological Fate of Chemicals* 44.5, pp. 672–682.

Imwong, M. et al. (2020). "Molecular Epidemiology of Resistance to Antimalarial Drugs in the Greater Mekong Subregion: An Observational Study". In: *The Lancet Infectious Diseases* 0.0.

Jimenez-Diaz, M. B. et al. (2009). "Improved Murine Model of Malaria Using Plasmodium Falciparum Competent Strains and Non-Myelodepleted NOD-scid IL2Rgammanull Mice Engrafted with Human Erythrocytes". In: *Antimicrobial Agents and Chemotherapy* 53.10, pp. 4533–6.

Jiménez-Díaz, M. B. et al. (2014a). "Animal Models of Efficacy to Accelerate Drug Discovery in Malaria". In: *Parasitology* 141.1, pp. 93–103.

Jiménez-Díaz, M. B. et al. (2013). "A New in Vivo Screening Paradigm to Accelerate Antimalarial Drug Discovery". In: *PLOS ONE* 8.6, e66967.

Jiménez-Díaz, M. B. et al. (2014b). "(+)-SJ733, a Clinical Candidate for Malaria That Acts through ATP4 to Induce Rapid Host-Mediated Clearance of Plasmodium". In: *Proceedings of the National Academy of Sciences* 111.50, E5455–E5462.

Jiménez-Díaz, M. B. et al. (2009). "Quantitative Measurement of Plasmodium-infected Erythrocytes in Murine Models of Malaria by Flow Cytometry Using Bidimensional Assessment of SYTO-16 Fluorescence". In: *Cytometry Part A* 75A.3, pp. 225–235.

Julien, J.-P. and H. Wardemann (2019). "Antibodies against Plasmodium Falciparum Malaria at the Molecular Level". In: *Nature Reviews Immunology* 19.12 (12), pp. 761–775.

Kamath, A. V. (2016). "Translational Pharmacokinetics and Pharmacodynamics of Monoclonal Antibodies". In: *Drug Discovery Today: Technologies*. Technology – Translational Pharmacology 21–22, pp. 75–83.

Khoury, D. S. et al. (2016). "Defining the Effectiveness of Antimalarial Chemotherapy: Investigation of the Lag in Parasite Clearance Following Drug Administration". In: *Journal of Infectious Diseases* 214.5, pp. 753–61.

Khoury, D. S. et al. (2017a). "Characterising the Effect of Antimalarial Drugs on the Maturation and Clearance of Murine Blood-Stage Plasmodium Parasites in Vivo". In: *International Journal for Parasitology* 47.14, pp. 913–922.

Khoury, D. S. et al. (2017b). "Host-Mediated Impairment of Parasite Maturation during Blood-Stage Plasmodium Infection". In: *Proceedings of the National Academy of Sciences of the United States of America* 114.29, pp. 7701–7706.

Khoury, D. S. et al. (2018). "Within-Host Modeling of Blood-Stage Malaria". In: *Immunological Reviews* 285.1, pp. 168–193.

Khoury, D. S. et al. (2020). "Malaria Parasite Clearance: What Are We Really Measuring?" In: *Trends in Parasitology* 36.5, pp. 413–426.

Kingston, H. W. et al. (2017). "Disease Severity and Effective Parasite Multiplication Rate in Falciparum Malaria". In: *Open forum infectious diseases* 4.4, ofx169–ofx169.

Kisalu, N. K. et al. (2018). "A Human Monoclonal Antibody Prevents Malaria Infection by Targeting a New Site of Vulnerability on the Parasite". In: *Nature Medicine* 24.4, pp. 408–416.

Knöchel, J. et al. (2018). "Understanding and Reducing Complex Systems Pharmacology Models Based on a Novel Input-Response Index". In: *Journal of Pharmacokinetics and Pharmacodynamics* 45.1, pp. 139–157.

Kock, M. de et al. (2018). "Population Pharmacokinetic Properties of Sulfadoxine and Pyrimethamine: A Pooled Analysis To Inform Optimal Dosing in African Children with Uncomplicated Malaria". In: *Antimicrobial Agents and Chemotherapy* 62.5.

Kontermann, R. E. (2009). "Strategies to Extend Plasma Half-Lives of Recombinant Antibodies". In: *BioDrugs: Clinical Immunotherapeutics, Biopharmaceuticals and Gene Therapy* 23.2, pp. 93–109.

Krause, A. et al. (2016). "Pharmacokinetic/Pharmacodynamic Modelling of the Antimalarial Effect of Actelion-451840 in an Induced Blood Stage Malaria Study in Healthy Subjects". In: *British Journal of Clinical Pharmacology* 82.2, pp. 412–421.

Kreutz, C. and J. Timmer (2009). "Systems Biology: Experimental Design". In: *The FEBS Journal* 276.4, pp. 923–942.

Kuhen, K. L. et al. (2014). "KAF156 Is an Antimalarial Clinical Candidate with Potential for Use in Prophylaxis, Treatment, and Prevention of Disease Transmission". In: *Antimicrobial agents and chemotherapy* 58.9, pp. 5060–5067.

Kyes, S. A. et al. (2007). "Antigenic Variation in Plasmodium Falciparum: Gene Organization and Regulation of the Var Multigene Family". In: *Eukaryotic Cell* 6.9, pp. 1511–1520.

Lamikanra, A. A. et al. (2007). "Malarial Anemia: Of Mice and Men". In: *Blood* 110.1, pp. 18–28.

Langhorne, J. et al. (2011). "The Relevance of Non-Human Primate and Rodent Malaria Models for Humans". In: *Malaria Journal* 10, p. 23.

Le Bihan, A. et al. (2016). "Characterization of Novel Antimalarial Compound ACT-451840: Preclinical Assessment of Activity and Dose-Efficacy Modeling". In: *PLoS Med* 13.10, e1002138.

Llanos-Cuentas, A. et al. (2018). "Antimalarial activity of single-dose DSM265, a novel plasmodium dihydroorotate dehydrogenase inhibitor, in patients with uncomplicated Plasmodium

falciparum or Plasmodium vivax malaria infection: a proof-of-concept, open-label, phase 2a study". In: *The Lancet Infectious Diseases*.

Loua, K and P. Milligan (2019). *Seasonal Malaria Chemoprevention Coverage Survey in Guinea, 2018*.

Macdonald, G (1957). *The Epidemiology and Control of Malaria*. London: Oxford University Press.

Macintyre, F. et al. (2017). "A Randomised, Double-Blind Clinical Phase II Trial of the Efficacy, Safety, Tolerability and Pharmacokinetics of a Single Dose Combination Treatment with Artefenomel and Piperaquine in Adults and Children with Uncomplicated Plasmodium Falciparum Malaria". In: *BMC medicine* 15.1, pp. 181–181.

Macintyre, F. et al. (2018). "Injectable Anti-Malarials Revisited: Discovery and Development of New Agents to Protect against Malaria". In: *Malaria journal* 17.1, pp. 402–402.

Maire, N. et al. (2006). "A Model for Natural Immunity to Asexual Blood Stages of Plasmodium Falciparum Malaria in Endemic Areas." In: *The American journal of tropical medicine and hygiene* 75 (2 Suppl), pp. 19–31.

Marquart, L. et al. (2015). "Evaluating the Pharmacodynamic Effect of Antimalarial Drugs in Clinical Trials by Quantitative Polymerase Chain Reaction". In: *Antimicrob Agents Chemother* 59.

Marshall, S. F. et al. (2016). "Good Practices in Model-Informed Drug Discovery and Development: Practice, Application, and Documentation". In: *CPT: Pharmacometrics & Systems Pharmacology* 5.3, pp. 93–122.

McCarthy, J. S. et al. (2011). "A Pilot Randomised Trial of Induced Blood-Stage Plasmodium Falciparum Infections in Healthy Volunteers for Testing Efficacy of New Antimalarial Drugs". In: *PLOS ONE* 6.8, e21914.

McCarthy, J. S. et al. (2016a). "Linking Murine and Human Plasmodium Falciparum Challenge Models in a Translational Path for Antimalarial Drug Development". In: *Antimicrob Agents Chemother* 60.

McCarthy, J. S. et al. (2017). "Safety, Tolerability, Pharmacokinetics, and Activity of the Novel Long-Acting Antimalarial DSM265: A Two-Part First-in-Human Phase 1a/1b Randomised Study". In: *Lancet Infect Dis* 17.6, pp. 626–635.

McCarthy, J. S. et al. (2016b). "A Phase II Pilot Trial to Evaluate Safety and Efficacy of Ferroquine against Early Plasmodium Falciparum in an Induced Blood-Stage Malaria Infection Study". In: *Malaria Journal* 15.1, p. 469.

McCarthy, J. S. et al. (2016c). "Efficacy of OZ439 (Artefenomel) against Early Plasmodium Falciparum Blood-Stage Malaria Infection in Healthy Volunteers". In: *Journal of Antimicrobial Chemotherapy* 71.9, pp. 2620–2627.

McCarthy, J. S. et al. (2019). "A Single-Dose Combination Study with the Experimental Antimalarials Artefenomel and DSM265 To Determine Safety and Antimalarial Activity against Blood-Stage Plasmodium Falciparum in Healthy Volunteers". In: *Antimicrobial Agents and Chemotherapy* 64.1.

McCarthy, J. S. et al. (2020). "A Phase 1, Placebo-controlled, Randomized, Single Ascending Dose Study and a Volunteer Infection Study to Characterize the Safety, Pharmacokinetics, and Antimalarial Activity of the Plasmodium Phosphatidylinositol 4-Kinase Inhibitor MMV390048". In: *Clinical Infectious Diseases*.

McClure, N. S. and T. Day (2014). "A Theoretical Examination of the Relative Importance of Evolution Management and Drug Development for Managing Resistance". In: *Proceedings. Biological Sciences* 281.1797.

McNamara, C. W. et al. (2013). "Targeting Plasmodium PI(4)K to Eliminate Malaria". In: *Nature* 504.7479, pp. 248–253.

Molineaux, L. et al. (2001). "Plasmodium Falciparum Parasitaemia Described by a New Mathematical Model". In: *Parasitology* 122 (Pt 4), pp. 379–91.

Monolix version 2016R1 (2016). Antony, France: Lixoft SAS.

Murithi, J. M. et al. (2020). "Combining Stage Specificity and Metabolomic Profiling to Advance Antimalarial Drug Discovery". In: *Cell Chemical Biology* 27.2, 158–171.e3.

Murray, L. et al. (2017). "Multiplication Rate Variation in the Human Malaria Parasite Plasmodium Falciparum". In: *Scientific Reports* 7.1, p. 6436.

Ménard, D. et al. (2016). "A Worldwide Map of Plasmodium Falciparum K13-Propeller Polymorphisms". In: *New England Journal of Medicine* 374.25, pp. 2453–2464.

Nagle, A. et al. (2012). "Imidazolopiperazines: Lead Optimization of the Second-Generation Antimalarial Agents". In: *Journal of Medicinal Chemistry* 55.9, pp. 4244–4273.

Nakazawa, S. et al. (2002). "Malaria Parasites Giving Rise to Recrudescence in Vitro". In: *Antimicrob Agents Chemother* 46.4, pp. 958–965.

NCT03707041 (2019). *Safety, Tolerability and Chemoprotective Activity of P218 in PfSPZ Challenge Model*. URL: `https://clinicaltrials.gov/ct2/show/record/NCT03707041` (visited on 08/11/2020).

Novartis (2016). *A Phase 1 Interventional, Sequential, Single-Site Study to Characterize the Effectiveness of Oral KAE609 in Reducing Asexual and Sexual Blood-Stage P. Falciparum Following Inoculation in Healthy Volunteers and Subsequent Infectivity to Mosquitoes.* URL: `https://www.novctrd.com/CtrdWeb/displaypdf.nov?trialresultid=17484`.

Nunes, J. K. et al. (2009). "Secreted Antibody Is Required for Immunity to Plasmodium Berghei". In: *J Infection and Immunity* 77.1, pp. 414–418.

O'Flaherty, K. et al. (2019). "Contribution of Functional Antimalarial Immunity to Measures of Parasite Clearance in Therapeutic Efficacy Studies of Artemisinin Derivatives". In: *Journal of Infectious Diseases* 220.7, pp. 1178–1187.

Okell, L. C. et al. (2017). "Mapping Sulphadoxine-Pyrimethamine-Resistant Plasmodium Falciparum Malaria in Infected Humans and in Parasite Populations in Africa". In: *Scientific Reports* 7.

OpenMalaria Github. URL: `https://github.com/SwissTPH/openmalaria/` (visited on 10/09/2020).

O'Flaherty, K. et al. (2017). "Immunity as a Predictor of Anti-Malarial Treatment Failure: A Systematic Review". In: *Malaria Journal* 16.1, p. 158.

Papaspiliopoulos, O. et al. (2007). "A General Framework for the Parametrization of Hierarchical Models". In: *Statistical Science* 22.1, pp. 59–73.

Paquet, T. et al. (2017). "Antimalarial Efficacy of MMV390048, an Inhibitor of Plasmodium Phosphatidylinositol 4-Kinase". In: *Science translational medicine* 9.387, eaad9735.

Patel, K. et al. (2013). "Mechanism-Based Model of Parasite Growth and Dihydroartemisinin Pharmacodynamics in Murine Malaria". In: *Antimicrobial Agents and Chemotherapy* 57.1, pp. 508–16.

Patel, K. et al. (2014). "Predicting the Parasite Killing Effect of Artemisinin Combination Therapy in a Murine Malaria Model". In: *Journal of Antimicrobial Chemotherapy* 69.8, pp. 2155–63.

Pellicciari, R. (2017). "Attrition in the Pharmaceutical Industry — Reasons, Implications, and Pathways Forward. Edited by Alexander Alex, C. John Harris, Dennis A. Smith". In: *ChemMedChem* 12.13, pp. 1097–1098.

Pemberton-Ross, P. et al. (2015). "Age-Shifting in Malaria Incidence as a Result of Induced Immunological Deficit: A Simulation Study". In: *Malaria Journal* 14.1, p. 287.

Penny, M. A. et al. (2015). "The Time-Course of Protection of the RTS,S Vaccine against Malaria Infections and Clinical Disease". In: *Malaria Journal* 14.1, p. 437.

Penny, M. A. et al. (2015). "Distribution of Malaria Exposure in Endemic Countries in Africa Considering Country Levels of Effective Treatment". In: *Malaria Journal* 14.

Penny, M. A. et al. (2016). "Public Health Impact and Cost-Effectiveness of the RTS,S/AS01 Malaria Vaccine: A Systematic Comparison of Predictions from Four Mathematical Models." In: *Lancet* 387.10016, pp. 367–375.

Phillips, M. A. et al. (2015). "A Long-Duration Dihydroorotate Dehydrogenase Inhibitor (DSM265) for Prevention and Treatment of Malaria". In: *Science translational medicine* 7.296, 296ra111.

Phillips, M. A. et al. (2016). "A Triazolopyrimidine-Based Dihydroorotate Dehydrogenase Inhibitor with Improved Drug-like Properties for Treatment and Prevention of Malaria". In: *ACS infectious diseases* 2.12, pp. 945–957.

Phillips, M. A. et al. (2017). "Malaria". In: *Nature Reviews Disease Primers* 3, p. 17050.

Phyo, A. P. et al. (2016a). "Antimalarial Activity of Artefenomel (OZ439), a Novel Synthetic Antimalarial Endoperoxide, in Patients with Plasmodium Falciparum and Plasmodium Vivax Malaria: An Open-Label Phase 2 Trial". In: *The Lancet. Infectious Diseases* 16.1, pp. 61–69.

Phyo, A. P. et al. (2016b). "Declining Efficacy of Artemisinin Combination Therapy Against P. Falciparum Malaria on the Thai-Myanmar Border (2003-2013): The Role of Parasite Genetic Factors". In: *Clinical Infectious Diseases: An Official Publication of the Infectious Diseases Society of America* 63.6, pp. 784–791.

Pitt, C. et al. (2017). "Large-Scale Delivery of Seasonal Malaria Chemoprevention to Children under 10 in Senegal: An Economic Analysis". In: *Health Policy and Planning* 32.9, pp. 1256–1266.

Plucinski, M. M. et al. (2015). "Robust Algorithm for Systematic Classification of Malaria Late Treatment Failures as Recrudescence or Reinfection Using Microsatellite Genotyping". In: *Antimicrobial Agents and Chemotherapy* 59.10, pp. 6096–100.

Pryce, J. et al. (2018). "Insecticide-Treated Nets for Preventing Malaria". In: *The Cochrane Database of Systematic Reviews* 11, p. CD000363.

R Core Team. R: A Language and Environment for Statistical Computing. URL: `http://www.R-project.org` (visited on 02/10/2017).

Rabinovich, R. N. et al. (2017). "malERA: An Updated Research Agenda for Malaria Elimination and Eradication". In: *PLOS Medicine* 14.11, e1002456.

Ranson, H. and N. Lissenden (2016). "Insecticide Resistance in African Anopheles Mosquitoes: A Worsening Situation That Needs Urgent Action to Maintain Malaria Control". In: *Trends in Parasitology*. Special Issue: Vectors 32.3, pp. 187–196.

Rasmussen, C. E. (2004). "Gaussian Processes in Machine Learning". In: *Advanced Lectures on Machine Learning: ML Summer Schools 2003, Canberra, Australia, February 2 - 14, 2003, Tübingen, Germany, August 4 - 16, 2003, Revised Lectures*. Ed. by O. Bousquet et al. Berlin, Heidelberg: Springer Berlin Heidelberg, pp. 63–71.

Reiker, T. et al. (2019). "Modelling Reactive Case Detection Strategies for Interrupting Transmission of Plasmodium Falciparum Malaria". In: *Malaria Journal* 18.1, p. 259.

Reiker, T. et al. (2021). "Emulator-Based Bayesian Optimization for Efficient Multi-Objective Calibration of an Individual-Based Model of Malaria". In: *Nature Communications* 12.1, p. 7212.

Reyburn, H. et al. (2005). "Association of Transmission Intensity and Age with Clinical Manifestations and Case Fatality of Severe Plasmodium Falciparum Malaria". In: *JAMA* 293.12, pp. 1461–1470.

Robbie, G. J. et al. (2013). "A Novel Investigational Fc-Modified Humanized Monoclonal Antibody, Motavizumab-YTE, Has an Extended Half-Life in Healthy Adults". In: *Antimicrobial Agents and Chemotherapy* 57.12, pp. 6147–6153.

Rogerson, S. J. et al. (2020). "Identifying and Combating the Impacts of COVID-19 on Malaria". In: *BMC Medicine* 18.1, p. 239.

Rosario, V. (1981). "Cloning of Naturally Occurring Mixed Infections of Malaria Parasites". In: *Science* 212.4498, pp. 1037–1038.

Ross, A. et al. (2006). "Relationships between Host Infectivity to Mosquitoes and Asexual Parasite Density in Plasmodium Falciparum". In: *The American Journal of Tropical Medicine and Hygiene* 75 (2 Suppl), pp. 32–37.

Ross, R (1911). *The Prevention of Malaria*. London: John Murray. 651–686.

Rottmann, M. et al. (2010). "Spiroindolones, a Potent Compound Class for the Treatment of Malaria". In: *Science* 329.5996, pp. 1175–1180.

Rottmann, M. et al. (2020). "Preclinical Antimalarial Combination Study of M5717, a Plasmodium Falciparum Elongation Factor 2 Inhibitor, and Pyronaridine, a Hemozoin Formation Inhibitor". In: *Antimicrobial Agents and Chemotherapy* 64.4.

RTS,S Clinical Trials Partnership (2014). "Efficacy and Safety of the RTS,S/AS01 Malaria Vaccine during 18 Months after Vaccination: A Phase 3 Randomized, Controlled Trial in Children and Young Infants at 11 African Sites". In: *PLoS medicine* 11.7, e1001685.

Runge, M. et al. (2020). "Applied Mathematical Modelling to Inform National Malaria Policies, Strategies and Operations in Tanzania". In: *Malaria Journal* 19.1, p. 101.

Sanz, L. M. et al. (2012). "P. Falciparum In Vitro Killing Rates Allow to Discriminate between Different Antimalarial Mode-of-Action". In: *PLOS ONE* 7.2, e30949.

Saralamba, S. et al. (2011). "Intrahost Modeling of Artemisinin Resistance in Plasmodium Falciparum". In: *Proceedings of the National Academy of Sciences of the United States of America* 108.

Schleiferböck, S. et al. (2013). "In Vitro and in Vivo Characterization of the Antimalarial Lead Compound SSJ-183 in Plasmodium Models". In: *Drug design, development and therapy* 7, pp. 1377–1384.

Schmidt, H. (2017). *IQRtools*.

Schneider, P. et al. (2012). "Virulence, Drug Sensitivity and Transmission Success in the Rodent Malaria, Plasmodium Chabaudi". In: *Proceedings. Biological Sciences* 279.1747, pp. 4677–85.

Simpson, J. A. et al. (2014). "Making the Most of Clinical Data: Reviewing the Role of Pharmacokinetic-Pharmacodynamic Models of Anti-Malarial Drugs". In: *AAPS Journal* 16.5, pp. 962–74.

Sinxadi, P. et al. (2020). "Safety, Tolerability, Pharmacokinetics and Antimalarial Activity of the Novel Plasmodium Phosphatidylinositol 4-Kinase Inhibitor MMV390048 in Healthy Volunteers". In: *Antimicrobial Agents and Chemotherapy*.

Slater, H. C. et al. (2017). "Mathematical Modelling to Guide Drug Development for Malaria Elimination". In: *Trends in Parasitology* 33.3, pp. 175–184.

Slater, M. et al. (2005). "Distinguishing Recrudescences from New Infections in Antimalarial Clinical Trials: Major Impact of Interpretation of Genotyping Results on Estimates of Drug Efficacy". In: *The American Journal of Tropical Medicine and Hygiene* 73.2, pp. 256–62.

Smith, D. L. et al. (2012). "Ross, Macdonald, and a Theory for the Dynamics and Control of Mosquito-Transmitted Pathogens". In: *PLOS Pathogens* 8.4, e1002588.

Smith, T. et al. (2006). "An Epidemiological Model of the Incidence of Acute Illness in Plasmodium Falciparum Malaria". In: *The American Journal of Tropical Medicine and Hygiene* 75 (2_suppl), pp. 56–62.

Sobol, I. M (2001). "Global Sensitivity Indices for Nonlinear Mathematical Models and Their Monte Carlo Estimates". In: *Mathematics and Computers in Simulation*. The Second IMACS Seminar on Monte Carlo Methods 55.1, pp. 271–280.

Somé, A. F. et al. (2014). "Selection of Drug Resistance-Mediating Plasmodium Falciparum Genetic Polymorphisms by Seasonal Malaria Chemoprevention in Burkina Faso". In: *Antimicrobial agents and chemotherapy* 58.7, pp. 3660–3665.

Stan Development Team (2018). *Stan Modeling Language Users Guide and Reference Manual*. 2.18.0.

Stan Development Team (2020). *RStan: The R Interface to Stan*.

Stanisic, D. I. et al. (2018). "Controlled Human Malaria Infection: Applications, Advances, and Challenges". In: *Infection and Immunity* 86.1.

Stein, M. (1987). "Large Sample Properties of Simulations Using Latin Hypercube Sampling". In: *Technometrics* 29.2, pp. 143–151.

Sulyok, M. et al. (2017). "DSM265 for Plasmodium Falciparum Chemoprophylaxis: A Randomised, Double Blinded, Phase 1 Trial with Controlled Human Malaria Infection". In: *The Lancet. Infectious Diseases* 17.6, pp. 636–644.

Svensson, U. S. et al. (2002). "Population Pharmacokinetic and Pharmacodynamic Modelling of Artemisinin and Mefloquine Enantiomers in Patients with Falciparum Malaria". In: *European Journal of Clinical Pharmacology* 58.5, pp. 339–51.

Tan, J. et al. (2018). "A Public Antibody Lineage That Potently Inhibits Malaria Infection by Dual Binding to the Circumsporozoite Protein". In: *Nature medicine* 24.4, pp. 401–407.

Tanner, M. et al. (2015). "Malaria Eradication and Elimination: Views on How to Translate a Vision into Reality". In: *BMC Med* 13, p. 167.

Tediosi, F. et al. (2006). "An Approach to Model the Costs and Effects of Case Management of Plasmodium Falciparum Malaria in Sub-Saharan Africa". In: *The American Journal of Tropical Medicine and Hygiene* 75 (2 Suppl), pp. 90–103.

Teuscher, F. et al. (2010). "Artemisinin-Induced Dormancy in Plasmodium Falciparum: Duration, Recovery Rates, and Implications in Treatment Failure". In: *Journal of Infectious Diseases* 202.

Thaithong, S. et al. (1983). "Susceptibility of Plasmodium Falciparum to Five Drugs: An in Vitro Study of Isolates Mainly from Thailand". In: *Transactions of The Royal Society of Tropical Medicine and Hygiene* 77.2, pp. 228–231.

Thapar, M. M. et al. (2005). "In Vitro Recrudescence of Plasmodium Falciparum Parasites Suppressed to Dormant State by Atovaquone Alone and in Combination with Proguanil". In: *Transactions of the Royal Society of Tropical Medicine and Hygiene* 99.1, pp. 62–70.

Traore, M. M. et al. (2020). "Large-Scale Field Trial of Attractive Toxic Sugar Baits (ATSB) for the Control of Malaria Vector Mosquitoes in Mali, West Africa". In: *Malaria Journal* 19.1, p. 72.

Tse, E. G. et al. (2019). "The Past, Present and Future of Anti-Malarial Medicines". In: *Malaria Journal* 18.1, p. 93.

Uwimana, A. et al. (2020). "Emergence and Clonal Expansion of in Vitro Artemisinin-Resistant Plasmodium Falciparum Kelch13 R561H Mutant Parasites in Rwanda". In: *Nature Medicine*, pp. 1–7.

Van Lenthe, M. et al. (2019). "Markers of Sulfadoxine–Pyrimethamine Resistance in Eastern Democratic Republic of Congo; Implications for Malaria Chemoprevention". In: *Malaria Journal* 18.1, p. 430.

Veiga, M. I. et al. (2010). "Antimalarial Exposure Delays Plasmodium Falciparum Intra-Erythrocytic Cycle and Drives Drug Transporter Genes Expression". In: *PLOS ONE* 5.8, e12408.

Villeval, J. L. et al. (1990). "Changes in Hemopoietic and Regulator Levels in Mice during Fatal or Nonfatal Malarial Infections. II. Nonerythroid Populations". In: *Experimental Parasitology* 71.4, pp. 375–85.

Wassmer, S. C. et al. (2015). "Investigating the Pathogenesis of Severe Malaria: A Multidisciplinary and Cross-Geographical Approach". In: *The American Journal of Tropical Medicine and Hygiene* 93 (3 Suppl), pp. 42–56.

Watanabe, S. (2010). "Asymptotic Equivalence of Bayes Cross Validation and Widely Applicable Information Criterion in Singular Learning Theory". In: *Journal of Machine Learning Research* 11, pp. 3571–3594.

Watson, J. et al. (2018). "Characterizing Blood-Stage Antimalarial Drug MIC Values In Vivo Using Reinfection Patterns". In: *Antimicrobial Agents and Chemotherapy* 62.7.

Weiss, D. J. et al. (2019). "Mapping the Global Prevalence, Incidence, and Mortality of Plasmodium Falciparum, 2000–17: A Spatial and Temporal Modelling Study". In: *The Lancet* 394.10195, pp. 322–331.

Wells, T. N. C. et al. (2015). "Malaria Medicines: A Glass Half Full?" In: *Nature Reviews. Drug Discovery* 14.

White, M. T. et al. (2014a). "Dynamics of the Antibody Response to Plasmodium Falciparum Infection in African Children". In: *The Journal of Infectious Diseases* 210.7, pp. 1115–1122.

White, N. J. (1997). "Assessment of the Pharmacodynamic Properties of Antimalarial Drugs in Vivo". In: *Antimicrobial Agents and Chemotherapy* 41.7, pp. 1413–22.

White, N. J. (2002). "The Assessment of Antimalarial Drug Efficacy". In: *Trends in Parasitology* 18.

White, N. J. (2011). "The Parasite Clearance Curve". In: *Malaria Journal* 10.

White, N. J. et al. (2017). "Split Dosing of Artemisinins Does Not Improve Antimalarial Therapeutic Efficacy". In: *Scientific Reports* 7.1, p. 12132.

White, N. J. (2017). "Malaria Parasite Clearance". In: *Malaria Journal* 16.1, p. 88.

White, N. J. et al. (2009). "Hyperparasitaemia and Low Dosing Are an Important Source of Anti-Malarial Drug Resistance". In: *Malaria Journal* 8.1, p. 253.

White, N. J. et al. (2014b). "Spiroindolone KAE609 for Falciparum and Vivax Malaria". In: *The New England Journal of Medicine* 371.5, pp. 403–410.

White, N. J. et al. (2016). "Antimalarial Activity of KAF156 in Falciparum and Vivax Malaria". In: *New England Journal of Medicine* 375.12, pp. 1152–1160.

Whitty, C. J. M. and E. Ansah (2019). "Malaria Control Stalls in High Incidence Areas". In: *BMJ* 365.

WHO. *WHO Target Product Profiles*. URL: `https://www.who.int/research-observatory/analyses/tpp/en/` (visited on 08/20/2020).

WHO (2009). *Methods for Surveillance of Antimalarial Drug Efficacy*. World Health Organization, Geneva: World Health Organization.

WHO (2010). *WHO Policy Recommendation on Intermittent Preventive Treatment during Infancy with Sulphadoxine-Pyrimethamine (SP-IPTi) for Plasmodium Falciparum Malaria Control in Africa*. World Health Organization, Geneva.

WHO (2012). *WHO Policy Recommendation: Seasonal Malaria Chemoprevention (SMC) for Plasmodium Falciparum Malaria Control in Highly Seasonal Transmission Areas of the Sahel Sub-Region in Africa*. World Health Organization, Geneva.

WHO (2013). *Seasonal Malaria Chemoprevention with Sulfadoxine-Pyrimethamine plus Amodiaquine in Children: A Field Guide*. World Health Organization, Geneva.

WHO (2015a). *Global Technical Strategy for Malaria 2016-2030*. World Health Organization, Geneva.

WHO (2015b). *Guidelines for the Treatment of Malaria*. WHO.

WHO (2016). *WHO Recommendation on Intermittent Preventive Treatment of Malaria in Pregnancy*. World Health Organization, Geneva.

WHO (2017). *Artemisinin and Artemisinin-Based Combination Therapy Resistance: Status Report*. URL: `http://www.who.int/iris/handle/10665/255213`.

WHO (2018). *World Malaria Report 2018*. URL: `http://www.who.int/iris/handle/10665/275867`.

WHO (2019). *World Malaria Report 2019*. World Health Organization, Geneva.

WHO (2020). *Country Profiles*. URL: `https://www.who.int/malaria/publications/country-profiles/en/`.

Wockner, L. F. et al. (2019). "Growth Rate of Plasmodium Falciparum: Analysis of Parasite Growth Data from Malaria Volunteer Infection Studies". In: *Journal of Infectious Diseases*.

Wunderlich, J. et al. (2012). "The Malaria Digestive Vacuole". In: *Frontiers in Bioscience (Scholar Edition)* 4, pp. 1424–1448.

WWARN (2015). "The Effect of Dosing Strategies on the Therapeutic Efficacy of Artesunate-Amodiaquine for Uncomplicated Malaria: A Meta-Analysis of Individual Patient Data". In: *BMC Medicine* 13.1, p. 66.

Yu, X.-Q. et al. (2017). "Safety, Tolerability, and Pharmacokinetics of MEDI4893, an Investigational, Extended-Half-Life, Anti-Staphylococcus Aureus Alpha-Toxin Human Monoclonal Antibody, in Healthy Adults". In: *Antimicrobial Agents and Chemotherapy* 61.1.

Yuthavong, Y. et al. (2012). "Malarial Dihydrofolate Reductase as a Paradigm for Drug Development against a Resistance-Compromised Target". In: *Proceedings of the National Academy of Sciences of the United States of America* 109.42, pp. 16823–16828.

Zaloumis, S. et al. (2012). "Assessing the Utility of an Anti-Malarial Pharmacokinetic-Pharmacodynamic Model for Aiding Drug Clinical Development". In: *Malaria Journal* 11, p. 303.

Zaloumis, S. G. et al. (2018). "In Silico Investigation of the Decline in Clinical Efficacy of Artemisinin Combination Therapies Due to Increasing Artemisinin and Partner Drug Resistance". In: *Antimicrobial Agents and Chemotherapy* 62.12.

Zhang, X. et al. (2015). "Sobol Sensitivity Analysis: A Tool to Guide the Development and Evaluation of Systems Pharmacology Models". In: *CPT: Pharmacometrics & Systems Pharmacology* 4.2, pp. 69–79.

Zongo, I. et al. (2015). "Randomized Noninferiority Trial of Dihydroartemisinin-Piperaquine Compared with Sulfadoxine-Pyrimethamine plus Amodiaquine for Seasonal Malaria Chemoprevention in Burkina Faso". In: *Antimicrobial Agents and Chemotherapy* 59.8, pp. 4387–4396.

Glossary

acquired immunity Specific immune response of vertebrates against an infection with a pathogen..

chemoprevention regular administration of a full treatment course for preventative purposes.

chemoprotection protection against infection through specifically designed interventions.

difference equations mathematical functions describing the difference between two states over time..

differential equations mathematical functions containing derivatives, used to describe the change of a variable over time.

drug resistance capacity of an organism to survive exposure to a drug. Reduces drug efficacy..

entomological inoculation rate number of infectious bites an individual receives per unit time (usually a year), provides information about the force of transmission .

erythrocyte Red blood cells, transporting oxygen throughout the body. Lack of erythrocytes causes anemia..

innate immunity Natural response mechanism of host organisms as a reaction to inoculation with a pathogen..

inoculation	Introduction of a organism into a host or culture medium..
lysis	disintegration of a cell through rupture of the cell membrane.
merozoites	Malaria parasite stage released into the blood after schizogony is completed. The released merozoites then infect new erythrocytes..
monoclonal antibody	antibodies produced by identical immune cells (cell clones) used to treat diseases .
NMRI mouse	Naval Medical Research Institute mouse, widely used experimental animal..
Parasitemia	presence of parasites in the blood, measured as parasite concentration per volume blood or the percentage of infected erythrocytes..
pharmacodynamics	description of the drug-effect over time.
pharmacokinetics	description of the drug-concentration profile of a drug after its application. Defined by its absorption, distribution, metabolism, and excretion..
phenotypic	Observable traits of organisms..
PKPD relationship	combination of pharmacokinetic and pharmacodynamic analysis to describe the drug effect over time in relation to the drug-concentration..
Plasmodium	Apicomplexan parasite, causative agent of malaria.
recrudescence	Re-growth of parasites after non-curative treatment with an anti-infective agent..
SCID mouse	mice with severe combined immunodeficiency, used in antimalarial drug development to study the efficacy of drugs in vivo.

sporogony	Reproduction via sporozoites. Typical for many apicomplexan parasites..
stage specificity	higher efficacy of an anti-infective agent against certain life cycle stages .

Appendix A

Supplementary Information Chapter 2- Ensemble modeling highlights importance of understanding parasite-host behavior in preclinical antimalarial drug development

Ensemble modelling highlights importance of understanding parasite-host behaviour in preclinical antimalarial drug development

Authors:
Lydia Burgert[1,2], Matthias Rottmann[1,2], Sergio Wittlin[1,2], Nathalie Gobeau[3], Andreas Krause[4], Jasper Dingemanse[4], Jörg J. Möhrle[1,2,3], Melissa A. Penny*[1,2]

[1] Swiss Tropical and Public Health Institute, Basel, Switzerland

[2] University of Basel, Basel, Switzerland

[3] Medicines for Malaria Venture, Geneva, Switzerland

[4] Idorsia Pharmaceuticals Ltd, Clinical Pharmacology, Allschwil, Switzerland

*Corresponding author: melissa.penny@unibas.ch

Supplement

Section 1: Data and Drugs

Overview of compounds and data used for analysis of parasite growth *P. berghei* and *P. falciparum* in their respective murine host and drug efficacy experiments.

Table S2.1: List of compounds including compound characteristics

Drug	Molecule class	Mode of action	Literature
ACT-451840	phenylalanine-based	Interaction with multidrug resistance protein-1 (PfMDR1), needs further investigation	[1,2]
CQ	4-aminoquinoline	Inhibits heme polymerization in food vacuole	[3]
MMV390048	2-aminopyridine	Inhibits phosphatidylinositol 4‑kinase (PfPI(4)K)	[3,4]
OZ439	peroxide	Peroxidative damage and oxidative stress through reductive activation by heme, needs further investigation	[5,6]

Table S2.2: Overview of data used in fitting parasite growth and drug action parameters (parasite density data), and concentration-time profiles (concentration time data). Doses are given in mg/kg.

	Data	Concentration time data	Parasite density data
***P. berghei* in normal mice**	Undisturbed parasite growth	-	No. mice: 215 No. experiments: 43 Mice per experiment: 2-5 Data source: Swiss TPH
	ACT-451840	No. mice: 12 No. experiments: 3 Mice per dose: 4 Quadruple dose: 100 Data source: Idorsia	No. mice: 69 No. experiments: 4 Mice per dose: 3-5 Single dose: 10, 15, 20, 25, 30, 60, 80, 100, 300 Triple dose: 3, 10, 2x15, 30, 50, 2x30, 100, 300 Data source: Idorsia
	CQ	No. mice: 2 No. experiments: 1 Mice per dose: 2 Single dose: 10, 100, 300 Data source: Swiss TPH	No. mice: 72 No. experiments: 8 Mice per dose: 2-5 Single dose: 3, 10, 30, 100 Quadruple dose: 3, 10, 30, 100 Data source: Swiss TPH
	MMV390048	No. mice: 9 No. experiments: 3 Mice per dose: 3 Single dose: 1, 10 Data source: MMV	No. mice: 65 No. experiments: 3 Mice per dose: 3-6 Single dose: 0.5, 1, 2, 3, 10, 25, 30 Quadruple dose: 0.3, 0.5, 0.8, 1, 3 Data source: Swiss TPH
	OZ439	No. mice: 6 No. experiments: 1 Mice per dose: 3 Single dose: 30, 100 Data source: MMV	No. mice: 220 No. experiments: 13 Mice per dose: 5-10 Single dose: 0.1, 0.3, 1, 1.5, 2, 3, 5, 10, 15, 20, 25, 30, 50, 100 Triple dose: 1, 3, 10 Data source: Swiss TPH
***P. falciparim in* NOD $^{scidIL-2R'\ c-/-}$ mice**	Undisturbed parasite growth	-	No. mice: 132 No. experiments: 32 Mice per experiment: 2-8 Data source: GSK, Swiss TPH, TAD
	ACT 451840	No. mice: 3 No. experiments: 1 Mice per dose:3 Single dose: 3 Data source: Idorsia	No. mice: 12 No. experiments: 1 Mice per dose: 3 quadruple dose: 3, 10, 30, 100 Data source: Idorsia
	CQ	No. mice: 4 No. experiments: 1 Mice per dose: 4 Single dose: 50 Data source: Swiss TPH	No. mice: 14 No. experiments: 3 Mice per dose: 2-3 Single dose: 50 mg/kg Quadruple dose: 2, 5, 10, 50 Data source: Swiss TPH
	MMV390048	No. mice: 48 No. experiments: 7 Mice per dose: 1-2 Double dose: 1,10 Quadruple dose: 0.25, 0.5, 1, 5, 10, 20 Data source: GSK, TAD	No. mice: 50 No. experiments: 7 Mice per dose: 1-2 Double dose: 1,10, Quadruple dose: 0.25, 0.5, 1, 5, 10, 20 Data source: GSK, TAD
	OZ439	No. mice: 34 No. experiments: 4 Mice per dose: 2 Single dose: 0.5, 1, 3, 5, 10, 20, 30, 50, 75, 100 Double dose: 25 Data source: GSK, Swiss TPH	No. mice: 48 No. experiments: 4 Mice per dose: 2 Single dose: 0.5, 1, 3, 5, 10, 20, 30, 50, 75, 100 Double dose: 25 Data source: GSK, Swiss TPH

Section 2: Mechanistic models

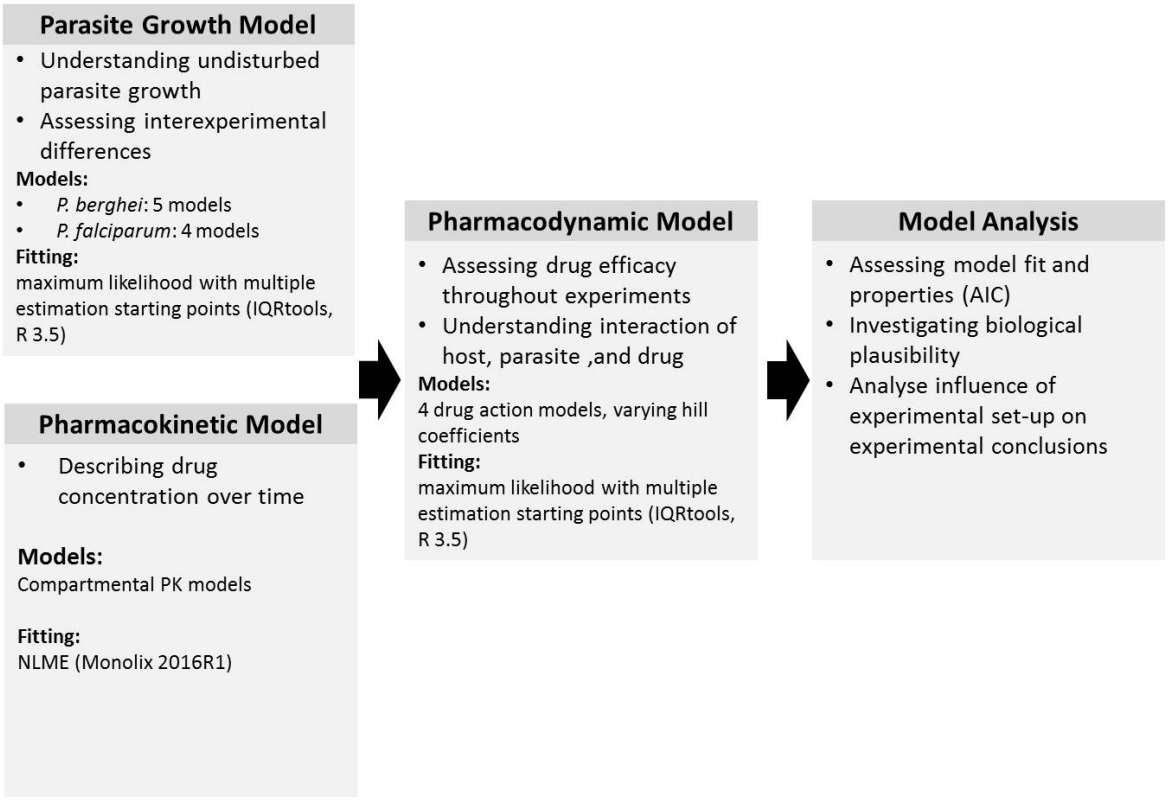

Figure S2.1: Standardized workflow for the systematic analysis of preclinical drug efficacy experiments. The workflow was designed to assist execution of consistent analysis of parasite growth and drug treatment experiments in a preclinical setting.

Supplementary information Chapter 2- Ensemble modelling highlights importance of understanding parasite-host behaviour in preclinical antimalarial drug development

Table S2.3: Equations (ordinary differential equations) for the parasite growth models. Models are annotated in a modular construction system. The equation for uninfected (X) and infected (Y) RBCs and merozoites (M) for the respective model are listed in the table below. The annotations represent mouse RBCs (m), human RBCs (h) and reticulocytes (R). Parameter annotations can be found in Table S2.4.

<table>
<tr>
<td>

Model a (base)

$\frac{dX_m}{dt} = \nu - \mu_{X_m} X_m - \beta X_m M$ *(S2.1)*

$\frac{dY_{Xm,1}}{dt} = \beta X_m M - \alpha Y_{Xm,1}$ (S2.2)

$\frac{dY_{Xm,i}}{dt} = \alpha Y_{Xm,i-1} - \alpha Y_{Xm,i}\ ,\ i = 2,..,n$ (S2.2.1)

$\frac{dM}{dt} = -\beta(X_m + Y_{Xm})M + \alpha r Y_{Xm,n} - \delta M$ *(S2.3)*

with: $Y_{Xm} = \sum_{i=1}^{n} Y_{Xm,i}$

$$P = \frac{Y_{Xm}}{X_m + Y_{Xm}} 100$$

and initial conditions: $X_{m,0} = X_{m,0}, \quad M_0 = 0$

$$Y_{Xm,0,i} = \omega \frac{\text{inoculum}}{Vn}$$

</td>
<td>

Model b (bystander)

$\frac{dX_m}{dt} = \nu - (\mu_{X_m} + \gamma)X - \beta X_m M$ (S2.4)

$\frac{dY_{Xm,1}}{dt} = \beta X_m M - \alpha Y_{Xm,1}$ (S2.2)

$\frac{dY_{Xm,i}}{dt} = \alpha Y_{Xm,i-1} - \alpha Y_{Xm,i}\ ,\ i = 2,..,n$ (S2.2.1)

$\frac{dM}{dt} = -\beta(X_m + Y_{Xm})M + \alpha r Y_{Xm,n} - \delta M$ (S2.3)

with : $Y_{Xm} = \sum_{i=1}^{n} Y_{Xm,i}$

$$\gamma = \frac{\gamma_{max} Y_{Xm}}{k\gamma_{50} + Y_{Xm}}$$

$$P = \frac{Y_{Xm}}{X_m + Y_{Xm}} 100$$

and initial conditions: $X_{m,0} = X_{m,0}, \quad M_0 = 0$

$$Y_{Xm,0,i} = \omega \frac{\text{inoculum}}{Vn}$$

</td>
</tr>
<tr>
<td>

Model c (comp. erythr.)

$\frac{dX_m}{dt} = \nu - \mu_{X_m} X_m - \beta X_m M$ (S2.1)

$\frac{dY_{Xm,1}}{dt} = \beta X_m M - \alpha Y_{Xm,1}$ (S2.2)

$\frac{dY_{Xm,i}}{dt} = \alpha Y_{Xm,i-1} - \alpha Y_{Xm,i}\ ,\ i = 2,..,n$ (S2.2.1)

$\frac{dM}{dt} = -\beta(X_m + Y_{Xm})M + \alpha r Y_{Xm,n} - \delta M$ (S2.3)

with: $Y_{Xm} = \sum_{i=1}^{n} Y_{Xm,i}$

$$\nu = \frac{\nu_{max}}{1 + \frac{X_m + Y_{Xm}}{k\nu_{50}}} X_{m,0}$$

$$P = \frac{Y_{Xm}}{X_m + Y_{Xm}} 100$$

and initial conditions: $X_{m,0} = X_{m,0}, \quad M_0 = 0$

$$Y_{Xm,0,i} = \omega \frac{\text{inoculum}}{Vn}$$

</td>
<td>

Model d (impaired maturation)

$\frac{dX_m}{dt} = \nu - \mu_{X_m} X_m - \beta X_m M$ (S2.1)

$\frac{dY_{Xm,1}}{dt} = \beta X_m M - lY_{Xm,1}$ (S2.2)

$\frac{dY_{Xm,i}}{dt} = lY_{Xm,i-1} - lY_{Xm,i}\ ,\ i = 2,..,n$ (S2.2.1)

$\frac{dM}{dt} = -\beta(X_m + Y_{Xm})M + lrY_{Xm,n} - \delta M$ (S2.3)

with: $Y_{Xm} = \sum_{i=1}^{n} Y_{Xm,i}$

$$l = \alpha - \frac{l_{max} Y_{xm}^2}{k_{l,50} X_{m,0} Y_{xm}^2}$$

$$P = \frac{Y_{Xm}}{X_m + Y_{Xm}} 100$$

and initial conditions: $X_{m,0} = X_{m,0}, \quad M_0 = 0$

$$Y_{Xm,0,i} = \omega \frac{\text{inoculum}}{Vn}$$

</td>
</tr>
</table>

Table S2.3: Equations (ordinary differential equations) for the parasite growth models. *Continued…*

<table>
<tr>
<td>

Model e (reticulocytes)

$\frac{dR}{dt} = \nu - \tau_R R - \beta\varepsilon RM$ (S2.5)

$\frac{dX_m}{dt} = \tau_R R - \mu_{X_m} X_m - \beta X_m M$ (S2.6)

$\frac{dY_R}{dt} = \beta\varepsilon RM - \tau_{YR} Y_R - \alpha Y_R$ (S2.7)

$\frac{dY_{Xm,1}}{dt} = \beta X_m M + \tau_{YR} Y_R - \alpha Y_{Xm}, 1$ (S2.8)

$\frac{dY_{Xm,i}}{dt} = \alpha Y_{Xm,i-1} - \alpha Y_{Xm,i}\ , i = 2,..,n$ (S2.8.1)

$\frac{dM}{dt} = -\beta(X_m + Y_{Xm})M - \beta\varepsilon(R + Y_R)\,M + \alpha r Y_{Xm,n} - \delta M$ (S2.9)

with:

$$Y_{Xm} = \sum_{i=1}^{n} Y_{Xm,i}$$

$$P = \frac{Y_{Xm} + Y_R}{X_m + R + Y_{Xm} + Y_R} 100$$

and initial conditions:

$$R_0 = R_0$$
$$X_{m,0} = X_{m,0}$$
$$Y_{R,0} = 0$$
$$Y_{Xm,0,i} = \omega \frac{\text{inoculum}}{Vn}$$
$$M_0 = 0$$

</td>
<td>

Model f (const. RBC decay)

$\frac{dX_h}{dt} = \text{inputRBC} - (\gamma + \lambda)X_h - \beta X_h M$ (S2.10)

$\frac{dX_m}{dt} = \nu - (\lambda + \mu_{X_m})X_m$ (S2.11)

$\frac{dY_{Xh,1}}{dt} = \beta X_h M - \alpha Y_{Xh,1} - (\gamma + \lambda + \varphi)Y_{Xh,1}$ (S2.12)

$\frac{dY_{Xh,i}}{dt} = \alpha Y_{Xh,i-1} - (\gamma + \lambda + \varphi)Y_{Xh,i} - \alpha Y_{Xh,i}\ , i = 2,..,n$ (S2.12.1)

$\frac{dM}{dt} = -\beta(X_h + Y_{Xh})M + \alpha r Y_{Xh,n} - \delta M$ (S2.13)

with:

$$Y_{Xh} = \sum_{i=1}^{n} Y_{Xh,i}$$

$$\nu = \frac{\nu_{max}}{1 + \frac{X_h + X_m}{k\nu_{50}}}$$

$$\gamma = \frac{\gamma_{max} Y_{Xh}}{k\gamma_{50} + Y_{Xh}}$$

$$P = \frac{Y_{Xh}}{X_h + X_m + Y_{Xh}} 100$$

$$H = \frac{X_h + Y_{Xh}}{X_h + X_m + Y_{Xh}} 100$$

and initial conditions:

$$X_h = H_0 10^{10}$$
$$X_{m,0} = (1 - H_0)10^{10}$$
$$Y_{Xh,0,1} = \omega \frac{\text{inoculum}}{Vn}$$
$$M_0 = 0$$

</td>
</tr>
</table>

Table S2.3: Equations (ordinary differential equations) for the parasite growth models. *Continued…*

<table>
<tr>
<td>

Model g (dd. RBC decay)

$$\frac{dX_h}{dt} = \text{inputRBC} - (\gamma + \lambda)X_h - \beta X_h M \quad \text{(S2.10)}$$

$$\frac{dX_m}{dt} = \nu - (\lambda + \mu_{X_m})X_m \quad \text{(S2.11)}$$

$$\frac{dY_{Xh,1}}{dt} = \beta X_h M - \alpha Y_{Xh,1} - (\gamma + \chi + \varphi)Y_{Xh,1} \quad \text{(S2.12)}$$

$$\frac{dY_{Xh,i}}{dt} = \alpha Y_{Xh,i-1} - (\gamma + \chi + \varphi)Y_{Xh,i} - \alpha Y_{Xh,i}\,, i = 2,..,n \quad \text{(S2.12.1)}$$

$$\frac{dM}{dt} = -\beta(X_h + Y_{Xh})M + \alpha r Y_{Xh,n} - \delta M \quad \text{(S2.13)}$$

with:

$$Y_{Xh} = \sum_{i=1}^{n} Y_{Xh,i}$$

$$\gamma = \frac{\gamma_{max} Y_{Xh}}{k\gamma_{50} + Y_{Xh}}$$

$$\chi = \frac{\chi_{max} N}{k\chi_{,50} + N}, N = X_h + X_m + Y_{Xh}$$

$$P = \frac{Y_{Xh}}{X_h + X_m + Y_{Xh}} 100$$

$$H = \frac{X_h + Y_{Xh}}{X_h + X_m + Y_{Xh}} 100$$

and initial conditions:

$$X_h = H_0 10^{10}$$

$$X_{m,0} = (1 - H_0)10^{10}$$

$$Y_{Xh,0,i} = \omega \frac{\text{inoculum}}{Vn}$$

$$M_0 = 0$$

</td>
<td>

Model h (human RBC)

$$\frac{dX_h}{dt} = \text{inputRBC} - (\gamma + \lambda)X_h - \beta X_h M \quad \text{(S2.10)}$$

$$\frac{dY_{Xh,1}}{dt} = \beta X_h M - \alpha Y_{Xh,1} - (\gamma + \lambda + \varphi)Y_{Xh,1} \quad \text{(S2.12)}$$

$$\frac{dY_{Xh,i}}{dt} = \alpha Y_{Xh,i-1} - (\gamma + \lambda + \varphi)Y_{Xh,i} - \alpha Y_{Xh,i}\,, i = 2,..,n \quad \text{(S2.12.1)}$$

$$\frac{dM}{dt} = -\beta(X_h + Y_{Xh})M + \alpha r Y_{Xh,n} - \delta M \quad \text{(S2.14)}$$

with:

$$Y_{Xh} = \sum_{i=1}^{n} Y_{Xh,i}$$

$$\gamma = \frac{\gamma_{max} Y_{Xh}}{k\gamma_{50} + Y_{Xh}}$$

$$P = \frac{Y_{Xh}}{X_h + Y_{Xh}} 100$$

and initial conditions:

$$X_h = H_0 10^{10}$$

$$Y_{Xh,0,i} = \omega \frac{\text{inoculum}}{Vn}$$

$$M_0 = 0$$

Model i (exponential)

$$\frac{dP}{dt} = p_{gr} Y \quad \text{(S2.15)}$$

with initial condition:

$$P_o = P_o$$

</td>
</tr>
</table>

Supplementary information Chapter 2- Ensemble modelling highlights importance of understanding parasite-host behaviour in preclinical antimalarial drug development

Table S2.4: Overview of model parameters of the mechanistic parasite growth models developed. Estimated parameters are denoted with Est. in the value column. (uninfected: uninf., infected: inf., calculated: calc., concentration: conc., erythrocyte: RBC)

Process	Model	Para-meter	Value	Unit	Description	Ref
Mouse RBC dyn.	a-c, f, g	ν	1.04×10^{7}	[cells/mLh]	Rate of RBCs production	[7]
Mouse RBC dyn.	a-g	μ_{X_m}	1.04×10^{-3}	[1/h]	Death rate of uninf. RBCs	[7]
Mouse RBC dyn.	c, f	ν_{max}	2.00×10^{-3}	[1/h]	Maximum effect of total RBC conc. on ν	
Mouse RBC dyn.	c, f	$k\nu_{50}$	1e10	[cells/mL]	Concentration of total RBC concentration achieving 0.5 ν_{max}	
P. berghei dyn.	a-c,e	α	0.042 n	[1/h]	Death rate of infected RBCs in each age stage	[7]
P. berghei dyn.	a-h	δ	0.5	[1/h]	Death rate of merozoite	[7]
P. berghei dyn.	e	τ_R	0.014	[1/h]	Maturation rate of uninf. reticulocytes	[8]
P. berghei dyn.	e	ε	Est.	[]	Attraction of parasite to reticulocyte	[8]
P. berghei dyn.	e	τ_{YR}	0.042	[1/h]	Maturation rate of inf. reticulocytes	[8]
P. berghei dyn.	d	α_0 $k_{l,50}$ l_{max}	0.042 n Est. 0.2	[1/h] [cells/mL] [1/h]	Base death rate of infected RBCs Conc. of Y_{Xm} achieving $0.5l_{max}$ Maximum death rate of inf. RBCs	[7]
P. falc. dyn.	f, h	λ	Est.	[1/h]	Base death rate of all RBCs	
P. falc. dyn.	g	χ	Est.	[1/h]	Total RBC conc. induced clearance of RBCs	
P. falc. dyn.	g	χ_{max}	Est.	[1/h]	Maximum effect of total RBC concentration on χ	
P. falc. dyn.	g	$k\chi_{,50}$	Est.	[cells/mL]	Total RBC conc. achieving 0.5 χ_{max}	
P. falc. dyn.	i	p_{gr}	Est.	[1/h]	Replication rate of parasite in exponential growth phase	
P. falc. dyn.	f-h	α	0.025 n	[1/h]	Death rate of inf. RBCs at each age stage	[9]
Parasite dyn.	a-h	n	12	-	Number of modeled parasite age stages	
Parasite dyn.	a-h	ω	Est.	[]	Viability of parasite inoculum	
Parasite dyn.	a-h	β	Est.	[cells/mLh]	Rate of merozoites- RBC contact resulting in infection (infectivity)	
Parasite dyn.	a-h	r	Est.	[]	Number of merozoites per inf. RBC	
Parasite dyn.	b, f-h	γ	Est.	[1/h]	Infection induced RBC clearance	
Parasite dyn.	b, f-h	γ_{max}	Est.	[1/h]	Maximum effect of inf. RBCs on γ	
Parasite dyn.	b, f-h	$k\gamma_{50}$	Est.	[cells/mL]	Conc. of inf. RBCs resulting $0.5\gamma_{max}$	
Parasite dyn.	f-h	φ	Est.	[1/h]	Base clearance of inf. RBCs	

Table S2.5: Overview of model parameters of the mechanistic parasite growth models developed. .

Continued…

Process	Model	Variable	Value	Unit	Description	Ref
RBC dyn.	a-g	X_m, X_h	-	[cells/mL] [cells/mL]	Mouse RBC conc. Human RBC conc.	
Parasite dyn.	a-e	Y_{Xm}, Y_R, Y_{Xh}.	-	[cells/mL] [cells/mL] [cells/mL]	Inf. mouse RBC conc. Inf. reticulocyte conc. Inf. human RBC conc.	
RBC. dyn	e	R		[cells/mL]	Reticulocyte conc.	
Parasite dyn.	a-h	M	-	[cells/mL]	Merozoite conc.	
Parasite dyn.	a-h	P	-	[%]	Parasitemia, Percentage inf. RBCs	
RBC dyn.	f-g	H	-	[%]	Hematocrit; Percentage human RBCs	
Mouse RBC dyn.	a-g	$X_{m,0}$	10^{10} or Calc.	[cells/mL]	Initial number of mouse RBCs	
RBC dyn.	a-h	$X_{h,0}$	Calc.	[cells/mL]	Initial number of human RBCs	
Mouse RBC dyn.	e	R_0	5^8	[cells/mL]	Initial number of reticulocytes, 5% of $X_{m,0}$	
RBC dyn.	f-h	H_0	Est.	[%]	Initial percentage of human RBCs	[8]
Parasite dyn.	i	P_0	Est.	[%]	Initial parasitemia	
Model input	a-h	inoculum	Data	[c]	Parasite Inoculum	
Model input	f-h	inputRBC	Data	[c]	RBC injections	
Mouse RBC dyn.	a-h	V	1.23	[mL]	Mouse blood volume	[10]

Table S2.6: Structural pharmacokinetic models. Models were built in a nested manner. No covariate model was developed. Models were evaluated based on difference in AIC and standard VPCs. Such that the one compartment model corresponding to the absorption and elimination strategies in the Table S2.6, Q_1 and V_{p1} were set to zero.

Absorption	Elimination	Equation (2 compartments)
1st order	linear	$\frac{dAd}{dt} = -k_a A_d + Input$ $\frac{dA_c}{dt} = k_a A_d - \frac{Cl}{V_c} A_c - \frac{Q_1}{V_c} A_c + \frac{Q_1}{V_{p1}} A_{p1}$ $\frac{dA_{p1}}{dt} = + \frac{Q_1}{V_c} A_c - \frac{Q_1}{V_{p1}} A_{p1}$
Michaelis-Menten	linear	$\frac{dAd}{dt} = -\frac{v_{max} A_d}{V_{max,50+A_d}} + Input$ $\frac{dA_c}{dt} = \frac{v_{max} A_d}{V_{max,50+A_d}} - \frac{Cl}{V_c} A_c - \frac{Q_1}{V_c} A_c + \frac{Q_1}{V_{p1}} A_{p1}$ $\frac{dA_{p1}}{dt} = + \frac{Q_1}{V_c} A_c - \frac{Q_1}{V_{p1}} A_{p1}$
linear	Linear and Michaelis-Menten	$\frac{dAd}{dt} = -k_a A_d + Input$ $\frac{dA_c}{dt} = k_a A_d - \frac{Cl}{V_c} A_c - \frac{Q_1}{V_c} A_c + \frac{Q_1}{V_{p1}} A_{p1} - \frac{v_{max} A_d}{V_{max,50+A_d}}$ $\frac{dA_{p1}}{dt} = + \frac{Q_1}{V_c} A_c - \frac{Q_1}{V_{p1}} A_{p1}$

Parameter	Unit	Description
k_a	[1/h]	Absorption rate constant
CL	[mL/h]	Drug Clearance
V_c	[mL]	Volume of distribution
Q_1	[1/h]	Inter-compartmental clearance
V_{p1}	[mL]	Volume of distribution of the peripheral compartment
v_{max}	[1/h]	Maximum process rate
$V_{max,50}$	[ng/mL]	Drug concentration with half-maximum process rate
Variable		
A_d	[ng]	Amount of drug in dosing compartment (depot)
A_c	[ng]	Amount of drug in central compartment
A_{p1}	[ng]	Amount of drug in peripheral compartment

Table S2.7: Drug action models fitted for each drug and parasite growth model combination. The effect *E* was added to the parameter of parasite death α for *model a-h* and directly subtracted from the growth rate p_{gr} in case of *model i*. Bold parameters are calibrated against data during this modeling step.

Model	Equation	Drug effect
Clearance	$\frac{dY}{dt} = (\dots) - \frac{\boldsymbol{E_{max}} C^{\gamma}}{\boldsymbol{EC_{50}^{\gamma}} + C^{\gamma}} Y$ $\frac{dY_{Cl}}{dt} = \frac{\boldsymbol{E_{max}} C^{\gamma}}{\boldsymbol{EC_{50}^{\gamma}} + C^{\gamma}} Y - \boldsymbol{Cl_Y} Y_{Cl}$	Parasites Y are damaged by the drug with direct effect, dead parasites Y_{Cl} are cleared with rate Cl_Y
Effect	$\frac{dC_e}{dt} = \boldsymbol{k_e}(C - C_e)$ $E = \frac{\boldsymbol{E_{max}} C_e^{\gamma}}{\boldsymbol{EC_{50}^{\gamma}} + C_e^{\gamma}}$	Reversible direct effect with additional effect compartment, incorporates time-delay in drug action
E_{max}	$E = \frac{\boldsymbol{E_{max}} C^{\gamma}}{\boldsymbol{EC_{50}^{\gamma}} + C^{\gamma}}$	Direct effect of the drug
Turnover	$E = \boldsymbol{k_R E_{max}} \left(\frac{C^{\gamma}}{\boldsymbol{EC_{50}^{\gamma}} + C^{\gamma}} - E \right)$	Indirect response

Parameter	Unit	Description
C	[mg/mL]	Drug concentration
C_e	[mg/mL]	Drug concentration in effect compartment
Cl_Y	[1/h]	Clearance rate for damaged parasites
E	[1/h]	Effect of the drug
EC_{50}	[mg/mL]	Drug concentration causing 50% of maximum effect
E_{max}	[1/h]	Maximum effect of the drug
k_e	[1/h]	First order rate constant for drug concentration in effect compartment
k_R	[1/h]	First order rate constant for biological intermediate
γ	[]	Hill-coefficient, parameter of steepness of the concentration-effect curve
Y_{Cl}	[cells/mL]	Parasites killed/damaged by the drug

Section 3: Parameter estimates

Table S2.8: Estimated parameter values of *P. berghei* and *P. falciparum* growth models. Parameter estimation was performed using data specified in Table S2.2 and equations noted in Table S2.3. Parameter ranges estimated over all experiments are given for parameters $\boldsymbol{\beta}$, $\boldsymbol{H_0}$, $\boldsymbol{P_0}$ and $\boldsymbol{p_{gr}}$. * range of values found over all experiments

Model	Description	Parameter (95% CI)	Unit	Error (prop, add [% parasitemia])
Model a (base)	β *	6.7e-11 – 1.7e-10	[cells/mLh]	0.35, 0.15
	r	14.5 (12.6;16.5)		
	ω	0.99 (0.99;0.99)		
Model b (bystander)	β *	1.94e-10 – 5e-10	[cells/mLh]	0.35, 0.15
	r	11.5 (10;13.2)		
	ω	0.28 (0.22;0.35)		
	y_{max}	0.02 (0.018;0.023)	[1/h]	
	ky_{50}	7.7e-5 (3.15e-5;1.9e-4)	[10^{10} cells/mL]	
Model c (comp. erythr.)	β *	7.1e-11 – 1.70e-10	[cells/mLh]	0.37, 0.15
	r	14.5 (12.7;16.5)		
	ω	0.99 (0.99;0.99)		
Model d (impaired maturation)	β *	9.8e-11 – 2.4e-10	[cells/mLh]	0.14, 0.14
	r	13.0 (11.4;14.9)		
	ω	0.74 (0.53;0.88)		
	$k_{l,50}$	0.12 (0.095;0.17)	[10^{10}cells/mL]	
Model e (reticulocytes)	β *	7.1e-11 – 1.2e-10	[cells/mLh]	0.39, 0.14
	r	10.6 (9.2;12.1)	[1/h]	
	ω	0.78 (0.12;0.99)		
	ε	5.1 (3.5;7.4)		
Model f (const. RBC decay)	β*	2.4e-10 – 1.6e-9	[cells/mLh]	0.31, 0.17
	H_0*	0.40 – 0.69		
	r	21.3 (18.6;24.5)		
	λ	0.010 (0.0099; 0.010)	[1/h]	
	γ_{max}	0.44 (0.38; 0.50)	[1/h]	
	$k\gamma_{50}$	0.24 (0.21; 0.27)	[cells/mL]	
	ω	0.29 (0.26; 0.33)		
	φ	0.030 (0.023; 0.0340)	[1/h]	
Model g (dd. RBC decay)	β*	2.0e-10 – 9.2e-10	[cells/mLh]	0.3, 0.001
	H_0*	0.40 – 0.65		
	r	22.8 (19.8;26.2)		
	ω	0.25 (0.18;0.34)		
	χ_{max}	0.018 (0.016;0.021)	[1/h]	
	$k\chi_{50}$	1.05 (0.91;1.18)	[10^{10} cells/mL]	
	γ_{max}	0.055 (0.041;0.074)	[1/h]	
	$K\gamma_{50}$	0.10 (0.09;0.12)	[10^{10} cells/mL]	
	φ	0.027 (0.016;0.047)	[1/h]	
Model h (human RBC)	β*	2.1e-10 – 8.8e-10	[cells/mLh]	0.34, 0.00010
	H_0*	0.40 – 0.65		
	r	22 (21.7;22.3)		
	ω	0.36 (0.28;0.46)		
	γ_{max}	0.067 (0.046;0.098)	[1/h]	
	$k\gamma_{50}$	0.20 (0.17;0.24)	[10^{10} cells/mL]	
	λ	0.008 (0.008;0.008)	[1/h]	
	φ	0.040 (0.030;0.047)	[1/h]	
Model i (exponential)	P_0	-1.03 -1.52	[log(P)]	
	p_{gr}	0.16 – 0.30	[1/h]	

Table S2.9: Estimates of the pharmacokinetic profile parameters for each investigated drug in infected mice. Estimates are given with their residual standard error [%]. Rates are given in [1/h], concentrations in [mg/mL] and volume in [mL]. Parameters were estimated using a NLME approach in Monolix (2016R1).

	Drug	comp	Abs.	Elim	k_a [1/h]	CL [mL/h]	V_c [mL]	Q_1 [1/h]	V_{p1} [mL]	v_{max} [1/h]	$V_{max,50}$ [ng/mL]	Rel. err
P. berghei in normal mice	ACT-451840	2	MM	lin.	-	51 (8)	91 (25)	1.09 (1.45e4)	0.08 (2.25e4)	0.89 (29)	5.47 (36)	0.31 (15)
	CQ	2	lin.	lin.	0.73 (23)	29 (5)	218 (12)	4.34 (47)	100 (24)			0.27 (11)
	MMV390048	1	lin.	MM, lin.	0.23 (16)	730 (13)	480 (21)			0.32 (21)	4.5 (121)	0.21 (11)
	OZ439	2	lin.	lin.	2.7 (63)	51 (14)	466 (19)	17 (211)	183 (534)			0.32 (25)
P. falciparum in NOD scidIL-2R$^{-/-}$	ACT-451840	1	lin.	lin.	0.047 (14)	210 (11)	109 (47)					0.27 (24)
	CQ	1	lin.	lin.	26 (7480)	68 (32)	630 (30)					0.17 (17)
	MMV390048	1	lin.	MM, lin.	30 (7)	130 (4)	280 (33)			0.68 (5)	20 (22)	0.34 (4)
	OZ439	2	lin.	lin.	2.84 (19)	1.7 (-)	686 (9)	63 (5)	1.71e5 (34)			0.52 (5)

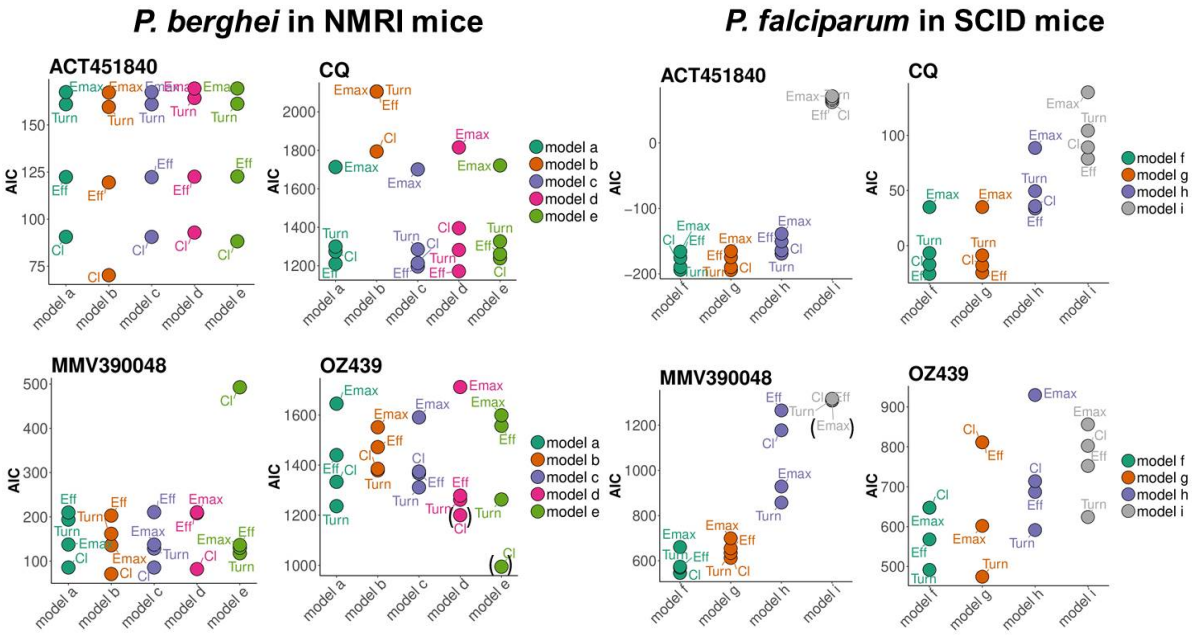

Figure S2.2: Selection of model of drug action based on AIC for the two murine experimental systems and four drugs. Models were selected based on lowest AIC and biological plausibility of the estimated parameters (E_{max}, EC_{50} and additional parameter). Models excluded due to biologically implausible parameters are set in parentheses.

Table S2.10: Estimated values of drug efficacy parameters. For each parasite growth model (PG), the drug action model with hill-coefficient *n* describing data best (ΔOFV) was chosen for comparison (see equations for drug action model in Table S2.6). Parameters are stated with their 95% confidence interval. Additional parameters are k_e for the effect model, k_R for the turnover model and Cl_Y for the clearance model.

	Drug	PG	Drug action	γ	EC_{50} [ng/mL] (95% CI)	E_{max} [1/h] (95% CI)	Add. parameter[1/h] (95 % CI)
***P. berghei* in normal mice**	ACT-451840	*a*	Clearance	5	1.1e2 (91;1.3 e2)	0.71 (0.41;1.2)	0.027 (0.025;0.029)
		b	Clearance	5	92 (82;1.0 e2)	0.50 (0.35;0.71)	0.026 (0.022;0.029)
		c	Clearance	5	1.1e2 (91;1.3 e2)	0.71 (0.41;1.2)	0.027 (0.025;0.029)
		d	Clearance	5	1e2 (85;1.2e2)	0.63 (0.41;0.97)	0.028 (0.026;0.031)
		e	Clearance	5	98 (85;1.1e2	0.60 (0.40;0.91)	0.032 (0.030;0.034)
	CQ	*a*	Effect	7	41 (39;43)	0.095 (0.093;0.097)	0.037 (0.036;0.038)
		b	Clearance	5	1.2e2 (98;1.4e2)	0.42 (0.35;0.50)	2.8e-3 (9.8e-5;4.8e-3)
		c	Effect	7	41 (39;43)	0.094 (0.092;0.096)	0.035 (0.034;0.037)
		d	Effect	2	46(43;50)	0.11 (0.11;0.11)	0.030 (0.028;0.031)
		e	Clearance	7	88 (83;94)	0.34 (0.33;0.35)	0.053 (0.051;0.055)
	MMV-390048	*a*	Clearance	5	3.7e2 (3.3e2;4.1e2)	0.61 (0.45;0.83)	0.039 (0.035;0.043)
		b	Clearance	7	2.8e2 (2.6e2;3.0e2)	0.39 (0.31;0.48)	0.036 (0.032;0.042)
		c	Clearance	5	3.7e2 (3.3e2;4.1e2)	0.61 (0.45;0.83;	0.039 (0.036;0.043)
		d	Clearance	5	3.1e2 (2.8e2;3.5e2)	0.45 (0.36;0.58)	0.041 (0.037;0.045)
		e	Turnover	2	2.2e2 (1.7e2;3.0e2)	0.19 (0.070;0.50)	0.055 (0.0054;0.55)
	OZ439	*a*	Turnover	7	49 (47;50)	0.93 (0.90;0.95)	0.013 (0.012;0.014)
		b	Turnover	7	49 (46;52)	0.94 (0.35;2.5)	0.013 (0.004;0.038)
		c	Turnover	7	42 (40;45)	0.28 (0.25;0.31)	0.060 (0.050;0.072)
		d	Turnover	7	46 (44;48)	0.84 (0.82;0.86)	0.015 (0.014;0.016)
		e	Turnover	7	46 (44;47)	0.91 (0.89;0.94)	0.014 (0.013;0.015)
***P. falciparum* in NOD scidIL-2R' c-/-**	ACT-451840	*f*	Turnover	5	17 (16;19)	0.093 (0.080;0.11)	0.062 (0.041;0.091)
		g	Turnover	5	17 (16;19)	0.095 (0.082; 0.11)	0.063 (0.062;0.073)
		h	Turnover	5	18 (17;19)	0.094 (0.082;0.11)	0.061 (0.041;0.088)
		i	Clearance	5	16 (15;18)	0.065 (0.062;0.067)	0.17 (0.14;0.19)
	CQ	*f*	Effect	7	71 (67;76)	0.098 (0.094;0.10)	0.044 (0.040;0.061)
		g	Effect	7	71 (67;75)	0.10 (0.095;0.10)	0.044 (0.038;0.059)
		h	Effect	7	70 (66;74)	0.098 (0.094;0.10)	0.045 (0.038;0.059)
		i	Effect	7	70 (66;75)	0.099 (0.092;0.11)	0.050 (0.042;0.060)
	MMV-390048	*f*	Clearance	2	1.2e2 (1.1e2;1.3e2)	0.090 (0.087;0.091)	0.071 (0.065;0.077)
		g	Clearance	5	1.1e2 (1.1 e2;1.2e2)	0.093 (0.091;0.096	0.068 (0.062;0.073)
		h	Turnover	7	1.1e2 (1.0e2;1.1e2)	0.082 (0.080;0.084)	0.073 (0.063;0.083)
		i	Clearance	5	32 (29;35)	0.12 (0.11;0.13)	0.025 (0.023;0.028)
	OZ439	*f*	Turnover	5	75 (71;79)	0.26 (0.25;0.26)	0.016 (0.015;0.017)
		g	Turnover	5	80 (76;85)	0.33 (0.32;0.34)	0.013 (0.012;0.014)
		h	Turnover	5	77 (73;82)	0.30 (0.30;0.31)	0.013 (0.013;0.014)
		i	Turnover	2	213 (197;230)	0.67 (0.63;0.72)	0.020 (0.018;0.023)

Section 4: Additional Findings

Table S2.11: Overview of experimental data of drug efficacy for *P. falciparum* infected NOD $^{scidIL\text{-}2R'\ c\text{-}/\text{-}}$ -mice treated with MMV390048 and OZ439. Only experiments conducted for sufficient duration parasites to recrudesce are listed. The total number of mice treated with the treatment regimen is split into mice cured and mice demonstrating recrudescence. For the remaining mice treatment did not decrease parasite numbers below the lower limit of quantification (0.01% parasitemia).

	Treatment regimen	no. mice	mice cured	mice with recrudescence	Time of recrudescence [hours after inoculation]
MMV390048	2×1 mg/kg	4	0	0	-
	2×10 mg/kg	5	0	2	336, 408
	4×0.25mg/kg	4	0	0	-
	4×0.5 mg/kg	8	0	0	-
	4×1 mg/kg	8	0	6	336, 456, 504, 504, 576, 624
	4×2.5 mg/kg	6	2	4	288, 576 ,576, 744
	4×5 mg/kg	2	2	0	-
	4×10 mg/kg	4	2	2	672,744
	4×20 mg/kg	2	2	0	-
OZ439	1×2.5 mg/kg	2	0	0	-
	1×5 mg/kg	2	0	0	-
	1×10 mg/kg	6	0	0	-
	1×20 mg/kg	2	0	2	288, 288
	1×30 mg/kg	2	0	2	336, 480
	1×50 mg/kg	2	0	2	576, 624
	1×75 mg/kg	2	0	2	408, 672
	1×100 mg/kg	2	2	0	-
	2×10 mg/kg	4	0	4	240, 240, 288, 336
	2×25 mg/kg	4	0	4	408, 456, 504, 672

Table S2.11: Individual slopes of parasite treatment curves and time of recrudescence for treatment with MMV390048 and OZ439 in SCID mice. The slopes of the parasite count curves after treatment were determined directly from the data.

MMV390048			OZ439		
Time of recrudescence [hours after inoculation]	**Dosing Regimen**	**-slope**	**Time of recrudescence [hours after inoculation]**	**Dosing Regimen**	**-slope**
288	4×2.5 mg/kg	0.0100	240	2×10 mg/kg	0.0030
336	4×1 mg/kg	0.0075	240	2×10 mg/kg	0.0021
336	2×10 mg/kg	0.0092	288	1×20 mg/kg	0.0281
408	2×10 mg/kg	0.0073	288	1×20 mg/kg	0.0264
456	4×1 mg/kg	0.0054	288	2×10 mg/kg	0.0020
504	4×1 mg/kg	0.0108	336	1×30 mg/kg	0.0256
504	4×1 mg/kg	0.0108	336	2×10 mg/kg	0.0061
576	4×1 mg/kg	0.0213	408	1×75 mg/kg	0.0174
576	4×2.5 mg/kg	0.0117	408	2×25 mg/kg	0.0085
576	4×2.5 mg/kg	0.0117	456	2×25 mg/kg	0.0058
624	4×1 mg/kg	0.0113	480	1×30 mg/kg	0.0281
672	4×10 mg/kg	0.0088	504	2×25 mg/kg	0.0071
744	4×2.5 mg/kg	0.0129	576	1×50 mg/kg	0.0291
744	4×10 mg/kg	0.0091	624	1×50 mg/kg	0.0337
			672	1×75 mg/kg	0.0296
			672	2×25 mg/kg	0.0080

Table S2.12: Regression analysis for slope of parasite treatment curve and recrudescence times. Ordinary linear regression (least-squares) was conducted to analyze the correlation between time of recrudescence (y) for each individual mouse and the slope of the parasite concentration curve after treatment calculated from individual mouse data (x_1, b_1), number of doses (x_2, b_2), and dosing amount (x_3, b_3) using the regression equation $y= b_1 x+ b_2 x + b_3 x +b_0$.We tested all combinations of predictors. The data used for the analysis can be found in Table S2.10 and Table S2.11.

	Slope b_1 (p-value)	**Regimen b_2 (p-value)**	**Dose b_3 (p-value)**	**Regression p-value**	**R^2**
MMV390048	13440 (0.240)	-	-	0.240	0.0392
	-	-	3.3 (0.761)	0.761	-0.07
	-	89 (0.116)	-	0.165	0.125
	9434 (0.404)	76 (0.194)	-	0.214	0.107
	16486 (0.187)	-	8.4 (0.454)	0.386	0.00625
	-	169 (0.0171)	23 (0.0608)	0.0492	0.317
	14558 (0.142)	163 (0.167)	27 (0.0300)	0.0442	0.401
OZ439	4936 (0.133)	-	-	0.133	0.0932
	-	-	4.5 (0.008)	0.00780	0.363
	-	-66 (0.396)	0	0.396	-0.01
	-	169 (0.00793)	23 (0.00793)	0.0183	0.377
	23486 (0.0215)	448 (0.0493)	-	0.0455	0.283
	249 (0.942)	-	4.4 (0.0359)	0.0340	0.314
	25009 (0.000267)	645 (0.000148)	6.2 (0.000112)	6.80e-5	0.786

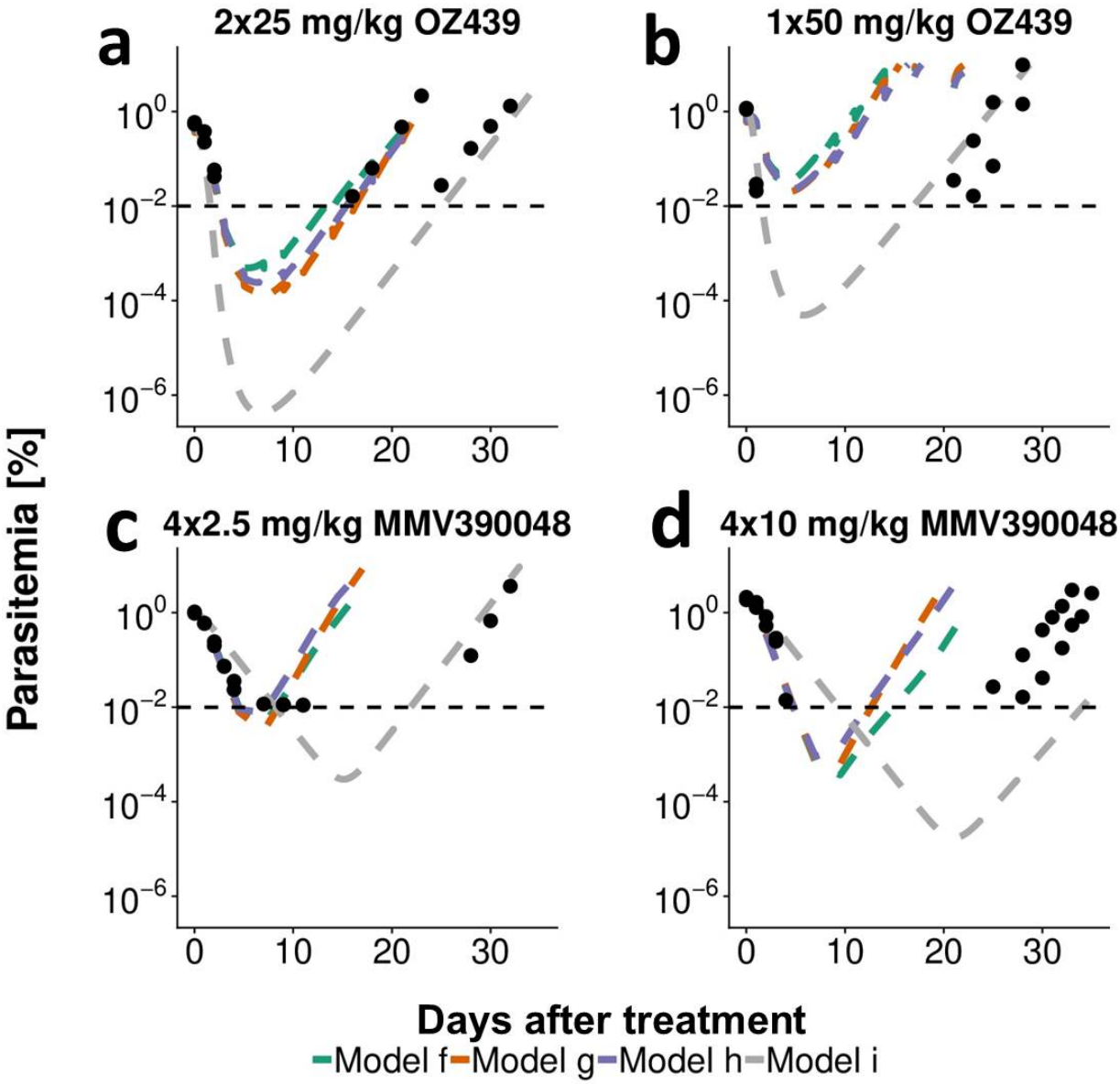

Figure S2.3: Typical fit of drug action models of SCID mice infected with *P. falciparum* demonstrating late recrudescence. Infection occurred at day 0 with an inoculum of 2×107-3.5×107 infected RBCs. Treatment commenced three days after inoculation in dosing intervals of 24 hours. Mice were treated with 2×25 mg/kg OZ439, 1×50 mg/kg OZ439, 4×2.5 mg/kg MMV390048 or 4×10 mg/kg MMV390048. n=2 mice for all doses shown.

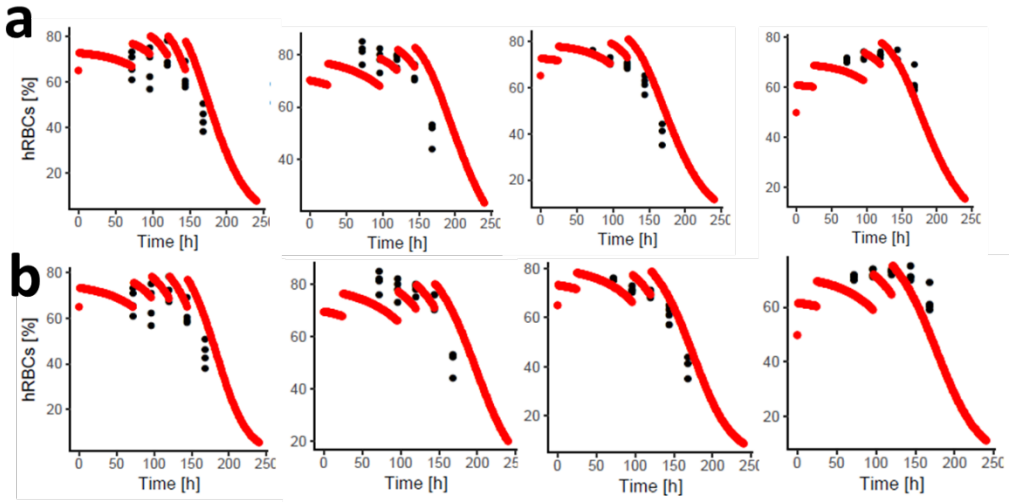

Figure S2.4: **The influence of ceasing human erythrocyte injections in SCID mice infected with *P. falciparum*.** Data (black •) and model output (red line) of four experiments, with human RBC injections ceasing before data collection, is shown for (a) *model f (const. RBC decay)* and (b) *model g (dd. RBC decay)*. RBC injections are indicated by sudden increase in hRBCs in the model output.

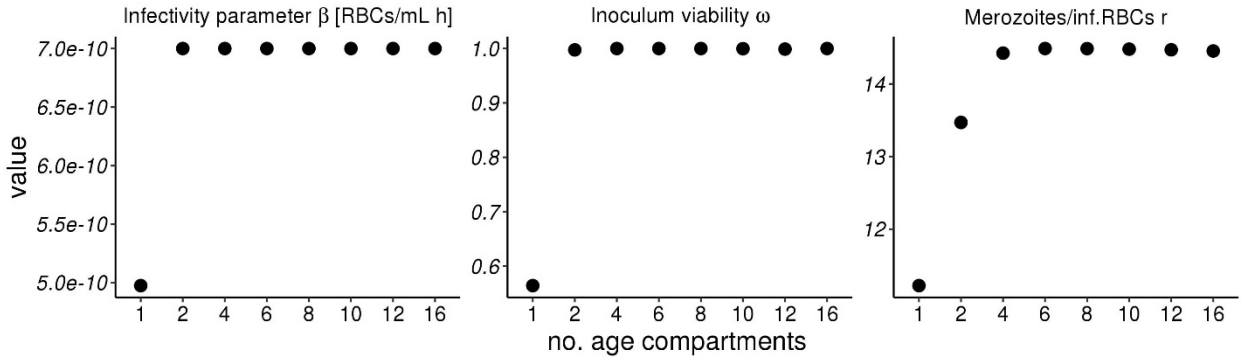

Figure S2.5: **Stability analysis conducted for the base structure of the models (corresponding to *model a (base)* towards the number of intra-erythrocytic parasite age-stages.** Total values of parameter estimates for *model a (base)* including n=1,2..,16 age compartments show the most prominent influence of the number of age compartments between one and two compartments with no distinctive contribution of additional age compartments. Considering the stability analysis and computational efficacy, we chose n=12 splitting the parasite life cycle in time-steps of two hours for *P.berghei* and four hours for *P.falciparum* considering the stability analysis and computational efficacy.

References

1 Boss, C. *et al.* Discovery and characterization of ACT-451840: an antimalarial drug with a novel mechanism of action. *ChemMedChem* **11**, 1995-2014, doi:10.1002/cmdc.201600298 (2016).

2 Le Bihan, A. *et al.* Characterization of novel antimalarial compound ACT-451840: preclinical assessment of activity and dose-efficacy modeling. *PLoS medicine* **13**, e1002138, doi:10.1371/journal.pmed.1002138 (2016).

3 Phillips, M. A. *et al.* Malaria. *Nature Reviews Disease Primers* **3**, 17050, doi:10.1038/nrdp.2017.50 (2017).

4 Paquet, T. *et al.* Antimalarial efficacy of MMV390048, an inhibitor of Plasmodium phosphatidylinositol 4-kinase. *Science translational medicine* **9**, doi:10.1126/scitranslmed.aad9735 (2017).

5 Dong, Y. *et al.* Structure-activity relationship of the antimalarial ozonide artefenomel (OZ439). *J Med Chem* **60**, 2654-2668, doi:10.1021/acs.jmedchem.6b01586 (2017).

6 Charman, S. A. *et al.* Synthetic ozonide drug candidate OZ439 offers new hope for a single-dose cure of uncomplicated malaria. *Proceedings of the National Academy of Sciences of the United States of America* **108**, 4400-4405, doi:10.1073/pnas.1015762108 (2011).

7 Hetzel, C. & Anderson, R. M. The within-host cellular dynamics of bloodstage malaria: theoretical and experimental studies. *Parasitology* **113**, 25-38 (1996).

8 Cromer, D., Evans, K. J., Schofield, L. & Davenport, M. P. Preferential invasion of reticulocytes during late-stage *Plasmodium berghei* infection accounts for reduced circulating reticulocyte levels. *International Journal for Parasitology* **36**, 1389-1397, doi:https://doi.org/10.1016/j.ijpara.2006.07.009 (2006).

9 Angulo-Barturen, I. *et al.* A murine model of falciparum-malaria by in vivo selection of competent strains in non-myelodepleted mice engrafted with human erythrocytes. *PLoS One* **3**, e2252, doi:10.1371/journal.pone.0002252 (2008).

10 Lloyd, S. W. M. in *Handbook of Laboratory Animal Management and Welfare* Vol. 3 Ch. 9, (Blackwell Publishing, 2003).

Appendix B

Supplementary Information Chapter 3- Parasite-host dynamics throughout antimalarial drug development stages complicate the translation of parasite clearance

Parasite-host dynamics throughout antimalarial drug development stages complicate the translation of parasite clearance

Running title: Parasite clearance in antimalarial drug development

AUTHORS: Lydia Burgert[1, 2], Sophie Zaloumis[3], Saber Dini[3], Louise Marquart [4], Pengxing Cao [5], Mohammed Cherkaoui[6], Nathalie Gobeau[6], James McCarthy[4], Julie A. Simpson[3], Jörg J. Möhrle[1, 2, 6], Melissa A. Penny*[1, 2]
AFFILIATIONS: [1] Swiss Tropical and Public Health Institute, Basel, Switzerland, [2] University of Basel, Basel, Switzerland, [3] Centre for Epidemiology and Biostatistics, Melbourne School of Population and Global Health, University of Melbourne, Melbourne, Australia, [4] QIMR Berghofer Medical Research Institute, Brisbane, Australia, [5] School of Mathematics and Statistics, University of Melbourne, Melbourne, Australia,[6] Medicines for Malaria Venture, Geneva, Switzerland

*Corresponding author: melissa.penny@unibas.ch

Email of other authors:
lydia.burgert@swisstph.ch
sophiez@unimelb.edu.au
saber.dini@unimelb.edu.au
Louise.Marquart@qimrberghofer.edu.au
pengxing.cao@unimelb.edu.au
cherkaouim@mmv.org
gobeaun@mmv.org
J.mccarthy@uq.edu.au
julieas@unimelb.edu.au
moehrlej@mmv.org

1. Data for drug efficacy in VIS

Table S3.1: Details of parasite clearance data used for estimating parameters of drug efficacy. The cohort name corresponds to the names provided in a previous analysis of parasite growth data from malaria Volunteer Infection Studies (VIS)[1]. The cohort number is linked to the parasite growth parameter estimation and corresponds to the cohorts shown in Fig. S7 and Fig. S8. The parasite growth (PG) and pharmacodynamic (PD) IDs are identifiers used in estimating the respective parameters.

Drug	Clinical trial registry	Cohort name*	No. Subj.	Dose [mg]	No. Cohort	PG ID	PD ID
MMV048	NCT02281344	MMV048_PIB: CH1	6	20	15	96-101	1-6
	NCT02783833	MMV049_PartB: CH1	7	40	26	163-170	7-13
	NCT02783833	MMV049_PartB: CH2	7	80	27	170-177	14-20
OZ439	ACTRN12612-000814875	OZ439:CH1	8	100	4	23-30	1-7
	ACTRN12612-000814875	OZ439:CH2	8	200	5	31-38	8-16
	ACTRN12612-000814875	OZ439:CH3	8	500	6	39-46	17-24

2. Pharmacokinetic (PK) models

Model structures

The drug-concentration after dosing with dose D [mg] is given by a two-compartment PK model with zero-order absorption for MMV048 and a two-compartment model with first-order absorption for OZ439. Below we provide the analytical solutions for both models (detailed by Monolix, http://mlxtran.lixoft.com/libraries). Individual PK parameters were used for estimation of drug action parameters in each human volunteer. Subsequent simulation utilised the population parameters. Both individual parameter and population level parameters can be found in Supplementary File 1. The PK parameter models and estimates were kindly provided by MMV, Geneva.

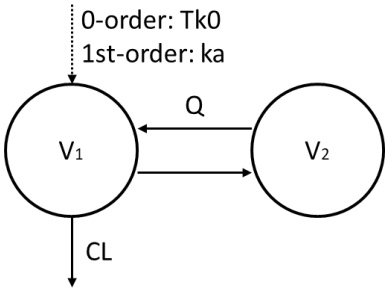

Figure S3.1: General schematic representation of a 2-compartment model with 0- or 1st order absorption process. V1 is the central compartment and V2 the peripheral compartment, rates of flow into and out of compartments are calculated with the equations given below.

2 compartment model with zero-order absorption

$$\mathbf{C(t)} = \begin{cases} \frac{\mathbf{D}}{\mathbf{T_{k0}}}\left[\frac{\mathbf{A}}{\boldsymbol{\alpha}}\left(\mathbf{1}-\mathbf{e}^{-\boldsymbol{\alpha}\mathbf{t}}\right)+\frac{\mathbf{B}}{\boldsymbol{\beta}}\left(\mathbf{1}-\mathbf{e}^{-\boldsymbol{\beta}\mathbf{t}}\right)\right] \textbf{ if } \mathbf{t} \le \mathbf{T_{k0}}, \textbf{else} \\ \frac{\mathbf{D}}{\mathbf{T_{k0}}}\left[\frac{\mathbf{A}}{\boldsymbol{\alpha}}\left(\mathbf{1}-\mathbf{e}^{-\boldsymbol{\alpha}\mathbf{T_{k0}}}\right)\mathbf{e}^{-\boldsymbol{\alpha}(\mathbf{t}-\mathbf{T_{k0}})}+\frac{\mathbf{B}}{\boldsymbol{\beta}}\left(\mathbf{1}-\mathbf{e}^{-\boldsymbol{\beta}\mathbf{T_{k0}}}\right)\mathbf{e}^{-\boldsymbol{\beta}(\mathbf{t}-\mathbf{T_{k0}})}\right] \end{cases} \quad \text{(S3.1)}$$

$$k_{10} = \frac{CL}{V_1};\ k_{12} = \frac{Q}{V_1};\quad k_{21} = \frac{Q}{V_2}$$

$$\beta = 0.5(k_{10} + k_{12} + k_{21} - \sqrt{(k_{10} + k_{12} + k_{21})^2 - 4k_{21}k_{10}}\ ;\quad \alpha = \frac{k_{21}\,k_{10}}{\beta};$$

$$A = \frac{1}{V_1}\frac{\alpha - k_{21}}{a - \beta}\ ;\quad B = \frac{1}{V_1}\frac{\beta - k_{21}}{\beta - a}$$

2 compartment model with linear absorption and lag-time

$$C(t) = \begin{cases} 0 \text{ if } t \le T_{lag}, \text{else} \\ D\left[Ae^{-\alpha\,(t-T_{lag})} + Be^{-\beta\,(t-T_{lag})} - (A+B)e^{-k_a\,(t-T_{lag})}\right] \end{cases} \quad \text{(S3.2)}$$

$$k_{10} = \frac{CL}{V_1};\ k_{12} = \frac{Q}{V_1};\quad k_{21} = \frac{Q}{V_2}$$

$$\beta = 0.5(k_{10} + k_{12} + k_{21} - \sqrt{(k_{10} + k_{12} + k_{21})^2 - 4k_{21}k_{10}}\ ;\quad \alpha = \frac{k_{21}\,k_{10}}{\beta};$$

$$A = \frac{k_a}{V_1}\frac{k_{21} - \alpha}{(k_a - a)(\beta - a)}\ ;\quad B = \frac{k_a}{V_1}\frac{k_{21} - \beta}{(k_a - \beta)(a - \beta)}$$

3. Parameter estimation

Table S3.2: Selection of the parasite growth model. The mechanistic parasite growth models S1-S3 differ in their hierarchical assignment of parameters to cohort and subject specific parameters. Based on the widely applicable information criterion (WAIC) we selected *model S3* for further analysis of drug action (referred to as *model S*). The correlation between $\boldsymbol{r_p}$ and $\boldsymbol{\delta}_p$ was calculated based of draws from the population posterior prediction.

Model	Hierarchy		WAIC (SE)	Correlation between $\boldsymbol{r_p}$ and $\boldsymbol{\delta}_p$
	Cohort	Subject		
S1	-	$ipl, \delta, r_p, \mu_{ipl}$ and σ_{ipl}	2024 (41)	0.75 (p≤0.01)
S2	r_p	ipl, μ_{ipl}, σ_{ipl} and δ	1850 (39)	0.84 (p≤0.01)
S3	r_p, μ_{ipl} and σ_{ipl}	ipl and δ	**1679 (40)**	0.84 (p≤0.01)
i		ipl and r_p	2574 (24)	-

Table S3.3: Selection of the drug effect model for treatment with MMV048 and OZ439. Per drug action model, four different hill constants were tested and models were selected per parasite growth (PG) model based on WAIC and additional observations made during the fitting process.

Drug	PG Model	Drug action	WAIC (SE)	hill	Additional observations after model fitting
MMV048	*S3*	Direct effect	1031 (41)	1	
			992 (36)	2	
			955 (33)	5	
			952 (34)	**7**	Directly low dose treatment model oscillation is out of phase with data
	S3	Direct effect+ growth retardation	901 (46)	1	
			835 (36)	2	
			774 (25)	**5**	Parasite oscillation after treatment captured in model
			779 (25)	7	
	i	Direct effect	1055 (30)	1	
			1012 (25)	2	
			973 (19)	5	
			969 (19)	**7**	Lower doses not well captured
OZ439	*S3*	Direct effect	866 (26)	1	
			850 (26)	2	
			841 (27)	**5**	Treatment effect after lower doses not well captured.
			842 (27)	7	
	S3	Direct effect+ growth retardation	685 (27)	1	
			657 (28)	**2**	
			657 (31)	5	Able to capture treatment effect after lower doses
			659 (31)	7	
	i	Direct effect	828 (18)	1	
			813 (18)	2	
			807 (19)	**5**	No drug effect for low doses
			809 (19)	7	

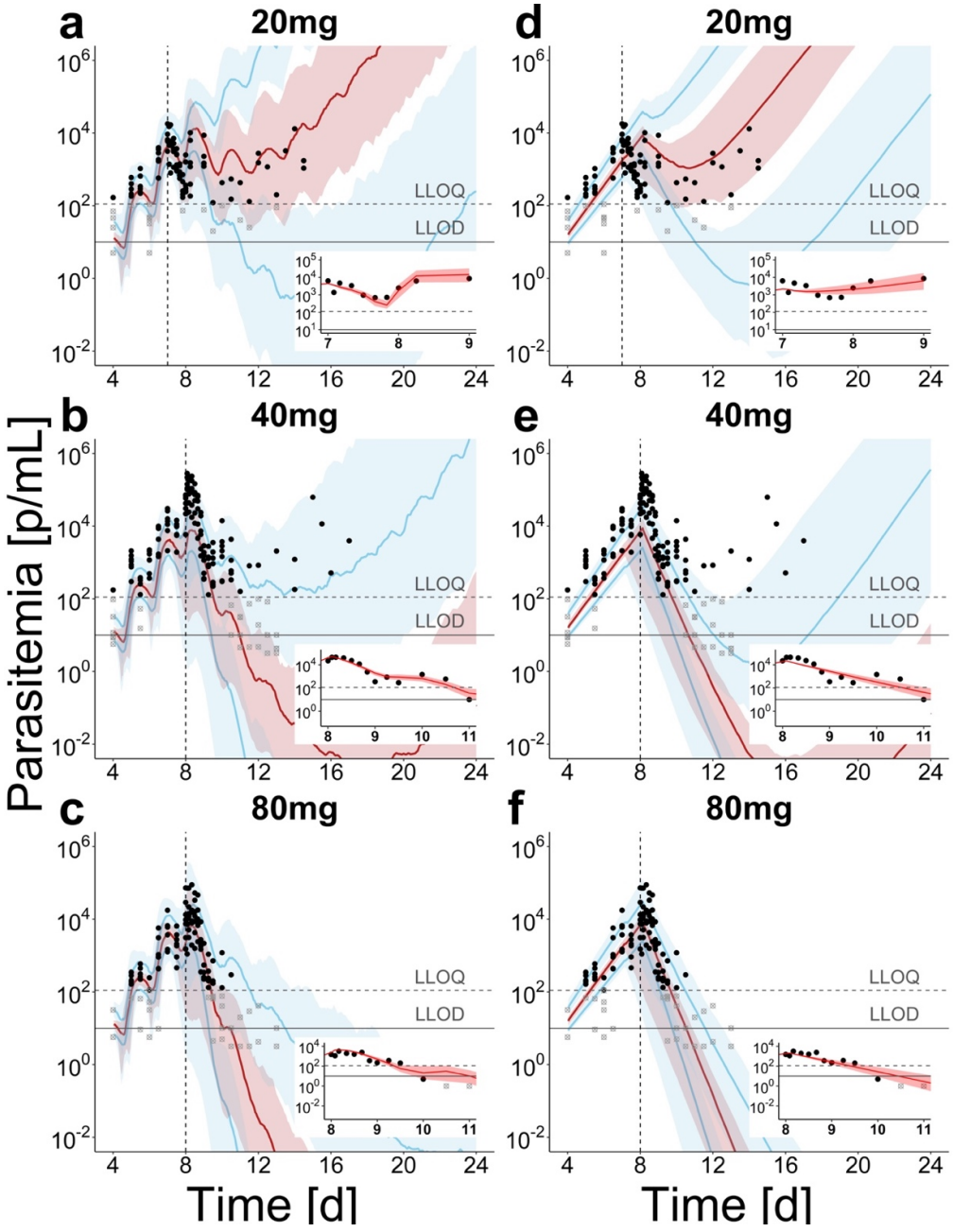

Figure S3.2: Population prediction after treatment with MMV048 in *P. falciparum*-human infection for mechanistic growth *model S* (a-c) and exponential *model i* (d-f) The median (red) and 90th percentile (blue) with credible intervals over 100 trials with 20 subjects is compared to individual parasite densities (•) in the respective treatment group. For each treatment group, parasite clearance of a typical subject (Subject 5, 13, and 17) immediately after treatment is illustrated with individual prediction (for all subjects see Supplementary Figure S3 and S4). The lower doses of 20mg and 40 mg MMV048 only show transient drug effect with parasitemia recrudescing in all subjects (see individual data in Supplementary Figure S3 and S4).In the 20 mg dose group **(a, d)**, *model S* predicts later recrudescence. After treatment with 40 mg **(b, e)**, treatment effects are overestimated for *model i*. Both models predict no recrudescence during the 24 days of follow-up for the highest dose (80mg **(c, f)**). However, predicted parasite clearance shows a larger range with *model S*. Vertical line (---) indicates time point of treatment and the horizontal lines LLOQ of 111 p/mL and LLOD of 10 p/mL.

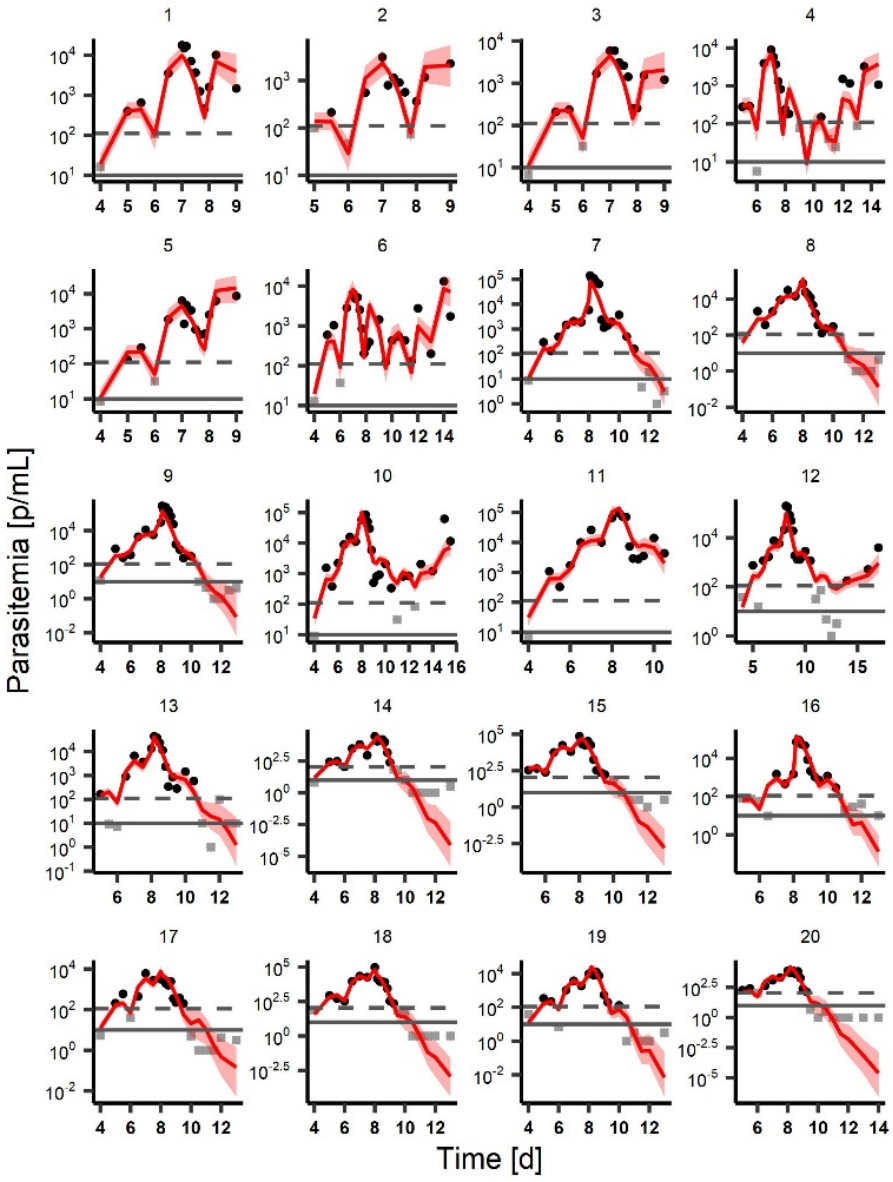

Figure S3.3: Individual posterior predictive check of parasite growth *model S* with a direct drug effect and additional growth retardation for the 20 subjects treated with MMV048 in VIS. Subjects are indicated by numbered title of each panel and were treated with 20 mg (Subjects 1-6, Cohort 15, day 7), 40 mg (Subjects 7-13, Cohort 26, day 8), and 80 mg (Subj. 14-20, Cohort 27, day 8) respectively. The periodicity in parasitemia is captured for all subjects before treatment. The model is able to describe treatment effects including recrudescence over all dose ranges. The median predicted parasitemia and its 90% credible interval are illustrated in red, with data above the LLOQ (---) in black and below in grey. Posterior predictions were generated as specified in Material and Methods.

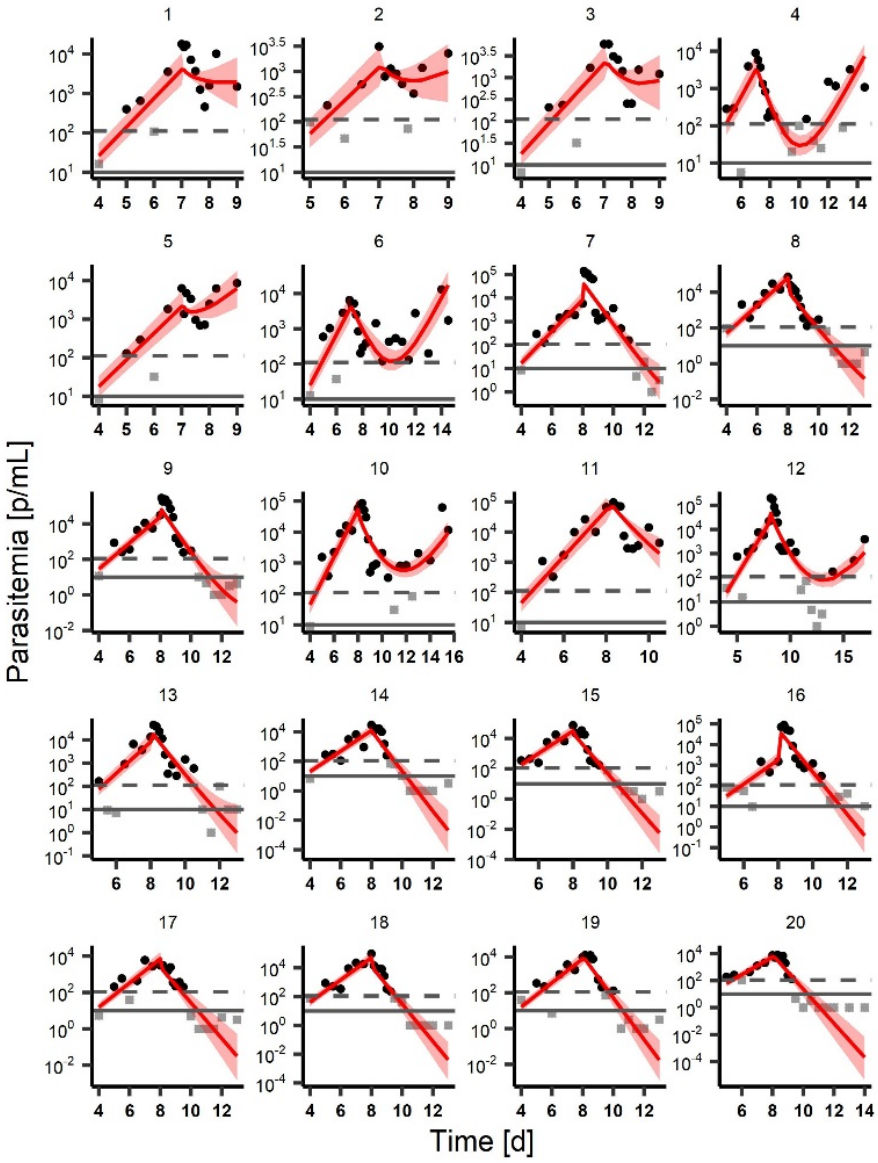

Figure S3.4: Individual posterior predictive check of parasite growth *model i* with a direct drug effect for the 20 subjects treated with MMV048 in VIS. Subjects are indicated by numbered title of each panel and were treated with 20 mg (Subjects 1-6, Cohort 15, day 7), 40 mg (Subjects 7-13, Cohort 26, day 8), and 80 mg (Subjects 14-20, Cohort 27, day 8) respectively. General trends in treatment are captured well for the two higher doses. After treatment with 20 mg, predictive intervals for subj. 1-5 are wide, capturing scenarios of increase and decrease of parasitemia after treatment. The median predicted parasitemia and its 90% credible interval are illustrated in red, with data above the LLOQ (---) in black and below in grey. Posterior predictions were generated as specified in Material and Methods.

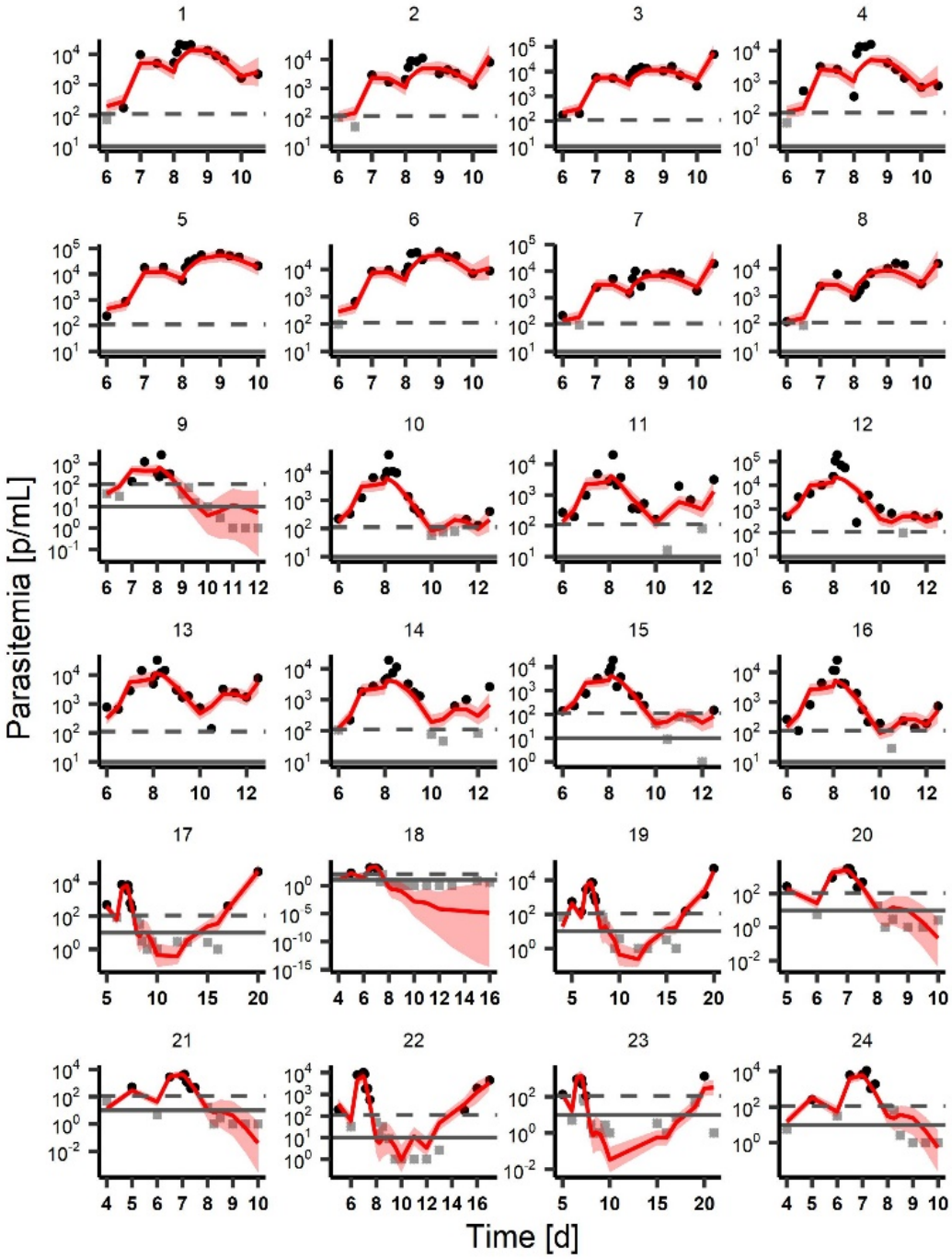

Figure S3.5: Individual posterior predictive check of parasite growth *model S* with a direct drug effect and additional growth retardation for the 24 subjects treated with OZ439 in VIS. Subjects are indicated by numbered title of each panel and were treated with 100 mg (Subjects 1-8, Cohort 4, day 8), 200 mg (Subjects. 9-16, Cohort 5, day 8), and 500 mg (Subjects 17-24, Cohort 6, day 7) respectively. After treatment with 100 mg, the model is able to capture the transient treatment effect of an initial increase directly after treatment and slight decrease around day 9. The model captures individual occurrence of recrudescence events well (Subj. 17, 19, 22, 23). The median predicted parasitemia and its 90% credible interval are illustrated in red, with data above the LLOQ (---) in black and below in grey. Posterior predictions were generated as specified in Material and Methods.

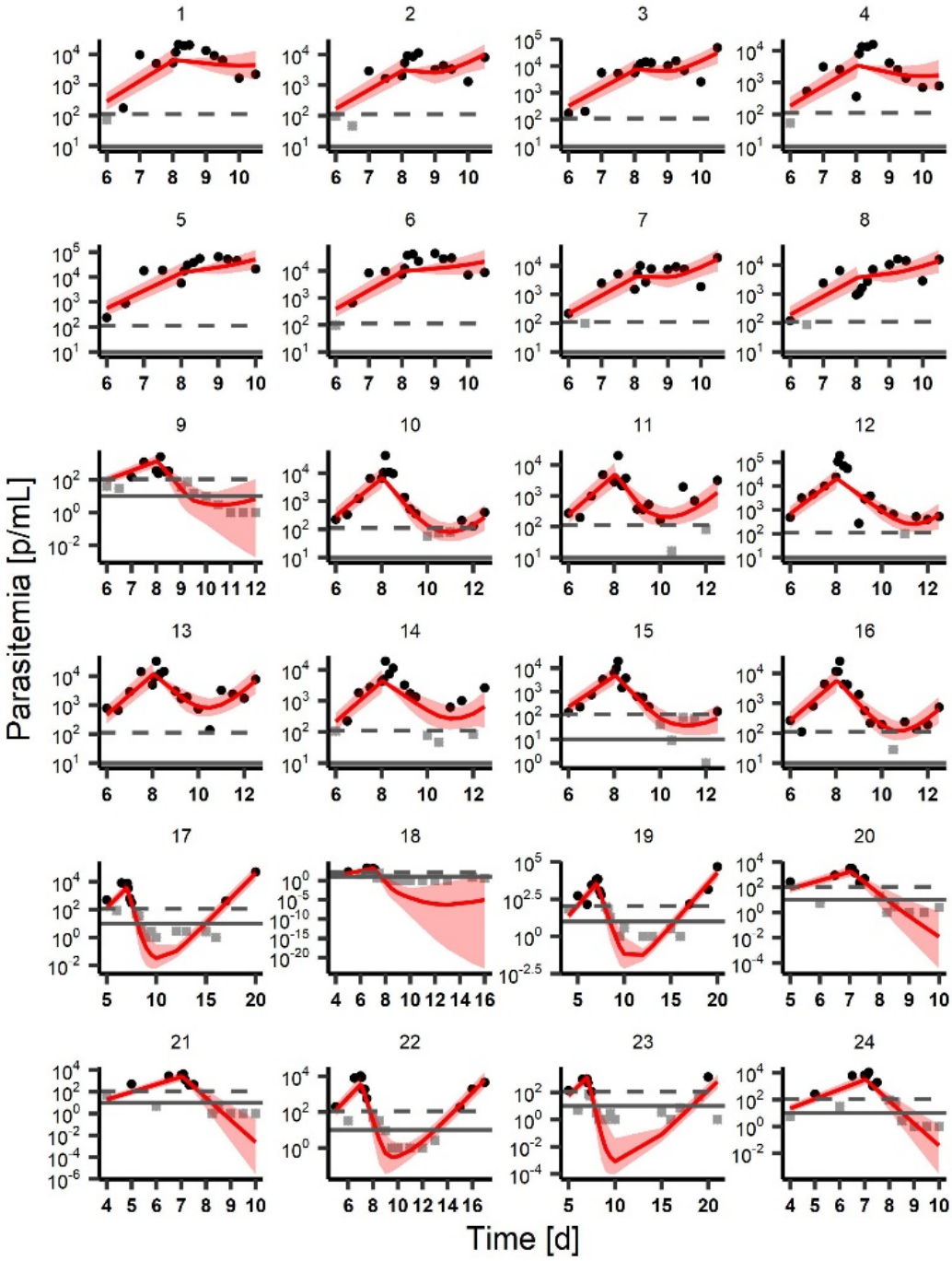

Figure S3.6: Individual posterior predictive check of parasite growth *model i* with a direct drug effect for the 24 subjects treated with OZ439 in VIS. Subjects are indicated by numbered title of each panel and were treated with 100 mg (Subjects 1-8, Cohort 4, day 8), 200 mg (Subjects 9-16, Cohort 5, day 8), and 500 mg (Subjects 17-24, Cohort 6, day 7) respectively. Model predictions are not capturing the transient treatment effect after treatment with 100 mg. The median predicted parasitemia and its 90% credible interval are illustrated in red, with data above the LLOQ (---) in black and below in grey. Posterior predictions were generated as specified in Material and Methods.

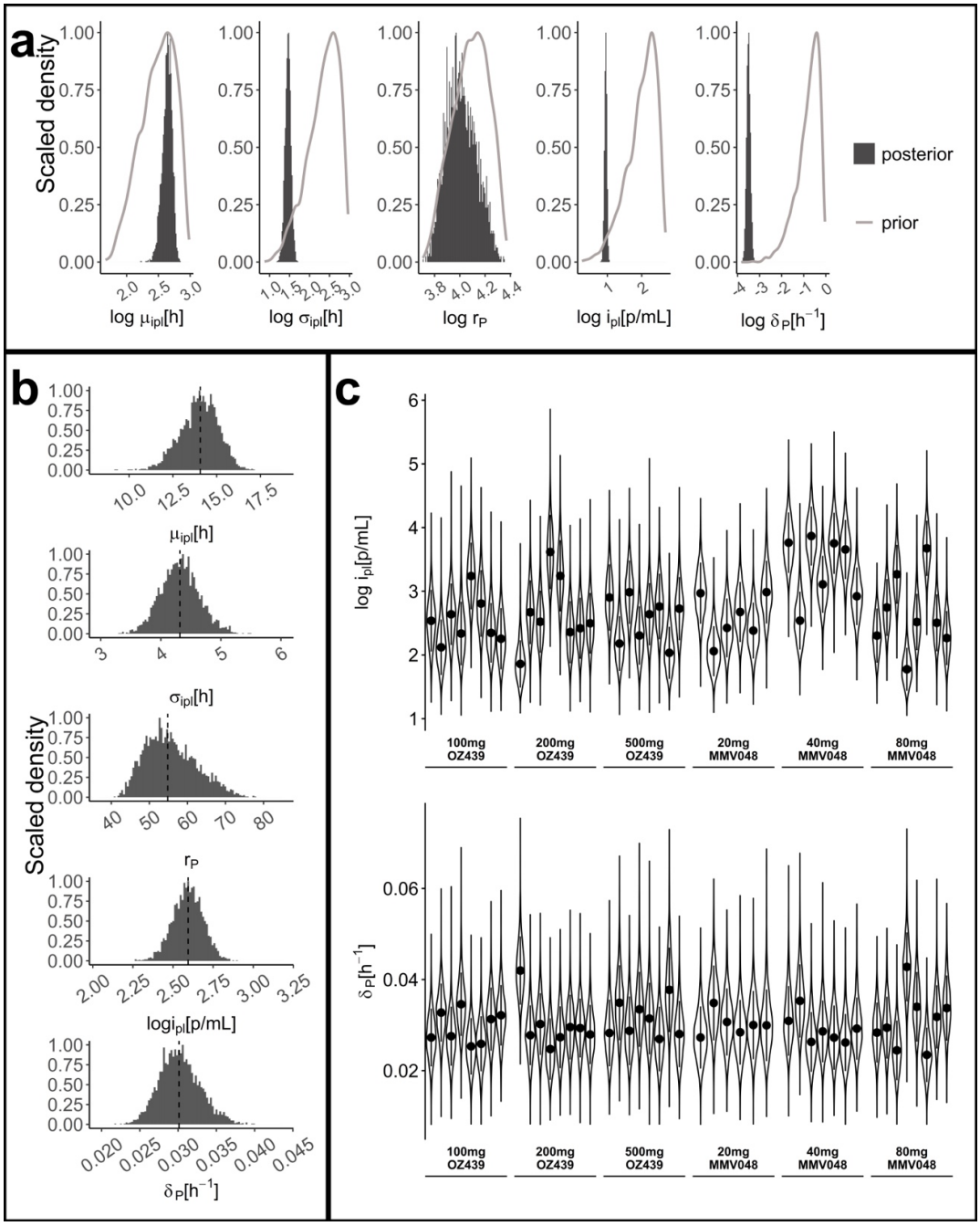

Figure S3.7: Prior and marginal posterior parameter distributions for mechanistic parasite growth *model S3* in *P. falciparum*-human infection over all cohorts and the subjects of interest. (a) Comparison of the scaled density of prior and posterior distribution, (b) population parameter estimates with their median, and (c) posterior distributions on a cohort or level (upper three panels) or for the subjects in the MMV048 and OZ439 cohorts. The parasite replication rate r_p exhibits week identifiability with congruent prior and posterior distributions (a) and posterior distributions of individual cohorts spanning the whole range between upper and lower bounds.

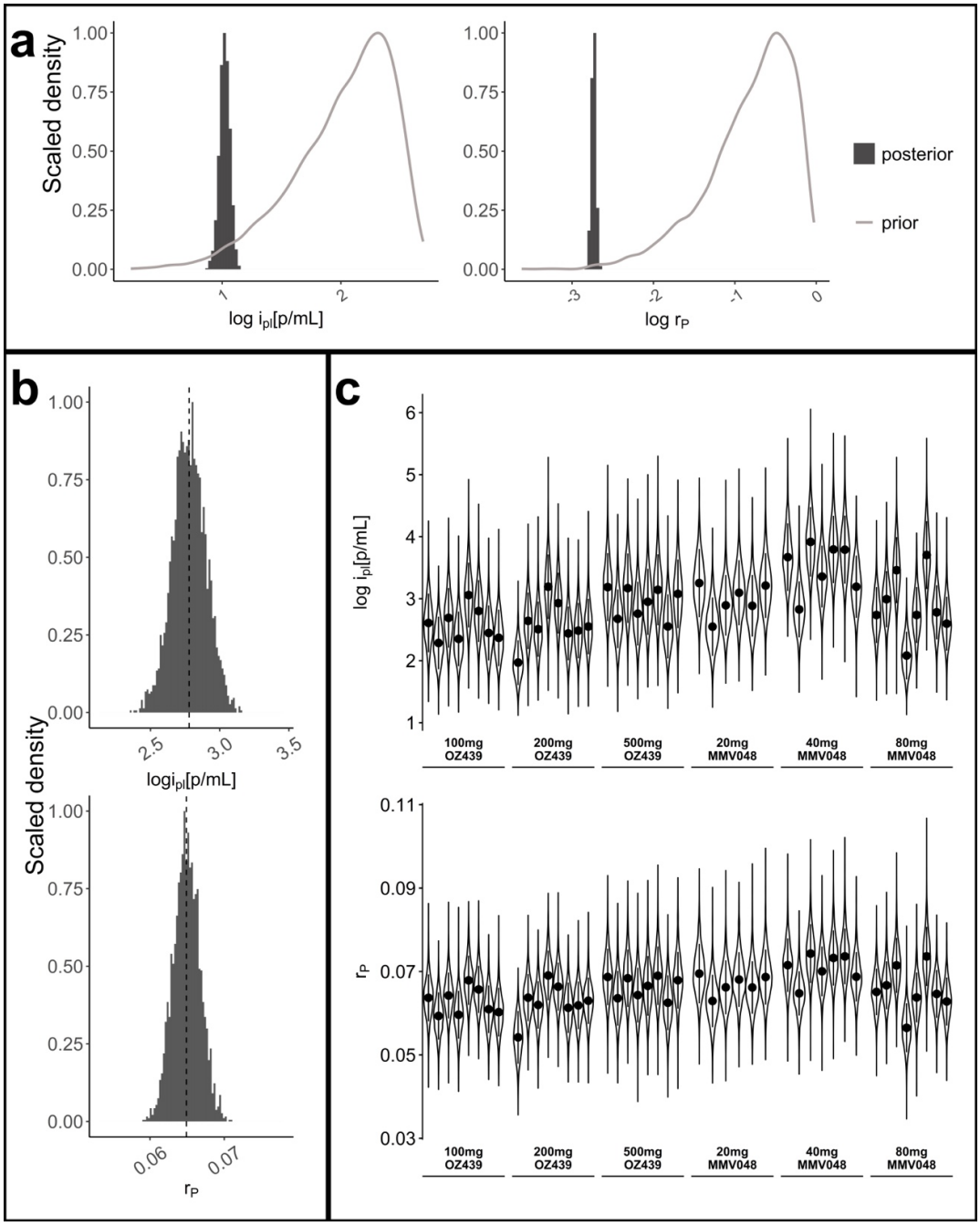

Figure S3.8: Prior and marginal posterior parameter distributions for exponential parasite growth *model i* in *P. falciparum*-human infection over all cohorts and the subjects of interest. (a) Comparison of the scaled density of prior and posterior distribution, (b) population parameter estimates with their median, and (c) posterior distributions on a cohort or level (upper three panels) or for the subjects in the MMV048 and OZ439 cohorts.

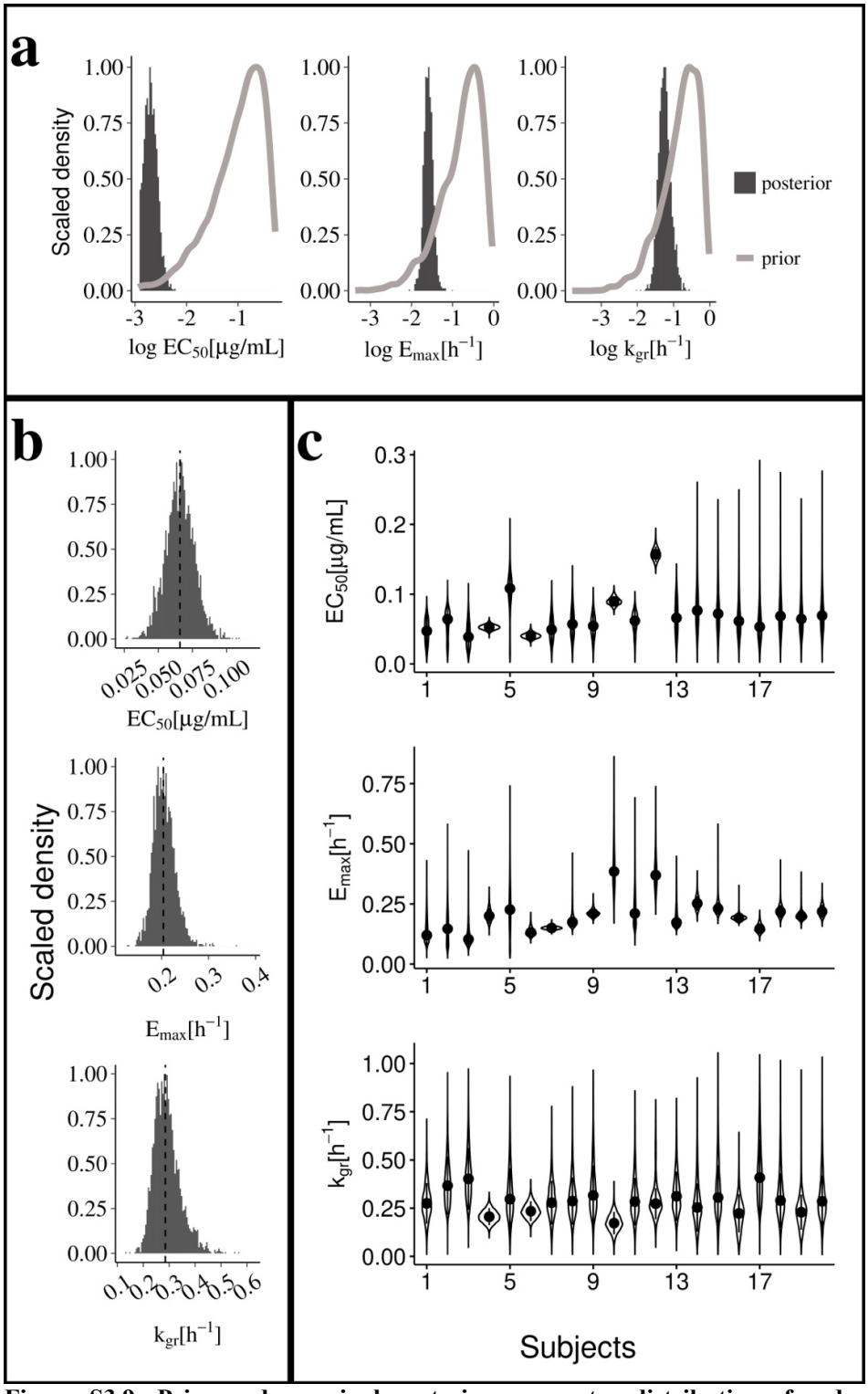

Figure S3.9: Prior and marginal posterior parameter distributions for drug efficacy parameters after treatment with MMV048 in *P. falciparum*-human infection for mechanistic growth *model S*-growth retardation (a) Comparison of the scaled density of prior and posterior distribution, (b) population parameter estimates with their median, and (c) posterior distributions on an individual level. There are identifiability issues of EC_{50} for subjects 14-17. As not all subjects in this dosing group (80mg) exhibited recrudescent, information on the efficacy of sub-curative drug concentration is missing for this dose group.

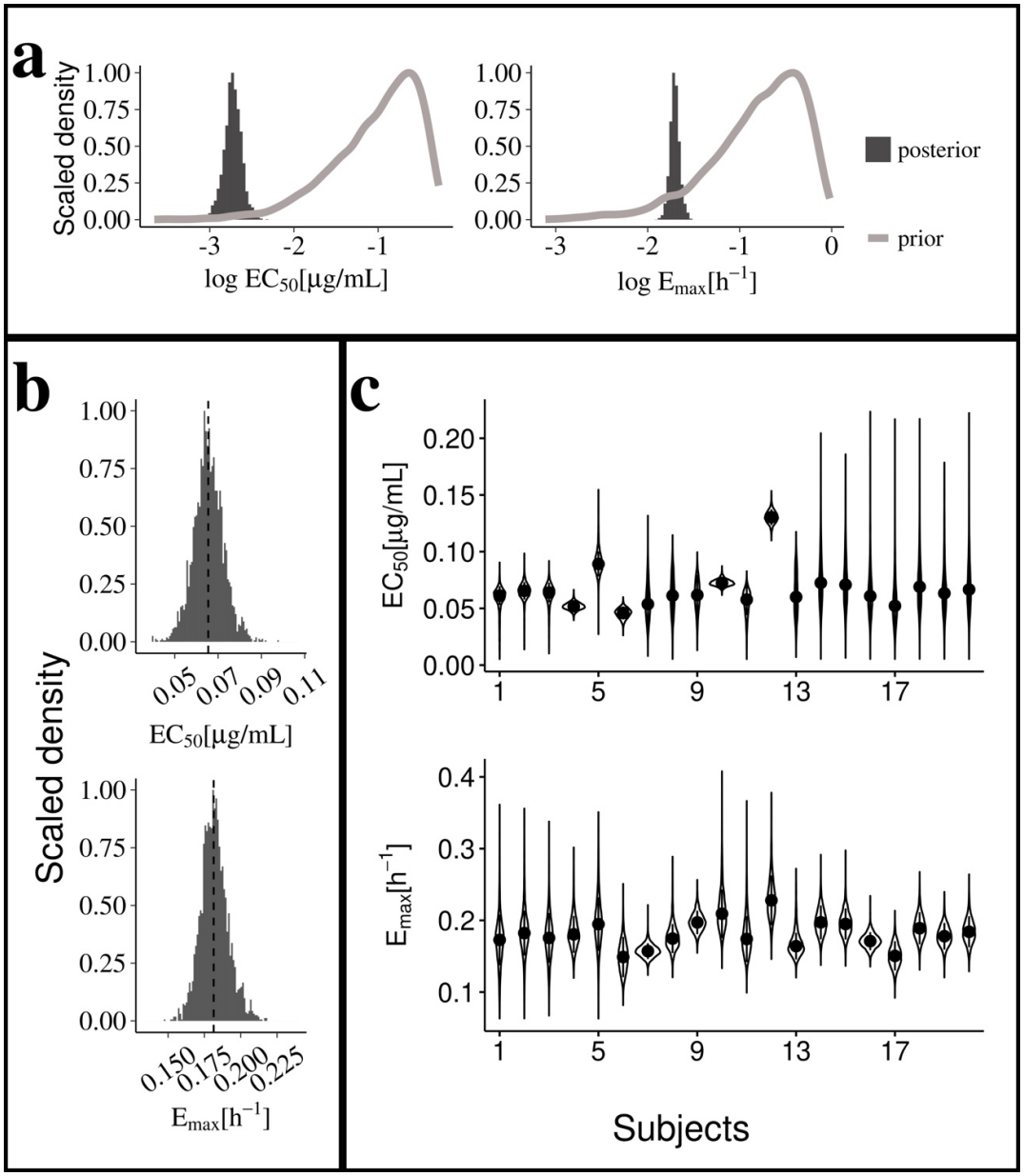

Figure S3.10: Prior and posterior marginal parameter distributions for drug efficacy parameters after treatment with MMV048 in *P. falciparum*-human infection for exponential growth *model i*-direct effect. There are identifiability issues of EC_{50} for subjects 14-17. As not all subjects in this dosing group (80mg) exhibited recrudescent, information on the efficacy of sub-curative drug concentration is missing for this dose group.

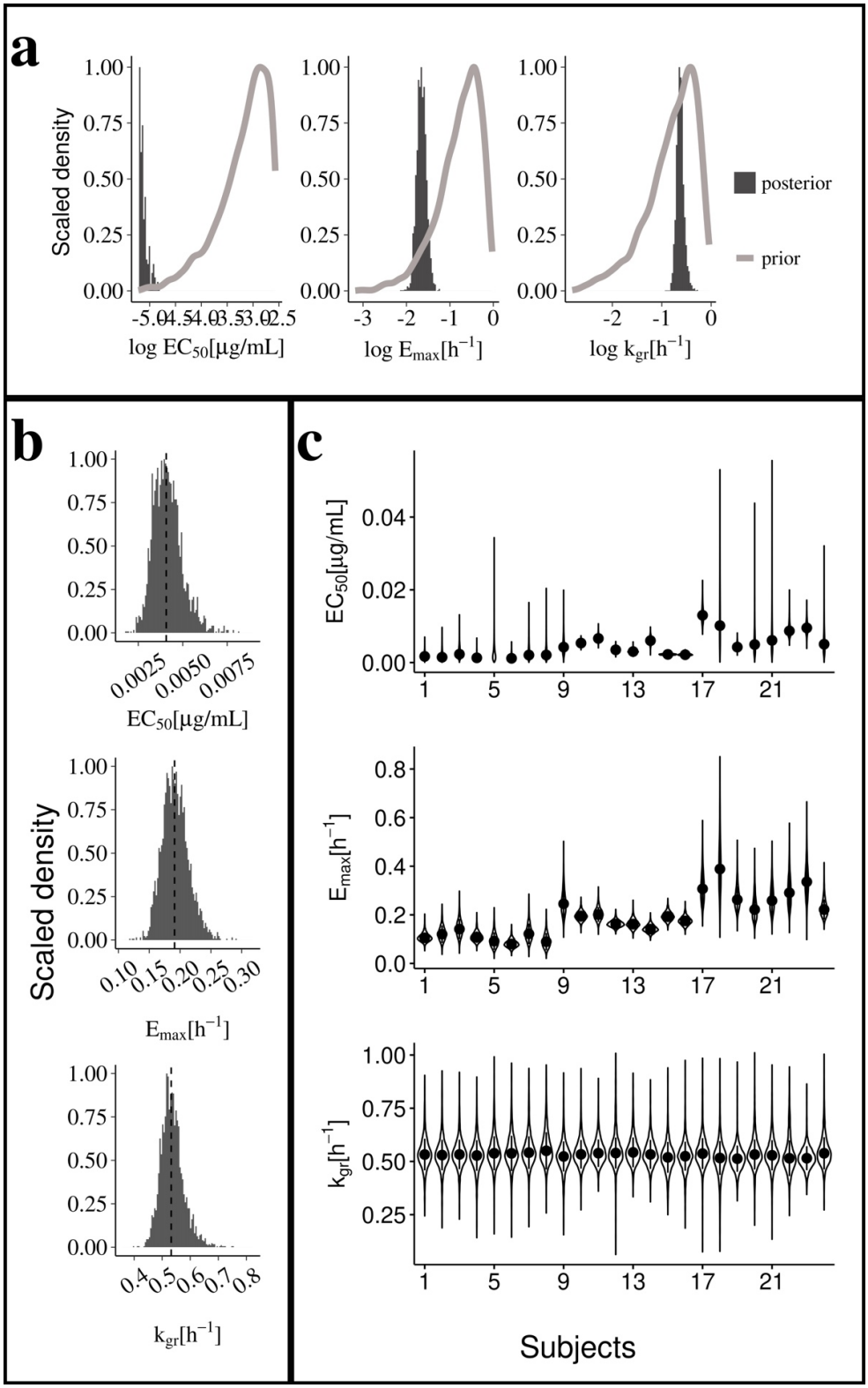

Figure S3.11: Prior and marginal posterior parameter distributions for drug efficacy parameters after treatment with OZ439 in *P. falciparum*-human infection for mechanistic growth *model S* with drug induced growth retardation. (a) Comparison of the scaled density of prior and posterior distribution, (b) population parameter estimates with their median, and (c) posterior distributions on an individual level.

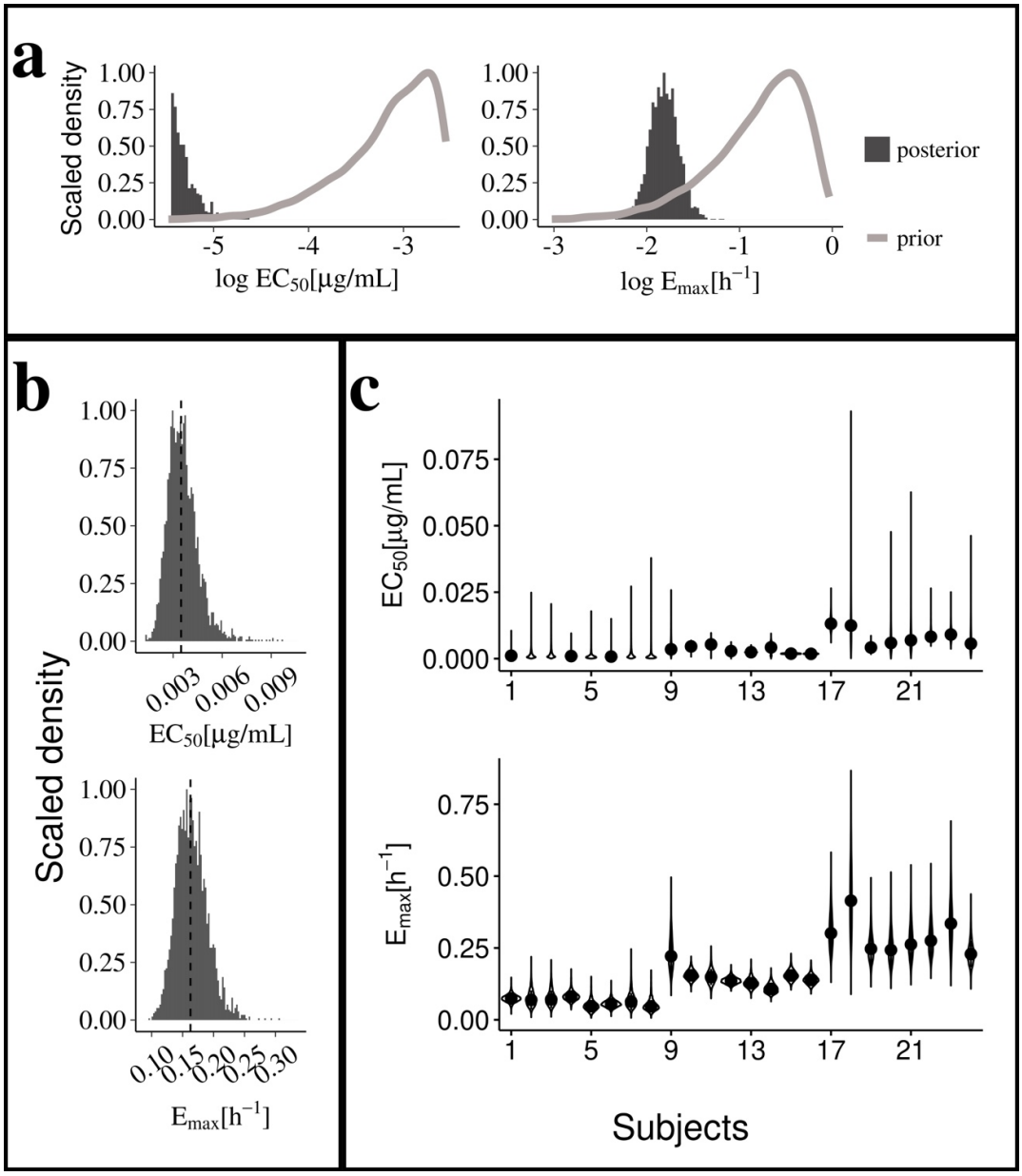

Figure S3.12 Prior and marginal posterior parameter distributions for drug efficacy parameters after treatment with OZ439 in *P. falciparum*-human infection for exponential growth *model i* and direct drug effect. (a) Comparison of the scaled density of prior and posterior distribution, (b) population parameter estimates with their median, and (c) posterior distributions on an individual level.

Table S3.4: Specification of simulation set-up for murine and human infection. Inputs into the model including dosing, parasite inoculum, and injections of human erythrocytes (hRBCs) were carried out as specified below.

	***P. berghei* - NMRI and *P.falciparum* -SCID**	***P. falciparum* - human**
Level of variability	Trial	Trial and subject
No. trials	1000	100
No. subjects/ dose/ trial	1	20
Simulation length [d]	20	30
No. doses	1	1
Dosing Time [d]	4	8
Parasite inoculum	*P. berghei*: 2e7 parasites *P. falciparum*: 3e7 parasites	Sampled i_{pl} [p/mL]
Body weight	0.021 kg	-
Blood volume	0.0025 L	-
Additional specification	P. falciparum: injection of 4.55e9 hRBC every 24 hours for the first week, then every 48 hours	-
Parameter sampling	Parameters previously estimated (1) were sampled from LN(μ,0.2μ) (Table S5)	Estimated variance-covariance matrix within parameter bounds [a, b] (Table 1)

Table S3.5: Summary of parameter estimates for murine malaria experiments of *P. berghei* -NMRI infection (*model a-model e*) and *P. falciparum*- SCID infection (*model f-model i*)(1). PD model selection, namely the best fitting structural drug action model for each drug are indicated in the drug action parameter column, with Cl_Y for delayed parasite clearance model and k_R for a turnover model. The parameters listed were sampled from a log-normal distribution LN(μ,0.2μ) for simulations. All other parameters were fixed to values specified in the Supplementary Material of previous growth analysis for murine malaria infection (1). * Range of values for infectivity parameter **β** and the initial percentage of human RBCs H_0 estimated over all experiments.

	Parasite growth parameter		Drug action parameter		
Model	**Parameter [Unit]**	**Mean estimate μ**	**Parameter**	**MMV-048**	**OZ439**
Model a-base	β * [cells/mLh]	6.7e-11 - 1.7e-10	EC_{50} [ng/mL]	3.7e2	49
	r	14.5	E_{max} [1/h]	0.61	0.93
	ω	0.99	Cl_Y or k_R [1/h]	Cl_Y=0.039	k_R=0.013
Model b-bystander	β* [c/mLh]	1.9e-10 - 5e-10	EC_{50} [ng/mL]	2.8e2	49
	r	11.5	E_{max} [1/h]	0.39	0.94
	ω	0.28	Cl_Y or k_R [1/h]	Cl_Y=0.036	k_R=0.013
	y_{max} [1/h]	0.02			
	ky_{50} [10^{10}c/mL]	7.7e-5			
Model c-comp. erythr.	β* [c/mLh]	7.1e-11-1.7e-10	EC_{50} [ng/mL]	3.7e2	42
	r	14.5	E_{max} [1/h]	0.61	0.28
	ω	0.99	Cl_Y or k_R [1/h]	Cl_Y=0.039	k_R =0.060
Model d-impaired maturation	β* [c/mLh]	9.8e-11 - 2.4e-10	EC_{50} [ng/mL]	3.1e2	46
	r	13.0	E_{max} [1/h]	0.45	0.84
	ω	0.74	Cl_Y or k_R [1/h]	Cl_Y=0.041	k_R=0.015
	$k_{l,50}$[10^{10}c/mL]	0.12			
Model e-reticulocytes	β *[c/mLh]	7.1e-11 - 1.2e-10	EC_{50} [ng/mL]	2.2e2	46
	r	10.6	E_{max} [1/h]	0.19	0.91
	ω	0.78	Cl_Y or k_R [1/h]	k_R=0.055	k_R=0.015
	ε	5.1			
Model f - const. RBC decay	β*[c/mLh]	2.4e-10 - 1.6e-9	EC_{50} [ng/mL]	1.2e2	75
	H_0*	0.40 – 0.69	E_{max} [1/h]	0.090	0.26
	r	21.3	Cl_Y or k_R [1/h]	Cl_Y=0.071	k_R=0.016
	λ[1/h]	0.010			
	γ_{max} [1/h]	0.44			
	$k\gamma_{50}$ [c/mL]	0.24			
	ω	0.29			
	φ [1/h]	0.030			

Table S3.5: Summary of parameter estimates for murine malaria experiments(1) of *P. berghei* -NMRI infection (*model a-model e*) and *P. falciparum*- SCID infection (*model f-model i*). Continued

Model	Parasite growth parameter		Drug action parameter		
	Parameter [Unit]	**Mean estimate μ**	**Parameter**	**MMV-048**	**OZ439**
Model f - const. RBC decay	β*[c/mLh]	2.4e-10 - 1.6e-9	EC_{50} [ng/mL]	1.2e2	75
	H_0*	0.40 – 0.69	E_{max} [1/h]	0.090	0.26
	r	21.3	x[1/h]	Cl_Y=0.071	k_R=0.016
	λ[1/h]	0.010			
	γ_{max} [1/h]	0.44			
	$k\gamma_{50}$ [c/mL]	0.24			
	ω	0.29			
	φ [1/h]	0.030			
Model g - dd. RBC decay	β*[c/mLh]	2.0e-10 - 9.2e-10	EC_{50} [ng/mL]	1.1e2	80
	H_0*	0.40 – 0.65	E_{max} [1/h]	0.093	0.33
	r	22.8	x [1/h]	Cl_Y=0.068	k_R=0.013
	ω	0.25			
	χ_{max} [1/h]	0.018			
	$k\chi_{,50}$[10^{10}c/mL]	1.05			
	γ_{max} [1/h]	0.055			
	K**γ_{50}**[10^{10} c/mL]	0.10			
	φ [1/h]	0.027			
Model h - human RBC	β*[c/mLh]	2.1e-10 - 8.8e-10	EC_{50} [ng/mL]	1.1e2	77
	H_0*	0.40 - 0.65	E_{max} [1/h]	0.082	0.30
	r	22	x [1/h]	k_R=0.073	k_R=0.013
	ω	0.36			
	γ_{max} [1/h]	0.067			
	$k\gamma_{50}$[10^{10} c/mL]	0.20			
	λ[1/h]	0.008			
	φ[1/h]	0.040			
Model i - exponential	P_0 [log(P)]	-1.03 - 1.52	EC_{50} [ng/mL]	32	213
	p_{gr} [1/h]	0.16 - 0.30	E_{max} [1/h]	0.12	0.67
			x [1/h]	Cl_Y=0.025	k_R=0.020

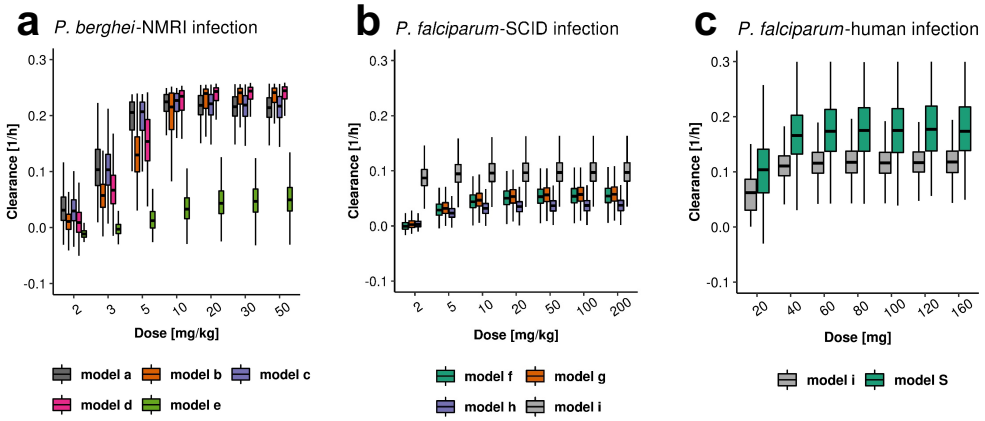

Figure S3.13: Parasitic clearance rates across the clinical development stages after single dose treatment with MMV048. Parasite clearance rates for *P. berghei* (a), *P. falciparum* in SCID (b) and *P. falciparum* in VIS (c) were calculated from simulation output using the methodology provided in (2). The difference in predicted clearance of *model e (reticulocytes)* for *P.berghei*-NMRI infection is caused by a difference in structural PD model (turnover) in comparison to *model a-d* (clearance). Because *model e* does not take the delayed clearance of dead parasites into account, it estimates slower parasite killing. In contrast, *model a-d* measure the actual killing of the drug and therefore higher clearance values. Delayed parasite recrudescence in lower doses influenced the estimation of parameters of drug action for *model i (exponential)* in *P. falciparum*-SCID infection, shifting them to higher drug efficacy estimates (lower EC_{50})**(1)**.

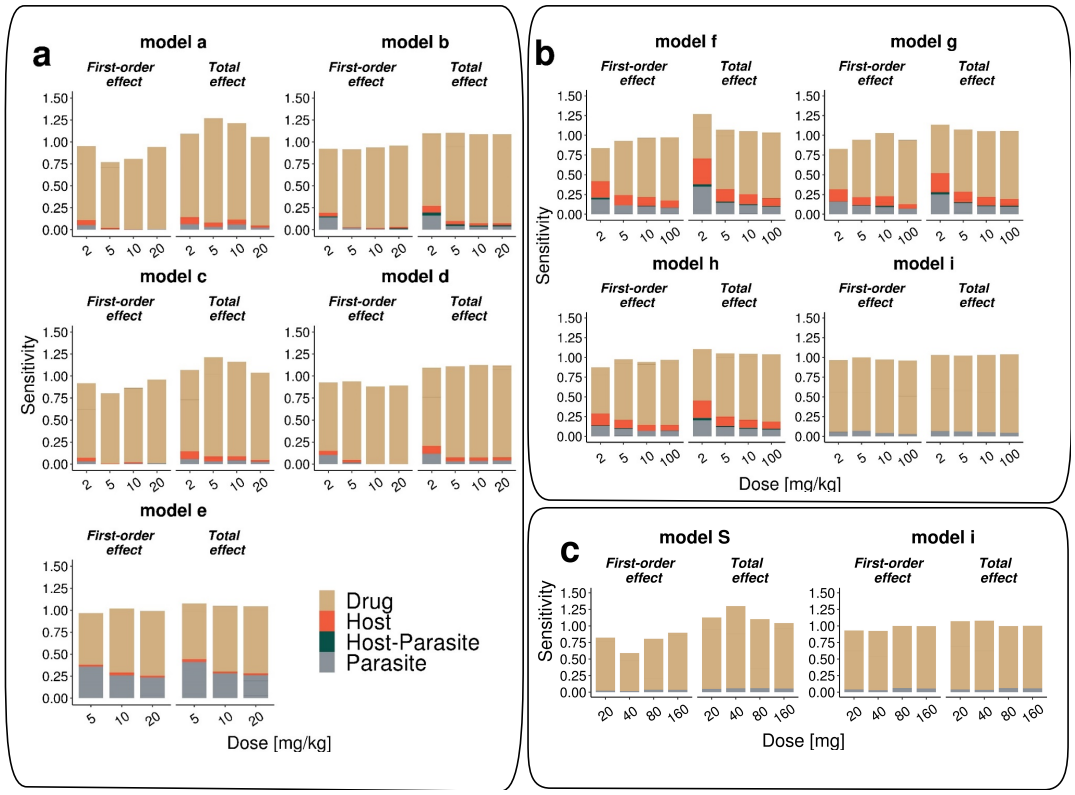

Figure S3.14: Sobol sensitivity analysis of parasite clearance after MMV048 treatment towards parameters of host, parasite, host-parasite, and drug dynamics for (a) *P. berghei* – NMRI , (b) *P. falciparum* – SCID, and (c) *P. falciparum*- human infection. In *P. berghei*-NMRI infection, parasite clearance after medium-high doses is highly sensitivity towards parameters of drug dynamics with the exception of *model e*. Here, the number of merozoites r and the preference for reticulocytes ε account for up to 40% of variance. Sobol indices could not be calculated for the 2 mg/kg dose group of *model e*, since the number of samples with quantifiable clearance was to small. Drug induced clearance in *P. falciparum*-SCID infections exhibits similar behavior for all mechanistic parasite growth *models f-h*. No noticeable influence of parasite and host parameters was found for *P. falciparum*-human infection. The first order effects measure individual parameter contributions and the total effect indices summarize individual and interactive parameter contributions to the outcome variance. The full set of individual parameter contributions can be found in Supplementary File 2.

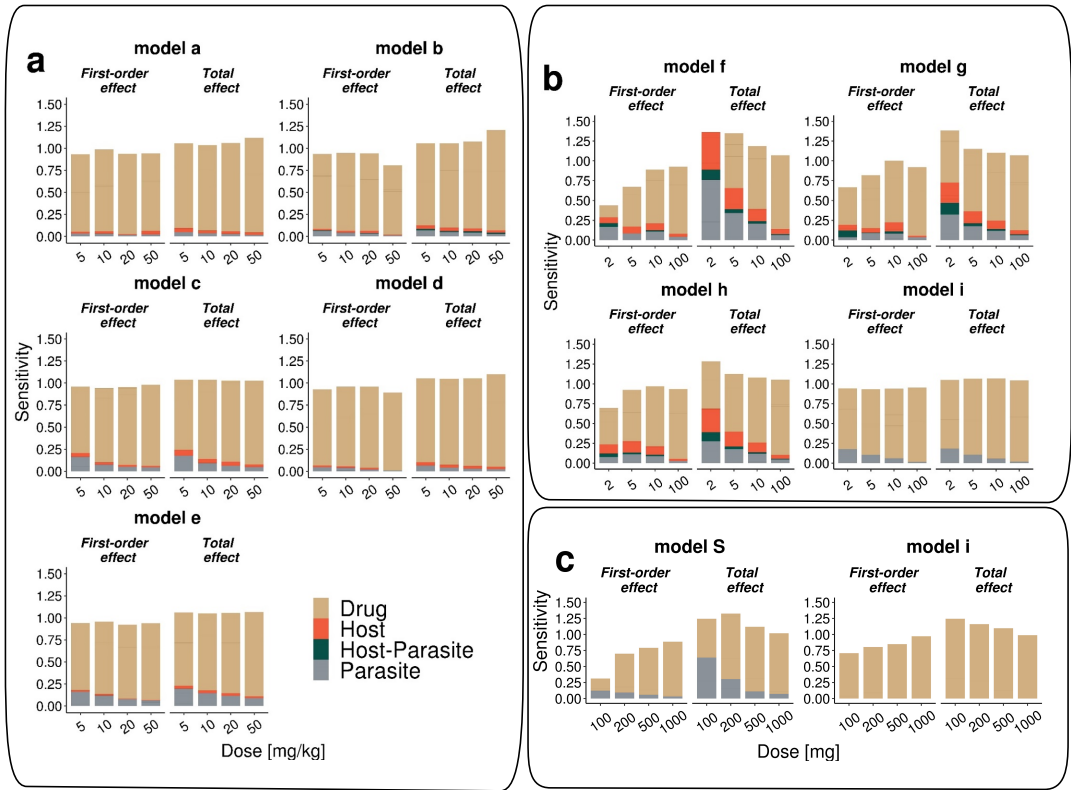

Figure S3.15: Sobol sensitivity analysis of parasite clearance after OZ439 treatment towards parameters of host, parasite, host-parasite, and drug dynamics for (a) *P. berghei* – NMRI , (b) *P. falciparum* – SCID, and (c) *P. falciparum*- human infection. In *P. berghei*-NMRI infection, parasite clearance after medium-high doses is highly sensitivity towards parameters of drug dynamics. Drug induced clearance in *P. falciparum*-SCID infections exhibits similar behavior for all mechanistic parasite growth *models f-h*, with lower dose ranges showing an increased sensitivity towards host and parasite parameters. *Model S* of *P. falciparum*-human infection shows an increased total effect of parasite parameters (see Discussion). No noticeable influence of parasite and host parameters was found for the exponential growth *model i*. The first order effects measure individual parameter contributions and the total effect indices summarize individual and interactive parameter contributions to the outcome variance. The full set of individual parameter contributions can be found in Supplementary File 2.

1. Burgert L, Rottmann M, Wittlin S, Gobeau N, Krause A, Dingemanse J, Möhrle JJ, Penny MA. 2020. Ensemble modeling highlights importance of understanding parasite-host behavior in preclinical antimalarial drug development. Sci Rep 10:4410.

2. Flegg JA, Guerin PJ, White NJ, Stepniewska K. 2011. Standardizing the measurement of parasite clearance in falciparum malaria: the parasite clearance estimator. Malar J 10.

Supplementary File 3.1 - Chapter 3: Parasite-host dynamics throughout antimalarial drug development stages complicate the translation of parasite clearance

Table SF 3.1: Population PK parameters for MMV390048 as provided by Monolix.

	parameter	**s.e. (lin)**	**r.s.e.(%)**
CL_pop	1.15	0.084	7
V1_pop	163	15	9
Q_pop	29.2	4.1	14
V2_pop	117	9.3	8
Tk0_pop	1.47	0.12	8
Standard deviation of the random effects:			
omega_CL	0.462	0.044	10
omega_V1	0.552	0.069	13
omega_Q1	0	-	-
omega_V2	0	-	-
omega_Tk0	0.682	0.054	8
a	0.000299	5.70E-05	19
b	0.213	0.0047	2

Table SF 3.2: Individual PK parameters for MMV390048 as provided by Monolix.

ID	Fabs0_mode	CL_mode	V1_mode	Q_mode	V2_mode	Tk0_mode
1	1.35	0.85	192.87	29.24	116.96	1.00
2	1.05	1.72	169.78	29.24	116.96	1.76
3	2.75	1.83	144.67	29.24	116.96	1.42
4	0.86	1.75	121.37	29.24	116.96	1.89
5	0.67	1.69	114.00	29.24	116.96	0.57
6	1.75	1.77	141.63	29.24	116.96	2.57
7	1.02	1.47	76.21	29.24	116.96	0.60
8	1.07	1.18	208.99	29.24	116.96	1.46
9	0.87	1.75	161.12	29.24	116.96	0.80
10	0.79	1.33	354.76	29.24	116.96	2.74
11	0.65	1.19	397.96	29.24	116.96	5.31
12	0.91	0.59	137.96	29.24	116.96	1.33
13	1.19	0.94	205.54	29.24	116.96	1.71
14	1.68	1.80	115.66	29.24	116.96	1.58
15	0.99	0.96	273.98	29.24	116.96	2.55
16	0.79	1.34	153.05	29.24	116.96	2.06
17	0.78	0.94	104.44	29.24	116.96	1.66
18	1.28	1.25	164.00	29.24	116.96	2.56
19	0.85	1.68	198.25	29.24	116.96	1.65
20	1.10	1.00	122.93	29.24	116.96	1.13

Table SF 3.3: Population PK parameters for OZ439 as provided by Monolix.

	parameter	**s.e. (lin)**	**r.s.e.(%)**
ka_pop	0.207	0.0138	6.67
CL_pop	57.6	4.06	7.05
beta_CL_tDOSELEVEL	-0.371	0.0984	26.5
V1_pop	139	12.7	9.13
Q1_pop	9.89	0.535	5.42
V2_pop	768	82.6	10.8
Tlag1_pop	0.416	0.0128	3.09
Standard deviation of the random effects:			
omega_ka	0.216	0.047	21.8
omega_CL	0.322	0.0498	15.5
omega_V2	0.378	0.0836	22.1
omega_Tlag1	0.124	0.0235	19

Table SF 3.4: Individual PK parameters for OZ439 as provided by Monolix.

ID	ka_mode	CL_mode	V2_mode	Q1_mode	V2_mode	Tlag1_mode	Dose [mg]
1	0.20	59.11	138.93	9.85	588.14	0.50	100
2	0.23	105.09	138.93	9.85	897.93	0.44	100
3	0.21	121.88	138.93	9.85	480.80	0.45	100
4	0.22	66.91	138.93	9.85	857.40	0.41	100
5	0.23	88.28	138.93	9.85	517.03	0.46	100
6	0.20	61.42	138.93	9.85	942.09	0.49	100
7	0.21	122.26	138.93	9.85	446.68	0.48	100
8	0.22	79.28	138.93	9.85	828.48	0.49	100
9	0.19	59.20	138.93	9.85	882.93	0.43	200
10	0.23	47.85	138.93	9.85	629.54	0.50	200
11	0.30	46.04	138.93	9.85	719.86	0.44	200
12	0.24	52.68	138.93	9.85	399.83	0.43	200
13	0.22	71.62	138.93	9.85	514.93	0.41	200
14	0.30	43.79	138.93	9.85	399.53	0.35	200
15	0.18	70.91	138.93	9.85	919.44	0.40	200
16	0.22	79.92	138.93	9.85	469.14	0.37	200
17	0.19	42.84	138.93	9.85	827.85	0.40	500
18	0.17	36.18	138.93	9.85	1115.89	0.48	500
19	0.17	73.18	138.93	9.85	754.11	0.40	500
20	0.20	36.65	138.93	9.85	1036.69	0.38	500
21	0.28	23.83	138.93	9.85	685.36	0.48	500
22	0.15	53.03	138.93	9.85	1275.33	0.49	500
23	0.16	51.00	138.93	9.85	968.26	0.36	500
24	0.19	30.87	138.93	9.85	886.38	0.38	500

Supplementary File 3.2 - Chapter 3: Parasite-host dynamics throughout antimalarial drug development stages complicate the translation of parasite clearance

Table SF 3.1: Sobol indices for parasite clearance of *P. berghei*-NMRI infection after treatment with OZ439.

Para-meter type	**Dose [mg/kg]**	**Para-meter**	***model a***	***model b***	***model c***	***model d***	***model e***	**Effect**
Drug	5	EC50	0.185	0.139	0.206	0.159	0.115	first-order effect
Drug	5	EMAX	0.443	0.461	0.539	0.476	0.455	first-order effect
Drug	5	kR	0.250	0.249	0	0.229	0.189	first-order effect
Drug	10	EC50	0.129	0.092	0.105	0.113	0.078	first-order effect
Drug	10	EMAX	0.510	0.507	0.727	0.555	0.506	first-order effect
Drug	10	kR	0.287	0.283	0	0.235	0.236	first-order effect
Drug	20	EC50	0.078	0.053	0.069	0.062	0.040	first-order effect
Drug	20	EMAX	0.529	0.526	0.796	0.607	0.538	first-order effect
Drug	20	kR	0.305	0.299	0.019	0.251	0.259	first-order effect
Drug	50	EC50	0.031	0.015	0.031	0.023	0.011	first-order effect
Drug	50	EMAX	0.534	0.494	0.858	0.615	0.588	first-order effect
Drug	50	kR	0.314	0.277	0.034	0.246	0.271	first-order effect
Host	5	CL	0.022	0.017	0.040	0.017	0.015	first-order effect
Host	10	CL	0.018	0.020	0.025	0.017	0.015	first-order effect
Host	20	CL	0	0.018	0.019	0.011	0	first-order effect
Host	50	CL	0.012	0	0.011	0	0	first-order effect
Parasite	5	attr	0	0	0	0	0.039	first-order effect
Parasite	5	beta	0	0	0.054	0	0.020	first-order effect
Parasite	5	r	0.029	0.053	0.109	0.042	0.104	first-order effect
Parasite	10	attr	0	0	0	0	0.028	first-order effect
Parasite	10	beta	0	0	0.019	0	0.013	first-order effect
Parasite	10	r	0.024	0.036	0.055	0.031	0.077	first-order effect
Parasite	20	attr	0	0	0	0	0.019	first-order effect
Parasite	20	beta	0	0	0.015	0	0	first-order effect
Parasite	20	r	0.015	0.027	0.037	0.017	0.055	first-order effect
Parasite	50	attr	0	0	0	0	0.019	first-order effect
Parasite	50	beta	0	0	0.011	0	0	first-order effect
Parasite	50	r	0.012	0.011	0.032	0.010	0.039	first-order effect
Drug	5	EC50	0.2141	0.162	0.222	0.190	0.133	total effect
Drug	5	EMAX	0.4771	0.496	0.560	0.507	0.485	total effect
Drug	5	kR	0.2708	0.274	0	0.253	0.213	total effect
Drug	10	EC50	0.1401	0.108	0.123	0.135	0.089	total effect
Drug	10	EMAX	0.5289	0.541	0.755	0.585	0.531	total effect
Drug	10	kR	0.2994	0.308	0	0.256	0.252	total effect
Drug	20	EC50	0.0936	0.061	0.081	0.074	0.053	total effect
Drug	20	EMAX	0.5668	0.581	0.817	0.645	0.571	total effect
Drug	20	kR	0.3414	0.342	0.025	0.276	0.286	total effect
Drug	50	EC50	0.0325	0.025	0.036	0.035	0.019	total effect
Drug	50	EMAX	0.6300	0.670	0.876	0.697	0.630	total effect
Drug	50	kR	0.4085	0.441	0.036	0.319	0.306	total effect
Host	5	CL	0.0298	0.026	0.049	0.024	0.022	total effect

Host	10	CL	0.0183	0.025	0.034	0.019	0.021	total effect
Host	20	CL	0	0.021	0.028	0.014	0	total effect
Host	50	CL	0.0099	0	0.017	0	0	total effect
Parasite	5	attr	0	0	0	0	0.052	total effect
Parasite	5	beta	0	0	0.060	0	0.024	total effect
Parasite	5	r	0.0379	0.057	0.116	0.051	0.120	total effect
Parasite	10	attr	0	0	0	0	0.039	total effect
Parasite	10	beta	0	0	0.027	0	0.016	total effect
Parasite	10	r	0.0279	0.042	0.064	0.034	0.090	total effect
Parasite	20	attr	0	0	0	0	0.030	total effect
Parasite	20	beta	0	0	0.020	0	0	total effect
Parasite	20	r	0.0208	0.033	0.042	0.023	0.071	total effect
Parasite	50	attr	0	0	0	0	0.026	total effect
Parasite	50	beta	0	0	0.014	0	0	total effect
Parasite	50	r	0.0126	0.022	0.033	0.017	0.050	total effect

Table SF 3.2: Sobol indices for parasite clearance of P. berghei-NMRI infection with MMV048.

Para-meter type	**Dose [mg/kg]**	**Para-meter**	***model a***	***model b***	***model c***	***model d***	***model e***	**Effect**
Drug	2	EC50	0.337	0.278	0.299	0.276	0	first-order effect
Drug	2	EMAX	0.500	0.447	0.549	0.500	0	first-order effect
Drug	5	EC50	0.061	0.107	0.049	0.086	0.044	first-order effect
Drug	5	EMAX	0.685	0.775	0.749	0.804	0.510	first-order effect
Drug	5	kR	0	0	0	0	0.034	first-order effect
Drug	10	EC50	0	0.020	0	0	0.019	first-order effect
Drug	10	EMAX	0.796	0.893	0.839	0.879	0.651	first-order effect
Drug	10	kR	0	0	0	0	0.056	first-order effect
Drug	20	EMAX	0.933	0.912	0.950	0.892	0.665	first-order effect
Drug	20	kR	0	0	0	0	0.065	first-order effect
Host	2	vmax	0.037	0.032	0.036	0.031	0	first-order effect
Host-Parasite	2	khmax	0	0.014	0	0	0	first-order effect
Parasite	2	beta	0.013	0.019	0	0.026	0	first-order effect
Parasite	2	r	0.041	0.121	0.027	0.076	0	first-order effect
Parasite	5	attr	0	0	0	0	0.072	first-order effect
Parasite	5	beta	0	0	0	0	0.037	first-order effect
Parasite	5	r	0	0.022	0	0.013	0.251	first-order effect
Parasite	10	attr	0	0	0	0	0.066	first-order effect
Parasite	10	beta	0	0	0	0	0.026	first-order effect
Parasite	10	r	0	0	0	0	0.167	first-order effect
Parasite	20	attr	0	0	0	0	0.058	first-order effect
Parasite	20	beta	0	0	0	0	0.029	first-order effect
Parasite	20	r	0	0	0	0	0.149	first-order effect
Drug	2	EC50	0.393	0.319	0.333	0.327	0	total effect
Drug	2	EMAX	0.544	0.493	0.586	0.552	0	total effect

Drug	5	EC50	0.255	0.140	0.193	0.136	0.053	total effect
Drug	5	EMAX	0.918	0.842	0.928	0.889	0.540	total effect
Drug	5	kR	0	0	0	0	0.040	total effect
Drug	10	EC50	0	0.042	0	0	0.018	total effect
Drug	10	EMAX	0.979	0.963	0.982	0.986	0.676	total effect
Drug	10	kR	0	0	0	0	0.054	total effect
Drug	20	EMAX	0.979	0.985	0.983	0.998	0.688	total effect
Drug	20	kR	0	0	0	0	0.067	total effect
Host	2	vmax	0.048	0.039	0.051	0.039	0	total effect
Host-Parasite	2	khmax	0	0.029	0	0	0	total effect
Parasite	2	beta	0.017	0.024	0	0.030	0	total effect
Parasite	2	r	0.048	0.138	0.038	0.087	0	total effect
Parasite	5	attr	0	0	0	0	0.090	total effect
Parasite	5	beta	0	0	0	0	0.044	total effect
Parasite	5	r	0	0.035	0	0.020	0.279	total effect
Parasite	10	attr	0	0	0	0	0.073	total effect
Parasite	10	beta	0	0	0	0	0.027	total effect
Parasite	10	r	0	0	0	0	0.181	total effect
Parasite	20	attr	0	0	0	0	0.067	total effect
Parasite	20	beta	0	0	0	0	0.029	total effect
Parasite	20	r	0	0	0	0	0.167	total effect

Table SF 3.3: Sobol indices for parasite clearance of P. falciparum-SCID infection after treatment with OZ439.

Para-meter type	**Dose [mg/kg]**	**Para-meter**	***model f***	***model g***	***model h***	***model i***	**Effect**
Drug	2	EC50	0.058	0.130	0.130	0.177	first-order effect
Drug	2	EMAX	0.081	0.250	0.286	0.329	first-order effect
Drug	2	kR	0.013	0.096	0.043	0.261	first-order effect
Drug	5	EC50	0.095	0.134	0.131	0.160	first-order effect
Drug	5	EMAX	0.315	0.362	0.363	0.380	first-order effect
Drug	5	kR	0.091	0.171	0.152	0.288	first-order effect
Drug	10	EC50	0.151	0.112	0.113	0.137	first-order effect
Drug	10	EMAX	0.392	0.437	0.457	0.409	first-order effect
Drug	10	kR	0.136	0.228	0.186	0.333	first-order effect
Drug	100	EC50	0.028	0.022	0.017	0	first-order effect
Drug	100	EMAX	0.587	0.534	0.575	0.517	first-order effect
Drug	100	kR	0.230	0.309	0.289	0.416	first-order effect
Host	2	bio2	0.025	0.010	0	0	first-order effect
Host	2	rmax	0.048	0.047	0.116	0	first-order effect
Host	5	Ccap	0.018	0	0	0	first-order effect
Host	5	rmax	0.068	0.057	0.126	0	first-order effect
Host	10	Ccap	0.020	0	0	0	first-order effect
Host	10	k50Ccmax	0	0.014	0	0	first-order effect
Host	10	kCcmax	0	0.014	0	0	first-order effect

Host	10	rmax	0.057	0.059	0.088	0	first-order effect
Host	100	rmax	0.029	0.018	0.028	0	first-order effect
Host-Parasite	2	kh50	0.031	0.022	0.011	0	first-order effect
Host-Parasite	2	khmax	0.017	0.062	0.035	0	first-order effect
Host-Parasite	5	kh50	0	0	0.013	0	first-order effect
Host-Parasite	5	khmax	0	0	0.010	0	first-order effect
Host-Parasite	10	kh50	0	0.014	0	0	first-order effect
Host-Parasite	10	khmax	0	0.014	0	0	first-order effect
Parasite	2	PG	0	0	0	0.177	first-order effect
Parasite	2	r	0.167	0.034	0.076	0	first-order effect
Parasite	5	beta	0	0	0.014	0	first-order effect
Parasite	5	PG	0	0	0	0.105	first-order effect
Parasite	5	r	0.084	0.081	0.097	0	first-order effect
Parasite	10	beta	0.013	0.020	0.013	0	first-order effect
Parasite	10	PG	0	0	0	0.058	first-order effect
Parasite	10	r	0.094	0.064	0.074	0	first-order effect
Parasite	100	PG	0	0	0	0.015	first-order effect
Parasite	100	r	0.040	0.032	0.027	0	first-order effect
Drug	2	EC50	0.110	0.203	0.171	0.208	total effect
Drug	2	EMAX	0.164	0.320	0.352	0.368	total effect
Drug	2	kR	0.049	0.134	0.073	0.293	total effect
Drug	5	EC50	0.144	0.171	0.153	0.197	total effect
Drug	5	EMAX	0.403	0.411	0.405	0.429	total effect
Drug	5	kR	0.146	0.203	0.172	0.332	total effect
Drug	10	EC50	0.176	0.132	0.126	0.164	total effect
Drug	10	EMAX	0.455	0.476	0.492	0.464	total effect
Drug	10	kR	0.163	0.250	0.203	0.383	total effect
Drug	100	EC50	0.044	0.031	0.026	0	total effect
Drug	100	EMAX	0.628	0.576	0.610	0.556	total effect
Drug	100	kR	0.260	0.338	0.312	0.459	total effect
Host	2	bio2	0.045	0.022	0	0	total effect
Host	2	rmax	0.323	0.125	0.253	0	total effect
Host	5	Ccap	0.056	0	0	0	total effect
Host	5	rmax	0.190	0.098	0.167	0	total effect
Host	10	Ccap	0.035	0	0	0	total effect
Host	10	k50Ccmax	0	0.015	0	0	total effect
Host	10	kCcmax	0	0.012	0	0	total effect
Host	10	rmax	0.104	0.067	0.108	0	total effect
Host	100	rmax	0.039	0.026	0.037	0	total effect
Host-Parasite	2	kh50	0.073	0.038	0.035	0	total effect
Host-Parasite	2	khmax	0.055	0.111	0.079	0	total effect

Host-Parasite	5	kh50	0	0	0.016	0	total effect
Host-Parasite	5	khmax	0	0	0.019	0	total effect
Host-Parasite	10	kh50	0	0.011	0	0	total effect
Host-Parasite	10	khmax	0	0.011	0	0	total effect
Parasite	2	PG	0	0	0	0.181	total effect
Parasite	2	r	0.532	0.237	0.234	0	total effect
Parasite	5	beta	0	0	0.028	0	total effect
Parasite	5	PG	0	0	0	0.107	total effect
Parasite	5	r	0.257	0.146	0.147	0	total effect
Parasite	10	beta	0.041	0.027	0.018	0	total effect
Parasite	10	PG	0	0	0	0.057	total effect
Parasite	10	r	0.168	0.091	0.101	0	total effect
Parasite	100	PG	0	0	0	0.018	total effect
Parasite	100	r	0.054	0.045	0.038	0	total effect

Table SF 3.4: Sobol indices for parasite clearance of *P. falciparum*-SCID infection after treatment with MMV390048.

Para-meter type	**Dose [mg/kg]**	**Para-meter**	***model f***	***model g***	***model h***	***model i***	**Effect**
Drug	2	ClY	0	0	0	0.405	first-order effect
Drug	2	EC50	0.118	0.131	0.098	0	first-order effect
Drug	2	EMAX	0.294	0.381	0.488	0.497	first-order effect
Drug	5	ClY	0	0	0	0.437	first-order effect
Drug	5	EC50	0.052	0.046	0.031	0	first-order effect
Drug	5	EMAX	0.635	0.682	0.715	0.486	first-order effect
Drug	5	kR	0	0	0.021	0	first-order effect
Drug	10	ClY	0	0	0	0.448	first-order effect
Drug	10	EC50	0.014	0.018	0	0	first-order effect
Drug	10	EMAX	0.735	0.775	0.765	0.482	first-order effect
Drug	10	kR	0	0	0.027	0	first-order effect
Drug	100	ClY	0	0	0	0.448	first-order effect
Drug	100	EMAX	0.797	0.813	0.786	0.483	first-order effect
Drug	100	kR	0	0	0.036	0	first-order effect
Host	2	Ccap	0.057	0	0	0	first-order effect
Host	2	kCcmax	0	0.016	0	0	first-order effect
Host	2	rmax	0.137	0.139	0.152	0	first-order effect
Host	5	Ccap	0.028	0	0	0	first-order effect
Host	5	kCcmax	0	0.012	0	0	first-order effect
Host	5	rmax	0.101	0.083	0.096	0	first-order effect
Host	10	Ccap	0.026	0	0	0	first-order effect
Host	10	k50Ccmax	0	0.011	0	0	first-order effect
Host	10	kCcmax	0	0.014	0	0	first-order effect
Host	10	rmax	0.085	0.076	0.076	0	first-order effect

Host	100	Ccap	0.021	0	0	0	first-order effect
Host	100	rmax	0.070	0.050	0.069	0	first-order effect
Host-Parasite	2	khmax	0.012	0	0	0	first-order effect
Parasite	2	beta	0.016	0.014	0	0	first-order effect
Parasite	2	PG	0	0	0	0.056	first-order effect
Parasite	2	r	0.172	0.144	0.122	0	first-order effect
Parasite	5	beta	0	0.013	0.011	0	first-order effect
Parasite	5	PG	0	0	0	0.062	first-order effect
Parasite	5	r	0.107	0.097	0.085	0	first-order effect
Parasite	10	beta	0	0.016	0	0	first-order effect
Parasite	10	PG	0	0	0	0.043	first-order effect
Parasite	10	r	0.091	0.075	0.066	0	first-order effect
Parasite	100	PG	0	0	0	0.030	first-order effect
Parasite	100	r	0.075	0.065	0.060	0	first-order effect
Drug	2	ClY	0	0	0	0.426	total effect
Drug	2	EC50	0.168	0.1660	0.117	0	total effect
Drug	2	EMAX	0.388	0.4408	0.530	0.518	total effect
Drug	5	ClY	0	0	0	0.449	total effect
Drug	5	EC50	0.071	0.0553	0.033	0	total effect
Drug	5	EMAX	0.675	0.7294	0.744	0.501	total effect
Drug	5	kR	0	0	0.024	0	total effect
Drug	10	ClY	0	0	0	0.466	total effect
Drug	10	EC50	0.022	0.0178	0	0	total effect
Drug	10	EMAX	0.771	0.8104	0.794	0.501	total effect
Drug	10	kR	0	0	0.032	0	total effect
Drug	100	ClY	0	0	0	0.472	total effect
Drug	100	EMAX	0.822	0.8543	0.810	0.514	total effect
Drug	100	kR	0	0	0.039	0	total effect
Host	2	Ccap	0.081	0	0	0	total effect
Host	2	kCcmax	0	0.0319	0	0	total effect
Host	2	rmax	0.233	0.1780	0.202	0	total effect
Host	5	Ccap	0.036	0	0	0	total effect
Host	5	kCcmax	0	0.0180	0	0	total effect
Host	5	rmax	0.115	0.0926	0.109	0	total effect
Host	10	Ccap	0.030	0	0	0	total effect
Host	10	k50Ccmax	0	0.0092	0	0	total effect
Host	10	kCcmax	0	0.0133	0	0	total effect
Host	10	rmax	0.091	0.0744	0.090	0	total effect
Host	100	Ccap	0.023	0	0	0	total effect
Host	100	rmax	0.073	0.0588	0.080	0	total effect
Host-Parasite	2	khmax	0.018	0	0	0	total effect
Parasite	2	beta	0.052	0.0428	0	0	total effect
Parasite	2	PG	0	0	0	0.065	total effect
Parasite	2	r	0.297	0.2091	0.177	0	total effect

Parasite	5	beta	0	0.0237	0.016	0	total effect
Parasite	5	PG	0	0	0	0.059	total effect
Parasite	5	r	0.131	0.1184	0.101	0	total effect
Parasite	10	beta	0	0.0176	0	0	total effect
Parasite	10	PG	0	0	0	0.049	total effect
Parasite	10	r	0.102	0.0853	0.082	0	total effect
Parasite	100	PG	0	0	0	0.043	total effect
Parasite	100	r	0.084	0.0799	0.072	0	total effect

Table SF 3.5: Sobol indices for parasite clearance of *P. falciparum*-human infection after treatment with OZ439.

Para-meter type	**Dose [mg]**	**Parameter**	***model i***	***model S***	**Effect**
Drug	100	EC50	0.035	0.029	first-order effect
Drug	100	Emax	0.672	0.160	first-order effect
Drug	200	add	0	0.015	first-order effect
Drug	200	EC50	0.089	0.087	first-order effect
Drug	200	Emax	0.715	0.504	first-order effect
Drug	500	EC50	0.012	0.075	first-order effect
Drug	500	Emax	0.837	0.658	first-order effect
Drug	1000	EC50	0	0.013	first-order effect
Drug	1000	Emax	0.972	0.841	first-order effect
Parasite	100	mu	0	0.037	first-order effect
Parasite	100	pmf	0	0.011	first-order effect
Parasite	100	sigma	0	0.075	first-order effect
Parasite	200	mu	0	0.060	first-order effect
Parasite	200	sigma	0	0.033	first-order effect
Parasite	500	mu	0	0.058	first-order effect
Parasite	1000	mu	0	0.032	first-order effect
Drug	100	EC50	0.31	0.605	total effect
Drug	100	Emax	0.94	0.715	total effect
Drug	200	add	0	0.039	total effect
Drug	200	EC50	0.27	0.323	total effect
Drug	200	Emax	0.89	0.661	total effect
Drug	500	EC50	0.13	0.200	total effect
Drug	500	Emax	0.97	0.808	total effect
Drug	1000	EC50	0	0.032	total effect
Drug	1000	Emax	0.99	0.914	total effect
Parasite	100	mu	0	0.272	total effect
Parasite	100	pmf	0	0.028	total effect
Parasite	100	sigma	0	0.339	total effect
Parasite	200	mu	0	0.155	total effect
Parasite	200	sigma	0	0.148	total effect
Parasite	500	mu	0	0.111	total effect
Parasite	1000	mu	0	0.072	total effect

Supplementary File 3.2 - Chapter 3: Parasite-host dynamics throughout antimalarial drug development stages complicate the translation of parasite clearance

Table SF 3.6: Sobol indices for parasite clearance of *P. falciparum*-human infection after treatment with MMV390048.

Para-meter type	**Dose [mg]**	**Parameter**	***model i***	***model S***	**Effect**
Drug	20	EC50	0.582	0.741	first-order effect
Drug	20	Emax	0.308	0.059	first-order effect
Drug	40	EC50	0.511	0.459	first-order effect
Drug	40	Emax	0.383	0.115	first-order effect
Drug	80	EC50	0	0.172	first-order effect
Drug	80	Emax	0.937	0.598	first-order effect
Drug	160	add	0	0.038	first-order effect
Drug	160	Emax	0.942	0.824	first-order effect
Parasite	20	pmf	0.041	0	first-order effect
Parasite	20	sigma	0	0.023	first-order effect
Parasite	40	pmf	0.030	0	first-order effect
Parasite	40	sigma	0	0.017	first-order effect
Parasite	80	pmf	0.062	0	first-order effect
Parasite	80	sigma	0	0.036	first-order effect
Parasite	160	pmf	0.055	0	first-order effect
Parasite	160	sigma	0	0.035	first-order effect
Drug	20	EC50	0.655	0.896	total effect
Drug	20	Emax	0.375	0.182	total effect
Drug	40	EC50	0.587	0.820	total effect
Drug	40	Emax	0.456	0.421	total effect
Drug	80	EC50	0	0.297	total effect
Drug	80	Emax	0.937	0.746	total effect
Drug	160	add	0	0.084	total effect
Drug	160	Emax	0.945	0.905	total effect
Parasite	20	pmf	0.041	0	total effect
Parasite	20	sigma	0	0.049	total effect
Parasite	40	pmf	0.035	0	total effect
Parasite	40	sigma	0	0.058	total effect
Parasite	80	pmf	0.061	0	total effect
Parasite	80	sigma	0	0.059	total effect
Parasite	160	pmf	0.057	0	total effect
Parasite	160	sigma	0	0.055	total effect

Appendix C

Supplementary Information Chapter 5- Parasite-host dynamics throughout antimalarial drug

Supplementary material for

Model informed target product profiles of long-acting-injectables for use as seasonal malaria prevention

Authors:

Lydia Burgert[1, 2], Theresa Reiker[1, 2], Monica Golumbeanu[1,2], Jörg J. Möhrle[1, 2, 3], Melissa A. Penny*[1, 2]

[1] Swiss Tropical and Public Health Institute, Basel, Switzerland

[2] University of Basel, Basel, Switzerland

[3] Medicines for Malaria Venture, Geneva, Switzerland

*Corresponding author: melissa.penny@unibas.ch

Table of Contents

1. General OpenMalaria specification and intervention set-up

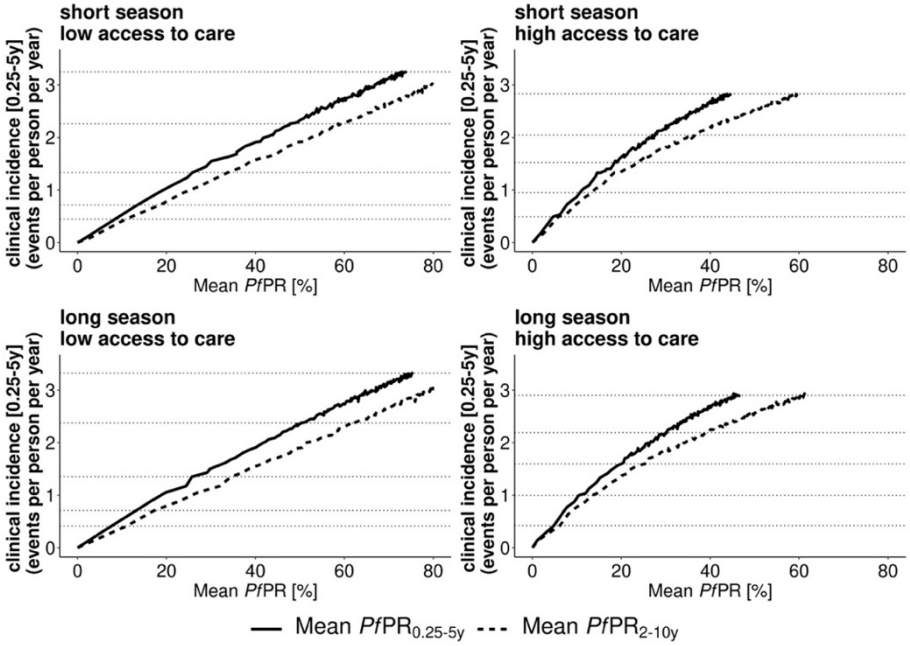

Fig A: Prevalence - incidence relationship in the simulated Open Malaria settings. The relationship between prevalence and incidence is displayed in the two simulated seasonal settings (Senegal/short season and Mali/long season) and health system access settings (low and high access) (Table 1) in absence of any interventions. The clinical incidence defined as the events per person per year in the target age-group (0.25-5 years of age) is shown for the corresponding mean prevalence over one year in the intervention age group (*Pf*PR$_{0.25\text{-}5y}$) and in children between 2-10 years (*Pf*PR$_{2\text{-}10y}$). The dotted horizontal lines mark the incidence settings, simulated for all downstream analyses and can be found in Table A.

Table A: Simulated prevalence – incidence settings. The force of transmission was defined by the entomological inoculation rate (EIR: mean number of infectious bites per person per year (pppy)). Across different transmission settings defined by access to healthcare (HC), EIR levels, and transmission seasonality, corresponding simulated annual mean malaria prevalence (*Pf*PR) and clinical incidence per person per year in the intervention age group are displayed for different age groups: 2 to 10 year olds (*Pf*PR$_{2\text{-}10y}$) and 0.25 to 5 years old (*Pf*PR$_{0.25\text{-}5y}$ and cases per person per year$_{0.25\text{-}5y}$). The adjustment of EIR between HC access settings ensures similar levels of case incidence simulated across transmission season settings.

		Short transmission season			**Long transmission season**		
HC Access	**EIR** [infectious bites pppy]	***Pf*PR $_{2\text{-}10y}$** [%]	***Pf*PR $_{0.25\text{-}5y}$** [%]	**Cases per person per year$_{0.25\text{-}5y}$**	***Pf*PR $_{2\text{-}10y}$** [%]	***Pf*PR $_{0.25\text{-}5y}$** [%]	**Cases per person per year$_{0.25\text{-}5y}$**
high	5	6	5	0.49	6	5	0.42
	9	13	11	0.95	13	10	1
	20	23	19	1.52	25	20	1.6
	47	37	28	2.04	39	30	2.2
	150	60	45	2.83	62	46	2.9
low	3	11	8	0.45	11	8	0.41
	4	19	13	0.72	17	13	0.71
	8	34	26	1.3	35	26	1.4
	28	59	48	2.3	62	50	2.4
	150	86	73	3.2	87	75	3.3

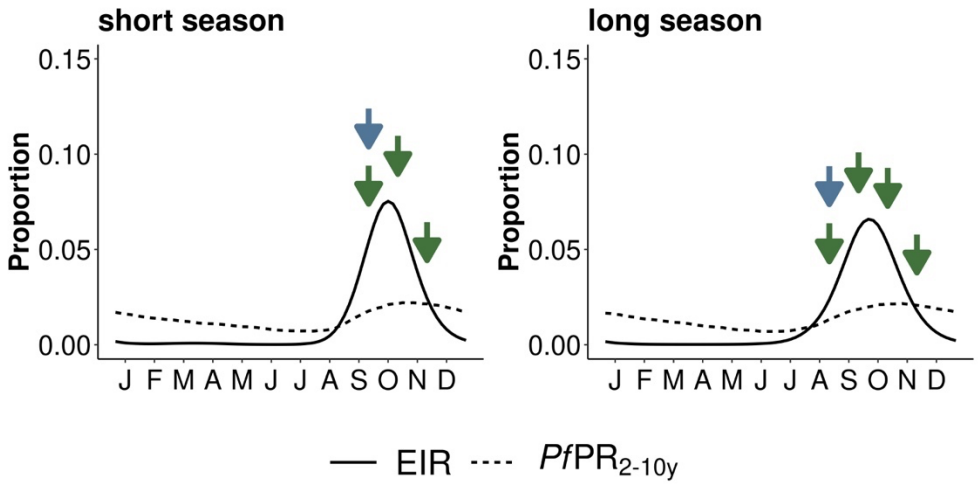

Fig B: Modelled malaria transmission pattern and simulated prevalence defining seasonality settings. The seasonality in malaria transmission is defined through the proportional EIR (solid line) in relation to the yearly EIR (input into the simulator). Here shown for a yearly EIR of 100 infectious bites per person per year. The dotted line represents the resulting scaled yearly prevalence profile. The arrows illustrate the administration of the preventative interventions of SMC-SP+AQ (green) and LAI (blue) in the two seasonal settings. Following WHO recommendations[1], SMC-SP+AQ was implemented monthly with the first dose administered before the peak and the second dose with the peak in malaria transmission.

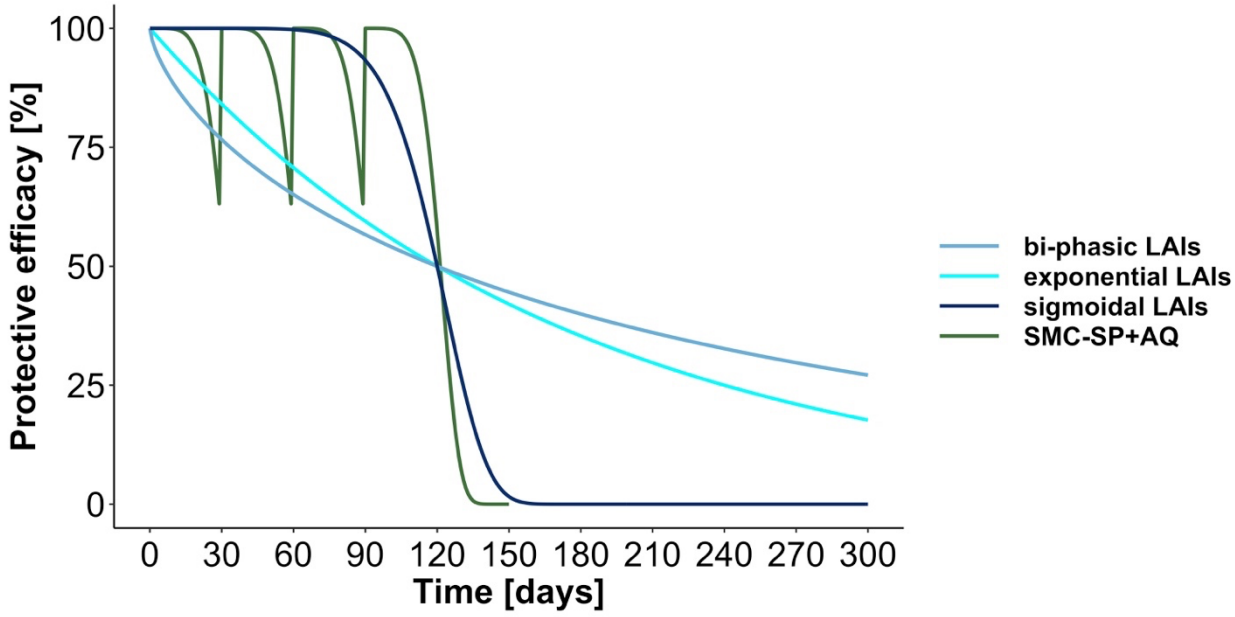

Fig C: Simulated protective efficacy decay shapes of long acting injectables (LAI) and seasonal malaria chemoprevention (SMC) over one transmission season. The LAI decay shapes were chosen such that they represent the three possible development streams of mAb (sigmoid decay), drug based (exponential decay), or vaccine like (biphasic) LAIs (blue solid line). Here, we illustrated a LAI protective efficacy half-life of 120 days and initial protective efficacy of 100 %. SMC – SP+AQ was parameterised as specified below and administered up to four times over the transmission season (green solid line). The parameterisation of the interventions is further specified in tablet.

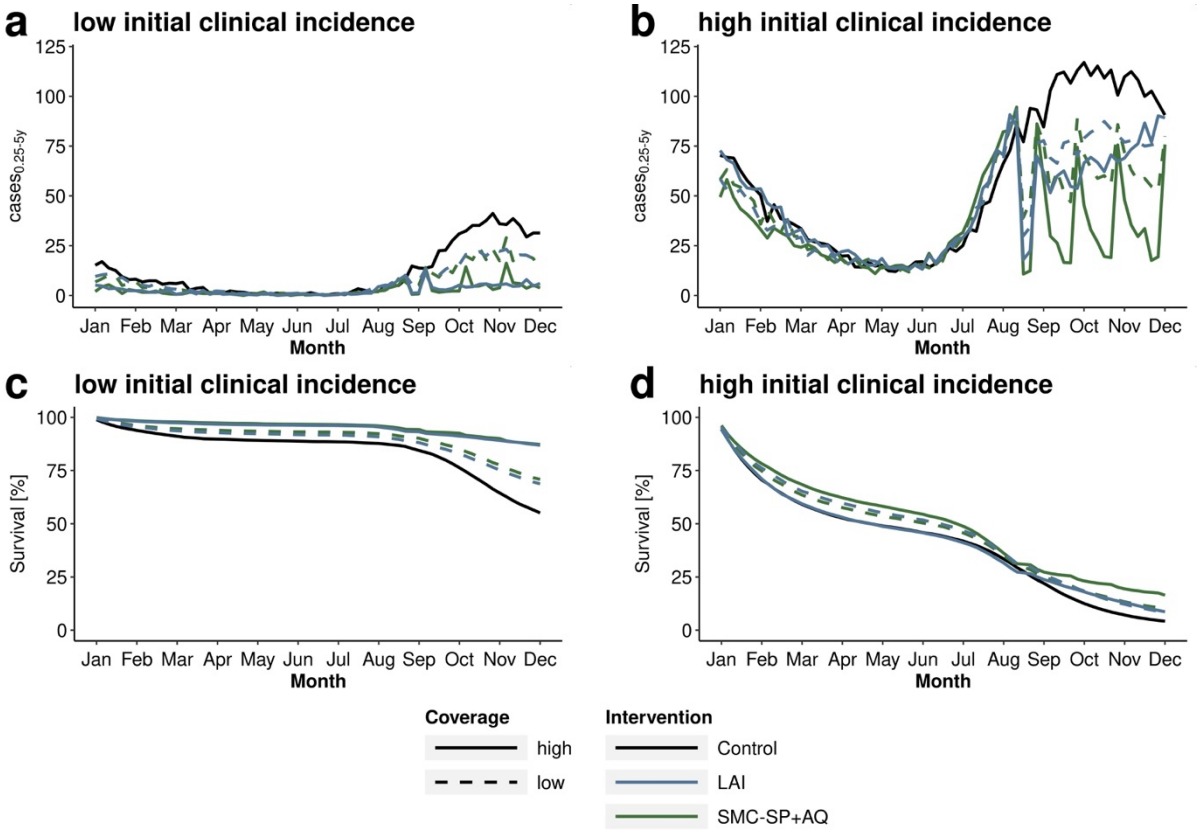

Fig D: Exemplary illustration of incidence and survival estimates of *sigmoidal LAIs* and SMC-SP+AQ in *implementation stages* over one implementation year. Plots are shown in **(a, c)** low initial clinical incidence settings (initial cases per person per year$_{0.25\text{-}5y}$ = 0.71) and **(b, d)** high initial clinical incidence settings (initial cases per person per year$_{0.25\text{-}5y}$ = 3.3) in long malaria transmission settings with low access to healthcare (E_{14}=0.1). The *sigmoidal LAIs* exhibit an initial protective efficacy over 95 % and protective efficacy half-life of 112 days. SMC-SP+AQ and LAIs were implemented at high deployment coverage (>90%, solid lines) and low deployment coverage (<50%, dashed lines). In low initial incidence settings **(a, c)** SMC-SP+AQ (green) is administered four times per season (Aug-Nov) with clinical incidence notably decreasing after each administration **(a, b)** compared to control settings with no implemented interventions (black). In contrast, the *sigmoidal LAIs* are only administered once at the beginning of the transmission season. With progressing season, the protective efficacy decays, resulting in an increase of clinical cases **(a, b)** and decrease in survival estimates **(c, d)** after LAI administration. In low clinical incidence settings, *sigmoidal LAIs* and SMC-SP+AQ are comparably effective at both coverage levels **(c)**. In contrast, the survival estimates in in high initial clinical incidence settings **(d)** reveal that *sigmoidal LAIs* at both coverage levels and SMC-SP+AQ at low coverage levels are all equally unable to prevent malaria cases. Shown here are the mean predictions over 5 stochastic *OpenMalaria* simulations.

2. Non-inferiority analysis

Survival analysis was performed using a Kaplan-Meier approach as specified in [2], with the K-M estimate $\hat{S}(t)$ derived via number of new clinical cases c_i at each time step t_i

$$\widehat{\boldsymbol{S}}(\boldsymbol{t}) = \prod_{\boldsymbol{i}:\boldsymbol{t_i}\leq\boldsymbol{t}} \mathbf{1} - \frac{\boldsymbol{c_i}}{\boldsymbol{N_{int}}}, \quad \textbf{Equ. S1}$$

with the standard error $\widehat{SE}$ calculated using the Greenwood formula

$$\widehat{\boldsymbol{SE}}(\boldsymbol{t}) = \left[\widehat{\boldsymbol{S}}(\boldsymbol{t})\right] \sqrt{\prod_{\boldsymbol{i}:\boldsymbol{t_i}\leq\boldsymbol{t}} \frac{\boldsymbol{c_i}}{\boldsymbol{N_{int}}(\boldsymbol{N_{int}}-\boldsymbol{c_i})}}. \quad \textbf{Eq. S2}$$

Non-inferiority analysis was conducted based on the survival statistics as described in [2]. The survival estimate (hazard ratio) for the standard of care SMC $\hat{S}_{SMC}$ (t) considering the desired margin of non-inferiority Δ defines the upper limit for non-inferiority γ :

$$\boldsymbol{\gamma} = \frac{\ln\left(\hat{\boldsymbol{S}}_{\boldsymbol{SMC}}-\Delta\right)}{\ln\left(\hat{\boldsymbol{S}}_{\boldsymbol{SMC}}\right)} \quad \textbf{Eq. S3}$$

The difference δ between the survival estimates of the standard of care SMC $\hat{S}_{SMC}$ (t) and new treatment (LAI) $\hat{S}_{LAI}$, is calculated on the log-log- scale and is equivalent to the logarithm of the ratio of cumulative hazards in the two groups

$$\delta = \ln\left(-\ln\left(\hat{S}_{SMC}\right)\right) - \ln\left(-\ln\left(\hat{S}_{LAI}\right)\right) = \ln\frac{\hat{H}_{SMC}(t)}{\hat{H}_{LAI}(t)} \quad \textbf{Eq. S4}$$

and its variance is calculated as follows:

$$Var(\delta) = \left\{\frac{1}{\ln(\hat{S}_{SMC})}\right\}^2 \frac{1}{{\hat{S}_{SMC}}^2}\, Var\left(\hat{S}_{SMC}\right) + \left\{\frac{1}{\ln(\hat{S}_{LAI})}\right\}^2 \frac{1}{{\hat{S}_{LAI}}^2}\, Var\left(\hat{S}_{LAI}\right) \quad \textbf{Eq. S5}$$

The confidence interval of the hazard ratio δ is given by $exp^{\delta\,[95\%\,CI:\,\delta\pm 1.96\times se(\delta)]}$. Non-inferiority is established if the upper limit of the derived 95% confidence interval, CI_{high}, of the hazard ratios δ between SMC and LAI lies below the upper limit for non-inferiority γ.

3. Emulator performance

Table B: Emulator performance for the investigated outcomes. The emulator performance was assessed by calculating the Pearson correlation coefficient (PCC) and the mean absolute error (MAE) between true and predicted values on a 20% holdout set for each investigated setting.

Outcome	PCC (median [min, max])	MAE (median [min, max])
upper limit for non-inferiority γ	0.9924 [0.8072, 0.9972]	0.0015 [0.0002, 0.0280]
upper limit of the hazard ratio	0.9945 [0.9472, 0.9978]	0.0229 [0.0094, 0.0791]
Clinical incidence SMC-SP+AQ, (cases per person per year$_{0.25\text{-}5y,\ SMC}$)	0.9964 [0.9787, 0.9986]	0.0142 [0.0060, 0.0428]
Clinical incidence LAIs, (cases per person per year$_{0.25\text{-}5y,\ LAI}$)	0.9947 [0.9562, 0.9985]	0.0136 [0.0055, 0.0488]

4. Additional analysis results in the clinical trial setting

Table C: Incidence reduction achieved through implementation of SMC-SP+AQ in a clinical trial setting. The mean incidence reduction was calculated in the clinical trial setting over three months in the short season setting and four months in the long season setting. Resistance to SMC-SP+AQ is implemented as a reduction in protective efficacy half-life from 32 to 20 days (half-life of 32 days parameterised from previous clinical trial data[3]).

		Short malaria transmission season	Long malaria transmission season
	EIR [infectious bites pppy]	**inc$_{red}$** [%]	**inc$_{red}$** [%]
No resistance to SMC-SP+AQ	5	90	87
	9	90	87
	20	90	88
	47	89	87
	150	88	86
Resistance to SMC-SP+AQ	3	79	76
	4	76	75
	8	76	72
	28	73	72
	150	73	71

5. Additional analysis results in the implementation setting

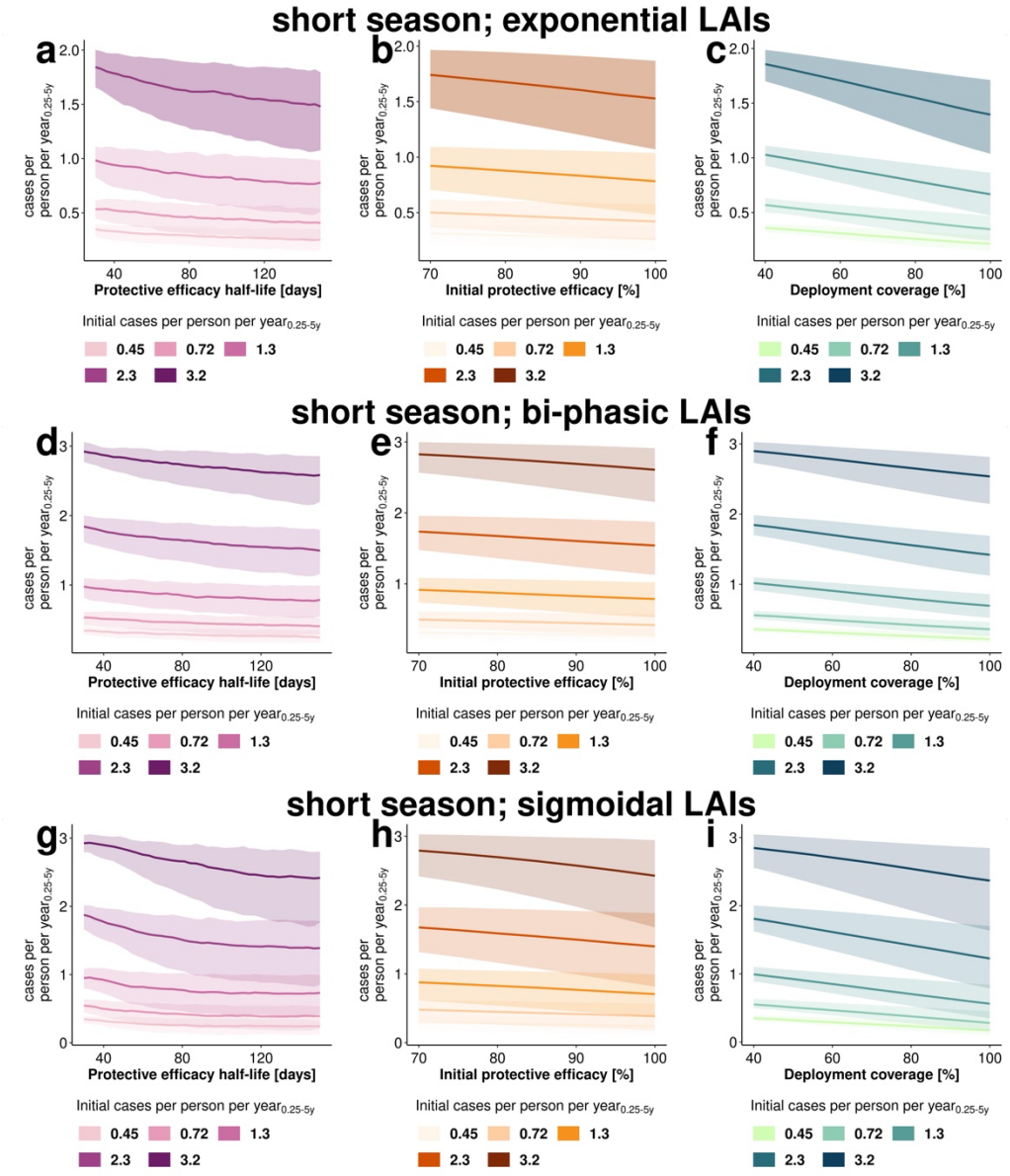

Fig E: Estimated impact of LAI properties and operational factors on the level of clinical incidence reduction. Results are shown for the implementation stage in a setting with low access to care (E_{14}=0.1) and short (Senegal-like) malaria transmission season, for **(a-c)** *exponential LAIs*, **(d-f)** *biphasic LAIs*, and **(g-i)** *sigmoidal LAIs*. Changes in clinical incidence measured as cases per person per $year_{0.25\text{-}5y}$ with increasing tool properties or deployment coverage across the parameter space are shown for for **(a, d, g)** half-life (30-150 d) , **(b, e, h)** initial efficacy (80-100%) and **(c, f, i)** coverage (40 -100 %). The lines represent the mean and the 95%- confidence bands (shaded area) capture the distribution of incidence reduction across all sampled values. Increasing color intensity represents increasing initial cases per person per $year_{0.25\text{-}5y}$). These results hold true for high access to healthcare settings. The conversion of initial cases per person per $year_{0.25\text{-}5y}$ to prevalence can be found in Table A.

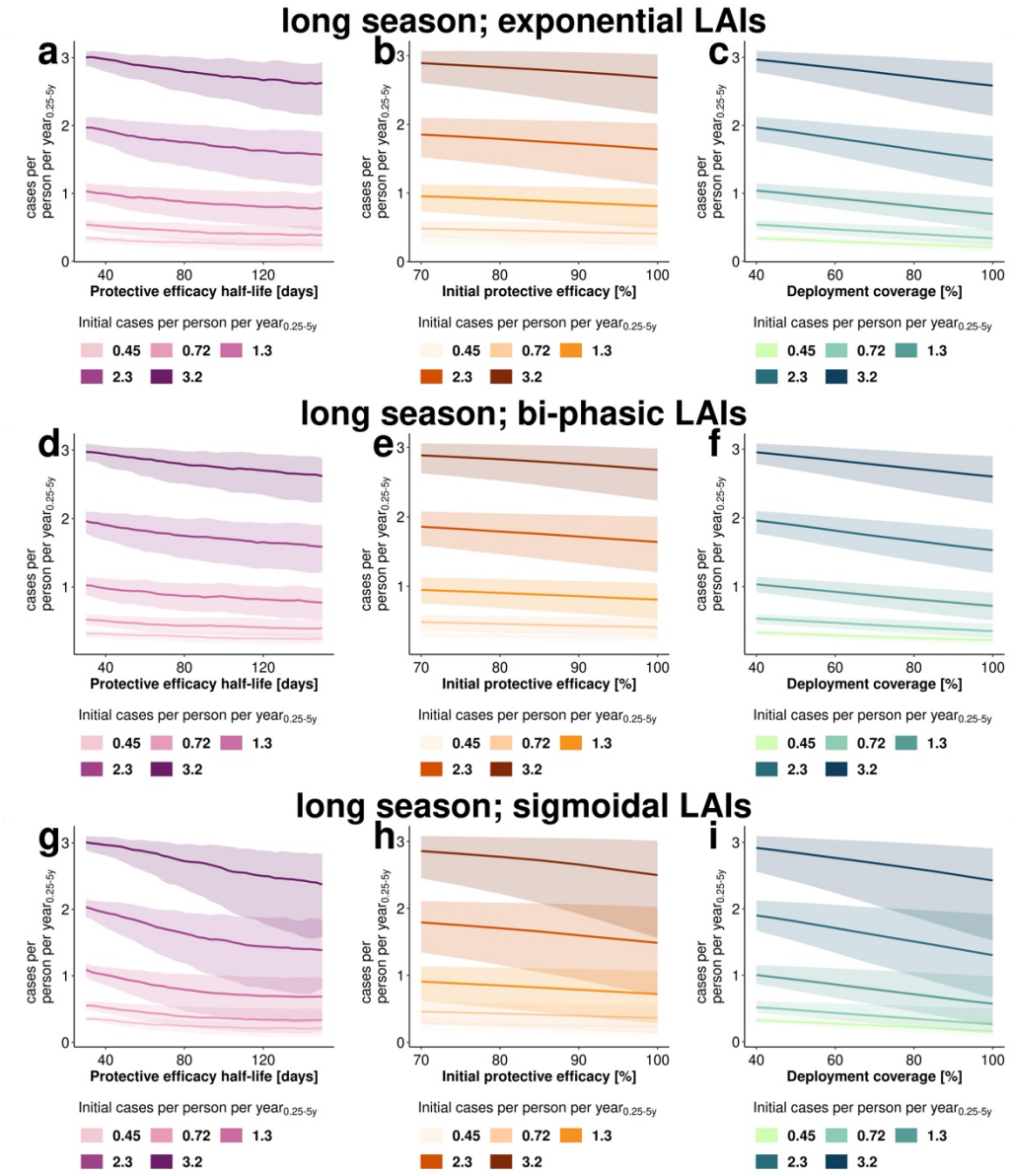

Fig F: Estimated impact of LAI properties and operational factors on the level of clinical incidence reduction. Results are shown for the implementation stage in a setting with low access to care (E_{14}=0.1) and long (Mali-like) malaria transmission season, for **(a-c)** *exponential LAIs*, **(d-f)** *biphasic LAIs*, and **(g-i)** *sigmoidal LAIs*. Changes in clinical incidence measured as cases per person per year$_{0.25\text{-}5y}$ with increasing tool properties or deployment coverage across the parameter space are shown for **(a, d, g)** half-life (30-150 d) , **(b, e, h)** initial efficacy (80-100%) and **(c, f, i)** coverage (40 -100 %). The lines represent the mean and the 95%- confidence bands (shaded area) capture the distribution of incidence reduction across all sampled values. Increasing color intensity represents increasing initial clinical incidence (cases per person per year$_{0.25\text{-}5y}$). These results hold true for high access to healthcare settings. The conversion of initial cases per person per year$_{0.25\text{-}5y}$ to prevalence can be found in Table A.

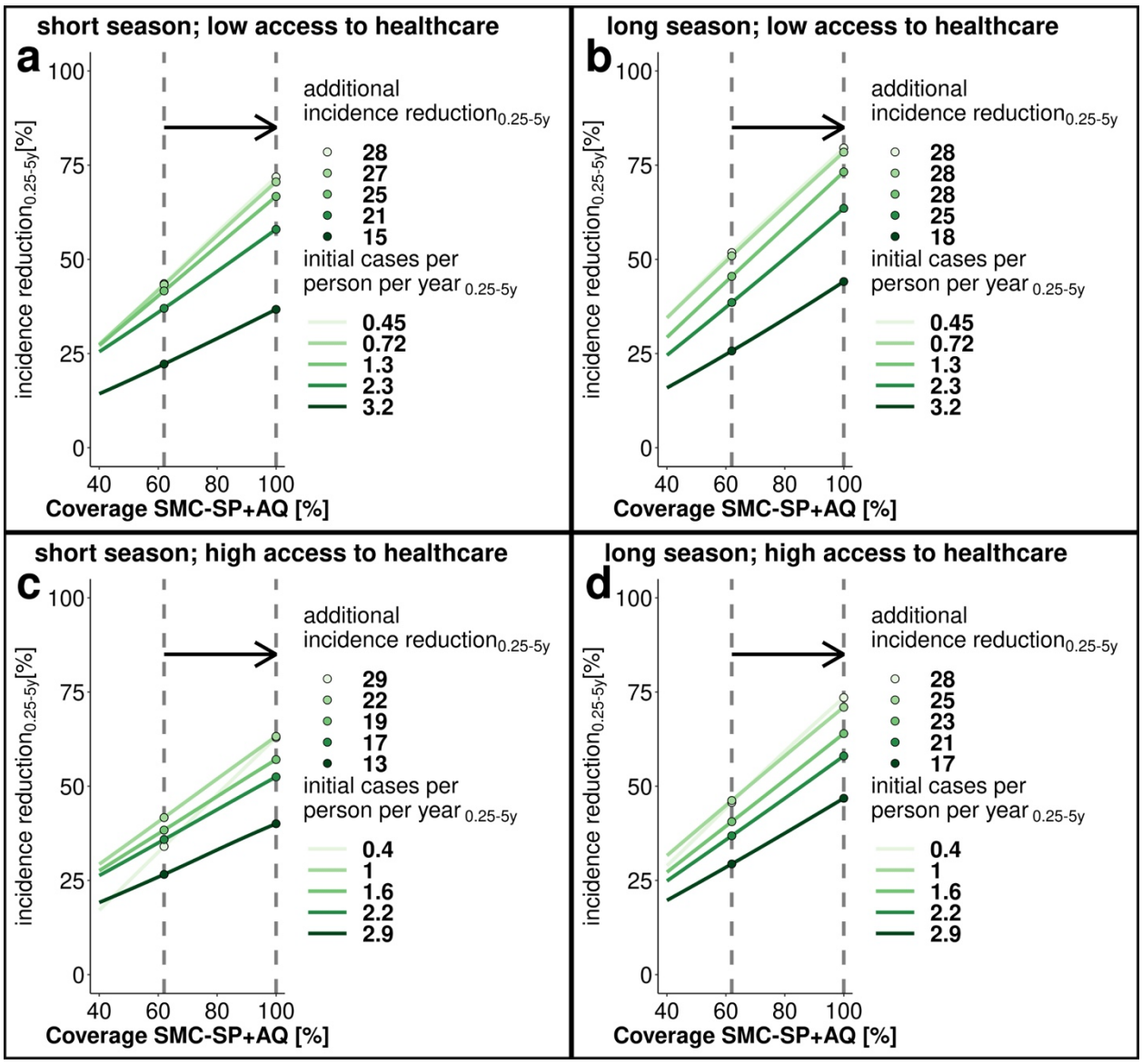

Fig G: Incidence reduction achieved through implementation of SMC-SP+AQ over varying deployment coverage. The results are shown for low **(a, b)** and high **(c, d)** access to healthcare and short **(a, c)** and long **(b, d)** malaria seasons. The colors indicate different initial clinical incidence before introduction of SMC-SP+AQ (initial cases per person per year$_{0.25\text{-}5y}$). The incidence reduction$_{0.25\text{-}5y}$ was calculated in the implementation scenario after one year of implementation. The grey lines indicate the additional incidence reduction $_{0.25\text{-}5y}$) achieved by increasing SMC-SP+AQ coverage from 62% to 100 %.

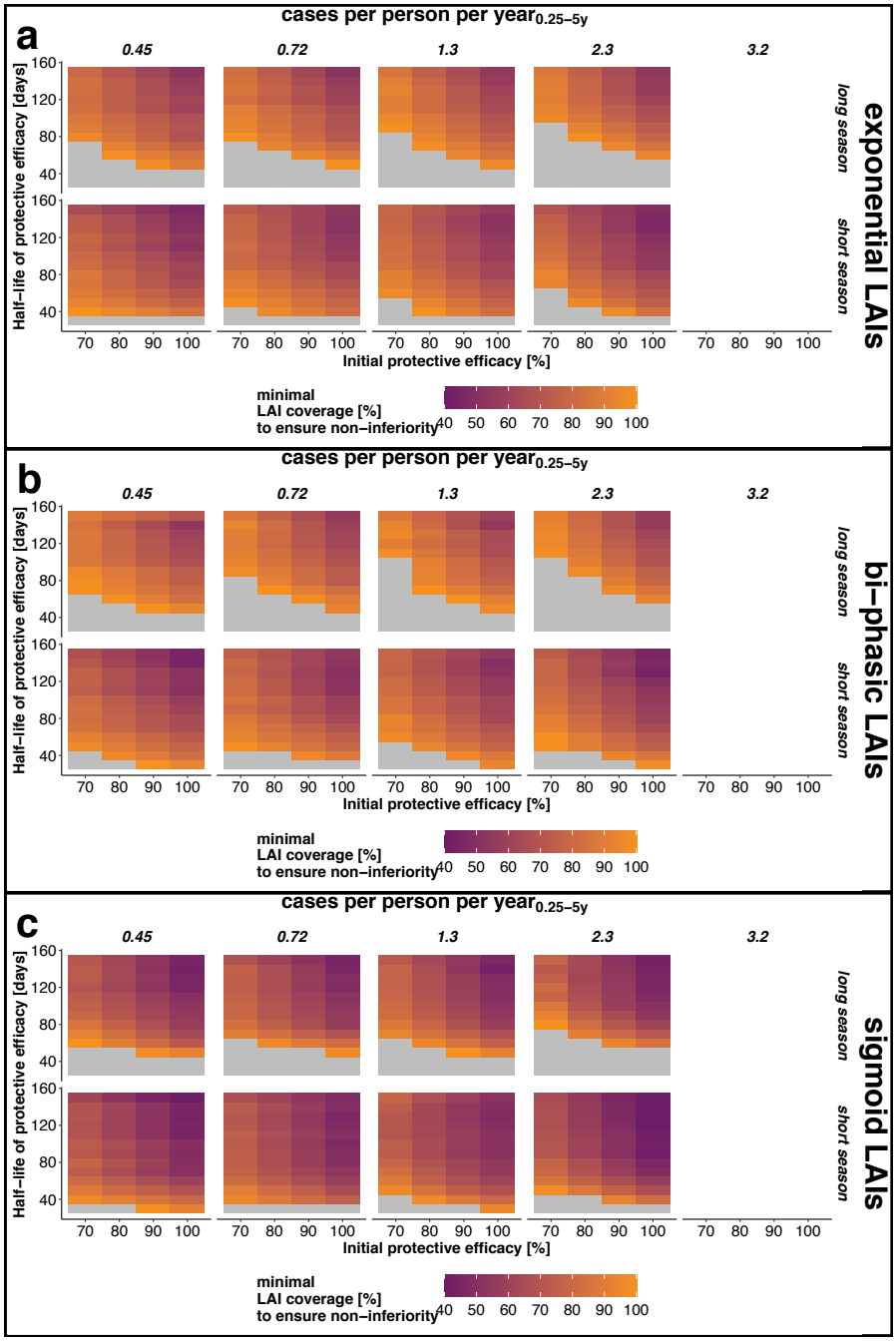

Fig H: Estimated minimal LAI coverage required during *implementation stages* to achieve non-inferiority in a given setting. Heatmap of the estimated minimal coverage (colour) of LAIs at which non-inferiority to SMC-SP+AQ (assuming a fixed SMC coverage of 60% in each of the 3 or 4 rounds) is achieved for different combinations of protective efficacy decay, initial protective efficacy and protective efficacy half-life. The results are displayed for intervention scenarios with a low access to care (E_{14}=0.1) in the two seasonal settings. In the grey area, non-inferiority could not be established for any combination of tool properties. The LAI coverage could not be optimized for high transmission settings (initial cases per person per year$_{0.25\text{-}5y}$=3.2) because they fail to sufficiently protect the targeted population from clinical malaria even at full deployment coverage. Therefore, optimisation of the LAI deployment coverage could not be conducted (Fig D).

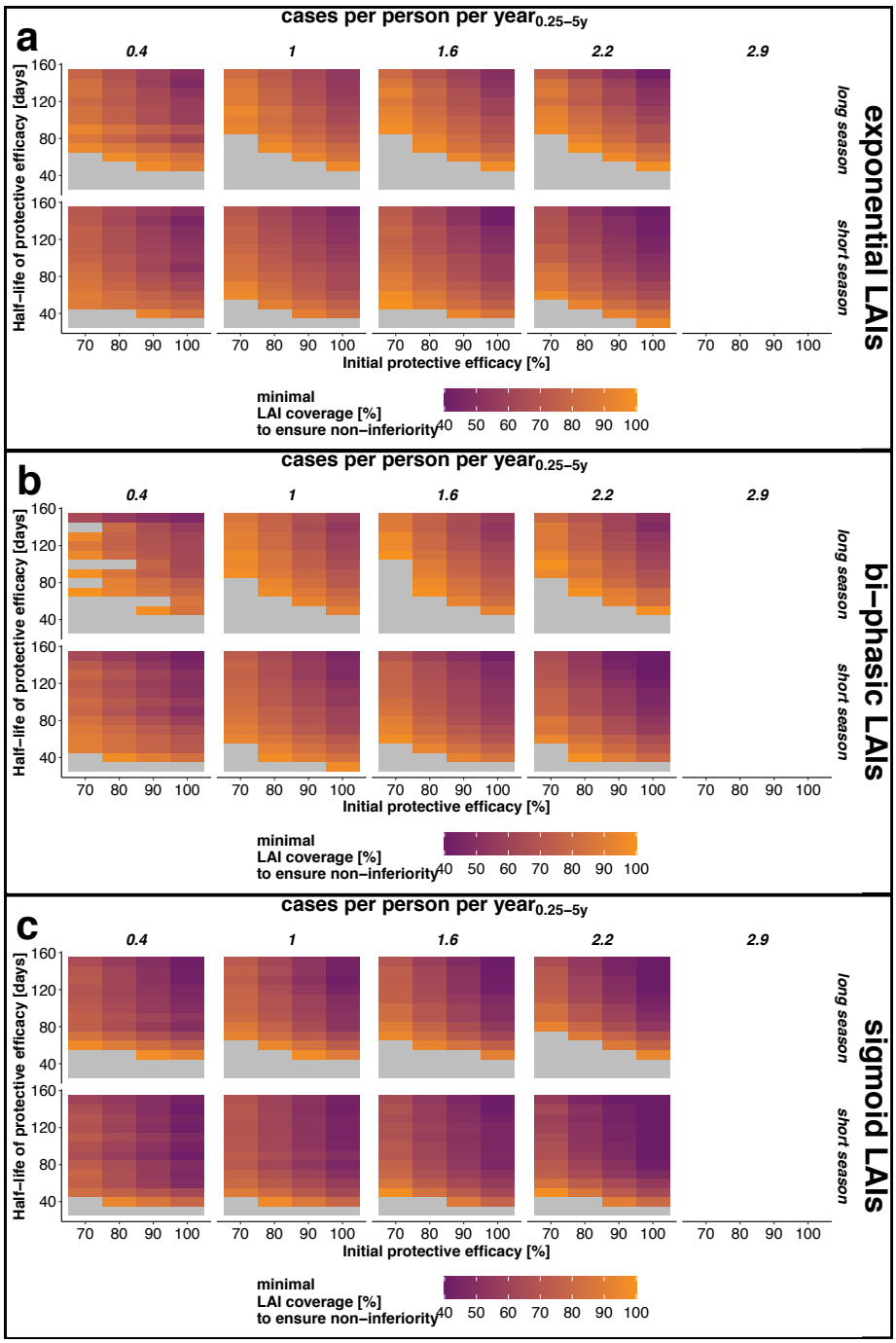

Fig I: Estimated minimal LAI coverage required during *implementation stages* to achieve non-inferiority in a given setting. Heatmap of the estimated minimal coverage (colour) of LAIs at which non-inferiority to SMC-SP+AQ (assuming a fixed SMC coverage of 60% in each of the 3 or 4 rounds) is achieved for different combinations of protective efficacy decay, initial protective efficacy and protective efficacy half-life. The results are displayed for intervention scenarios with a high access to care (E_{14}=0.5) in the two seasonal settings. In the grey area, non-inferiority could not be established for any combination of tool properties. The LAI coverage could not be optimized for high transmission settings (initial cases per person per year$_{0.25\text{-}5y}$=2.9) because they fail to sufficiently protect the targeted population from clinical malaria even at full deployment coverage. Therefore, optimisation of the LAI deployment coverage could not be conducted (Fig D).

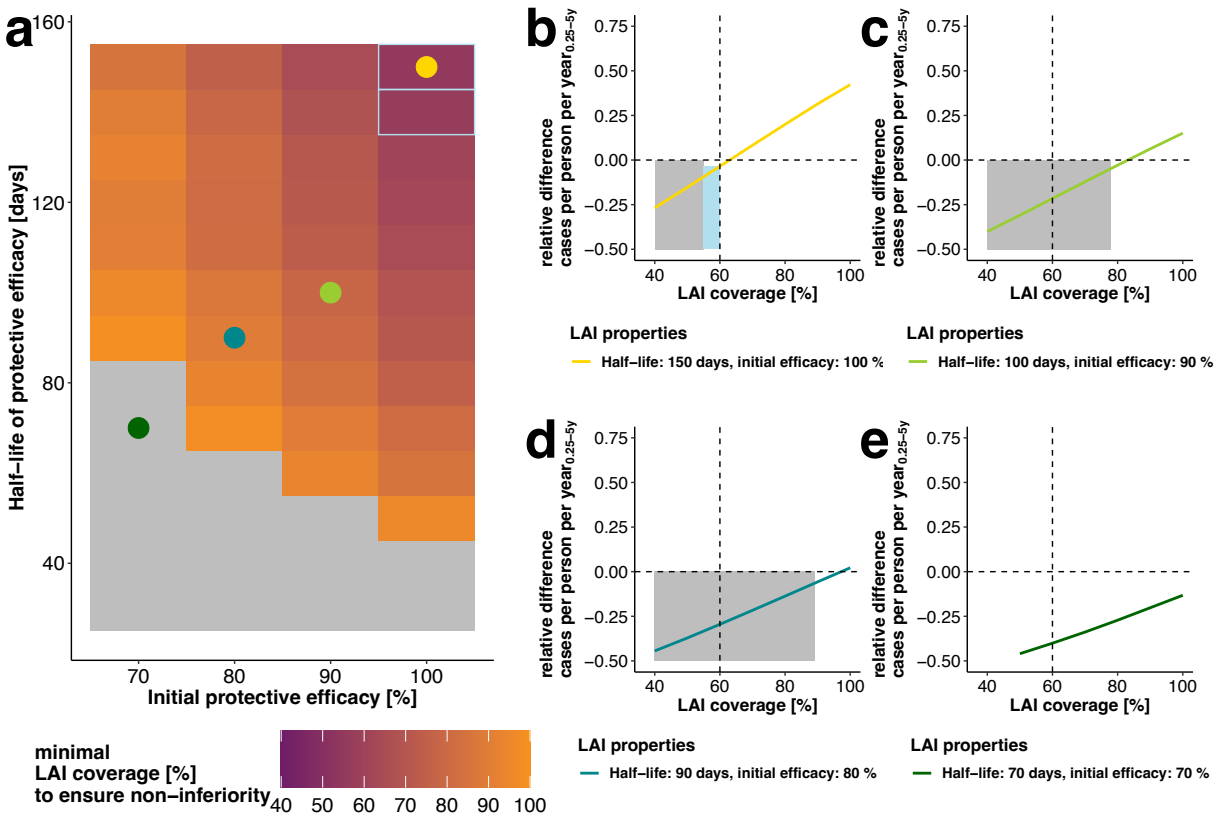

Fig J: Estimated minimal LAI coverage required during *implementation stages* to achieve non-inferiority in a given setting and predicted gains in cases averted of subsequent *exponential* LAI coverage increments. ((a) Heatmap of the estimated minimal coverage (colour) of *sigmoidal LAIs* at which non-inferiority to SMC-SP+AQ (assuming a fixed SMC coverage of 60%) is achieved for different combinations of *exponential LAI* efficacy and half-life. The results are displayed for intervention scenarios with an underlying disease burden of 1.4 cases per person per year$_{0.25\text{-}5y}$, long malaria transmission season and low access to treatment (E_{14}=0.1). In the grey area, non-inferiority could not be established for any coverage. For the tool characteristics within the light-blue frames, non-inferiority could be reached with a LAI coverage under the reference SMC-SP+AQ coverage of 60%. The coloured dots represent four illustrative LAI profiles of **(b)**150 days half-life and 100% initial efficacy (yellow), **(c)** 100 days half-life and 90% initial efficacy (light green), **(d)** 90 days half-life and 80% initial efficacy (blue), and **(e)** 70 days half-life and 70% initial efficacy (dark green, e). **(b-e)**. Corresponding predicted relative differences in cases per person per year$_{0.25\text{-}5y}$ (Eq. 5) are calculated for the illustrative LAIs (coloured dots) in (a) in the last implementation year (5 years after LAI introduction) over all LAI coverages as compared to SMC-SP+AQ at 60% coverage (vertical dotted line). The predicted positive increase in relative difference in yearly clinical cases (above the dotted horizontal line) means more clinical cases are averted with LAIs than with SMC-SP+AQ. It thus illustrates the benefit of increasing *exponential LAI*-coverage above the minimal required coverage to achieve non-inferiority (shown by the grey coloured area). In the light-blue area in (b), a LAI coverage lower than the SMC-SP+AQ coverage is sufficient to establish non-inferiority.

6. Parameterization of SMC-SP+AQ to clinical trial data

Seasonal malaria chemoprotection (SMC) was implemented as sulfadoxine–pyrimethamine+amodiquine (SP-AQ) treatment and calibrated to a randomized non-inferiority trial of dihydroartemisinin-piperaquine with SP-AQ, conducted between August 2009 and January 2010 in rural western Burkina Faso Zongo et al.(2015)[3]. Decay of protective efficacy of SPAQ in the field over time was extracted from Fig3 in Zongo et al.(2015)[3] and used to parameterized the decay functions as specified in *OpenMalaria* using a least squares approach combined with a Gaussian-Process optimization. The trial described in Zongo et al.(2015)[1] was rebuilt in OM settings listed in Table D.

Table D: Inputs into OpenMalaria (OM) to check adequate parameterization of SMC-SP-AQ

	Parameter	Value	Ref.
Vector specification	Mosquito species [% of total abundance]	*An. funestus*: 42% indoor, 31% outdoor *An. gambiae*: 14% indoor, 13% outdoor	[4]
	Total EIR	154	[4]
	Seasonality in malaria transmission [monthly EIR]	*An. funestus*: Aug 23, Sep 16, Oct 0, Nov 3.1 *An. gambiae*: Aug 40, Sep 50, Oct 16, Nov 6.4	[4]
Health system	Access to treatment	2003 / 2006 Effective coverage E_{14} [%]: 50 / 50 OM 5-day probability E_5 [%]: 24.12 / 24.12	[5, 6]
	Malaria treatment	First line: Arthemeter-Lumefantrine Treatment failure/Severe malaria: Quinine	[5]
Vector Interventions	Coverage of ITNs	2006-2008: 14%	[5]
	ITN coverage during trial	27%	[3]
Seasonal malaria chemoprevention	Timing of interventions	SMC: 15 Aug, 15.Sep, & 15 Oct 2009 Follow-up: 1 Sep, 1 Oct & 1 Nov 2009	[3]
	Protective efficacy of SP+AQ	$E(t) = E_0\, e^{-\left(\frac{t}{L}\right)^k \log(2)}$ Parameter ranges for LHS sampling: Half-life L: [20, 60] days Shape parameter k: [1, 10] Initial efficacy E_0: [0.7, 1]	[3]

We used Latin-Hypercube sampling (LHS) to generate 5000 samples of the decay function parameters for protective efficacy (L, k, E_0) within the parameter bounds given in Table D. The trial was simulated with these parameters and five seeds per parameter-set for the intervention and control cohort. The protective efficacy E of SMC - SP+AQ in the simulated trial compared to the simulated controls (without intervention) was extracted by comparing cases per person (cpp) between the intervention group (cpp_{int}) and control group (cpp_{cont}) over the trial period as follows:

$$\boldsymbol{E = 1 - \frac{cpp_{int}}{cpp_{cont}}} \qquad \textbf{Equ. S6}$$

The residual sum of squares (RSS) between the protective efficacy given in Zongo et al.(2015)[3] and protective efficacy from OM simulations was extracted and a Gaussian process (GP) regression was trained to predict the RSS between trial results and OM simulation with the parameters of the protective efficacy decay.

The true over predicted RSS of the hold-out of 1000 data points is shown in Fig K.

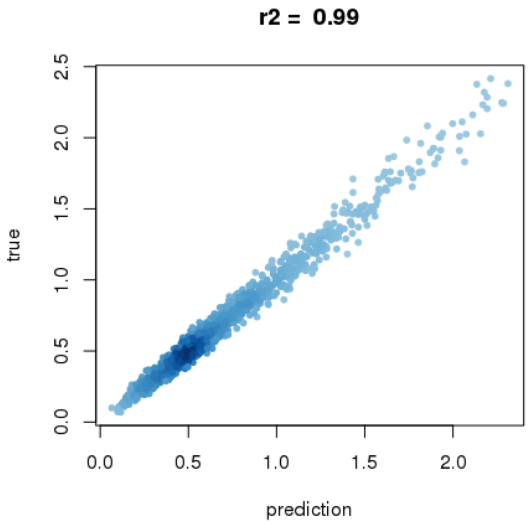

Fig K: True over predicted RSS of the GP.

The GP was then optimized via non-linear optimization using the augmented Lagrange method (function gosolnp, R-package Rsolnp). We optimized the mean predicted error +/- one or two standard deviation of the residual sum of squares (RSS) between the protective efficacy in Zongo et al.(2015)[3] and the OM simulation output. The parameters of the decay function returned by the optimization process were re-simulated with OM and the RSS extracted (*RSS OM*). The OM simulation resulting in the least RSS was then selected for further analysis.

Table E: Results of the GP optimization. The results of the optimization *RSS optim* is compared with the *predicted (pred.) RSS* by the GP and the RSS extracted from OM simulations (median of 5 seeds) conducted with the respective parameters (*RSS OM*). The solver was restarted 20 times and the number of random parameters generated for every restart was set to n.sim=500.

	kdecay	Half-life	Initial efficacy	RSS optim	RSS pred	RSS OM
Min. RSS before optimisation	6.35	32.5	0.97	-	0.0842	0.0601
mean	5.40	31.3	1.0	0.0538	0.0538	**0.0556**
Mean +sd	5.29	31.5	1.0	0.0882	0.0542	0.0583
Mean - sd	5.58	31.0	1.0	0.0186	0.0545	0.0538
Mean + 2*sd	5.28	31.5	1.0	0.0895	0.0541	0.0556
Mean – 2*sd	5.62	31.1	1.0	0.0172	0.0544	0.0739

The OM implementation of the best parameter set for the intervention cohort is able to well capture the protective efficacy described in [3]. The protective efficacy (Fig L), cumulative hazard (Fig M) and prevalence over time (Fig N) provide more insight into the trial results and comparison with OM outputs.

Table F: Comparison of trial results of Zongo et al., 2015 [3] and model outputs using the model specification in Table D with the best parameter set. The compared time-points correspond to the time-points compared in [3]. The difference in prevalence of parasitemia in December 2009 in the untreated cohort are caused by ongoing but decreasing transmission in December (see Fig C) and unclear definition of data time-point in [3].

	Zongo et al., 2015	**OM [min, max]**
Prevalence of parasitemia [%] in August 2009, intervention cohort	45	45 [44, 48]
Prevalence of parasitemia [%] in September 2009, untreated cohort	61	60 [57, 65]
Cumulative hazard for fever with any parasitemia intervention cohort	0.22	0.14 [0.13, 0.15]
Cumulative hazard for fever with any parasitemia intervention cohort	0.92	1.01 [0.93, 1.12]
Prevalence of parasitemia [%] in November 2009, intervention cohort	12	19 [18, 20]
Prevalence of parasitemia [%] in December 2009, untreated cohort	36	46 [39, 48]

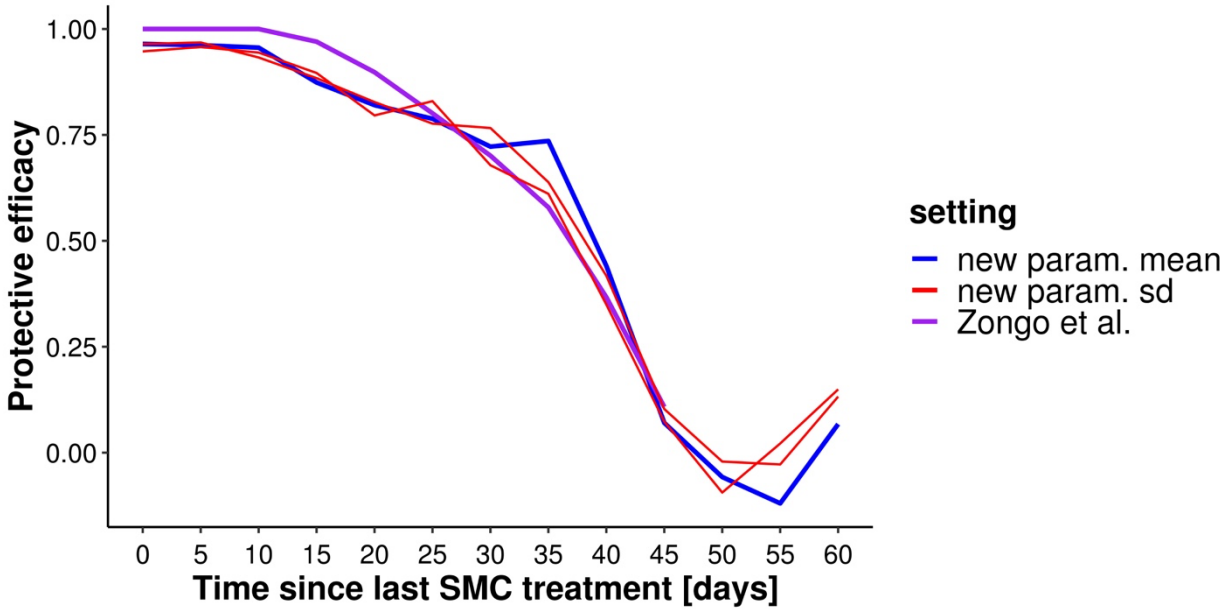

Fig L: Decay of protective efficacy of SMC-SP+AQ over time. Population protective efficacy over time in the trial setting. The purple line represents the protective efficacy as extracted from Zongo et al.(2015) [3]. The new parameterization after optimization and uncertainty are shown in blue and red.

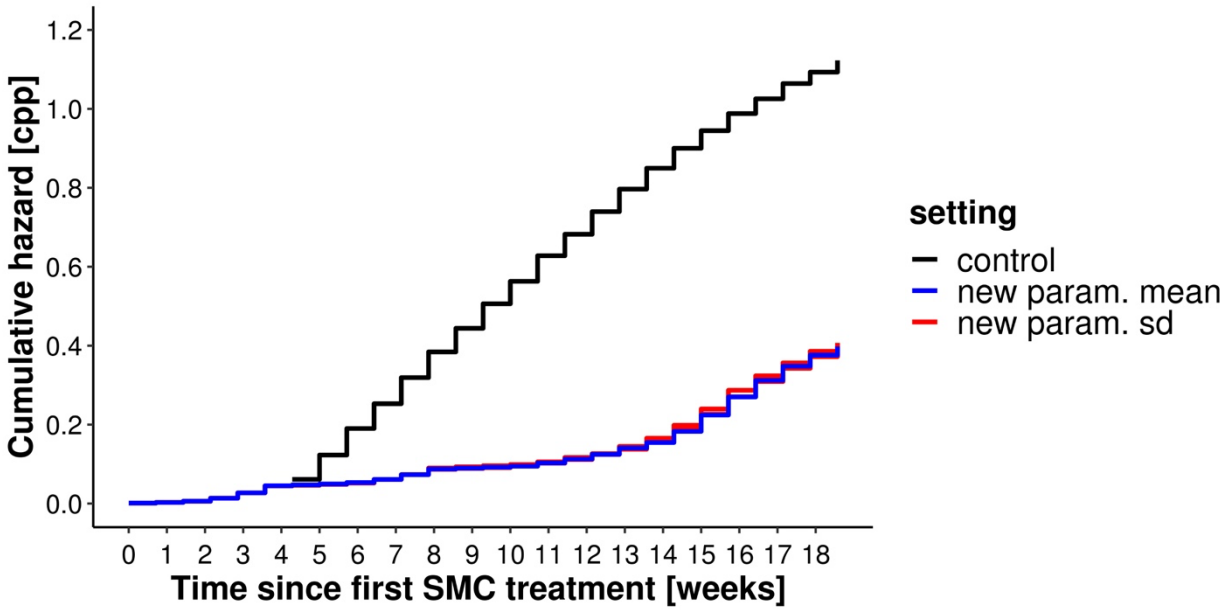

Fig M: Cumulative hazard of malaria in children who received SMC with SP-AQ (blue) compared to controls (black). The cumulative hazard over time was calculated using the Nelson-Aalen estimator. See Fig 2 in Zongo et al.(2015)[3] for comparison.

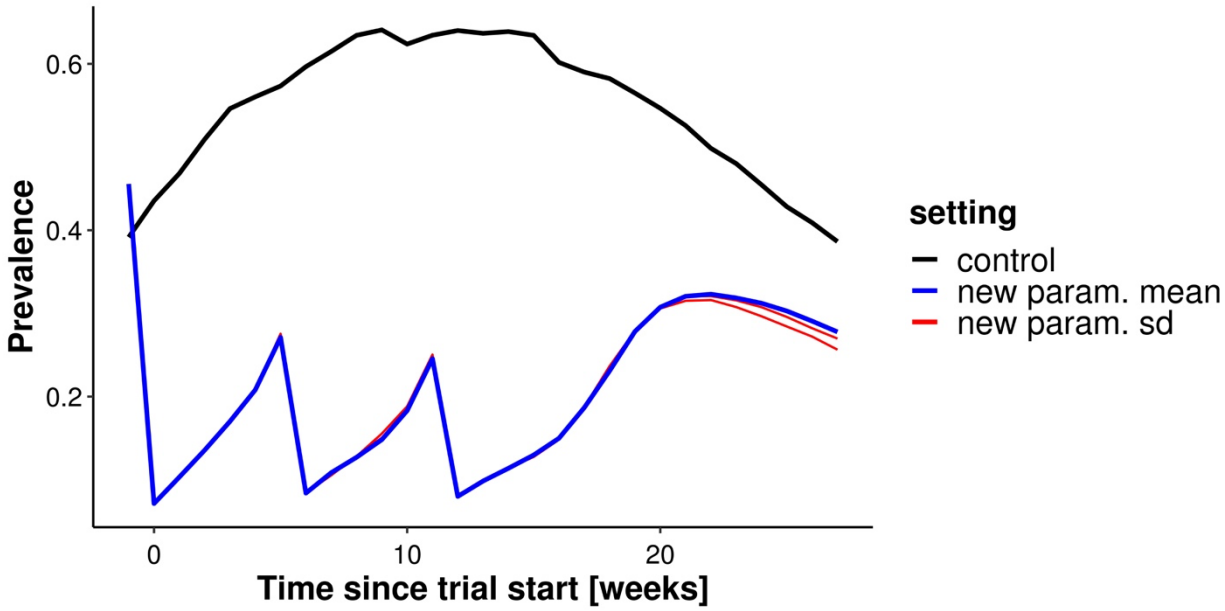

Fig N: Prevalence of malaria in children who received SMC with SP-AQ (blue) compared to controls (black) over the trial. The prevalence in the intervention cohort is decreasing with each SMC round every month and then slowly increasing again. At the same time, the prevalence in the control group is increasing with the ongoing malaria transmission season. After the last SMC round, there is an increase of prevalence caused by still ongoing transmission. Simultaneously, the transmission intensity is already decreasing as can be seen in the control cohort prevalence.

References

1. WHO. WHO Policy Recommendation: Seasonal Malaria Chemoprevention (SMC) for Plasmodium falciparum malaria control in highly seasonal transmission areas of the Sahel sub-region in Africa. (World Health Organization, 2012).

2. Dahal, P. et al. Statistical methods to derive efficacy estimates of anti-malarials for uncomplicated Plasmodium falciparum malaria: pitfalls and challenges. Malar. J. **16**, 430–430 (2017).

3. Zongo, I. et al. Randomized Noninferiority Trial of Dihydroartemisinin-Piperaquine Compared with Sulfadoxine-Pyrimethamine plus Amodiaquine for Seasonal Malaria Chemoprevention in Burkina Faso. Antimicrob. Agents Chemother. **59**, 4387–4396 (2015).

4. Dabire, K. R. et al. Anopheles funestus (Diptera: Culicidae) in a humid savannah area of western Burkina Faso: bionomics, insecticide resistance status, and role in malaria transmission. J Med Entomol **44**, 990–7 (2007).

5. WHO. World malaria report 2008. (World Health Organization, 2008).

6. Penny, M. A. et al. Distribution of malaria exposure in endemic countries in Africa considering country levels of effective treatment. Malar. J. **14**, 384 (2015).